Fall 2020

Application of Excitation-Emission Matrices to Fluorescent Dye Tracing of Groundwater Flow

Cayla M. Baughn
Western Kentucky University, cb7427@gmail.com

APPLICATION OF EXCITATION-EMISSION MATRICES TO FLUORESCENT DYE TRACING OF GROUNDWATER FLOW

A Thesis
Presented to
The Faculty of the Department of Geography and Geology
Western Kentucky University
Bowling Green, Kentucky

In Partial Fulfillment
Of the Requirements for the Degree
Master of Science

By
Cayla Baughn

May 2020

APPLICATION OF EXCITATION-EMISSION MATRICES TO FLUORESCENT DYE TRACING OF GROUNDWATER FLOW

Date Recommended: July 25, 2020

Groves, Christopher Digitally signed by Groves, Christopher Date: 2020.08.06 13:40:06 -05'00'

Chris Groves, Director of Thesis

Patricia Kambesis Digitally signed by Patricia Kambesis Date: 2020.08.06 15:26:11 -05'00'

Patricia Kambesis

Fredrick D. Siewers Digitally signed by Fredrick D. Siewers Date: 2020.08.06 15:01:31 -05'00'

Fred Siewers

Cathleen Webb Digitally signed by Cathleen Webb Date: 2020.08.06 16:08:59 -05'00'

Cathleen Webb

Ranjit T. Koodali Digitally signed by Ranjit T. Koodali Date: 2020.08.06 16:20:27 -05'00'

Associate Provost for Research and Graduate Education

ACKNOWLEDGMENTS

I would first like to extend to my advisor, Dr. Chris Groves, and the Crawford Hydrology Laboratory my sincere gratitude for providing the monetary and laboratory resources necessary to facilitate the completion of this thesis and my graduate experience as a whole. I would also like to thank my thesis committee, including Drs. Groves, Patricia Kambesis, Fred Siewers, and Cate Webb, for their input through the development and completion of this thesis.

I would like to personally thank Dr. May for supporting me and for all of our times joking around. Your classes were one of the best parts of my program. Autumn Turner, thank you for being such a joy to work with at CHL. I hope our paths cross often! Cesalea Osborne and Josh Allison, thank you for being the sincerest of friends ever since we first met, for always believing in me, and for your optimism. I hope your happiness knows no limits! Thank you also Colleen Hoskins and Austin Dewitz. You were true friends last summer when I worked on this research at night in the truck in Nevada and it seemed like it would never happen. I'm thankful to have you as friends even now.

Finally, I would like to thank my family and Manny Jimenez for their undying love, support, patience, kindness, and unfailing sense of humor. Thank you, Mom, for always being there for me, no matter what, even when your FCA shirt is on! Thank you, Granny and Grandpa, for being the best grandparents I could ever want and for being darn good field buddies too! Thank you, Mim and Dad, for helping me keep things in perspective by being plain funny. Thank you, Scarlett, for being the sister I never had but always wanted. Finally, Manny, thank you for all this time you've spent with me, your love, patience, and thank you for all of our adventures. Time for the next one.

TABLE OF CONTENTS

LIST OF FIGURES

LIST OF TABLES

APPLICATION OF EXCITATION-EMISSION MATRICES TO FLUORESCENT DYE TRACING OF GROUNDWATER FLOW

Cayla Baughn May 2020 198 Pages

Directed by: Chris Groves, Patricia Kambesis, Fred Siewers, and Cathleen Webb

Department of Geography and Geology Western Kentucky University

Fluorescent dye tracing of groundwater is a technique employed particularly in carbonate rock karst regions to examine karst hydrology by mapping underground flow paths. It is important to understand the hydrology of karst environments because solutionally-enlarged conduits may allow the rapid influx of contaminants into the groundwater system. Fluorescent dye tracing involves the injection of a fluorescent dye into an appropriate injection site (sinking streams, sinkholes, or even through soil flushed with water) and is followed by sampling at sites where the dye may be recovered (typically springs). Various methods exist by which sampling may occur, but all methods ultimately result in laboratory analysis of samples through the application of fluorescence spectrophotometry.

In Western Kentucky University's Crawford Hydrology Laboratory, two-dimensional synchronous scanning is applied to aqueous samples that potentially contain fluorescent dyes to quantify the concentration of the dye in the sample and thus determine flow paths between dye injection and recovery sites. Sometimes this analysis is impeded by complications, including background fluorescence and challenges associated with concurrent use of multiple fluorescent dyes. This research explores potential solutions to these issues through the application of *three-dimensional synchronous scanning*.

Both two and three-dimensional synchronous scanning were applied to collections of dilutions of the fluorescent dyes, fluorescein (FL), eosin (EO), rhodamine WT (RWT), and sulphorhodamine B (SRB), as well as a collection of anthropogenically-impacted water samples pulled from the Lost River Groundwater Basin in Bowling Green, Kentucky, following the injection of FL. Although measurement of dye concentration proves to be challenging, three-dimensional synchronous scanning provides an additional method to distinguish FL from EO in aqueous water samples and an additional method by which it may be determined if a particular dye compositionally dominates a sample that contains more than one fluorescent dye. Furthermore, through this study, a preliminary characterization of the background fluorescence of the Lost River was conducted; a preliminary parameter set for the three-dimensional analysis of the fluorescent dyes, FL, EO, RWT, and SRB was developed; and preliminary spectral fingerprints were developed for the fluorescent dyes, FL, EO, RWT, and SRB.

1. Introduction, Background, and Objectives

1.1 Karst Aquifer/Flow Systems

Karst landscapes that cover 10-20% of the Earth's surface are characterized by the dissolution of underlying carbonate rocks (most commonly limestone and dolomite) by carbonic acid that forms as a result of the interaction between water and carbon dioxide gas (Figure 1). The term "karst" may also be used to describe a landscape that is comprised of karst-like features developed in gypsum or salt-based rock types. Karst is uniquely valuable as an irreplaceable landscape on the Earth's surface, as a home to a variety of rare and endemic species especially adapted to life in cave environments, and as the supplier of a significant portion of the world's fresh water. Furthermore, karst landscapes act as a natural carbon sink (Freeze and Cherry 1979; Palmer 1981; Crawford and Hoffman 1989; Palmer 1991; Sasowsky 2000; Currens 2002; Palmer 2007; De Waele et al. 2009; Goldscheider 2012).

Features that are commonly found in karst areas include *sinkholes*, or closed depressions in the landscape where land is subsiding due to bedrock dissolution; *springs*, or locations where groundwater emerges from an aquifer to become surface flow; and *sinking streams*, or streams that originate as surface flow but abandon their channels and divert underground (locations along streams and within sinkholes where surface flow is lost to the subsurface are called *swallets*). Caves are another widely recognized karst feature that are the focus of extensive scholarly study and recreational interest (Freeze and Cherry 1979; Palmer 1981; Ryan and Meiman 1996; Currens 2002; Goldscheider and Andreo 2007; Palmer 2007; Goldscheider et al. 2008).

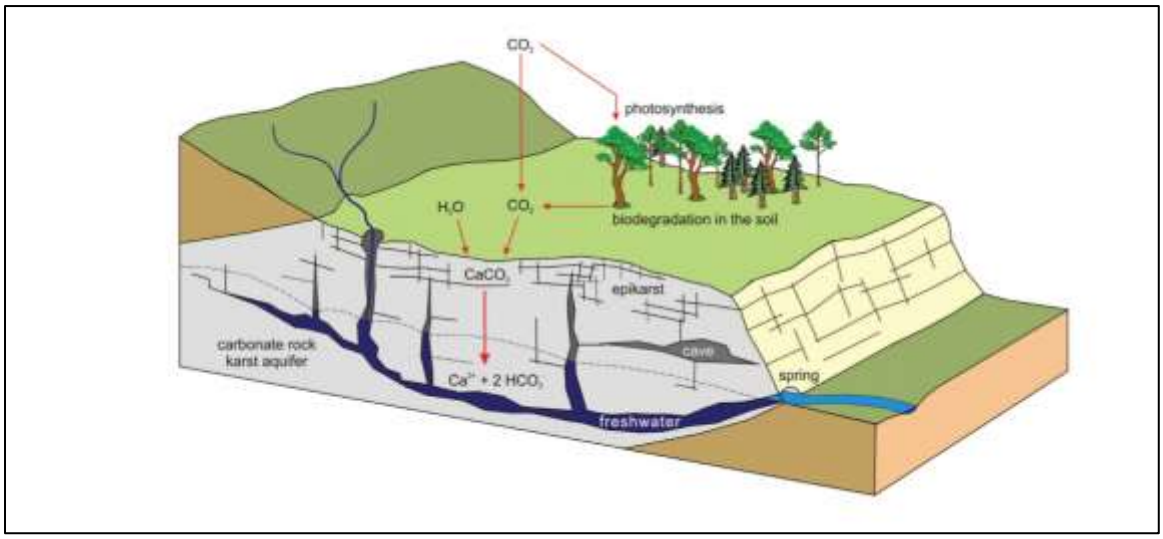

Figure 1: Development of Karst (Goldscheider 2012).

In Kentucky, well-developed karst terrain comprises approximately 38% of the topography, and 55% of Kentucky's topography is underlain by strata conducive to the formation of karst features (Currens 2002). Kentucky is home to Mammoth Cave, the longest known cave system in the world. The karst regions of Kentucky may be divided into four regions: The Western Pennyroyal, the central Kentucky Inner Bluegrass, the Eastern Pennyroyal, and the Pine Mountain region (Figure 2) (Palmer 1981; Currens 2002).

Unlike groundwater basins in non-karstic regions, subsurface flow patterns in karst landscapes do not necessarily mimic those of the surface water above and are therefore much more difficult to map and delineate (Currens 2002; Goldscheider and Andreo 2007). Differential dissolution of underlying strata may yield unpredictable underground flow paths that extend beyond the subsurface drainage basin to divert flow from adjacent subsurface basins, that are variable in size, and that can transport disparate

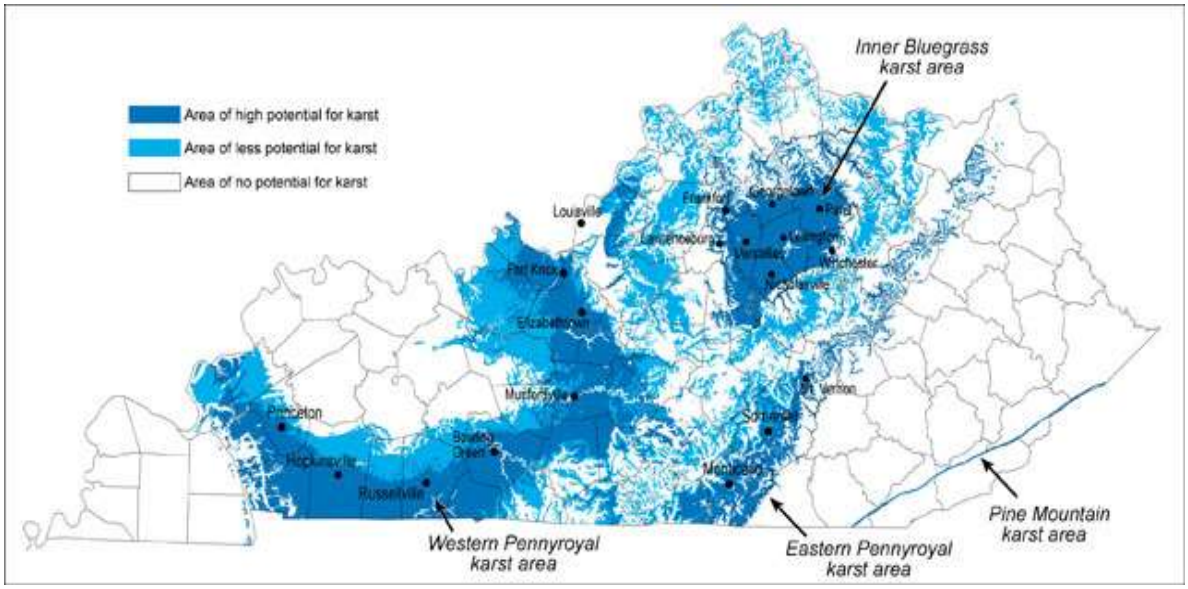

Figure 2: Karst regions of Kentucky (Currens 2002).

volumes of water (Palmer 1991; Baedke and Krothe 2000; Sasowsky 2000; Currens 2002). Flow variations within the aquifer may cause conduits to fill in or empty due to heterogeneous sediment accumulation and conduits may change shape, destination, join, or split in accordance with the volume of fluid and sediment within them (Goldscheider et al. 2008).

Karst aquifers are often characterized by particularly severe vulnerability to contamination by chemicals, bacteria, viruses, and other contaminants (Figure 3). Other types of aquifers in porous or fractured media are usually composed of low-permeability strata within which flow is limited to fractures and pore spaces. Groundwater movement in non-karst aquifers is usually substantially slower than in karst aquifers, and, due to its prolonged journey through minute spaces, is often leached of contaminants by physical, chemical, and biological processes much more effectively than karstic groundwater (Crawford and Hoffman 1989; Palmer 1991; Currens 2002). Contrastingly, karst regions are characterized by bedrock dissolution and large underground conduit systems. Surface

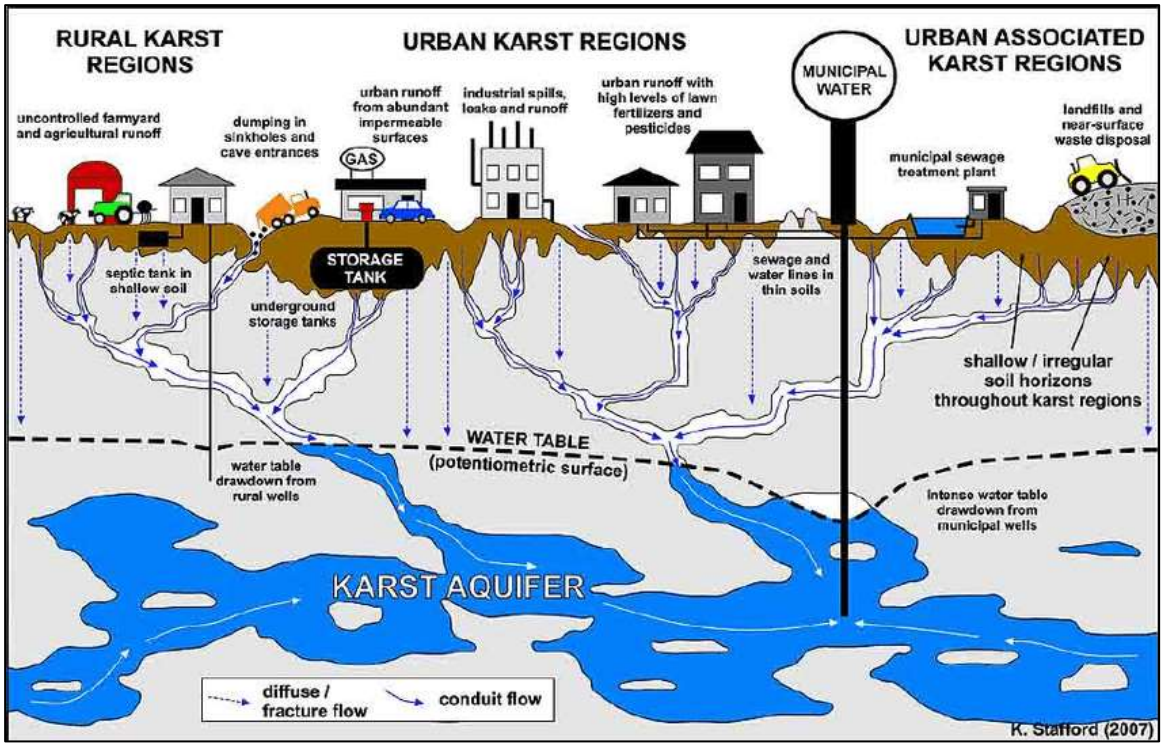

Figure 3: Potential sources of contaminants in karst terrain (Margane 2011).

water that infiltrates the subsurface in a karst landscape, whether via swallets or through percolation and infiltration through the vadose (unsaturated) zone, can move rapidly through the subsurface and has markedly less opportunity for filtration (Crawford and Hoffman 1989; Palmer 1991; Currens 2002; Goldscheider et al. 2007).

Contamination of karst aquifers is particularly severe during storm runoff events which generate *flood pulses*. Flood pulses move downstream more quickly than the normal flow rate. In fact, in *phreatic* (water-filled) conduits, flood pulses move through the system almost instantaneously, while they can move through the system much more quickly than the normal flow rate in *vadose* (air-filled) conduits. Contamination of karst groundwater systems typically worsens during storm events when flood pulses that bear unfiltered runoff move through conduits much more quickly than in non-karst aquifers (Pronk et al. 2006; Göppert and Goldscheider 2007; Goldscheider et al. 2008). Water

pushed through the groundwater network during flood pulses resurfaces at cave and surficial springs that may serve as drinking water sources. Thus, even karst drinking water sources characterized by acceptable water quality during relatively dry conditions may be punctuated by temporary microbial influxes (Pronk et al. 2007). The sinuous nature of karst and the potential for rapid transmission of contaminants into the subsurface often necessitates the use of tracer tests to identify the recharge area to the specific karst hydrologic system, aid in the determination of contaminant source(s), and to aid in the delineation of potential contaminant pathways.

1.2 Significance and Research Objectives

Groundwater contamination may yield a wide variety of challenges, from damaging fragile ecosystems to contaminating drinking water supplies. In karst regions, the intensity of the sometimes-devastating consequences of groundwater contamination is amplified. It is imperative to delineate underground flow paths and elucidate the connectivity between them so that contaminant pathways and significant contamination events may be anticipated, mitigated, or even prevented.

Tracer tests are the most common tool used to delineate groundwater flow paths in karst aquifers and a preponderance of related scientific literature has arisen in accordance with this fact. The objectives of the current research are to contribute to this body of literature by advancing the analytical laboratory aspect of tracer testing by rigorously evaluating the potential of three-dimensional synchronous scanning (the detection of fluorescence dye tracers by fluorescence spectrometry in three dimensions rather than the conventional two dimensions) to: 1) discriminate the fluorescent dye

spectra of four common fluorescent dyes from one another, 2) discriminate fluorescent dye spectra of four common fluorescent dyes from background fluorescence in an anthropogenically-affected sampling environment, and 3) enhance existing or establish new fluorescent dye detection and quantification methods in the field of dye tracing.

2. Literature Review

2.1 Fluorescent Dye Tracing Tests: Field Procedures

Tracer tests are tests that involve the injection of a *tracer*, or a compound used to tag and track moving water, into the local groundwater system, often by injection into a sinking stream or swallet (Baedke and Krothe 2000; Smart and Karunaratne 2002; Smart and Simpson 2002; Goldscheider et al. 2008). Although there are many types of tracers, including salts, isotopes, bacteria, lanthanide-labeled clay, and fluorescent microspheres, fluorescent dyes are perhaps the most popular because it is possible to detect them at extremely low concentrations and they exhibit limited toxicological and ecotoxicological effects (Behrens at al. 2001; Göppert and Goldscheider 2007; Goldscheider et al. 2008). *Fluorescent dyes* are "synthetic organic compounds that absorb light at specific wavelengths and emit fluorescence light at longer wavelengths" (Weiss 1943; Goldscheider et al. 2008, p. 28). Tracer tests are comprised of three primary components: field procedures, laboratory procedures, and data processing and interpretation. Tracer test field procedures include delineation of the study area, literature review, karst hydrogeological inventory, background fluorescence investigation, and in some locations, acquisition of a dye trace permit. Through some studies of contaminated aquifers, a *matrix interference* investigation is also required to evaluate the potential interference of contaminants in the dye trace. The laboratory-based element of tracer tests includes sample processing, preparation of standard dilutions, and analysis. Analysis is followed by interpretation of results.

The initial steps of the tracer test characterize the study area. The study area boundaries are defined by locations where the water table is known to be higher than at

the proposed dye injection site, or where a definite discharge boundary has been reached (i.e. a river or large perennial stream). Following the delineation of the study area, a review of relevant literature and karst hydrogeologic inventory (KHI) are conducted. The latter involves the exploration of all relevant waterways (springs, cave and surface streams, ponds, and lakes) usually by walking or canoe to identify any relevant karst features and potential monitoring locations. Each of these features is assigned a unique identification code, plotted on a topographic map, and pertinent hydrological and physical feature data is recorded (feature sketch, basic water quality parameter measurements, etc.) (Kass 1992; Crawford Hydrology Laboratory 2019).

After a full KHI is performed, a *background fluorescence* investigation should be conducted to identify and measure any preexistent fluorescence in the relevant waterways (i.e. *background fluorescence*). This information will aid in choosing the type and concentration of the tracer. Methods of measuring fluorescent dyes in the field will be discussed shortly and background fluorescence will be discussed in a later section as a general challenge to the analysis of fluorescent dyes (Kass 1992; Wehry 1997; Smart and Karunaratne 2002; Smart and Simpson 2002; Meus et al. 2006; Shimadzu 2015; Crawford Hydrology Laboratory 2019).

After conducting a background fluorescence investigation, a matrix inference investigation may be performed if necessary. A *matrix interference investigation* is an investigation that seeks to discover the degree to which the properties of the dye are influenced by particularities of the matrix in which the analyte is contained. Peculiarities may include abnormally low or high pH values or elevated total dissolved solids concentrations. These peculiarities may be attributed to anthropogenic influence or the

natural environment. It is ideal that the analytical measurement is *not* significantly impacted by the matrix. The matrix interference investigation usually involves comparison of the measurement of the analyte suspended in the original matrix to a *laboratory* or *reagent blank*, a sample comprised of a matrix of known characteristics that does not contain any concentration of the analyte, and a *laboratory-fortified matrix*, or an additional sample to which a known amount (at least ten times the minimum reporting level) of the analyte of interest has been added, among other possible quality control and quality assurance measures (American Public Health Association 1999; Thompson and Ellison 2005).

Matrix interference investigations are more common in discrete sampling studies through which the fluorescent dye tracer is suspended in a natural aqueous matrix and when evaluating potential influences of a new eluent in integrative sampling studies (American Public Health Association 1999; Thompson and Ellison 2005). These studies will be described shortly. Following the matrix interference investigation (if applicable), a dye trace permit application must be submitted to the proper authorities and approved (through the Kentucky Division of Water in the state of Kentucky) (Crawford Hydrology Laboratory 2019).

After these preparations have been made, the tracer test may be conducted in the field. In light of the results of the KHI and background fluorescence investigation, appropriate fluorescent dye(s) and dye injection point(s) must be chosen. Cave streams, sinking streams, sinkholes, and swallets are usually chosen as dye injection sites because flow moving through these karst features will rapidly carry the fluorescent dye into the groundwater system (Kass 1992; Benischke et al. 2007). However, if water is not

naturally flowing through these features at the time of injection, it may be necessary to "flush" the tracer into the karst aquifer using a large volume of water (Goldscheider et al. 2008). After the dye has been injected, an appropriate sampling regime must be enacted. Types of sampling regimes include both integrative and quantitative methods.

Integrative sampling through qualitative tracing is an economical, useful, and popular sampling method through which nylon mesh bags of granulated high-grade coconut charcoal called *dye receptors* (Figure 4) are placed at strategic locations in flow channels over a specified period, usually one to two weeks (Currens 2002; Smart and Simpson 2002; Palmer 2007; Goldscheider et al. 2008; L.A. Bledsoe, personal communication, December 22, 2018). Placement locations are chosen based upon the likelihood of the injected dye arriving at the location during the trace—if it is plausible that the injected dye will arrive at a given location, dye receptors are placed prior to the dye injection to capture any tracer that might arrive. It is absolutely key to identify and monitor every possible dye emergence location. The fluorescent dye will adsorb onto the charcoal in the dye receptor if it passes through the site and after the allotted time period, the dye receptors are collected and processed in a laboratory (Baedke and Krothe 2000; Smart and Simpson 2002; Palmer 2007; Goldscheider et al. 2008).

Quantitative sampling allows for more detailed measurement of hydrologic information, including time to initial arrival of the tracer at the sampling site, peak concentration point, fluorescent dye percent recovery, estimation of cross-sectional areas and volumes of phreatic conduits, and center of mass via discrete and continuous

Figure 4: Charcoal dye receptors.

sampling methods (Palmer 2007; Goldscheider et al. 2008). *Discrete* quantitative sampling may be described as manual or automated sampling undertaken at specified time intervals at sites likely to intercept the fluorescent dye, which eventually results in time-series data of fluorescent dye concentrations at the sampling sites (Baedke and Krothe 2000; Palmer 2007; Goldscheider et al. 2008).

Continuous quantitative sampling permits the most detailed data acquisition using *submersible fluorimeters*, i.e. automatic water samplers or *in-situ* electronic data loggers. These devices can take measurements at time resolutions as high as one measurement per several seconds and allow the measurement of up to three fluorescent dyes

simultaneously, in addition to turbidity and temperature. However, continuous quantitative sampling is typically much more expensive than integrative sampling (Ryan and Meiman 1996; Sasowsky 2000; Palmer 2007; Goldscheider et al. 2008).

Whatever the method, it is always imperative that the dye trace technicians take ample precaution to ward against *autocontamination*, or inadvertent contamination with dye. Autocontamination is also a potential source of contamination when creating the fluorescent dye solutions from powdered dyes prior to injection or when creating standard dilutions from powdered dyes in the laboratory (Smart and Karunaratne 2002).

2.2 Tracer Tests: Laboratory Procedures

2.2.1 Sample Processing and Preparation of Standard Dilutions

After collection, water samples and dye receptors are checked in and processed in a laboratory. In the WKU Crawford Hydrology Laboratory (CHL) where this research was performed, water samples are processed first by washing the outside of the collection vessel (typically a glass screw-cap vial) with a diluted bleach solution and then by washing the outside of the vessel with water. Water samples are then labeled and stored in the dark at 5 °C ± 2°C until analysis. Dye receptors are processed by washing for 30 seconds on each side with a high-pressure water stream and then dried in a drying oven for a minimum of 12 hours at 50 °C ± 5 °C. Once the receptors are dry, 1 g ± .02 g of charcoal from each sample is removed and eluted with an alkaline alcohol mixture deemed “Smart Solution” (named for pioneering hydrologist, Peter Smart, and composed of ammonia hydroxide, propanol, and water) to transfer any dye adsorbed onto the charcoal into the eluent. One duplicate sample per twenty samples is created and

analyzed with the sample set. Eluent samples are labeled and stored in the dark at 5 °C ± 2°C until analysis (Crawford Hydrology Laboratory 2019).

Prior to analysis of the samples, fluorescent dye standard dilutions must be created to calibrate the instrument and to periodically check the instrument's calibration. Two low concentration and one high concentration standard dilutions are analyzed at the beginning and end of each sample set in the CHL. In addition, after every 20 samples, two low concentration standard dilutions must be analyzed to verify the calibration of the instrument throughout the analysis. Fluorescent dye standard dilutions are made using deionized water as the diluent for water samples and Smart Solution as the diluent for eluent samples. Only the process of making standard dilutions in water will be discussed here because water samples are the subject of this research (PerkinElmer 2000; Bledsoe 2019 (a); Bledsoe 2019 (b)).

Through the course of this research, fluorescent dye standard dilutions were either created from concentrated fluorescent dye standards stored in CHL or made from powdered fluorescent dyes and subsequent serial dilution. Fluorescent dye standard dilutions were rarely, if ever, made from low concentration working dilutions because it is well-established that dilute solutions are less stable than concentrated ones (PerkinElmer 2000; Alexander 2005). First, powdered fluorescent dye of a purity guaranteed by the supplier must be dried in an oven at 120°F overnight. Powdered dyes are dried in an oven outside the CHL to prevent possible contamination of the lab. The oven used to dry the powdered dye is thoroughly decontaminated using a bleach solution after each use to prevent contamination of later powdered dyes. The powdered dye is then portioned by weight using a sub-milligram precision analytical balance, precise to .001 g.

The measured portion of powdered dye is added to an ultra-clean amber bottle within a precision of .0200 g of the target portion. Then, deionized water is added to the amber bottle to within .0200 g of 100 g. The solution is then capped and the powdered dye is allowed to dissolve completely, thus creating a 1% stock standard dilution. 1% stock dilutions of every dye are used to create the spectra of standard dilutions in water volumetrically. These dilutions may either be made by serial dilution or by direct dilution of the 1% stock solution (Alexander 2005).

Following the creation of standard fluorescent dye dilutions, laboratory analysis may be conducted. Potential types of fluorescence laboratory analyses include UV/visible absorption spectroscopy, chemiluminescence, phosphorescence spectrometry, and fluorescence spectrometry (Wehry 1997). Fluorescence spectrometry is the method utilized in the CHL and is the subject of this research (Crawford Hydrology Laboratory 2019).

2.2.2 Analysis Using Fluorescence Spectrometry: Procedures

Fluorescence spectrometry is used in the CHL to analyze water samples collected in the progression of a dye trace. The CHL utilizes a Shimadzu RF-6000 spectrofluorophotometer and LabSolutionsRF software. Laboratory analytical procedures proceed as follows: first, the laboratory's spectrofluorophotometer is allowed to equilibrate for 30 minutes to allow the xenon bulb to stabilize. Simultaneously, samples are allowed to warm in a water bath for a maximum of 15 minutes to reach a temperature of 30° C, which is verified by an independent, regularly calibrated thermometer. A single laboratory blank (a verified reference vial of deionized water), a control blank (a vial of

the water that was used to create the fluorescent dye standard dilutions), and the set of standard dilutions are also added to the water bath and allowed to warm. Analysis of the laboratory blank is used to measure the Raman scattering of water at 350 nm. It is common practice to measure the Raman line of water at 348 nm to validate instrument stability and to evaluate any instrumental drift (Baker and Spencer 2004; Hudson et al. 2008; Bledsoe 2019b).

The set of standard dilutions usually includes a minimum of two fluorescent dyes whose emission ranges span alternate portions of the electromagnetic spectrum to verify the linearity of the instrument's calibration. Standard dilutions should be chosen that represent the fluorescent dyes likely to be found in the water samples. If more than these two fluorescent dyes are thought to be present in the water samples, standard dilutions of the additional dyes should be included in the standard dilution set as well. Two practical quantitation limit (PQL) (lowest concentration of the fluorescent dye the instrument is calibrated to measure) and one high-concentration standard dilution should be present for each fluorescent dye in the set of standard dilutions. Table 1 shows PQL standard dilutions used in the CHL (Bledsoe 2019b).

Following the 30-minute equilibration period, an evaluation of the signal-to-noise ratio (SNR) is initiated to define the instrument's sensitivity. The instrument is used to measure a laboratory blank (and thereby the Raman line of water) at an excitation wavelength of 350 nm. The *instrumental signal* is defined as a digital signal between 0 and 2^N-1where N is the number of bits in the Analogue-to-Digital (A/D) converter on the instrument. *Instrumental noise* is defined as the variation of the signal around a mean

Table 1: Practical quantitation limits on analysis of fluorescent dyes analyzed in the CHL (Bledsoe 2019b).

Fluorescent Dye Common Name (Chemical Name)	Low Scan in ppb	Low Scan in ppb	High Scan in ppb	Approx. Peak Center	Dye Abbreviation
PTSA	0.100	1.000	100	391.8	PT
Optical Brightener (Tinopal CBS-X)	0.100	1.000	100	397.0	OB
D&C Green #8	0.050	0.100	100	492.8	G8
Fluorescein (Uranine C)	0.010	0.050	10	510.8	FL
Eosine	0.010	0.100	100	536.2	EO
FD&C Red #3	0.100	1.000	100	546.0	R3
D&C Red #28 (Phloxine)	0.010	0.100	100	556.7	R28
Rhodamine WT	0.010	0.100	100	577.1	RWT
Sulphorhodamine B	0.010	0.100	100	584.3	SRB

value. The CHL utilizes the rms (root mean square) signal to noise measurement method to calculate instrument noise, where

$$\boldsymbol{Root\ Mean\ Square}\ (\hat{\sigma}) = \sqrt{\frac{1}{n-1}\sum_{i=1}^{n}(x_i - \bar{\mu}^2)} \qquad (1)$$

where n is the sample size, x is the sample mean, and μ is the population mean. Through this method, the root mean squared value of the noise fluctuations over a specified baseline section is computed in the software—CHL specifies a 10-minute baseline section. After calculating the noise rms value, the software computes the SNR by dividing the peak signal average by the rms noise value of the peak signal (measured over the specified baseline interval). This measurement ensures that the signal of the instrument is at least 1000 times the signal of the background noise. This stipulation ensures the signal to noise ratio receives a "passing" result, which is required to continue

analysis consistent with CHL methodology (Baker and Genty 1999; PerkinElmer 2000; Shimadzu 2012; Thomas 2012; Bledsoe 2019b; Ibsen Photonics A/S 2020).

Following a successful signal to noise ratio test, the instrument is used to measure the synchronous spectra of the laboratory blank, a laboratory control, a set of standard dilutions, and samples, in that order. All samples are initially analyzed using high-sensitivity parameters developed for low-concentration samples (samples that contain low concentrations of fluorescent constituents). Following analysis of the samples, the laboratory control and standard dilutions are analyzed a second time to verify calibration of the instrument to and through the analysis period. If some or all of the samples prove to be high-concentration samples, these samples are analyzed using low-sensitivity instrument parameters that were developed for the analysis of high-concentration samples. High-concentration samples contain high concentrations of fluorescent constituents and are characterized by a fluorescence intensity of more than 1,000 fluorescence intensity units or a concentration of more than 100 parts per billion (ppb). It is possible to save both low and high-sensitivity parameter settings within the software program and the CHL has established standard low and high-concentration analysis parameters that were used for all synchronous scan measurements throughout the course of this research. Figure 5 and Table 2 display the settings and peak parameters used to analyze both low and high concentration water samples (Bledsoe 2019a; Bledsoe 2019b).

If any samples contain high concentrations of fluorescent constituents, low-sensitivity instrument parameters must be loaded into the software program and a laboratory blank, a set of high-concentration standard dilutions, and the high-concentration samples must be analyzed. It is not necessary to analyze a laboratory

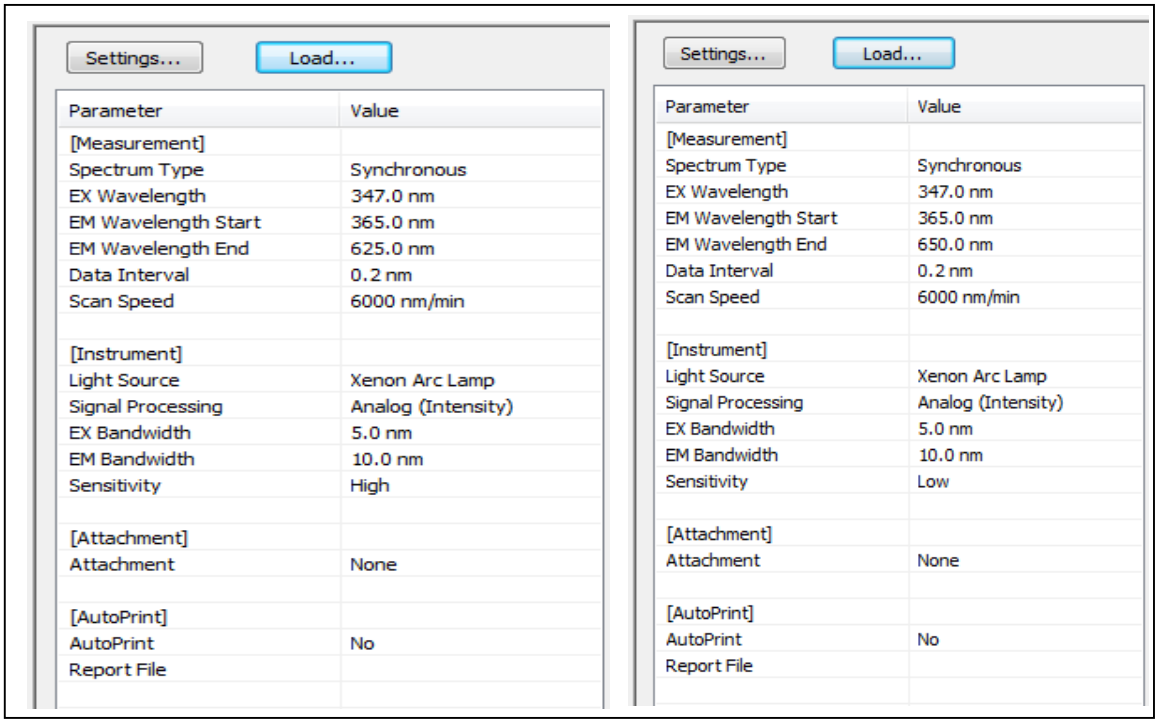

Figure 5: High and low sensitivity two-dimensional synchronous scanning parameters employed routinely in the CHL throughout the analysis period and through the course of this research.

Table 2: Fluorescein, eosin, rhodamine WT, and sulphorhodamine B peak parameters regularly consulted to define the respective fluorescent dye peaks in the CHL throughout the analysis period.

Dye	Start	End	Center
Fluorescein	492.8	528.8	510.8
Eosin	518.2	554.2	536.2
Rhodamine WT	558.9	594.9	576.9
Sulphorhodamine B	565.8	601.8	583.8

control in low sensitivity setting because any irregularities in the spectra of the laboratory control would presumably be too fine to be measured using the low-sensitivity setting. It is also unnecessary to analyze PQL standard dilutions because the instrument is configured to quantify concentrations far above the PQL in low sensitivity mode. Instead, a single high-concentration standard dilution is chosen to represent each fluorescent dye

that the samples are suspected to contain. These standard dilutions are analyzed to verify the linearity of the calibration at high concentrations. The set of high concentration standard dilutions is analyzed prior to the analysis of the samples, as well as following sample analysis. After any high-concentration samples are analyzed in low-sensitivity mode, a final signal-to-noise ratio is measured and must demonstrate passing results to validate the preceding analyses (Bledsoe 2019b).

In addition to measurement of synchronous spectra of all samples, two additional operations are performed during the analysis process: determination of the peak area and peak pick. These operations allow the laboratory technician to measure the area of a fluorescence peak displayed on a synchronous scan and discriminate fluorescence peaks from the overall fluorescence spectra, all within the software program. As displayed in the table below, the peak area function allows the technician to save pairs of beginning and end-point wavelengths (called *peak beginning* and *peak end*—the beginning and ending points of a spectral peak along the x-axis of the synchronous scan) that have been determined to be specific to a certain fluorescent compound. The *peak center* may also aid in the determination of the fluorescent compound that is indicated by the spectral range (Smart and Laidlaw 1977; Smart and Karunaratne 2002; Smart and Simpson 2002; Bledsoe 2019a; Bledsoe 2019b; Crawford Hydrology Laboratory 2019).

The software program calculates the *peak area* of the fluorescence peak, which is directly translatable to concentration of fluorescent compound in parts per billion (ppb) by the calibration process. The instrument is recalibrated periodically in response to shifting of peak centers of the spectral ranges of known fluorescent compounds. Shifting peak centers potentially indicate shifting of the spectral ranges of the compounds and/or

instrument drift. Through the recalibration process, standard dilutions of known concentrations are analyzed three times to gain an average area measurement. To determine the divisor parameter, the known concentration of the standard dilution is divided by the dilution's measured area. The new divisor parameter is then used in peak area calculations to produce the corresponding fluorescent compound concentration (Shimadzu 2012; Bledsoe 2019b). By way of this calibration procedure, it is common practice to calculate concentrations of fluorescent dyes through the analysis of synchronous spectra in the Crawford Laboratory (Alexander 2005; Bledsoe 2019b).

The *Peak Pick* function allows the laboratory technician to elucidate particular peaks in the continuous synchronous spectra by setting a threshold value and a peak point value. The *threshold value* is a fluorescence intensity value over which the software program will consider the segment of spectra as deviant from the spectral norm. Spectra that fluoresce at a greater fluorescence intensity than the threshold indicates the presence of a substance that is too fluorescent to be a common component of the background fluorescence and is potentially a portion of a spectral peak. The *point pick* value is the spectral range (in units of nanometers) in either direction from the peak center within which the spectra will be assigned to the peak center as a portion of the identified peak. The point pick metric is essentially a data aggregation value. For example, if the peak point is set to 5, then spectra within 5 nm of the peak center will be assigned to the specified peak and classified as a portion of the peak (Bledsoe 2019a; Gilbert Vial, personal communication, November 2, 2018). Following measurement of the peak area and peak pick, data QAQC and interpretation are executed, and the laboratory analysis procedures conclude.

2.3 Challenges to Analytical Fluorescence Measurement in Hydrology

Fluorescence spectrometry analytical methods in the Crawford Hydrology Laboratory are robust and well-established, as are dye trace field procedures. These methods are also well-documented in the body of scientific literature. However, several challenges still exist to the accurate measurement of fluorescent dyes. For many of these challenges, the solutions are limited or not yet developed. Several challenges exist related to the accurate detection and measurement of fluorescent dyes using fluorescence spectrometry. These challenges include background fluorescence, quenching (sometimes caused by interactions of certain metal ions), variations in temperature and pH, and inner filter effects. *Background interference* is a common analytical challenge and is defined as the instance in which a fraction of the observed value(s) arises from sources external to the investigation at hand (Smart and Karunaratne 2002). Fluorescent background interference, or background fluorescence, may arise from natural or anthropogenic sources, all of which are composed of fluorescent compounds that emit fluorescence in the same emission wavelength range as the injected dyes (Kass 1992; Goldberg and Weiner 1993; Wehry 1997; Smart and Karunaratne 2002; Smart and Simpson 2002; Meus et al. 2006; Shimadzu 2015; Crawford Hydrology Laboratory 2019).

There are two standard field monitoring strategies that assist in the elimination of interference by background fluorescence: *pre-monitoring* at the site(s) of interest and *analog monitoring*. Pre-monitoring at a site (or sites) entails collecting samples at the site(s) prior to the dye trace to either calculate the average background fluorescence or collect sufficient data to extrapolate a trend in background fluorescence throughout the dye trace period. The average or extrapolated background fluorescence is then subtracted

from the measured fluorescence to obtain the "true" fluorescent dye concentration. A fundamental assumption of pre-monitoring is that the overall trend in background fluorescence is consistent and that spontaneous events that contribute background fluorescence (for instance, vehicular collisions) are rare and/or insignificant (Smart and Karunaratne 2002; Alexander 2005). Fluorescent dyes that are not detected or are detected in low concentrations at the site of the trace will be selected as the tracer(s) in most instances to limit interference by background fluorescence. This is the method typically employed in the CHL (Crawford Hydrology Laboratory 2019).

Analog monitoring entails monitoring background fluorescence at a second site or system thought to be analogous to the location of the dye trace based on the local hydrogeology, land-use type, soil type, vegetation, and other relevant factors. Background fluorescence measured at the analog site is subtracted from the fluorescence measurements made at the dye trace site to obtain the "true" fluorescence concentration values. A drawback of the analog monitoring method is that there are no specific or widely accepted criteria for classifying a system as an analog site (Smart and Karunaratne 2002). Both methods may fail to account for unexplained shifts in the spectral form of the broad background fluorescence peak and since background fluorescence may be altered substantially by isolated contamination events, standard extrapolation corrected procedures which require a standard spectral form may be rendered challenging or impossible (Smart and Karunaratne 2002, p. 498).

Dye trace technicians sometimes inject copious amounts of the tracer into the hydrological system to ensure the dye may be measured at a level significantly higher than the background fluorescence. However, this method is not always feasible,

especially when bright red or green waterways might raise local concern or extended exposure might cause harm to local ecological communities. Dye trace technicians also sometimes use more than one tracer dye at a time in a given system. This method is potentially more expensive than using a single tracer and in highly-contaminated systems it may be difficult to find two appropriate fluorescent dyes that fluoresce significantly above the background fluorescence and do not themselves share overlapping emission wavelength ranges (Smart and Karunaratne 2002).

Fluorescent background interference, or background fluorescence, is unique to each flow system and is determined by the organic chemical hydrology of the stream—it is especially sensitive to contaminant history and local runoff processes (Smart and Karunaratne 2002). Background fluorescence is contributed by many forms of human activity in addition to certain natural processes. Anthropogenic background fluorescence sources include vehicular collisions that contribute fluorescein (a popular fluorescent tracing dye and a component of antifreeze) and petroleum products that contain highly fluorescent polycyclic aromatic hydrocarbons (PAHs). Tissue mills produce effluent that contains optical brighteners and fluorescent whitening agents that sometimes leach into waterways. Unlined landfills or landfills in which the liner is failing produce effluent that contains humic and fulvic-like fluorescence. Fluorescence that takes the spectral form of the protein, tryptophan, may leach out of landfills as well (Wehry 1997; Baker 2002; Patra and Mishra 2002; Smart and Simpson 2002; Baker and Curry 2004).

Common sources of natural background fluorescence include both organic and inorganic complexes. Organic complexes such as humic and fulvic acids—amino-acid groups within proteins that are derived from decomposed plant material in the overlying

soil—display a broad peak in the synchronous scan. Other organic background interference sources include flora and fauna organic material and organic pollutants, the latter of which may display more defined peaks and peak clusters in the synchronous scan, especially at ultraviolet (short) wavelengths (Baker and Genty 1999; Smart and Karunaratne 2002). Inorganic compounds like UO^{2+} and Mn^{2+} may also contribute to background fluorescence (Baker and Gentry 1999). Thus, many regions of the light spectrum are susceptible to background interference—the orange region of the spectrum (540-600 nm) is reportedly the most robust and least susceptible to influence by background contamination, while green (490-540 nm) and blue (390-490 nm) dyes are the most susceptible to interference by organic background interference (Smart and Karunaratne 2002). Blue fluorescent dyes include Amino G acid and Photine CU; green fluorescent dyes include the popular dye fluorescein, in addition to pyranine and lissamine FF; and orange fluorescent dyes include rhodamine B, rhodamine WT, and sulphorhodamine B (Smart and Laidlaw 1977).

As discussed previously, field strategies undertaken to mitigate the effects of background fluorescence by using very large amounts of dye may fail to account for the full spectrum of background fluorescence, may cause alarm in local communities, may be more costly, and in extreme cases may have ecological impacts while not necessarily providing significant benefits. Analytical techniques to distinguish dye tracers from background fluorescence in the laboratory are limited as well. The existing analytical methods to separate fluorescence peaks caused by natural or anthropogenic background fluorescence from the emission peaks of fluorescent dyes include the application of non-

linear curve-fitting software that is specifically designed for spectral analysis and separation of spectral peaks (i.e. PeakFit) (Smart and Karunaratne 498).

In addition to background fluorescence and quenching effects, variations in pH and temperature may also influence the measurement of synchronous spectra. Sample temperature changes affect the viscosity of the sample and thus influence the number of collisions of the molecules of the fluorescent component(s) within the sample and the solvent molecules. Fluorescence intensity is sensitive to these changes. In fact, in many types of samples, it has been shown that each rise of 1°C correlates to a loss of 1-2% of the fluorescence intensity of the synchronous scan spectra of the sample. Some biological samples may even fluoresce at a 10% difference in intensity in response to each degree (in °C) of temperature change. It is recommended that temperature-dependent samples be analyzed while in a constant-temperature (thermostatted) cell holder, although it is usually sufficient to analyze all samples at room temperature (PerkinElmer 2000; Shimadzu 2015).

Variations in pH may also influence fluorescence intensity. Water samples of pH values between 7.0 and 8.5 are not likely to experience pH-related quenching or fluorescence wavelength changes, but pH and fluorescence intensity have been shown to be positively correlated and relatively small variations in pH will sometimes dramatically influence the intensity and spectral form of a fluorescence peak (Baker and Genty 1999; PerkinElmer 2000; Hudson et al. 2008).

Finally, the inner filter effect may also substantially affect interpretation and accurate measurement of the synchronous scan spectra. *Inner-filter effects* occur when a component of the sample shares the absorbance spectra of the fluorescent component of

interest and thus decreases the excitation energy reaching the fluorescent component of interest. The inner-filter effect may also occur when the absorbance spectra of a component of the sample overlaps with the emission spectra of the component of interest, which causes a reduction in the number of photons that are emitted by the component of interest and reach the measuring apparatus (Wehry 1997; PerkinElmer 2000). More simply, an inner-filter effect may be described as the "reabsorption of emitted energy by surrounding molecules in concentrated solutions" (Hudson et al. 2008, p. 6). Inner-filter effects may result from the presence of dissolved organic matter (DOM), among other constituents (Baker and Spencer 2004). In consideration of these challenges to synchronous scanning, it may be expedient to conduct a more informative, perhaps even more robust analysis of the fluorescent sample. One such method is called three-dimensional synchronous scanning and produces the three-dimensional synchronous scan, or as they are more often called, the excitation-emission matrix.

2.4 Three-Dimensional Synchronous Scanning

Another, potentially more informative type of fluorescence measurement, and the focus of this research, is *three-dimensional synchronous scanning*. Three-dimensional synchronous scanning is conducted by measuring the emission signal within a designated range of emission wavelengths (λ_{Em}) per each set excitation wavelength in a set range of excitation wavelengths (λ_{Ex}). The fluorescence intensity is recorded for every possible pair of emission and excitation wavelengths within the designated ranges to create a full spectral "fingerprint" of the substance. This combination of spectra is commonly referred to as an *excitation-emission matrix (EEM)* (Figure 6) and results in a three-dimensional

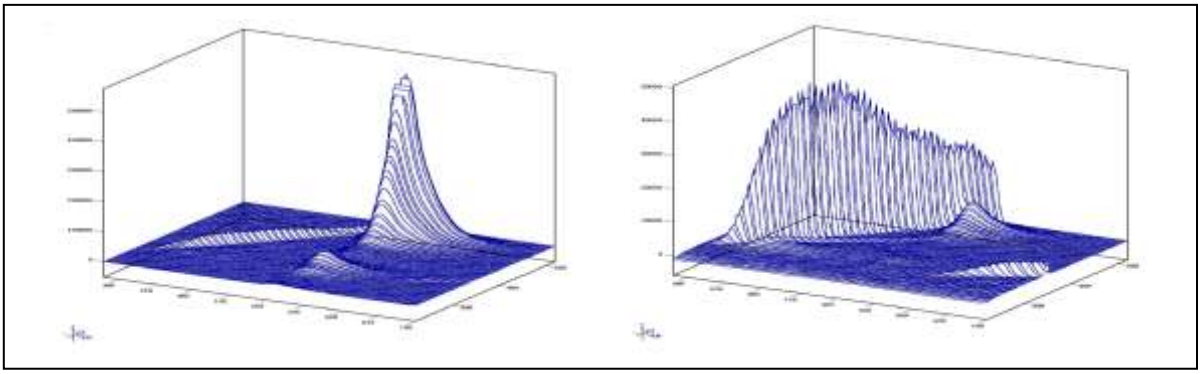

Figure 6: (Left to right) EEMs of 1 ppb and 100 ppb standard dilutions of fluorescein used in this research.

graph or contour diagram wherein excitation wavelength is represented on the *y*-axis (right hand side of the graph), emission wavelength is represented on the *x*-axis (front side of graph), and fluorescence intensity is represented on the (vertical) *z*-axis. EEMs are very useful for distinguishing complex materials from one another (for example, petroleum or biological fluids) by serving as *spectral fingerprints* for unique fluorophores and provide more information than the standard two-dimensional synchronous scan (Goldberg and Weiner 1993; Wehry 1997; Baker and Lamont-Black 2001; Baker 2002; Baker and Curry 2004; Soltzberg et al. 2008).

Since three-dimensional synchronous scanning is simply a dimensional extension of two-dimensional synchronous scanning, the principles of Stoke's Shift, quantum fluorescent yield, and quantum efficiency apply (see discussion of fluorescence theory in Appendix A). Here the *wavelength offset (Δλ)* is considered, which is the difference in nanometers between the wavelength of light that the instrument operator sets to excite the substance and the wavelength of light absorbed or emitted by the substance that the instrument operator chooses to measure. An appropriate value of *Δλ* must be chosen to produce an optimum EEM as well. However, three-dimensional synchronous scanning is sometimes used as a tool to determine the appropriate Δλ choice for synchronous

scanning, which is possible through the simultaneous, complete display of λ_{Ex} and λ_{Em} in the EEM. The EEM may be scrutinized to determine where the fluorescent components of concern exhibit their emission and excitation maxima and thus define the optimum $\Delta\lambda$ for use during analysis. The determination of the optimum $\Delta\lambda$ is an important use of the EEM (Rubio et al. 1986).

EEMs typically measure λ_{Ex} and λ_{Em} = ~200 - ~500 nm and their usefulness is well-established in the literature through a myriad of applications. These applications include characterizing the fluorescence of effluent from tissue mills and landfills, dissolved organic matter in various marine and freshwater environments, the fluorescence of various oceanic water bodies for the purpose of differentiating water masses, fishery effluent, sewage, natural organic matter and the accompanying speciation of trace metals in solution, phenol contamination, defining the chemical structure of natural organic matter, and developing spectral fingerprints for a range of petroleum products (Sierra et al. 1994; Coble 1995; Baker and Lamont-Black 2001; Baker 2002; Wu et al. 2003; Baker and Curry 2004; Fiore et al. 2013; Qianqian et al. 2014).

Due to EEM's ability to display more information than two-dimensional synchronous scans, they are not always as susceptible to the general analytical challenges that affect synchronous scanning capabilities. For instance, display of the full spectral range of the λ_{Ex}, λ_{Em}, and fluorescence intensity in a single plot may render inconsequential the effects of quenching (see Appendix A—a process by which other chemical constituents within the substance prevent it from fluorescing when irradiated), variations in temperature, and variations in pH, which alter the fluorescence intensity of the fluorescent components of a sample. Since the full spectral range of the sample may

be displayed, fluorescent sample components may still be identified and characterized by their displayed λ_{Ex} and $\lambda_{Em,}$ even at low or altered fluorescence intensities. However, EEMs may still be vulnerable to inner-filter effect and it remains to be seen if EEMs may aid in the discrimination between background fluorescence and the fluorescent component of interest (in the case of the present research, four common fluorescent dyes). The use of EEMs also necessitates the consideration of a few other analytical challenges, including light scattering and so-called red and blue shifts.

2.5 Scattering and Red and Blue Shifts

There are two primary types of scattering that may interfere with three-dimensional synchronous scanning: Rayleigh and Raman (Figure 7). *Rayleigh scattering* results from the scattering of light caused by the presence of certain molecules, particulates, or air bubbles in the sample (Shimadzu 2015). Rayleigh scattering may be displayed as the most intense fluorescence in EEMs in the analysis of weakly fluorescent samples, but it often does not substantially interfere in synchronous scanning or three-dimensional synchronous scanning. If Rayleigh scattering is present in an EEM, it will be displayed at the wavelength(s) of the excitation radiation and will appear at wavelengths twice and/or even three times the wavelength of the excitation light. For instance, if an EEM utilizes a range of λ_{Ex} = 200-400, then the second order light will be scattered from 400-600 nm and from 600 nm to the final wavelength of the λ_{Ex}, respectively. When excitation light is scattered and appears in the EEM at two and three times the excitation wavelength range, it is called *second* and *third order light*, respectively. Rayleigh

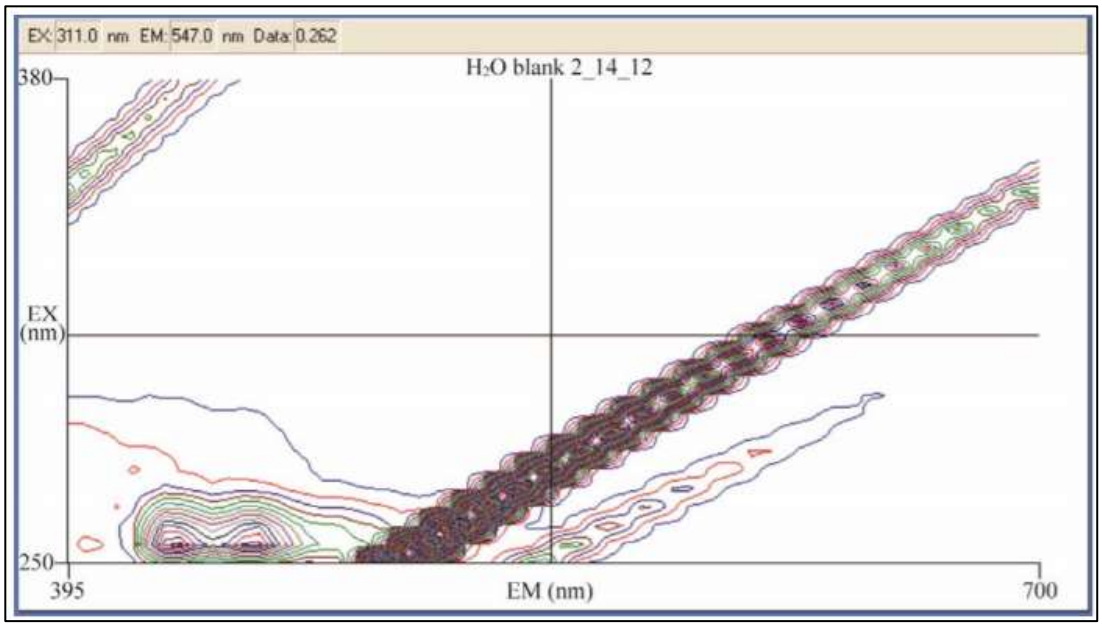

Figure 7: Rayleigh scattering (distinct central diagonal feature), primary Raman scattering (diagonal feature at upper left), and secondary Raman scattering (diagonal feature at lower right) (Soltzberg et al. 2012).

scattering may sometimes be mitigated by allowing any particulate matter in the sample to settle to the bottom below the irradiated range (*pathlength*) of the sample. It may also be mitigated by installation of a short wavelength-cutting filter inside the instrument that blocks transmission of radiation at about 220 nm, or through installation of several filters (Rubio et al. 1986; Hudson et al. 2008; Soltzberg et al. 2008; Shimadzu 2015; personal communication, Gilbert Vial, Molecular Spectroscopy Product Specialist Shimadzu Scientific Instruments, November 1, 2018).

During the Rayleigh scattering process, some of the scattered excitation light may be converted into vibrational and rotational energy. This light, by its intermediate conversion into vibrational and rotational energy, is reduced to a lower energy and longer wavelength than the excitation light, which results in a weak emitted light that may interfere with or be attributed to the fluorescence of the component of interest. This type of scattering may be subdivided into Stokes and anti-Stokes scattering, but the sum of

them is referred to as *Raman scattering*. The amount of energy abstracted into Raman scattering is always constant (PerkinElmer 2000; Shimadzu 2015).

Raman scattering, like Rayleigh scattering, appears at wavelengths that are longer than the λ_{Ex}. However, unlike Rayleigh scattering, the intensity of Raman scattering is not strongly correlated with concentration of fluorescent constituents in the sample and it may be possible to distinguish between Raman scattering and the fluorescence of the component of interest by changing the λ_{Ex} of the EEM. This method may assist in discrimination between the Raman scattering and the fluorescence of the component of interest because the Raman scattering will always be separated from the λ_{Ex} by a consistent wavelength frequency, regardless of the wavelength(s) of the excitation light. Therefore, if the Raman scatter overlaps with the λ_{Em} of the EEM, the two may be differentiated by lowering or raising the λ_{Ex} in the direction away from the λ_{Em}. In other words, by increasing the $\Delta\lambda$. Since the Raman scatter will always appear at a certain distance from the λ_{Ex}, increasing the separating of the λ_{Ex} from the λ_{Em} will ensure that the Raman scattering occurs within the wavelengths of the offset between λ_{Ex} and λ_{Em} rather than in the λ_{Em} (PerkinElmer 2000; Shimadzu 2015).

In addition to scattered light, spectral shifts may also provide a challenge to analytical measurement using three-dimensional scanning. *Red shift*, or *bathochromic shift*, is defined as the shift from shorter wavelengths to longer wavelengths in the spectral form, specifically the λ_{Em} and the emission maxima. This shift can be caused by changes in physical and chemical properties of the sample, including formational changes that permit vibrational energy losses of the promoted electrons, an increase in the number of aromatic rings condensed in a straight chain, and conjugated double bonds (Wu et al.

2003; Sierra et al. 2005). Alternately, blue shift is the shifting of the spectral form, or, specifically, the λ_{Em} and the emission maxima, from longer wavelengths to shorter wavelengths (Wu et al. 2003; Baker and Spencer 2004). Blue shifts have been shown to correspond to greater fractions of large molecular size and more hydrophobic nature of natural organic matter (Wu et al. 2003).

2.6 Research Objectives

Three-dimensional synchronous scanning is a well-developed tool that has been used to characterize a wide variety of fluorescent substances. The challenges to this type of scanning have been explored and documented. Although extensive research has been conducted related to the use of three-dimensional synchronous scanning and the application of EEMs to various environmental issues, limited research has been conducted to investigate the use of three-dimensional synchronous scanning in fluorescent dye tracing. The objectives of the current research are to rigorously evaluate the potential of three-dimensional synchronous scanning and EEMs to offer improved tools for fluorescent dye tracing, potentially allowing better: 1) discrimination the fluorescent dye spectra of four common fluorescent dyes from one another, 2) discriminate fluorescent dye spectra of four common fluorescent dyes from background fluorescence in anthropogenically-effected sampling environments, and 3) enhance existing or establish new fluorescent dye detection and quantification methods in the field of dye tracing.

3. Study Area (in the Field)

3.1 Introduction

A fluorescent dye trace utilizing the fluorescent dye fluorescein was conducted in the Lost River Groundwater Drainage Basin and samples were collected outside the mouth of Lost River Cave in Bowling Green, Kentucky. The water samples collected in the course of the project were later analyzed in the CHL to facilitate evaluation of the ability of three-dimensional synchronous scanning to differentiate between anthropogenic background fluorescence and the fluorescence spectra of the fluorescent dye, fluorescein. The Lost River was regarded as an optimum dye trace location due to its lengthy history of anthropogenic contamination.

3.2 The Lost River Groundwater Basin

3.2.1 Physiographic Setting

The Lost River Groundwater Basin (LRGB) is a karst drainage system located in Bowling Green, Warren County, Kentucky in the southeastern United States, which is generally considered a humid subtropical climate zone (Groves 1987; Granger et al. 2001; Ingram et al. 2013). The LRGB is located on the Pennyroyal Plateau in the Interior Low Plateaus region of the United States, which, in addition to the neighboring Mitchell Plains in Indiana and the Highland Rim in Tennessee, is a classic sinkhole plain characterized by gently rolling topography and dominated by a plethora of sinkholes and other karst features (Groves 1987). The LRGB encompasses 143 km^2 and is largely drained by a solutionally-enlarged subsurface conduit network within the Mississippian St. Louis and St. Genevieve Limestones (Groves 1987).

Based on National Oceanic and Atmospheric Administration (NOAA) 1981-2010 Climate Normals calculated from data collected at the Bowling Green Warren County Airport station, the Lost River Groundwater Basin has been characterized by an average minimum annual temperature of 47 ºF and an average maximum annual temperature of 69 ºF. However, temperatures may vary from an average minimum winter temperature of 28.4 ºF to an average maximum summer temperature of 88.2 ºF. The average annual precipitation depth in the Lost River Groundwater Basin is 49.9 inches (NOAA 2020).

3.2.2 Hydrogeology of the Lost River Groundwater Basin

Most of the caves in Warren County, Kentucky are *water table caves*, or caves that form near the water table due to a high hydraulic conductivity setting (*hydraulic conductivity* describes the rate at which groundwater can be transmitted through the aquifer) and the presence of *confining layers*, or geologic layers that are less permeable and soluble than the surrounding layers and impede or prevent diffusion of groundwater. Given adequate elapsed time, mature karst systems will develop water-table caves (Crawford and Hoffman 1989; De Waele et al. 2009).

In the process of forming water-table caves, confining layers prevent groundwater from flowing vertically further into the subsurface. Instead, groundwater is forced to flow laterally through the subsurface, sometimes directly on top of the confining layer in a high conductivity setting so that groundwater rapidly flows laterally across the confining layer. The confining layers that define the formation of water-table caves in Warren County are the Lost River Chert Bed of the Mississippian St. Genevieve Limestone and

the Corydon “Ball Chert” member of the Mississippian St. Louis Limestone (Crawford and Hoffman 1989).

3.2.3 Extent of the Lost River Groundwater Basin

The Lost River Groundwater Basin extends from its headwaters near the town of Woodburn, Kentucky about 19 miles to just south of Bowling Green, Kentucky where the Lost River merges with Jennings Creek to ultimately flow into the Barren River. The drainage basin is about 14 km wide at its widest from Drake’s Creek in the east to just east of Rockfield, Kentucky in the west. The LRGB headwaters are situated in the southern part of the LRGB near Woodburn, Kentucky where several surface streams flow across a partially impervious clay-chert surface (the Mississippian Lost River Chert Bed) and sink into the Ste. Genevieve limestone. These streams combine to become the Lost River as they flow northward atop the Corydon Member of the St. Louis Limestone. The Lost River may be observed at the Church Karst Window in the central part of the Basin along the initial portion of its trajectory, and again at the Lost River Blue Hole where the Lost River emerges and flows atop the Lost River Chert bed for 120 meters before diverting into the subsurface through the large Lost River Cave entrance. Lost River Cave is a water-table cave that has formed in about 10 meters of the St. Louis Limestone (Groves 1987; Crawford and Hoffman 1989; Blair et al. 2012).

The Lost River then flows from Lost River Cave beneath the city of Bowling Green and resurfaces permanently at the Lost River Rise (Figure 8). The Lost River Rise is a large spring where the Lost River emerges from beneath a low bluff formed in the

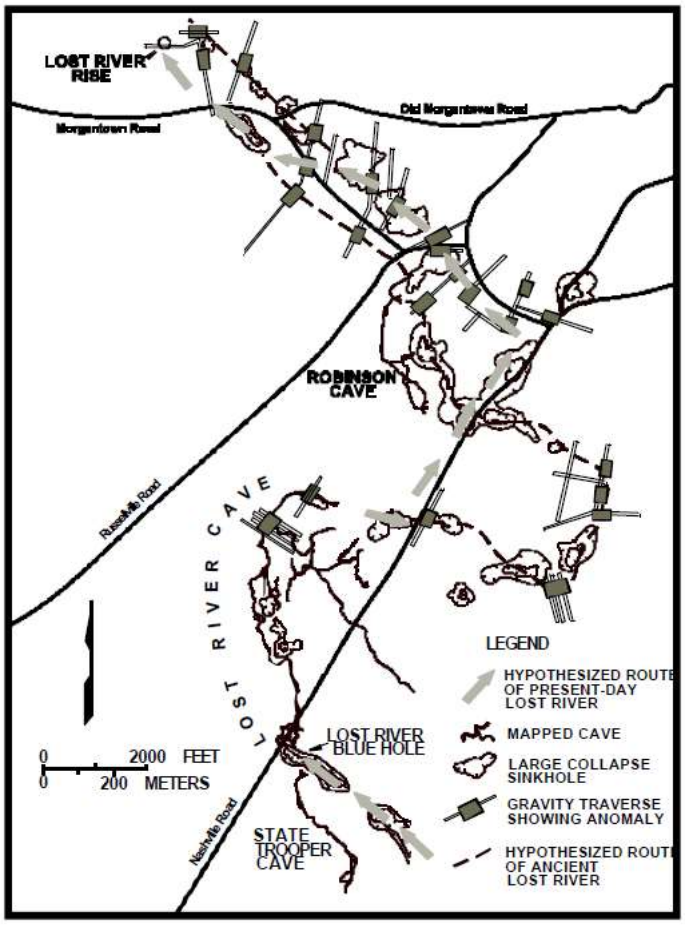

Figure 8: Hypothesized trajectory of the current and ancient Lost River from upstream of the Lost River Blue Hole to the Lost River Rise where it ultimately resurfaces before joining with Jennings Creek and flowing into the Barren River. (Crawford 2000).

Ste. Genevieve Limestone. The Lost River flows about 230 m from the Lost River Rise to meet Jennings Creek with which it combines and ultimately flows into the Barren River (Groves 1987; Crawford and Hoffman 1989; Blair et al. 2012). Groundwater in the LRGB is significantly impacted by historical and contemporary contamination, especially since the basin contains much of the city of Bowling Green, which itself contains more than 50,000 people and significant urban, commercial, and industrial development (Crawford and Hoffman 1989).

3.2.4 Cultural and Contamination History of the Lost River Groundwater Basin

As early as the 1930s, the large open entrance of Lost River Cave was used as a nightclub and the large open dance floor in the mouth of the cave served as a cool place to enjoy sweltering summer Bowling Green nights (Figure 9) (Tejada 1985). The nightclub was closed in later years, but the dancefloor and cave entrance are still used to host events like weddings and concerts and guided boat tours will allow the curious visitor to float on the Lost River into the Lost River Cave (Blair et al. 2012). In addition to boat tours and weddings, the park in which Lost River Cave is situated, owned by Western Kentucky University but managed by a non-profit group "Friends of Lost River," also includes walking trails, a gift shop, and ziplines.

Although recreation in and around Lost River Cave is encouraged and even monetized now, there were likely periods in Bowling Green's past when such recreation in Lost River Cave (and other caves in Bowling Green) was discouraged. In 1969, homes along Riverwood Street were discovered to contain gasoline fumes, and the same homes were evacuated in 1981 due to explosive concentrations of gasoline fumes in the basements. Other homes were also affected by gasoline fumes, including homes on Chestnut Street and Nashville Road. In 1982, toxins including benzene and methylene chloride were detected in the Lost River. These toxins entered the Lost River through leakage of chemical-containing underground storage tanks (USTs) owned by a local chemical company into the local groundwater system that entered a local pond through a spring. The pond overflowed into the Lost River (Crawford 1984).

Figure 9: Interior of Lost River Cave and example of event held within Lost River Cave (LostRiverCave.org n.d.).

In 1984 and 1985 as well, cave exploration and visitation were replaced with air and water quality monitoring when toxic and explosive vapors were measured in Bowling Green houses, schools, and apartment buildings that were built over contaminated cave systems. These vapors may have resulted from volatilized chemicals that entered the subsurface as liquids through spills on the soil surface, which rapidly transmitted the chemicals into the subsurface. Leaking USTs and deliberate discharge of chemicals into the subsurface may have also contributed to the accumulation of fumes in cave systems and structures built atop them. One study reported that, as of the publication date in 1984, at least three considerable UST spills had released more than 35,000 liters of diesel fuel into a portion of the groundwater system that flowed to Lost River Cave (Crawford

1984). By 1985, at least six factories had been identified that either spilled or directly discharged chemicals into the cave systems beneath Bowling Green (Crawford 1984; Tejada 1985). Subsurface contamination such as this is potentially prolonged through the accumulation of contaminants in natural traps in the cave systems where the chemicals float atop the water's surface and become sequestered in lithologic features or can adhere to cave ceilings and walls (Crawford 1984; Tejada 1985).

In March of 1984, the Centers for Disease Control (CDC) announced a public health advisory for the city of Bowling Green due to the detection of toxic and sometimes explosive vaporized chemicals like benzene, toluene, methylene chloride, xylene, and other volatile organic compounds (VOCs) above the allowable concentration in non-occupational settings (Tejada 1985; Groves 1987). The CDC health advisory sparked EPA involvement by way of a Superfund emergency response in June 1984, as well as intensive efforts to locate cave passages in the city of Bowling Green. These efforts included an evaluation of the relationship between the Lost River and the toxic and explosive vapors (Tejada 1985; Groves 1987; Crawford 2000).

In addition to VOCs, other contaminants have been measured in the Lost River, including pesticides. A 5-month study was conducted in 2001 by the United States Geological Survey (USGS) in conjunction with the Kentucky Department of Agriculture to collect water samples every 2 weeks from May to September 2001. The study measured significant concentrations of pesticides in the Lost River Blue Hole Spring. These pesticides were acetochlor (0.099 µg/L), chlorpyrifos (0.011 µg/L), metribuzin (0.011 µg/L), and tebuthiuron (0.043 µg/L) (Crain 2002). Due to the substantial contaminant history of the Lost River Groundwater Basin, including but not limited to

toxic and explosive VOCs, pesticides, petroleum products (whose fluorescence has been investigated and substantiated through numerous studies), and other common anthropogenic contamination resultant from a heavily urbanized watershed, the Lost River Groundwater Basin was regarded as an optimum dye trace location to test the ability of three-dimensional synchronous scanning to discriminate between fluorescent dyes and background fluorescence.

4. Methods

4.1 Process Overview

The objectives of the current research are to evaluate the ability of three-dimensional synchronous scanning to improve the following two procedures in the CHL: discrimination of the fluorescent dye spectra of four common fluorescent dyes from one another and discrimination of the fluorescent dye spectra of four common fluorescent dyes from background fluorescence in anthropogenically-affected sampling environments. It is also an ancillary objective of this research to enhance existing or establish new fluorescent dye detection and quantification methods in the field of dye tracing.

To satisfy the objectives of this research, fluorescent dye standard dilutions of four common fluorescent dyes (fluorescein, eosin, rhodamine WT, and sulphorhodamine B) were first analyzed using two-dimensional synchronous scanning to create a catalogue of synchronous scans that represent the current method of fluorescent dye measurement in the CHL. These fluorescent dye standard dilutions were then analyzed using three-dimensional synchronous scanning to allow comparison between two-dimensional synchronous scans and EEMs in the simplest case. Next, fluorescein and eosin standard dilutions were mixed in equal parts to create 1:1 mixtures of the standard dye dilutions. These mixed dilutions were analyzed using both two-dimensional synchronous scanning and three-dimensional synchronous scanning to facilitate comparison of the ability of each method to discriminate between fluorescent dyes that emit fluorescence in overlapping emission wavelength (λ_{Em}). This process was reproduced for rhodamine WT and sulphorhodamine B standard dilutions as well. Finally, natural samples likely to be

impacted by anthropogenic contamination were collected from the Lost River at the mouth of the Lost River Cave in Bowling Green, Kentucky following an injection of fluorescein into the Lost River. The samples were analyzed using both two and three-dimensional synchronous scanning to facilitate the comparison of the ability of each method to discriminate between commonly used fluorescent dyes and background fluorescence in anthropogenically-affected waterways. All successful synchronous scans and EEMs produced through the course of this research are displayed in the Results section and Appendix B.

4.2 General Laboratory Methods

All analyses through the course of this research were conducted in the Crawford Hydrology Laboratory (CHL), a laboratory housed at Western Kentucky University's main campus in Bowling Green, Kentucky that specializes in field and laboratory fluorescent dye trace techniques both for research and applied groundwater studies for environmental consulting firms, government agencies, and other clients. CHL personnel assisted in the fluorescent dye trace of the Lost River and the creation of fluorescent dye standard dilutions. The fluorescent dye trace, sample processing, sample storage, and analysis components of the research were all conducted with respect to established CHL field and research procedures.

All water samples were processed, stored, and analyzed in the CHL (see the Literature Review for a review of CHL standard laboratory procedures). Analysis of water samples was conducted in the CHL on a Shimadzu RF-6000 spectrofluorophotometer. The Shimadzu RF-6000 measures spectra within the 200-900

nm wavelength range, measures emission spectra with a resolution of 1.0 nm, and measures wavelength with a ± 1.0 nm accuracy. The Shimadzu RF-6000 is equipped with a short-wavelength cutting filter that mitigates effects of Rayleigh scattering, and is also equipped with correction functions established at the time of installation that mitigate the idiosyncrasies of various instrument components to produce only true spectra which are comparable between instrument manufacturers, models, and over time (Shimadzu 2015). Laboratory procedures developed in accordance with manufacturer recommendations are in place to mitigate the effects of Raman scattering (Shimadzu 2015).

Primary components of the spectrofluorophotomer include the 150-watt xenon arc lamp source light, excitation diffraction grating monochromator, excitation monitor (silicon photodiodide detector), emission diffraction grating monochromator, and emission detector (photomultiplier tube) (Figures 10 and 11). The 150-watt *xenon arc lamp* is the source of excitation radiation in the analyses and is the most common light source built within spectrofluorophotometers. The output of the light source is essentially a continuum which is defined by a number of sharp lines by which exact excitation wavelengths may be distinguished and selected (PerkinElmer 2000; Shimadzu 2015).

The *diffraction grating monochromators* are monochromators that dictate the spectral distribution of both the excitation radiation and the radiation emitted from the analyte. They are fitted with diffraction gratings that further regulate the quantity of excitation and emission radiation. It is the presence of both the emission and excitation monochromators in the instrument that permits the development of three-dimensional synchronous scans. The monochromators allow the production of EEMs because they

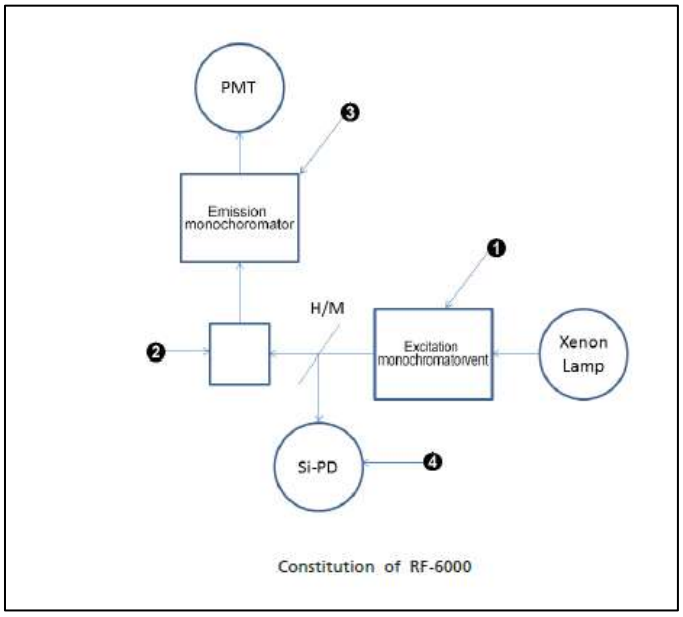

Figure10: General configuration of the Shimadzu RF-6000 spectrofluorophotometer (Shimadzu 2015).

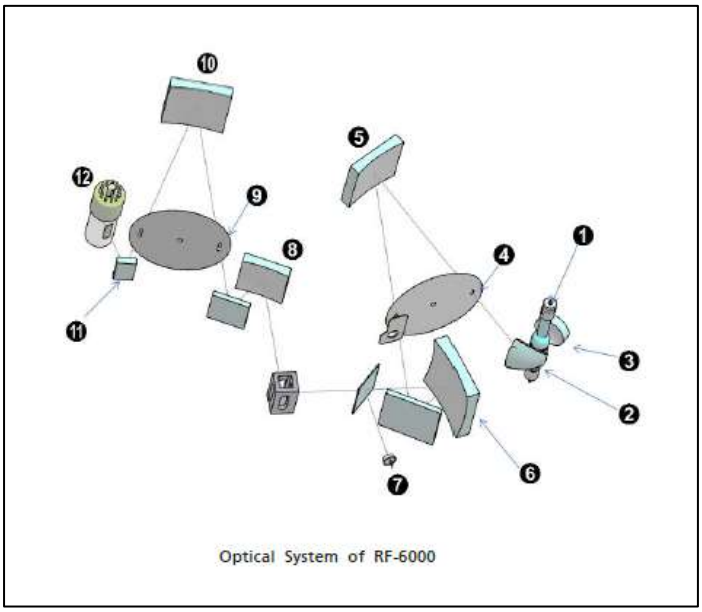

Figure 11: Shimadzu RF-6000 optical system (Shimadzu 2015).

control the quantity of excitation light that is permitted to reach the analyte and the quantity of emitted light that is permitted to be measured by the emission detector. The monochromators perform this function by controlling the width of the slits that allow light to enter and exit the sample chamber. Narrow slits (less light) correspond to greater resolution and lower sensitivity while wide slits (more light) correspond to lower

resolution and greater sensitivity. The excitation monitor and emission detector measure the intensity of the spectra of light used to excite the analyte and the spectral range of the emission radiation of the analyte, respectively (PerkinElmer 2000; Shimadzu 2015).

Monochromators also dictate the wavelength offset ($\Delta\lambda$) discussed previously. If the following conditions are true, then the interval between the excitation spectra and the emission spectra is called the wavelength offset $\Delta\lambda$: the monochromators are set to allow the detection of a set spectra of both emission and excitation radiation, the measured spectra of the emission and excitation radiation is separated by a sufficient interval to prevent substantial interference by Raman scattering, and the light exiting and entering the monochromators is measured at a constant rate (the *scanning rate*) (Rubio et al. 1986). The analyte is contained within the Shimadzu RF-6000 within a cell holder which is the target of the excitation radiation. Square and round cuvettes have often been employed in spectrofluorophotometric analyses. Square cuvettes are advantageous because it is simpler to ensure that pathlength (*pathlength*, in this instance, is the length of the path of the excitation radiation through the analyte) and parallelism are maintained during their manufacturing. Round cuvettes are advantageous because they are more universally useful and are cheaper than square cuvettes. However, the nature of fluorescence measurement does not necessitate the maintenance of exact parallelism or pathlength parameters and there are inexpensive alternatives to round cuvettes, like inexpensive standard glass laboratory test tubes. Samples analyzed through this study were contained in standard glass laboratory test tubes with no known loss of analytical precision (PerkinElmer 2000).

4.3 Single Standard Dilutions

Benchtop experiments and fluorescence spectrometric analyses were conducted at the CHL. The dyes fluorescein (FL), eosin (EO), rhodamine WT (RWT), and sulphorhodamine B (SRB) were chosen due to their prevalent usage in groundwater dye tracing and because the FL and EO pair and the RWT and SRB pair, respectively, emit fluorescence in overlapping λ_{Em} (Table 3). FL, EO, RWT, and SRB standard dilutions were created from high-concentration stock solutions stored in the CHL for laboratory use or were created from guaranteed-purity powdered dyes through a serial dilution process. Two-dimensional synchronous scans and EEMs of single standard dilutions were produced through analysis of a set of fluorescent dye serial dilutions regularly used in the CHL for the calibration of the Shimadzu RF-6000 and through analysis of a set of fluorescent dye standard dilutions created specifically for use through this research.

Table 3: Peak area parameters and peak overlap ranges of FL and EO and RWT and SRB.

Dye	Em Start (nm)	Em End (nm)	Center (nm)	λ_{Em} Overlap (nm)	Overlap (nm)
Fluorescein	492.8	528.8	510.8	518.2 - 528.8	10.6
Eosin	518.2	554.2	536.2		

Dye	Em Start (nm)	Em End (nm)	Center (nm)	λ_{Em} Overlap (nm)	Overlap (nm)
Rhodamine WT	558.9	594.9	576.9	565.8 - 594.9	29.1
Sulphorhodamine B	565.8	601.8	583.8		

4.4 Mixed Standard Dilutions

A full set of fluorescent dye standard dilutions was created through an order-of-magnitude serial dilution process for the creation of mixed fluorescent dye standard

dilutions. 100 ppm concentration dilutions of FL, EO, RWT, and SRB were created by mixing 1 g of a 1% stock solution with 100 g of deionized water (± .02 g). Solutions ranging in concentration from 10 ppm to the lowest concentration, 0.1 ppb, of FL, EO, RWT, and SRB were created by mixing 5 g of a standard dilution with 50 g of deionized water (± .02 g). The result of this process was a set of standard dilutions that ranged in concentration from .01 PPB to 100 PPB. The standard dilutions were analyzed using two-dimensional synchronous scanning and the measured concentrations fell within 10% of the target concentrations, except for 1 ppb FL, which fell within 15% of its target concentration (Table 4, Figure 12).

Mixed dilutions were created from the set of single standard dilutions by mixing 2.5 ml aliquots of every FL standard dilution with 2.5 ml aliquots of every EO standard dilution to create a total of 25 unique 5 ml total volume 1:1 ratio mixed standard dilutions. The same procedure was followed to create 25 unique 5 ml total volume 1:1 ratio RWT and SRB mixed standard dilutions. Dye mixtures are named using abbreviations of the two dye names (a combination of FL and EO or RWT and SRB), followed by numbers showing the relative proportions of the dye concentrations. A mixture of FL and EO, for example, composed of one part of the former to ten of the latter would be designated FLEO 1:10.

4.5 Lost River Cave Grab Samples

Lost River Cave (LRC) Samples were collected from the Lost River just outside the Lost River Cave entrance from September 15, 2018 to September 16, 2018 using a discrete sampling technique (ISCO 3700 automatic water sampler) over a 12-hour

sampling period. Samples were collected every 30 minutes beginning at 18:00 on the 15th and ending at 05:30 on the 16th. Samples were processed in the CHL in accordance with previously discussed CHL standard procedures. LRC field samples were analyzed using two-dimensional synchronous scanning on November 1, 2018 and were analyzed using three-dimensional synchronous scanning on April 14, 2019 after development of three-dimensional synchronous scanning parameters. Single standard dilutions, mixed standard solutions, and Lost River Cave field samples were processed and stored in accordance with previously described laboratory processing procedures prior to and following the analysis period.

Table 4. Target and measured concentrations of standard dilutions used to create the mixed standard dilution set. All standard dilutions fell within 10% of their target concentrations except FL 1 ppb. FL 1 ppb fell within 15% of the target concentration.

Single Solution	Target Concentration (ppb)	10% Tolerance Range (ppb)	Concentration (ppb)
FL	1	0.90 - 1.10	0.854
FL	10	9.00 - 11.0	9.591
EO	1	0.90 - 1.10	0.963
EO	10	9.00 - 11.0	9.758
EO	100	90 - 110	94.759
RWT	1	0.90 - 1.10	1
RWT	10	9.00 - 11.0	10.4
RWT	100	90 - 110	90.304
SRB	1	0.90 - 1.10	1
SRB	10	9.00 - 11.0	9.8

4.6 Two-Dimensional Synchronous Scanning

Two-dimensional synchronous scanning was conducted using the Shimadzu RF-6000 and the accompanying software, LabSolutions RF, in Spectrum mode, in accordance with standard CHL analysis procedures. The instrument was permitted to equilibrate for 30 minutes and samples were warmed to 30 °C in a water bath. All

analyses were preconditioned by a passing signal to noise ratio and followed by a passing signal to noise ratio to verify instrumental sensitivity throughout the analysis period. The Raman line of water was measured at 350 nm using the high sensitivity setting prior to any analysis through the measurement of a laboratory blank. The Raman fluorescence spectra was subtracted from the fluorescence spectra of each sample to eliminate interference by Raman scattering.

All samples were first analyzed using the high-sensitivity setting and were analyzed using the low-sensitivity setting as well if the concentration of the sample exceeded 100 ppb or if the fluorescence exceeded 1000 intensity units. Intermediate standards were run

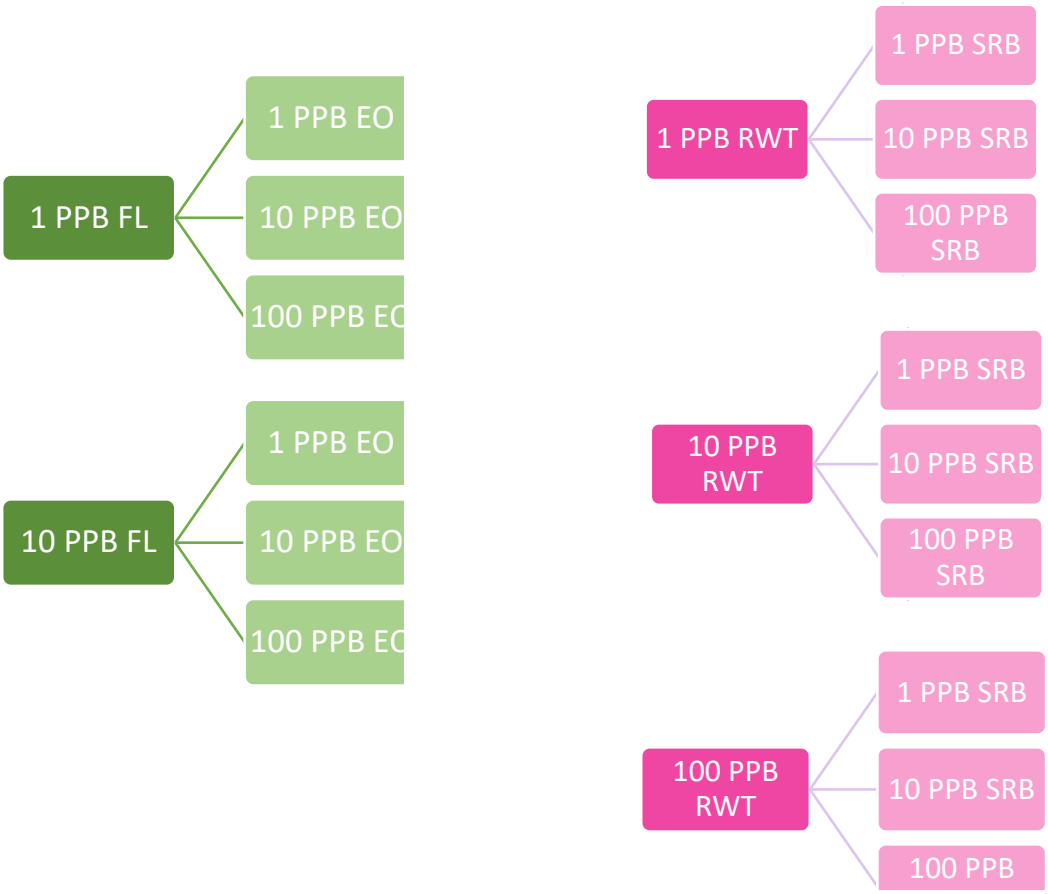

Combinations

1 PPB FL + 1 PPB EO
1 PPB FL + 10 PPB EO
1 PPB FL + 100 PPB EO

10 PPB FL + 1 PPB EO
10 PPB FL + 10 PPB EO

10 PPB FL + 100 PPB EO

Combinations

1 PPB RWT + 1 PPB SRB
1 PPB RWT + 10 PPB SRB
1 PPB RWT + 100 PPB SRB

10 PPB RWT + 1 PPB SRB
10 PPB RWT + 10 PPB SRB
10 PPB RWT + 100 PPB SRB

100 PPB RWT + 1 PPB SRB
100 PPB RWT + 10 PPB SRB
100 PPB RWT + 100 PPB SRB

Figure 12: Mixed standard dilution combinations of FL and EO and RWT and SRB.

were run every 20 samples to check for instrumental drift. No instrumental drift was identified through the course of this research. For single and mixed standard dilutions, high-sensitivity two-dimensional synchronous scanning proceeded in the following order: laboratory blank, control, standard dilutions (from low to high concentration), control. This sequence was replicated using low-sensitivity two-dimensional synchronous scanning for any high-concentration standard dilutions and analysis of a control was omitted.

For samples, high-sensitivity two-dimensional synchronous scanning proceeded in the following order: laboratory blank, control, standard dilutions (from low to high concentration, minimum of two concentrations to verify linearity of the instrument calibration for the dye of interest, one of the standard dilutions was the PQL), samples, standard dilutions, control. For any high-concentration samples, the sequence was repeated using the low-sensitivity instrument setting and 100 ppb concentration standard dilution(s). Analysis of the control was omitted.

4.6.1 Two-Dimensional Synchronous Scanning Parameters and Settings

The high and low sensitivity instrument settings are controlled by the excitation monochromator diffraction grating that regulates the intensity of excitation light used to excite the sample. Instrument sensitivity is directly related to the intensity of light from the xenon arc lamp—brighter, or more intense, light from the lamp (excitation radiation) initiates the emission of more intense light from the sample, provided that the given sample contains fluorescent components. When the instrument is configured to use the high sensitivity setting, the excitation monochromator diffraction grating is open to the

maximum extent possible to collect the largest amount of light. Through the low sensitivity instrument setting, the aperture in the diffraction grating is not opened as widely, which limits the quantity of excitation light that may reach the sample and thus limits the intensity of the light that is emitted by any fluorescent components in the sample (Shimadzu 2015).

Analysis of samples using the appropriate instrument sensitivity is critical because high sensitivity analysis of highly concentrated samples may result in prohibitive inner-filter effects and red-shifting of the λ_{Em}. Additionally, if a highly concentrated sample is analyzed using the high sensitivity instrument setting, the excitation radiation may be absorbed around the light-sample interface and may not fully penetrate the center of the sample. Spectrofluorophotometers are generally designed to measure light emitted from the center of samples, so reduction in the amount of excitation radiation reaching the center of the sample will result in reduced intensity of the λ_{Em} (Shimadzu 2015).

Standard CHL procedure dictates that all samples be analyzed first using the high sensitivity setting (Table 5) to capture even the most subtle synchronous spectra. If the concentration of the dye exceeds 100 ppb or if the intensity of the synchronous spectra exceeds 1,000 intensity units anywhere along its λ_{Em}, the sample is analyzed using the low sensitivity setting. If the synchronous spectra is observed to be affected by inner-filter effects, red-shifting, or abnormal peak shape, the samples are diluted by orders of magnitude as necessary and reanalyzed using the low sensitivity setting. The necessity to dilute such samples may often be perceived by visual observation (the sample may be extremely dark or iridescent) (Bledsoe 2019b). See the figure below for the standard CHL parameters for analysis of water samples.

Table 5: Two-dimensional high and low sensitivity synchronous scanning parameters.

Sensitivit	Excitation (nm)	λ_{Em} (nm)	Steps (nm)	Ex Bandwidth (nm)	Em Ba (r	Scanning Rate (nm/min)
High	347	365 - 625	0.2	5	10	6000
Low	347	365 - 650	0.2	5	10	6000

Two-dimensional synchronous scanning is conducted in the CHL by displaying the λ_{Em} of a sample from 365-650 nm (low sensitivity) or 365 – 625 (high sensitivity) at an 0.2 nm data interval at Ex = 347 nm. The CHL employs an 18 nm $\Delta\lambda$. The scan speed is set to 6000 nm/min and the Ex and Em bandwidths are set to 5.0 and 10.0 nm, respectively. The *data interval* is the interval at which data are measured and reported. The *scan speed* is the speed at which the instrument conducts the analysis (measures the λ_{Em} at the intervals specified by the data interval value along the chosen range of Em values). The *bandwidth* is the acceptable range of deviation from the given Ex or Em value (i.e. if the Ex = 347 nm and the bandwidth is set to 5.0 nm, then the true Ex values are 347 ± 2.5 nm).

Selection of a proper data interval and scanning speed ensures collection of data at an acceptable resolution and balance of timely data acquisition, and integrity of the data, respectively. Selection of an appropriate bandwidth for both Ex and Em ensures selection of an appropriate margin of error (Keppy and Allen 2008). Both the data interval and bandwidth parameters contribute to the overall relatively continuous or disjunctive appearance of EEMs. The parameters discussed here were those routinely and successfully used in the CHL for the analysis of client samples through the course of this research (August 2017-May 2019) and were employed through this study to allow direct comparison of current and novel methods in the CHL. These parameters are substantiated

by successful routine use and the fact that these parameters allow the measurement of the synchronous spectra of most fluorescent substances that may be present in natural water samples (personal communication, Gilbert Vial, Shimadzu Scientific Instruments Molecular Spectroscopy Product Specialist, 2018).

4.7 Three-Dimensional Synchronous Scanning

All single standard dilutions, mixed standard dilutions, and LRC samples were analyzed first using two-dimensional synchronous scanning, as described above. Two-dimensional synchronous scanning of known-concentration standard dilutions was also conducted to verify instrument calibration prior to and following each three-dimensional analysis run. It is not possible to calculate peak area within the software's 3D Spectrum mode; thus, it is not possible to verify instrument calibration using peak area/concentration measurements within the standard, unmodified 3D Spectrum mode of the program (personal communication, Gilbert Vial, Shimadzu Scientific Instruments Molecular Spectroscopy Product Specialist, 2019).

After verifying instrument calibration using two-dimensional synchronous scanning of standard dilutions of known concentrations, all samples were analyzed using the Shimadzu RF-6000 and accompanying LabSolutions RF Software in 3D Spectrum mode. Standard CHL analysis procedures employed prior to two-dimensional analyses were also employed prior to three-dimensional synchronous scanning. The instrument was permitted to equilibrate for 30 minutes and samples were warmed to 30 °C in a water bath. All analyses were preconditioned by a passing signal to noise ratio and followed by a passing signal to noise ratio to verify instrumental sensitivity throughout the analysis

period. However, not all samples were first analyzed using the high sensitivity setting since the appropriate sensitivity setting was identified through the two-dimensional analyses. This is especially pertinent since the 3D Spectrum mode does not provide a method to calculate peak area within the program and concentration limitations (100 ppb) may not be used to identify appropriate sensitivity settings in 3D Spectrum mode (personal communication, Gilbert Vial, Shimadzu Scientific Instruments Molecular Spectroscopy Product Specialist, 2019).

It was not necessary to run intermittent standard dilutions every 20 samples to verify the instrument calibration through the LRC sample analysis period because fluorescein was only measured in four of the LRC samples as identified during two-dimensional synchronous scanning (thus only four LRC samples were analyzed in 3D Spectrum mode). High sensitivity three-dimensional synchronous scanning of single and mixed standard dilutions proceeded in the following order: laboratory blank, control, standard dilutions (from low to high concentration), control. This sequence was replicated using low sensitivity three-dimensional synchronous scanning for any high-concentration standard dilutions and analysis of a control was omitted. For samples, high sensitivity three-dimensional synchronous scanning proceeded in the following order: laboratory blank, control, samples, control. Analysis of standard dilutions was omitted since the instrument calibration was verified prior to the three-dimensional analysis run using two-dimensional synchronous scanning. For any high-concentration samples, the sequence was repeated using the low sensitivity instrument setting and analysis of the control was omitted. All three-dimensional analyses were followed by verification of

instrument calibration through two-dimensional analysis of standard dilutions of known concentrations.

4.7.1 Published Three-Dimensional Synchronous Scanning Parameters

An intrinsic requirement to meet the project research objectives was to choose a set of three-dimensional synchronous scanning parameters that would allow the capture of the fullest EEM possible of each of the four fluorescent dyes (FL, EO, RWT, and SRB) in the least amount of time while sacrificing the least data resolution. To develop an appropriate parameter set, three-dimensional synchronous scanning parameter sets presented in thirteen publications were taken into consideration; experimental analyses were conducted using a modified subset of these parameter sets; and, finally, a single parameter set was chosen to produce all EEMs presented in Appendix B of this research.

The parameters presented in thirteen publications were considered through the search for an applicable three-dimensional synchronous scanning parameter set. See Table 6 for a complete collection of the parameter sets considered through the course of this research in alphabetical order by author. To develop a set of parameters that would allow the capture of the fullest EEM possible of each of the four fluorescent dyes in the least amount of time while sacrificing the least data resolution, it was necessary to meet certain parameter specifications. First, the λ_{Em} measured during the analysis must include, at a minimum, the full λ_{Em} of each of the four fluorescent dyes at Ex = 347 nm (the chosen excitation wavelength for two-dimensional synchronous scanning analyses in the CHL). Ideally, the parameter set would include the full λ_{Em} of each of the four dyes, and thus the widest λ_{Ex} and λ_{Em} possible, as well as lower Em wavelengths where natural

organic substances such as humic and fulvic acids are known to emit fluorescence (Baker and Genty 1999; Wu et al. 2003; Sierra et al. 2005; Hudson

Source	Excitation Range (nm)	Steps (nm)	Emission Range (nm)	Steps (nm)	Slitwidth (nm)	Ex Bandwidth (nm)	Em Bandwidth (nm)	Scanning Rate (nm/min)	Total Scan Time
Baker 2001	250-400	5	300-500	0.5	5				
Baker 2002	250-420	5	280-500	0.5	5				
Baker and Curry 2004	200-370	5	250-500	0.5	5				
Baker and Genty 1999	220-400	5	300-500	0.5	5				
Baker and Genty 1999 (fulvic acid peak only)	290-340	2 < nm < 5	395-430	0.5	5				
Baker and Lamont-Black 2001	250-425	5	300-500	0.5	5				
Baker and Spencer 2004	250-400	5	300-500	0.5	5				
Fiore et al. 2013 (preliminary)	220-520	1	280-700	1					
Fiore et al. 2013 (final)	200-482	3	280-700	5					
Hudson et al. 2008	200-400	5	280-500	5	5			9600	
Muller et al. 2008	250-400	5	280-500	5					
Qianqian et al. 2014	200-600	10	200-600	1				6000	
Sierra et al. 2005	250-410	10	260-700	1		4	4		
Soltzberg et al. 2012	250-380		395-700					1200	< 8 min per scan
Wu et al. 2003	250-550	9	250-650		0.25 millimeters	2	2		

Table 6: Three-dimensional synchronous scanning parameters considered through the course of the present research.

et al. 2008; Muller et al. 2008). However, a sufficient $\Delta\lambda$ between the λ_{Ex} and λ_{Em} must be maintained to minimize Raman scattering and wider scanning ranges mandate longer scan times, especially if requiring fine data resolution. Development of a suitable three-dimensional synchronous scanning parameter set required the balancing of the following priorities: 1) wide λ_{Em}, 2) appropriate $\Delta\lambda$, 3) reasonable scan time, and 4) sufficient spectral data resolution.

The research conducted by Baker (2001, 2002), Baker and Curry (2004), Baker and Genty (1999), Baker and Lamont-Black (2001), Baker and Spencer (2004), Hudson et al. (2008), Muller et al. (2008), and Qianqian et al. (2014) sought to characterize a wide array of natural and anthropogenically-impacted aqueous sources and components. The research presented in these studies characterized riverine water samples upstream, downstream, and at the outfalls of sewage treatment plants; riverine water samples upstream, downstream, and at the outfall of a tissue mill; landfill leachate within landfill sites, as well as landfill-adjacent clean and contaminated groundwater samples; overall characterization of groundwater percolating in four cave systems; dissolved organic matter (DOM) in groundwater from a variety of relatively unimpacted groundwater sources; both relatively pristine and contaminated (industrial, sewage treatment plant, and stormwater effluent) riverine samples, as well as estuarine samples that received contributions from these riverine sources; fluorescence intensities of tryptophan-like, tyrosine-like, and humic-like compounds for a wide range of samples, including natural surface waters, sewage effluent, industrial effluent, and waters that have experienced known pollution events; humic-like, tyrosine-like, and tryptophan-like components of dissolved organic carbon (DOC) in rainwater; and, finally, phenol dissolved in both

distilled and natural water aliquots. Although these studies were very informative in the development of the overall technique of three-dimensional synchronous scanning, the research presented in these studies considered an λ_{Em} too narrow to be applicable in the research herein described. With the exception of Qianqian et al. (2014), the maximum Em wavelength scanned in each of these studies was no more than 600 nm, which would prohibit the capture of even a full FL EEM when Ex = 347 nm, much less a full EO, RWT, or SRB EEM. Qianqian et al. (2014) scanned a maximum Em wavelength of 600 nm, which is insufficient to capture the full λ_{Em} of SRB when Ex = 347 nm.

After eliminating the aforementioned studies, the following studies were considered: Fiore et al. (2013), Sierra et al. (2005), Soltzberg et al. (2012), and Wu et al. (2003) (Table 7).

Table 7: Three-dimensional synchronous scanning parameters considered through the present research after eliminating those parameters that did not meet the initial research requirements.

Source	λ_{Ex} (nm)	Steps (nm)	λ_{Em} (nm)	Steps (nm)	Ex Bandwidth (nm)	Em Bandwidth (nm)	Scanning Rate (nm/min)	Repetition
Fiore et al. 2013 Prelim 3D	220-520	1	280-700	1				
Sierra et al. 2005 3D	250-410	10	260-700	1	4	4		
Soltzberg et al. 2012	250-380		395-700				1200	< 8 min per scan
Wu et al. 2003 3D	250-550	10	250-650	0.2	2	2		

The research presented in these studies sought to characterize a variety of riverine water samples, including relatively pristine samples, samples impacted by industrial discharges (fishery and sewage treatment plant effluents), sewage treatment plant effluent, and fishery effluent; a set of fulvic and humic acids extracted from marine, estuarine, lacustrine, and terrestrial environments; 65 water solutions of dyes from the Schweppe

Library of Synthetic Organic Dyes; and natural organic matter (NOM) in Suwannee River Fulvic Acid, Adlrich Humic Acid, and a natural riverine sample. The parameters utilized in these studies were acceptable because they included a sufficiently wide λ_{Em} (maximum beginning Em = 395 nm and minimum ending Em = 650 nm). However, the Soltzberg et al. (2012) parameters were later removed from consideration due to the exclusion of λ_{Em} = 200-395 nm, which would have limited measurement of natural organic fluorescent compounds, such as humic and fulvic acids (see Table 6). Parameter sets employed in the remaining three studies (Fiore et al. 2013, Sierra et al. 2005, and Wu et al. 2003) were used in the experimental development of preliminary EEMs of fluorescent dye standard dilutions.

4.7.2 Three-Dimensional Synchronous Scanning Experimental Parameters

Parameter sets employed by Fiore et al. (2013), Sierra et al. (2005), and Wu et al. (2003) (Tables 8 and 9) were modified and replicated in the LabSolutions RF Software and used to develop preliminary EEMs of fluorescent dye standard dilutions. Fiore et al. (2013) did not define bandwidth or scanning rate metrics for the parameter set. The default scanning rate of 6000 nm/min and Ex/Em bandwidths of 5 and 10 nm, respectively, were chosen to complete the parameter set. The Sierra et al. (2005) parameter set replicated in the

Table 8: Three-dimensional synchronous scanning parameters as discussed in the original publications.

Original Source Parameters	Excitation Range (nm)	Steps (nm)	Emission Range (nm)	Steps (nm)	Ex Bandwidth (nm)	Em Bandwidth (nm)	Scanning Rate (nm/min)
Fiore et al. 2013 Prelim 3D	220-520	1	280-700	1			
Sierra et al. 2005 3D	250-410	10	260-700	1	4	4	
Wu et al. 2003 3D	250-550	10	250-650	0.2	2	2	

Table 9: Versions of published parameters (see Table 8 above) adapted for experimentation in the present research.

Adapted Parameters	Excitation Range (nm)	Steps (nm)	Emission Range (nm)	Steps (nm)	Ex Bandwidth (nm)	Em Bandwidth (nm)	Scanning Rate (nm/min)
Fiore et al. 2013 Prelim 3D	220-520	2	280-700	5	5	10	6000
Sierra et al. 2005 3D	250-410	10	260-700	1	5	5	6000
Wu et al. 2003 3D	250-550	10	250-650	0.2	3	3	6000

LabSolutions RF Software was nearly identical to the published parameter set, except the experimental parameter set employed Ex/Em bandwidths of 5 nm and 5 nm, rather than 4 nm and 4 nm, and the scanning speed was set to the default scanning speed (6000 nm/min). The Wu et al. (2003) parameter set replicated in the LabSolutions RF Software was nearly identical to the published parameter set as well, except the experimental parameter set employed Ex/Em bandwidths of 3 nm and 3 nm, respectively, rather than 2 nm and 2 nm, and the scanning speed was set to the default scanning speed (6000 nm/min).

The final experimental parameter set was chosen on the basis of optimum parameter settings, as well as general aesthetics of the experimental EEMs because many of the parameter settings are quite similar. The replicated Fiore et al. (2013), Sierra et al.

(2005), and Wu et al. (2003) experimental parameter sets employed an λ_{Ex} that spanned 300, 160, and 300 nm, respectively, and an λ_{Em} that spanned 420, 440, and 400 nm, respectively. Each of the studies considered all portions of the electromagnetic spectrum known to be relevant to this research, including the shorter Em wavelengths where natural organic substances are known to emit fluorescence and the full λ_{Em} of FL, EO, RWT, and SRB when Ex = 347 nm. The default scanning rate of 6000 nm/min was used for each of the three experimental parameter sets as well.

Sierra et al. (2005) used an λ_{Ex} that is nearly half that considered by Fiore et al. (2013) and Wu et al. (2003), which resulted in the rejection of the Sierra et al. (2005) experimental parameter set. The replicated Fiore et al. (2013) experimental parameter set (Table 10) was selected for the production of EEMs of FL, EO, RWT, and SRB rather than Wu et al. (2003) because the replicated Fiore et al. (2013) experimental parameter set utilized similar data intervals for both Ex and Em and wider Ex/Em bandwidths than Wu et al. (2003). These two artifacts resulted in the production of more visually continuous EEMs than the more disjunctive EEMs produced using the replicated Wu et al. (2003) experimental parameter set (Figure 13).

Table 10: Parameter set adapted from Fiore et al. (2013) used in the production of final EEMs and contour diagrams through the course of this research.

Excitation Range (nm)	Steps (nm)	Emission Range (nm)	Steps (nm)	Ex Bandwidth (nm)	Em Bandwidth (nm)	Scanning Rate (nm/min)
220-520	2	280-700	5	5	10	6000

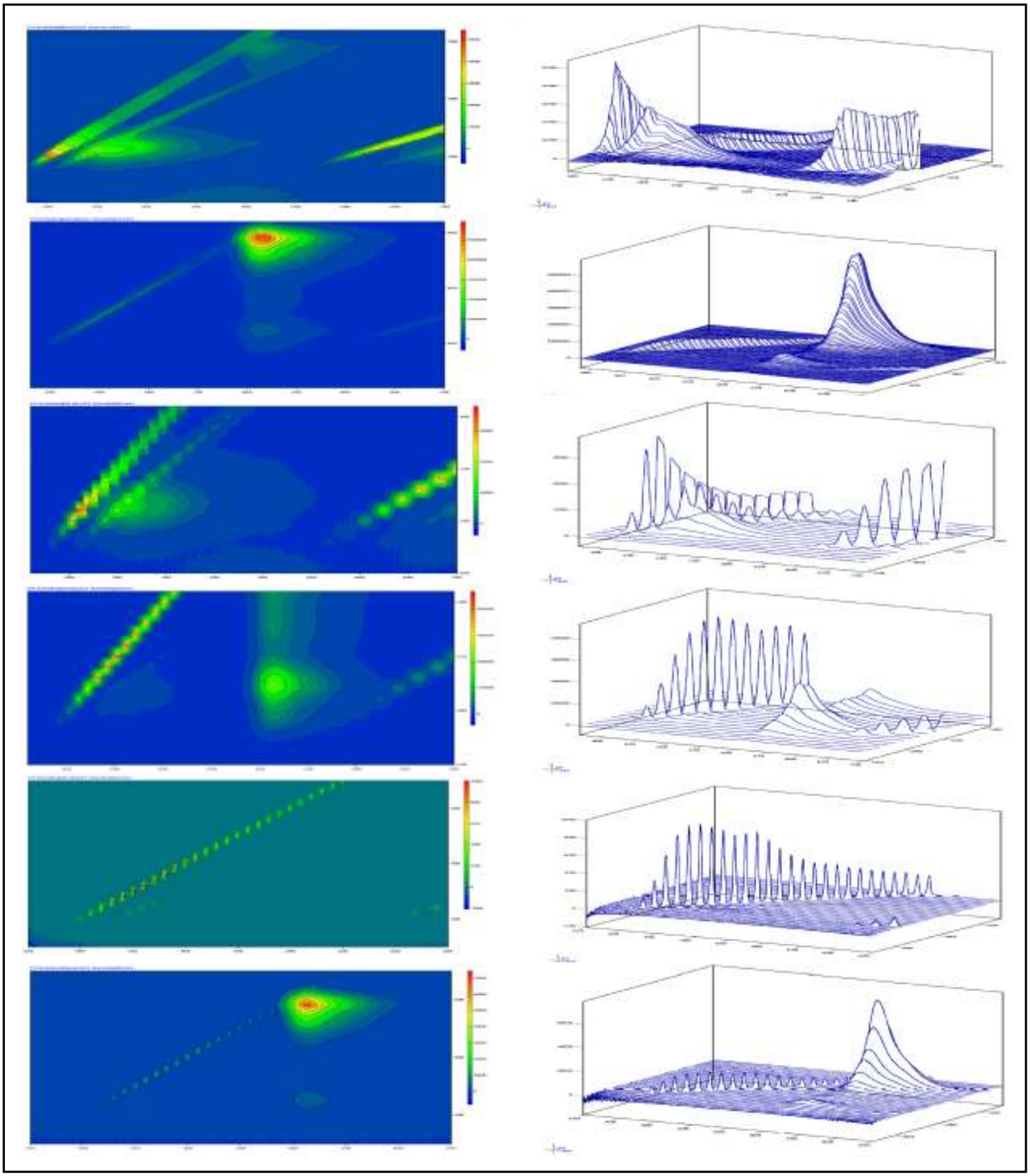

Figure 13: Compared contour diagrams and EEMs of FL 0.1 ppb (odd row) and FL 100 ppb (even row) standard dilutions created using Fiore et al. (2013) (rows 1 and 2), Sierra et al. (2005) (rows 3 and 4), and Wu et al. (2003) (rows 5 and 6) adapted parameter sets (from top to bottom). X-axis range = 280 - 700, Y-axis range = 220 – 520 nm.

5. Results

5.1 Two-Dimensional Synchronous Scans of Single Dye Dilutions

As discussed in the Methods section, the two-dimensional synchronous scanning parameters employed in the creation of two-dimensional synchronous scans are those that were successful and routinely utilized in the CHL. Single dilution two-dimensional synchronous scans serve the purpose of demonstrating the fluorescence peaks of four common fluorescent dyes diluted in DI water, free from natural or anthropogenic fluorescence—an ideal case that is unlikely in the natural world but serves as baseline data.

All samples were first analyzed using the high sensitivity setting and were analyzed using the low sensitivity setting only if the concentration of the sample exceeded 100 ppb or if the fluorescence exceeded 1000 intensity units. The appearance of instrumental "noise" is greatly reduced in low sensitivity two dimensional synchronous scans due to the coarser measurement scale. Synchronous scans were produced by measuring the λ_{Em} of four fluorescent dyes diluted in DI water at Ex = 347 nm. Note that although the λ_{Em} is only recorded in response to Ex = 347 nm, the instrument actually produces Ex radiation along a range of Ex wavelengths. The λ_{Em} are only displayed in respond to a single Ex wavelength due to the inherent limitations of a two-dimensional graphing space and the nature of two-dimensional synchronous scanning. It is also relevant to note that two-dimensional synchronous scans are significantly less time-consuming to develop than contour diagrams and EEMs using the LabSolutions RF Software (30 seconds vs. 10-15 minutes, dependent upon parameter specifications).

The two-dimensional synchronous scans demonstrate that fluorescent dye concentration is positively correlated with fluorescence intensity in the absence of measurement obstacles like quenching and inner-filter effects. Each fluorescent dye will respond to a given wavelength of light from the instrument's lamp by emitting light of certain wavelengths at a consistent range of fluorescence intensities. It is the consistency of the Ex-Em relationship of a fluorescent substance that permits identification of fluorescent substances by two-dimensional synchronous scanning and interpretation of contour diagrams/EEMs as signature, or "fingerprint," spectral forms of fluorescent substances.

5.2 Single Dye Dilution EEMs and Contour Diagrams

The high and low sensitivity settings used in three-dimensional synchronous scanning are similar to those used for two-dimensional synchronous scanning. The instrumental configuration and applications of the settings are identical for the production of both two-dimensional synchronous scans and contour diagrams/EEMs (Figures 14 and 15). The appearance of instrumental noise is greatly reduced in low sensitivity (as compared to high sensitivity) contour diagrams/EEMs, just as it is in the two-dimensional synchronous scans. Also note that three of the most consistent and apparent fluorescence patterns in the single dilution contour diagrams and EEMs are caused by scattered light. These three fluorescence patterns often disrupt the view of the dye fluorescence centers and will be discussed in detail in the Discussion section.

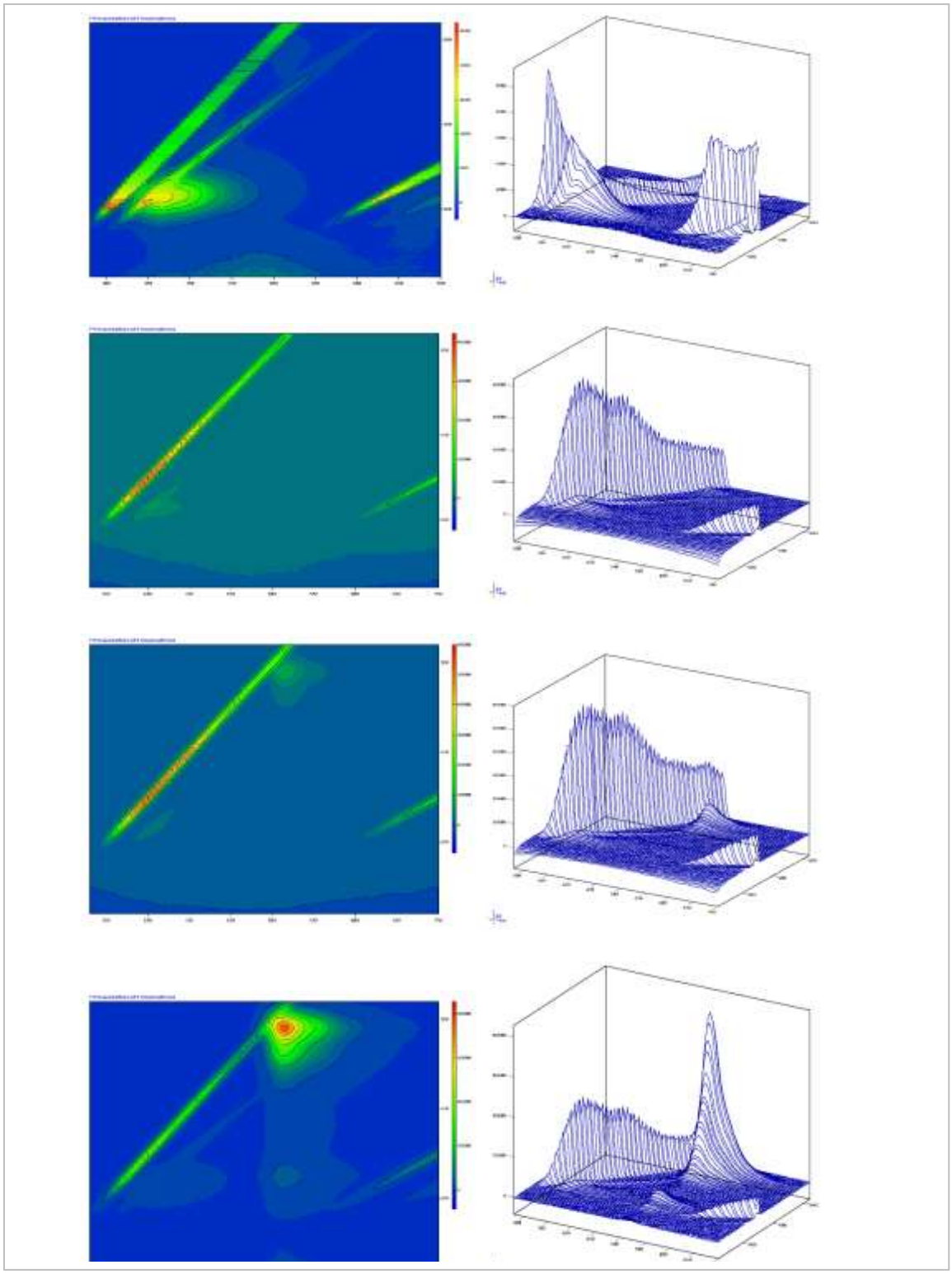

Figure 14: (Top to bottom) fluorescein single dye dilution .01, 0.1, 1, and 10 ppb EEMs and contour diagrams. X-axis range = 280 - 700 is nm, Y-axis range = 220 – 520 nm.

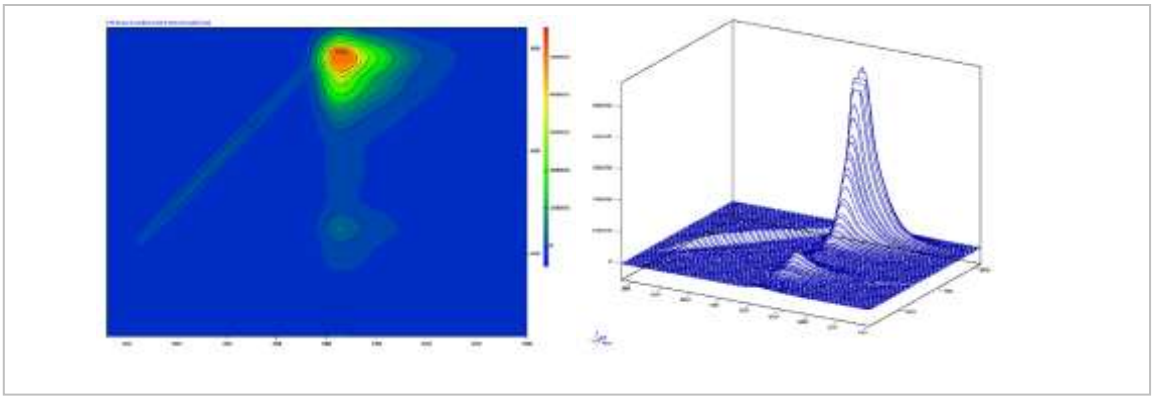

Figure 15: fluorescein single dye dilution 100 ppb EEM and contour diagram. *X*-axis range = 280 - 700 is nm, *y*-axis range = 220 – 520 nm.

.01, 0.1, 1, 10, and 100 ppb concentrations of FL were analyzed to produce single dye dilution contour diagrams/EEMs. The FL fluorescence center is not identifiable in EEMs and contour diagrams of .01 and 0.1 ppb FL standard dilutions where scattered light dominates the spectra. However, interference by scattered light diminishes as higher fluorescent dye concentrations increase due to the corresponding higher fluorescence intensity. The full FL fluorescence center may be seen in EEMs and contour diagrams of 1 – 100 ppb FL standard dilutions, which indicates that the λ_{Ex} includes sufficiently long Ex wavelengths to capture the full FL fluorescence center. Notice the asymmetry of the FL fluorescence center where the area is skewed in the *x*-direction and diminished in the *y*-direction. This may be an artifact resultant from the Ex/Em relationship, or it may be due to the scaling of the *x* and *y* axes. Notice also the "tail" on the right-most portion of the FL fluorescence center. The fluorescence center exhibits the greatest spread from the highest fluorescence intensity point toward the southeast quadrant of the graph space (greater Ex and lower Em wavelengths).

Like FL, EO may exhibit the greatest spread in its fluorescence center from the highest fluorescence intensity point toward the southeast portion of the graph space, but it

is difficult to verify this potentially shared trait since EO is less fluorescent than FL at comparable concentrations and the EO fluorescence center is not fully captured by the chosen λ_{Ex}. Unlike FL, the chosen λ_{Ex} only captures a portion of the EO fluorescence center at high concentrations. The EO fluorescence center is not identified in EEMs and contour diagrams of .01, 0.1, and 1 ppb concentration standard dilutions and is only partially visible in 10 and 100 ppb EO EEMs and contour diagrams (Figure 16). The partial EO fluorescence centers captured in the 10 and 100 ppb EEMs and contour diagrams are not entirely symmetrical—a characteristic shared by the FL fluorescence centers. Because the EO fluorescence center is not captured in the .01, 0.1, and 1 ppb EEMs and contour diagrams, it is only possible to determine that scattered light intersects the EO 10 and 100 ppb concentration standard dilution fluorescence centers. The

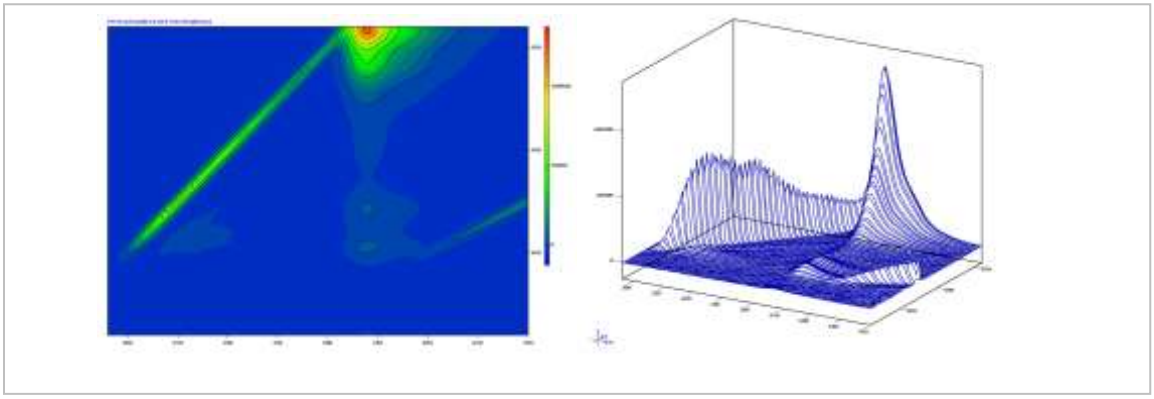

Figure 16: Three-dimensional synchronous scan of eosin 100 ppb single dye dilution. *X*-axis range = 280 - 700 is nm, *y*-axis range = 220 – 520 nm.

scattered light may contribute extraneous peak area to these fluorescence centers.

Like EO, the RWT fluorescence center is not fully depicted by the chosen λ_{Ex}. The RWT fluorescence center is not identifiable in EEMs and contour diagrams at concentrations lower than 100 ppb—scattered light dominates the spectra at concentrations lower than 100 ppb and even at 100 ppb the RWT fluorescence center is only partially visible. The RWT fluorescence center may share the shape of the EO and

FL fluorescence centers (the center is concentrated primarily to the right, at greater excitation wavelengths, of the greatest intensity point), but it is difficult to make a definitive statement about the shape of the RWT fluorescence center since it is not visible in EEMs and contour diagrams of RWT standard dilutions less than 100 ppb concentration and is only partially visible at 100 ppb. However, the 100 ppb RWT EEM and contour diagram (Figure 17) do display a fluorescence pattern composed of three distinct fluorescence centers distributed below the primary RWT fluorescence center in the southeast portion of the contour diagram/EEM. This fluorescence pattern is not

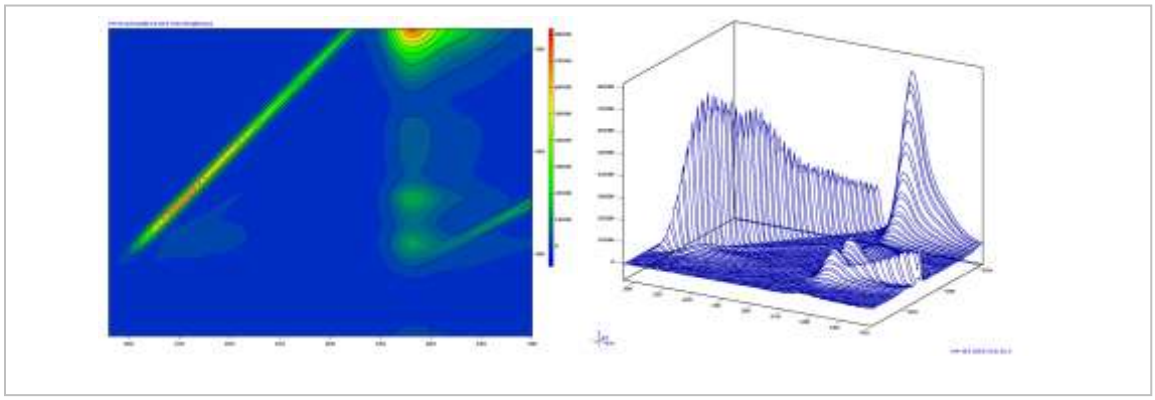

Figure 17: Three-dimensional synchronous scan of 100 ppb rhodamine WT single dye dilution. *X*-axis range = 280 - 700 is nm, *y*-axis range = 220 – 520 nm.

observed in the high concentration FL and EO EEMs and contour diagrams.

Like EO and RWT, the SRB fluorescence center is not fully depicted by the chosen λ_{Ex} — the SRB fluorescence center is only visible at SRB concentrations 10 ppb and higher. At concentrations lower than 10 ppb, scattered light dominates the SRB EEMs/contour diagrams. Like the high concentration FL, EO, and RWT EEMs and contour diagrams, the majority of the area of the SRB fluorescence center is skewed to the right of the highest intensity point. Interestingly, the SRB EEMs/contour diagrams (Figure 18) share the fluorescence pattern displayed in the 100 ppb RWT EEM and

contour diagram that is characterized by secondary fluorescence centers in the southeast direction of the primary fluorescence center.

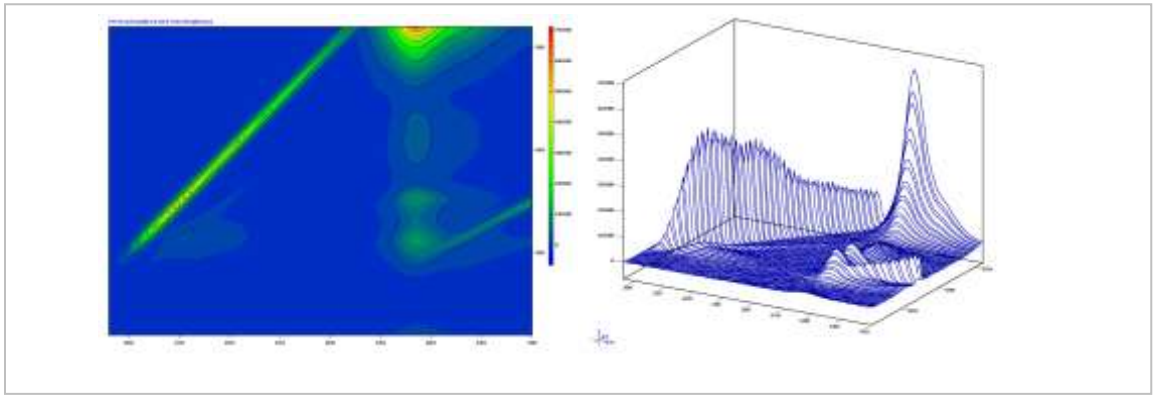

Figure 18: Three-dimensional synchronous scan of sulphorhodamine B 100 ppb single dye dilution. *X*-axis range = 280 - 700 is nm, *y*-axis range = 220 – 520 nm.

5.3 Two-Dimensional Synchronous Scans of Mixed Dye Dilutions

Standard dilutions were created for FL, EO, RWT, and SRB at 1, 10, and 100 ppb concentrations and mixed to create mixed standard dilutions. Mixed standard dilutions were not created using any dilution less than 1 ppb in concentration because three-dimensional synchronous scanning revealed that fluorescence centers of the four dyes were not visible if the dilutions were concentrated less than 1 ppb. There is no obvious reason to suppose that the fluorescence centers not detected through analysis of the low concentration single standard dilutions would be detected through analysis of low concentration mixed standard dilutions. Mixed dye dilutions were also not created using 100 ppb FL because FL fluoresces so intensely that measurement of such a highly concentrated FL dilution as 100 ppb is outside the measurement capabilities of the instrument in its current configuration. The quantum yield—resulting in a larger fluorescence intensity per unit of dye— of FL exceeds that of EO, RWT, or SRB.

The two-dimensional synchronous scans of the mixed dye dilutions demonstrate the appearance of two-dimensional synchronous scans affected by the presence of fluorescent dyes that share overlapping λ_{Em}. This is a plausible scenario in natural waters since dyes like FL are used in products as commonplace as antifreeze and thus often exist at considerable concentrations in natural waterways due to anthropogenic influence. Overlapping λ_{Em} may result in inaccurate peak area measurement and dye concentration calculation. FL and EO share overlapping λ_{Em}, as do RWT and SRB.

Two dyes mixed into a solution may appear as one primary fluorescence peak with a substantial "shoulder" in the peak, rather than as two distinct peaks that share peak area. In the case of FLEO 1:1, FL and EO share a common λ_{Em} in response to Ex = 347 nm. EO appears as a shoulder on the primary FL fluorescence peak because, although these dyes are mixed into water at the same concentrations (1 ppb each), the quantum yield of FL is higher than that of EO. The FLEO 1:10 two-dimensional synchronous scan (Figure 19) displays FL as a shoulder on the primary EO fluorescence peak because, although EO is of a lower fluorescence quantum yield than FL, EO is ten times more concentrated than FL in this sample. Peak area is shared between FL and EO, which might result in inaccurate peak area and concentration calculations.

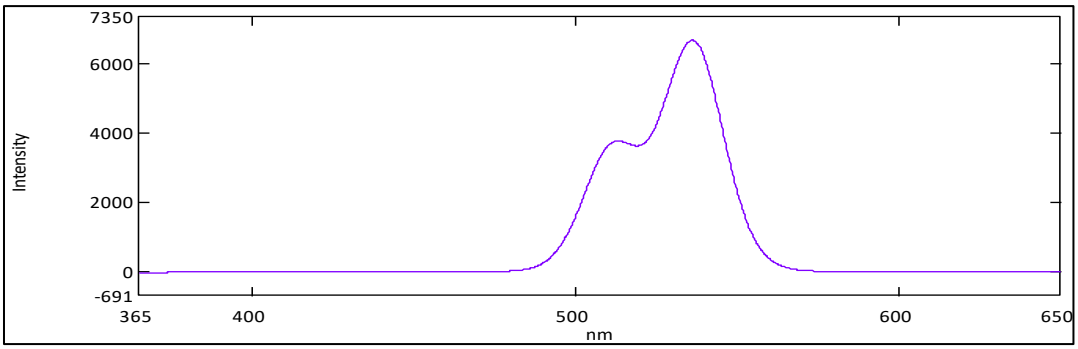

Figure 19: Two-dimensional synchronous scan of a FLEO 1:10 mixed dye dilution where fluorescein is depicted as a shoulder on the eosin fluorescence peak.

These miscalculations might then result in inaccurate estimation of flow paths, residence times, etc. following a dye trace. The FLEO 1:100 two-dimensional synchronous scan displays 1 ppb FL entirely hidden by the 100 ppb EO fluorescence peak. FL is indistinguishable from EO. Analysis of this sample might result in the loss of any information related to the FL in a dye trace.

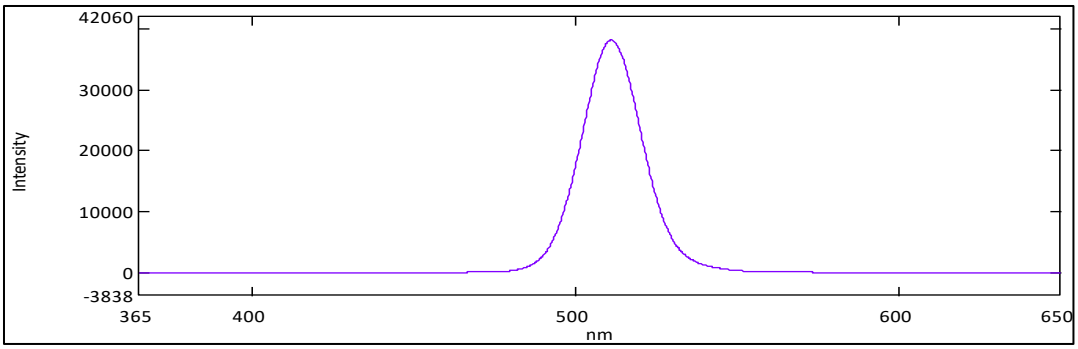

Figure 20: Two-dimensional synchronous scan of a FLEO 10:1 mixed dye dilution where the eosin fluorescence peak is subsumed by the fluorescein fluorescence peak.

The FLEO 10:1 synchronous scan displays 1 ppb EO entirely absorbed by the FL fluorescence peak due to FL's higher quantum yield (Figure 20). The FLEO 10:10 synchronous scan displays EO as a small shoulder on the larger FL fluorescence peak and peak are is shared between the two dyes. The FLEO 10:100 synchronous scan displays FL and EO as components of a bimodal peak where EO is the highest intensity peak. Peak discrimination might be possible through the application of PeakFit or other curve-fitting software, but otherwise it may be difficult to derive quantitative information from the trace, including dye concentrations.

The RWTSRB 1:1, RWTSRB 1:10, RWTSRB 1:100, RWTSRB 10:1, RWTSRB 10:10, and RWTSRB 10:100 synchronous scans display RWT and SRB as a single, indistinguishable peak. Peak area may be difficult to determine for each dye and it may be difficult to derive quantitative information related to the trace. The RWTSRB

100:1 synchronous scan displays RWT and SRB as two discriminate peaks with only slight potential sharing of peak area and high fluorescence intensity. The intensities of the two dyes are remarkably close even though RWT is one hundred times the concentration of SRB. This is especially interesting because, as displayed in the single dilution synchronous scans, RWT and SRB fluoresce at comparable intensities at the same concentration (Figure 21). The RWTSRB 100:10 and RWTSRB 100:100 tsynchronous scans display only one homogenous fluorescence peak featuring no shoulders. Peak area is entirely shared between the RWT and SRB dyes and it may be difficult to derive any information from the trace related to the respective concentrations of RWT and SRB.

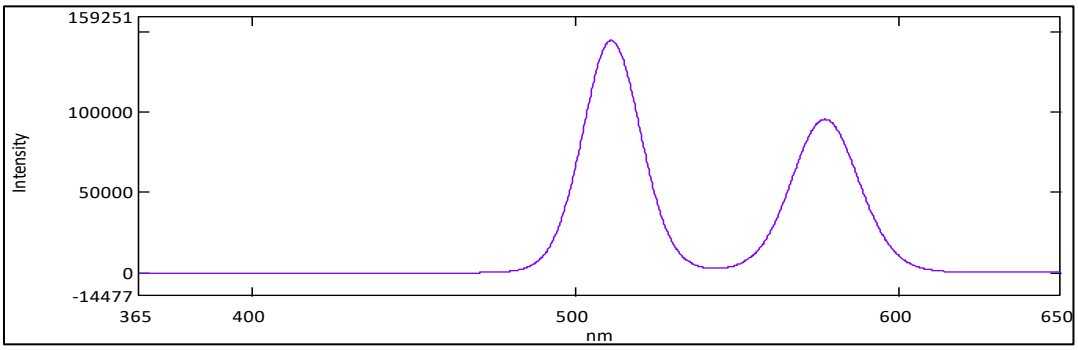

Figure 21: Three-dimensional synchronous scan of RWTSRB 100:1 mixed dye dilution where each dye is depicted as a discriminate fluorescence peak.

5.4 Mixed Standard Dilution EEMs and Contour Diagrams

Mixed standard dilutions were analyzed using three-dimensional synchronous scanning following application of two-dimensional synchronous scanning to produce EEMs and contour diagrams for each of the mixed standard dilutions. As in the EEMs and contour diagrams produced of single standard dilutions, fluorescence patterns resultant from scattered light may result in the contribution of superfluous area to the fluorescence centers and oftentimes distort the shape of the fluorescence centers. The FLEO 1:1 contour diagram/EEM exhibits an identifiable fluorescence center that is only

slightly divided by the longer Ex wavelength boundary (upper boundary of the graph space). The center is of similar intensity as the most central light scatter pattern and is intersected by the scattered light, which may contribute superfluous peak area. The FLEO 1:10 contour diagram/EEM exhibits a high intensity center shifted upward to such a degree that the highest intensity center is intersected by the upper limit of the λ_{Ex}. The high intensity center is also intersected by scattered light and the area of the center is broader and rounder than the center displayed in the FLEO 1:1 contour diagram/EEM. The FLEO 1:100 contour diagram (Figure 22) displays a high intensity fluorescence center that is exaggerated downward and intersected by scattered light. The longest λ_{Ex} wavelength boundary intersects the fluorescence center above the highest intensity point and secondary fluorescence centers may be seen between Ex = 300 - 400 nm, adjacent to but not intersected by scattered light. These secondary fluorescence centers are distinct from the primary fluorescence centers. The FLEO 10:1 contour diagram displays one primary fluorescence center, which is almost entirely within the graph space and intersected by scattered light, and several secondary fluorescence centers.

The primary center is continuous with the secondary centers in the lower reaches of the contour diagram and the secondary centers are synonymous with those that were observed in the FLEO 1:100 contour diagram between Ex = 275 - 350 nm. The FLEO 10:10 contour diagram displays one primary fluorescence center that is almost entirely within the graph space and is intersected by scattered light. The contour diagram also displays several secondary fluorescence centers that are continuous with the

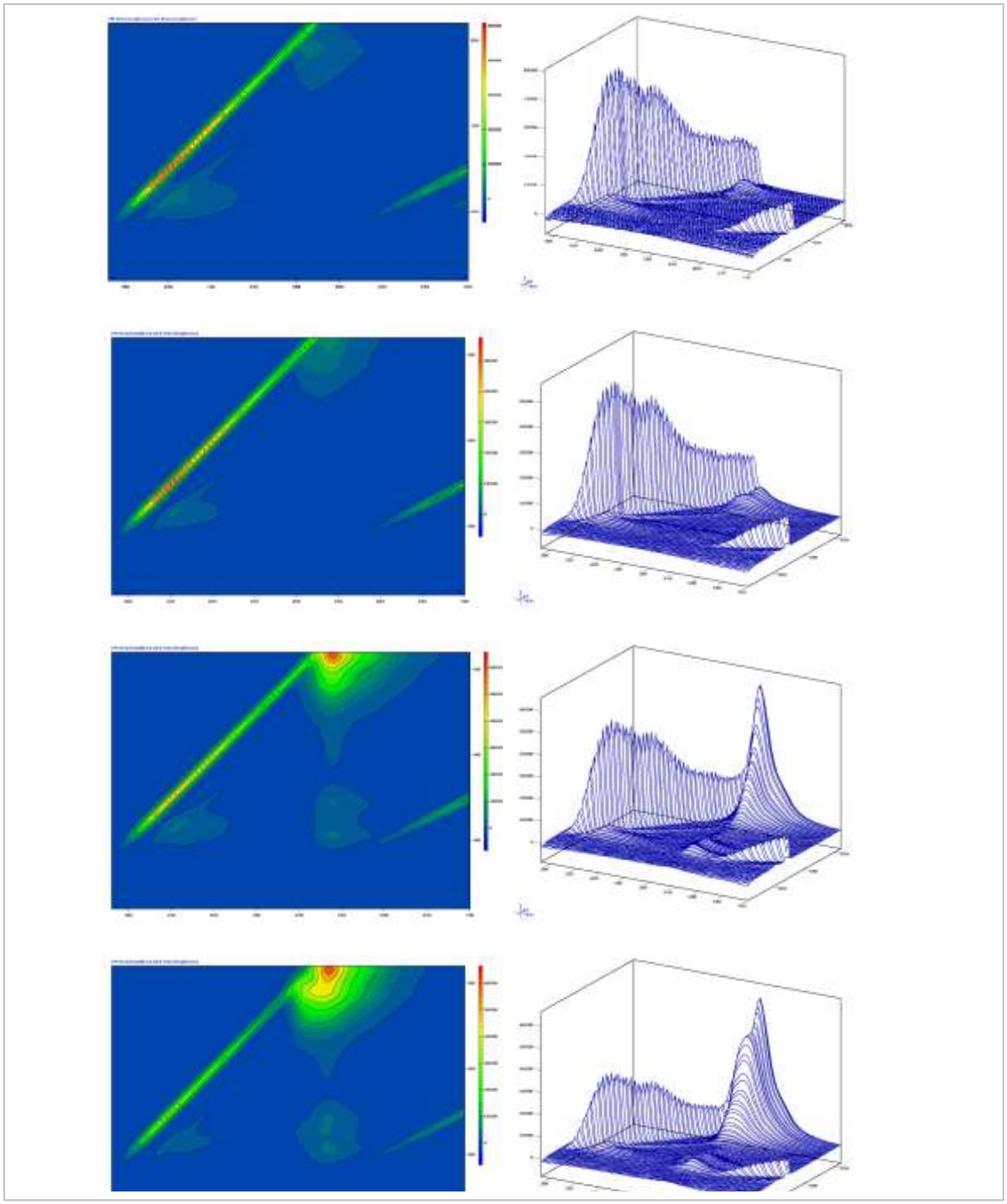

Figure 22: Top to bottom, three-dimensional synchronous scans of FLEO 1:1, FLEO 1:10, FLEO 1:100, and FLEO 10:100 mixed dye dilutions. *X*-axis range = 280 - 700 is nm, *y*-axis range = 220 – 520 nm.

primary fluorescence center. The FLEO 10:100 contour diagram displays one primary fluorescence center that is intersected by the longest wavelength Ex boundary above the highest intensity center. The primary center is not continuous with the secondary fluorescence centers below it and is intersected by scattered light.

The RWTSRB 1:1 contour diagram (Figure 23) does not display any fluorescence centers other than fluorescence patterns attributable to scattered light. The RWTSRB 1:10 contour diagram displays a primary fluorescence center intersected by the longest wavelength Ex boundary far below the highest intensity center, rendering only the bottom edge of the primary fluorescence center visible in the contour diagram. It is not possible to determine if the contour diagram is intersected by scattered light (though it likely is since contour diagrams/EEMs have usually displayed primary fluorescence centers intersected by scattered light). The RWTSRB 1:100 contour diagram displays a primary fluorescence center intersected by the longest wavelength Ex boundary far below the highest intensity center as well. It is not possible to determine if the primary fluorescence center is intersected by scattered light. Secondary fluorescence centers are visible below the primary fluorescence center and not all of the secondary fluorescence centers are continuous with one another. The bottommost secondary fluorescence center (located at shortest Ex wavelengths) is intersected by scattered light.

The RWTSRB 10:1 contour diagram displays a primary fluorescence center that is not continuous with the secondary fluorescence centers and is intersected by the uppermost boundary of the graph below the highest intensity center. The secondary fluorescence centers located in the lowermost portions of the graph space are continuous with one another and are intersected by scattered light. The RWTSRB 10:10 contour

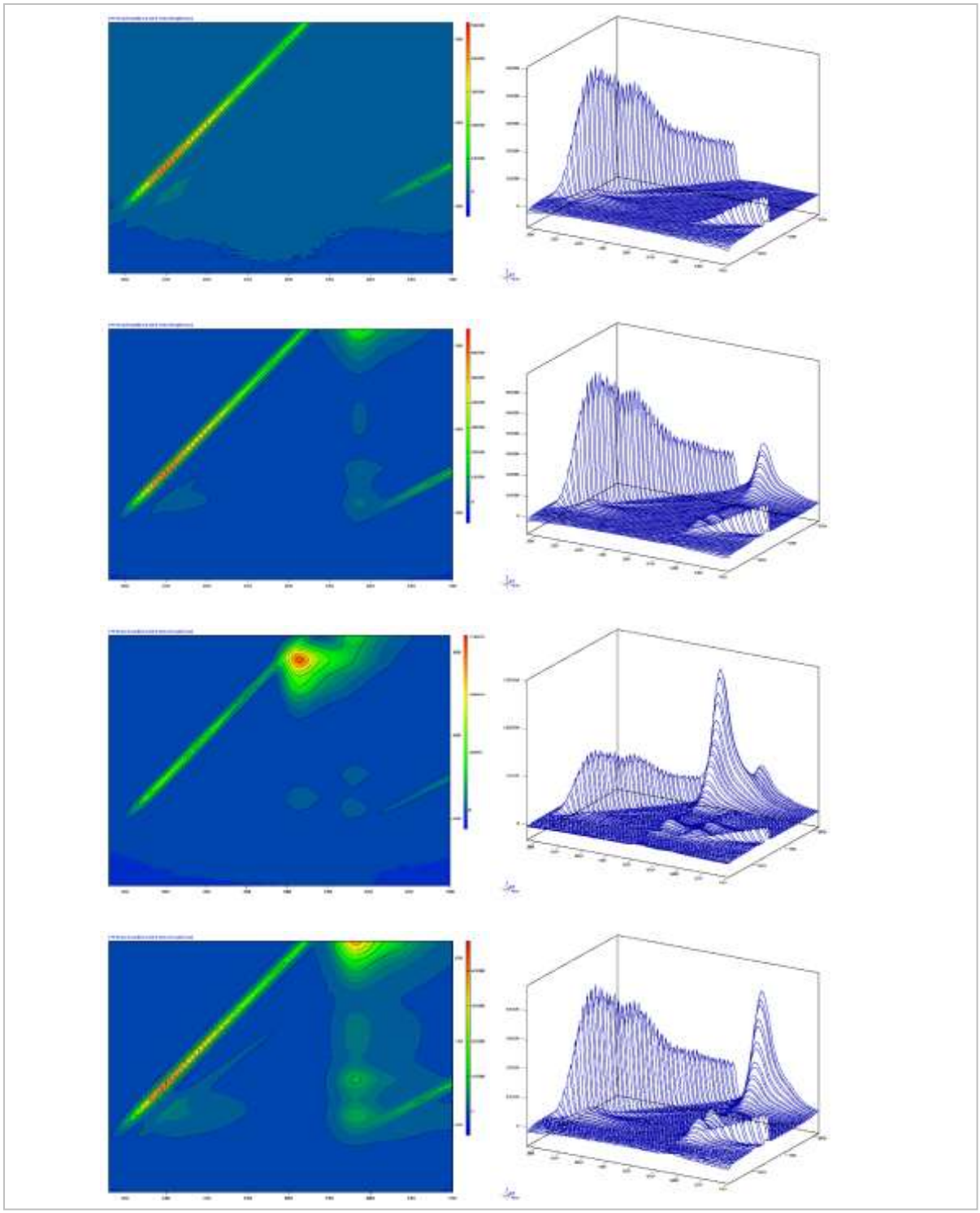

Figure 23: Top to bottom, three-dimensional synchronous scans of RWTSRB 1:1, 1:100, 100:1, and 100:10 mixed dye dilutions. *X*-axis range = 280 - 700 is nm, *y*-axis range = 220 – 520 nm.

diagram displays a primary fluorescence center that is not continuous with the three secondary fluorescence centers in the southern portion of the diagram and is intersected by the uppermost boundary of the contour diagram. The secondary fluorescence centers are not continuous with one another and the bottommost fluorescence center is intersected by scattered light. The RWTSRB 10:100 contour diagram displays primary and secondary fluorescence centers that are continuous with one another. Although the primary fluorescence center is still intersected below the highest intensity center by the uppermost boundary of the contour diagram, it is clear that the primary fluorescence center is intersected by scattered light.

The RWTSRB 100:1 contour diagram displays the usual primary and secondary fluorescence centers, but these centers do not demonstrate the regular pattern and shape. A single primary fluorescence center occupies the top central and right portions of the contour diagram and is not intersected below its high intensity center. The majority of the primary center is located within the graph space, with the exception of an arm-like feature of moderate fluorescence intensity that extends to the upper right off the graph space (into longer Em and Ex wavelengths). Two secondary fluorescence centers may be seen below the primary fluorescence center, but a third secondary center to the left (shorter Em wavelengths) of the usual secondary fluorescence centers may also be observed. None of the secondary fluorescence centers are intersected by scattered light.

The RWTSRB 100:10 contour diagram is quite different than the 100:1 contour diagram and exhibits something more akin to the usual pattern. The primary fluorescence center is bisected by the longest Ex wavelength boundary and intersected by scattered light. The primary fluorescence center is continuous with the secondary centers below it,

which are also continuous with one another. The secondary fluorescence centers are intersected by scattered light, especially the secondary center located at the shortest Ex wavelengths. The central of the three secondary fluorescence centers exhibits a zone of higher intensity than the other two secondary fluorescence centers.

The RWTSRB 100:100 contour diagram exhibits the trend observed in the transition between the RWTSRB 100:1 to 100:100 contour diagrams in which the fluorescence centers become increasingly continuous and the primary fluorescence center moves further and further upward and off the graph space (into longer and longer Ex wavelengths). The leftmost (short Em wavelengths) fluorescence center adjacent to the scattered light artifact is reduced in area and intensity and seems to no longer be intersected by scattered light. The primary fluorescence center is intersected by the uppermost graph boundary (longest Ex wavelength) below the highest intensity center and is not continuous with the secondary fluorescence centers. The secondary centers are continuous with one another and the secondary centers in the lowermost portion of the graph space are intersected by scattered light. The lower two secondary fluorescence centers are of greater fluorescence intensity than the uppermost secondary fluorescence center.

5.5 Two-Dimensional Synchronous Scans of Lost River Cave Samples

LRC samples were collected using an autosampler over a period of 24 hours following an injection of FL and were named 001-0 through 024-0. The samples were first analyzed using two-dimensional synchronous scanning (Figure 24) and those that

contained the injected dye were analyzed using three-dimensional synchronous scanning. The two-dimensional synchronous scans of samples 001-0 through

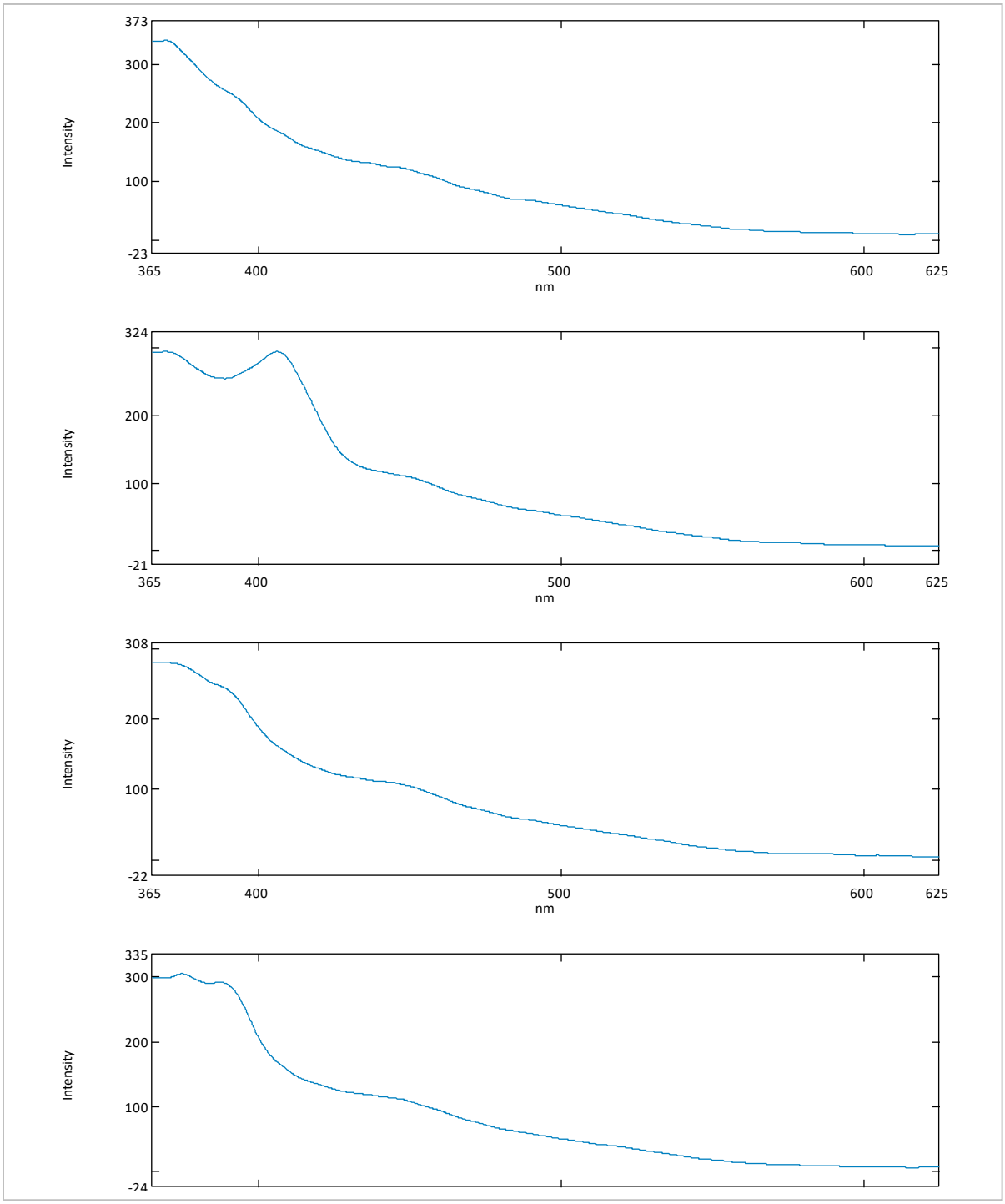

Figure 24: Top to bottom, two-dimensional synchronous scans of Lost River Cave 008, 009, 013, and 020 water samples.

008-0 seem to display measurable background fluorescence, but there is only a discernible peak between λ_{Em} = ~430 - ~460 nm. The 009-0 scan displays a pronounced fluorescence peak between λ_{Em} = ~385 - ~430 nm. The 010-0 and 011-0 scans display only the λ_{Em} = ~430 - ~460 nm fluorescence peak. The 012-0 and 013-0 scans display a more pronounced shoulder on the steep portion of the large peak between λ_{Em} = ~390 - ~400 nm, which may correspond to the fluorescence peak identified in sample 009-0 from λ_{Em} = ~385 - ~430 nm. Peaks are displayed at λ_{Em} = ~390 - ~400 nm and λ_{Em} = ~430 - ~460 nm in the 014-0 through 021-0 scans, with minor (~10 nm) variations in the λ_{Em} of the peaks and peak intensities.

The injected dye (FL) is first detected in the 022-0 scan (Figure 25) from λ_{Em} = 492.8 - 528.8 nm at a concentration of .004 ppb. It should be noted that this concentration is below the lowest concentration FL PQL standard dilution and so is not within the calibrated range of the instrument. The minor fluorescence peaks located at λ_{Em} = ~390 - ~400 nm and λ_{Em} = ~430 - ~460 nm are also present.

FL was measured in the 023-0 scan at greater than 600 fluorescence intensity units and a concentration of 0.092 ppb. The minor fluorescence peaks at λ_{Em} = ~390 - ~400 nm and λ_{Em} = ~430 - ~460 nm are present. The minor fluorescence peaks at λ_{Em} = ~390 - ~400 nm and λ_{Em} = ~430 - ~460 nm are barely discernible in the 024-0 scan and FL is too highly concentrated to be measured using the high sensitivity instrument setting. The 024-0 scan was produced using a low sensitivity instrument setting. The minor fluorescence peaks located at λ_{Em} = ~390 - ~400 nm and λ_{Em} = ~430 - ~460 nm are not easily discerned due to the scaling of the *y*-axis, which also minimizes the appearance

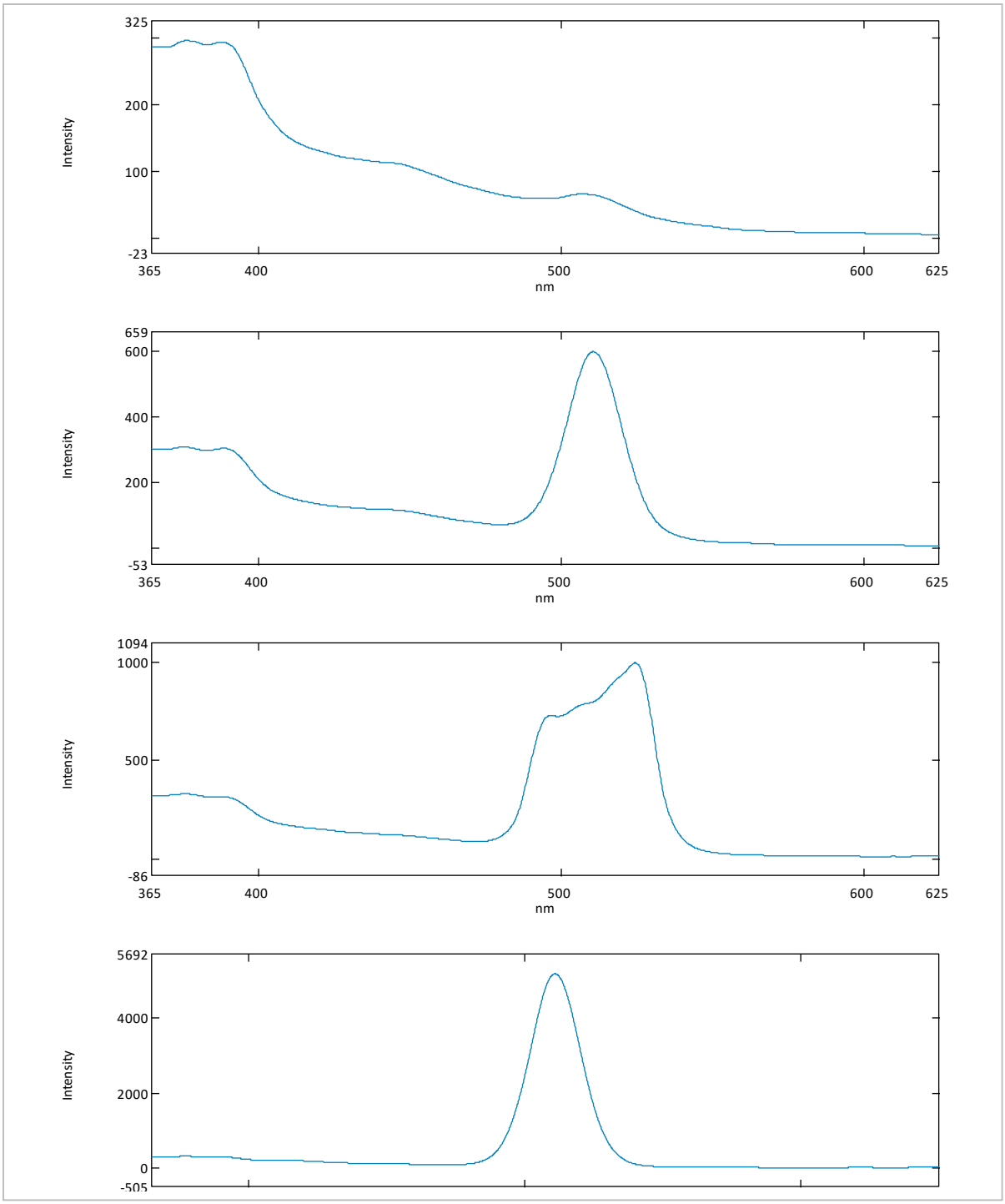

Figure 25: Top to bottom, two-dimensional synchronous scans of Lost River Cave 022, 023, high sensitivity 024, and low sensitivity 024 water samples.

of instrumental noise. The measured FL concentration is 0.849 ppb and fluoresces at about 5,000 fluorescence intensity units. The highest fluorescence intensity demonstrated either by noise or the three identifiable peaks at λ_{Em} = ~385 - ~430 nm, ~390 - ~400 nm,

and ~430 - ~460 nm was measured at 275 - 425 intensity units. The highest fluorescence intensity was measured at about 5,000 intensity units in the 024-0 sample that contained concentrated FL. Notice that only samples 022-0, 023-0, and 024-0 contain the injected FL. The sampling regime only collected the beginning of the breakthrough curve, which began at and was collected in sample 022-0.

5.6 Lost River Cave EEMs and Contour Diagrams

Two-dimensional synchronous scans of the LRC samples (Figure 26) demonstrated that only samples 022-0, 023-0, and 024-0 contained the injected tracer dye, FL. These samples, in addition to 021-0, were analyzed using three-dimensional synchronous scanning. Sample 021-0 was analyzed using three-dimensional synchronous scanning to ensure that any trace of FL that was not detected using two-dimensional synchronous scanning might be measured using three-dimensional synchronous scanning. The 021-0 contour diagram displays an irregularly (angular)-shaped fluorescence center in the lower left portion of the graph space (low Em and Ex wavelengths). The angularity of the fluorescence center is potentially caused by intersecting scattered light and the center seems to have two high intensity centers. There are also two forms of scattered light present in the bottom right (low Ex and high Em wavelengths) portion of the contour diagram, though neither artifact is obviously intersecting the fluorescence center. The only observable fluorescence patterns in the contour diagram are artifacts resultant from scattered light. No background fluorescence or instrumental noise is distinguishable, likely due to the coarse scale of the contour diagram, although the chosen λ_{Ex} and λ_{Em} should encompass the likely ranges of background fluorescence.

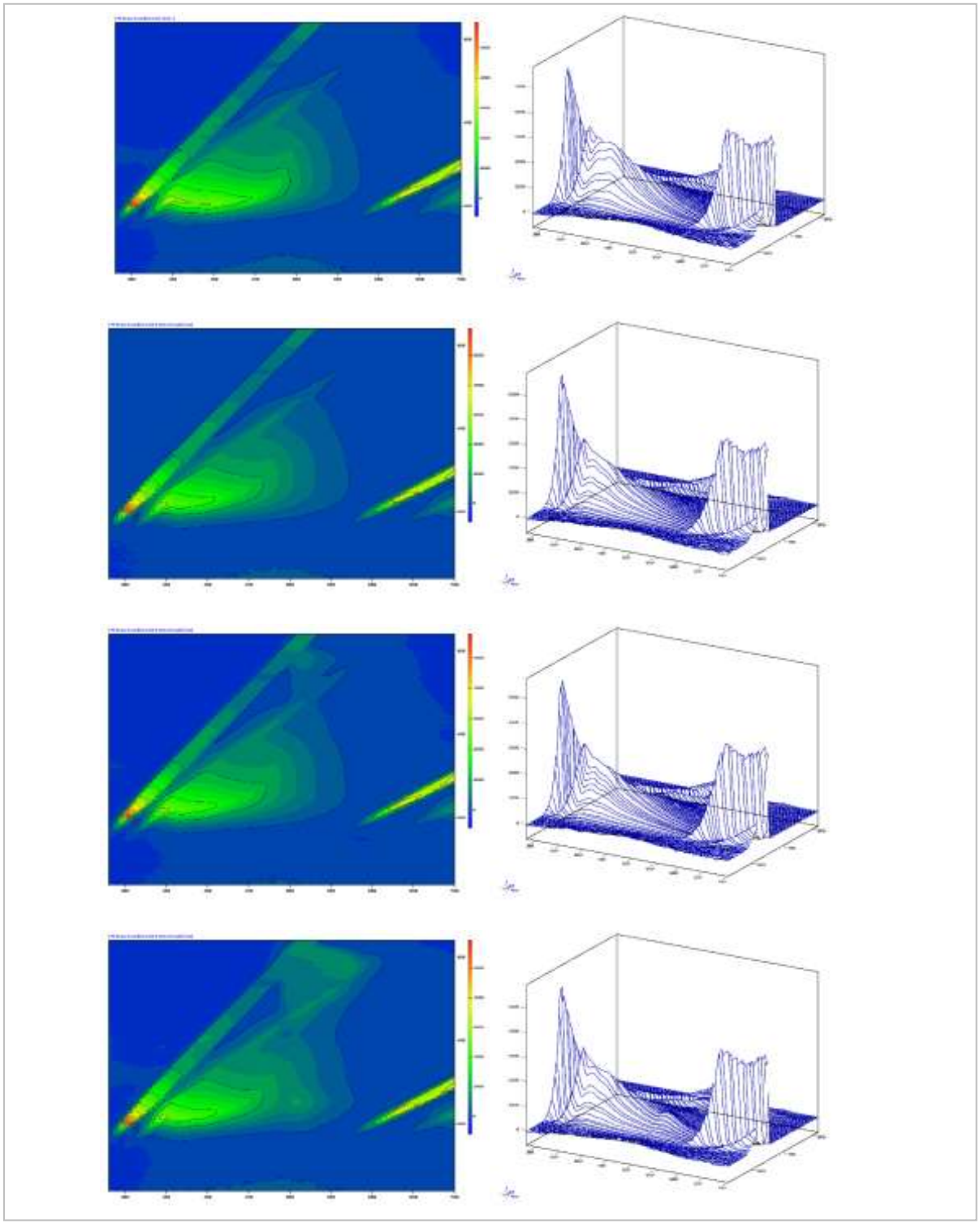

Figure 26: Top to bottom, three-dimensional synchronous scans of Lost River Cave 020, 021, 022, and 023 water samples. *X*-axis range = 280 - 700 is nm, *y*-axis range = 220 – 520 nm.

The 022-0 contour diagram is identical to 021-0 except the primary fluorescence center seems to be characterized by only one high intensity center. This is interesting since 021-0 does not contain any FL dye and 022-0 does. The 023-0 contour diagram is identical to the 022-0 contour diagram except that the scattered light may entirely intersect the primary fluorescence center in the 023-0 contour diagram and skew the primary fluorescence center to the upper right (long Em and Ex wavelengths). Additionally, a second fluorescence center seems to be present northward of the primary fluorescent center, though it is of lower intensity than the primary fluorescence center. The 024-0 contour diagram displays a new fluorescence center at the lower center (short Ex, mid Em) of the contour diagram. The primary fluorescence center is much more angular and extends as an "arm" upward along the left-most fluorescence pattern caused by scattered light, where the arm-like feature completely joins with the scattered light. The irregularity of the primary fluorescence center is likely a result of the FL concentration exceeding the measurement capabilities of the high sensitivity instrument setting.

6. Discussion

It should be noted that all measurements associated with three-dimensional synchronous scanning are made with an associated error of ± 5 nm due to the chosen data interval (also called "steps") of 5 nm employed in the production of EEMs and contour diagrams. All measurements associated with two-dimensional synchronous scans are made with an associated error of ± 0.2 nm due to the data interval of 0.2 nm employed in the production of two-dimensional synchronous scans. Also note that fluorescence centers are considered unique and characteristic through this study if and only if they are of a greater fluorescence intensity than any ubiquitous background fluorescence in the EEM/contour diagram. Occasionally a general fluorescence pattern of extremely low fluorescence intensity is adjacent to and surrounds unique fluorescence centers. This weakly-fluorescent pattern does not constitute a unique fluorescence center, nor is it interpreted to "link" unique fluorescence centers into a single fluorescence center.

6.1 Single Dye Dilution EEMs and Contour Diagrams

Characteristics that may be used to differentiate FL and EO through both two and three-dimensional synchronous scanning include locations of FL and EO λ_{Em} maxima and the respective beginning and ending wavelengths of their λ_{Em}. Some researchers have distinguished between various fluorescent substances by qualitative inspection of the shapes of their fluorescence centers (Soltzberg et al. 2012). This method is not applicable in the examination of FL and EO EEMs/contour diagrams produced through this research because both FL and EO share a common contour shape and location. However, the application of three-dimensional synchronous scanning revealed a characteristic peculiar

to EO EEMs/contour diagrams that may be used to discriminate between FL and EO that would not otherwise be possible through the application of two-dimensional synchronous scanning alone as applied through this research.

FL EEMs/contour diagrams (Figure 27) are characterized by two fluorescence intensity centers: one primary fluorescence center in the northcentral portion of the graph space (λ_{Ex} = 420 – 522 nm, λ_{Em} = 480 – 610 nm), and one secondary fluorescence center present in the southcentral portion of the graph space (λ_{Ex} = 312 – 340 nm, λ_{Em} = 500 – 536 nm). These two fluorescence centers are continuous with one another by a low-intensity fluorescence pattern. Both the 10 and 100 PPB FL EEMs/contour diagrams display this pattern, though these specific fluorescence center measurements were produced from the 100 PPB FL contour diagram. Note that the long Ex wavelength boundary is an approximation because the long wavelength Ex boundary of the graph space severs the uppermost portion of the FL 100 PPB fluorescence center.

All long Ex wavelength boundaries established by approximation through this research were established by measuring the wavelength span between the shortest Ex wavelength boundary and the longest Ex wavelength boundary of the graph space (520 nm). The difference between the shortest Ex wavelength boundary of the fluorescence center and 520 nm was added to 520 nm to establish the approximate long Ex wavelength boundary of the fluorescence center. It should be noted that one limitation of this method is the assumption that fluorescence centers are symmetrical about their Em (*y*) axis. Evidence will be provided in the Discussion that invalidates this assumption and future efforts should endeavor to measure the entirety of the FL, EO, RWT, and SRB fluorescence centers.

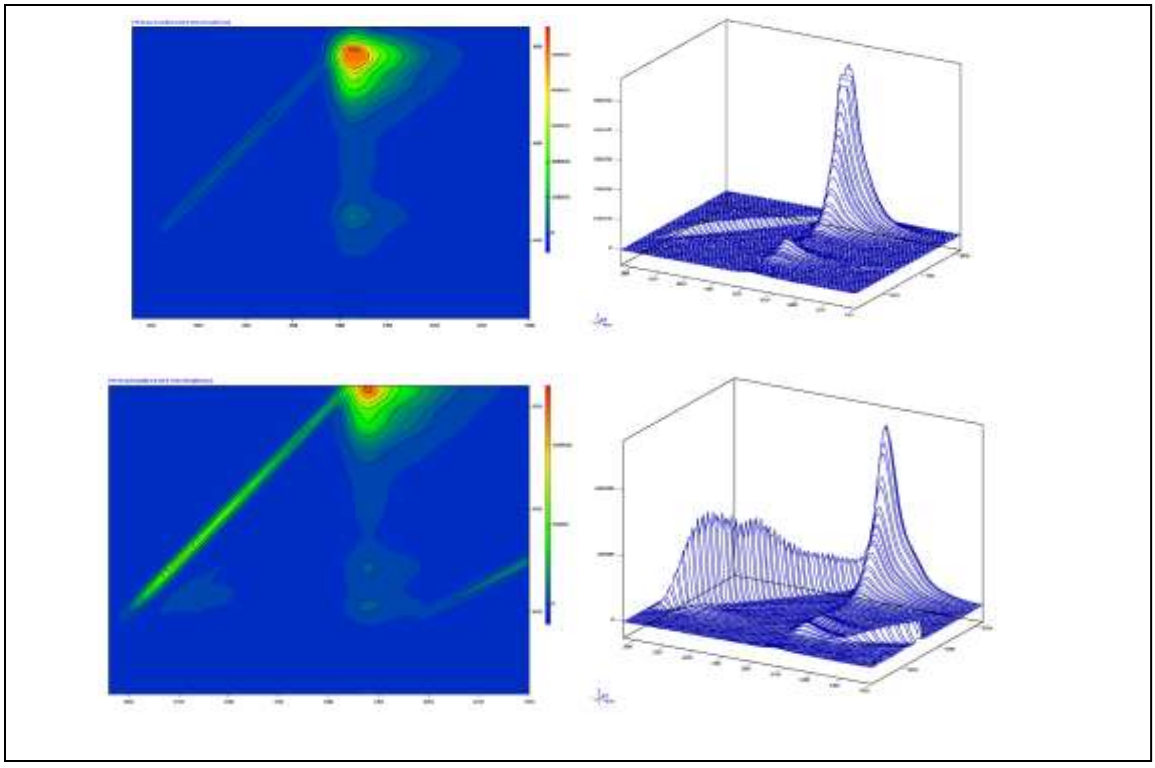

Figure 27: Comparison of fluorescein 100 ppb and eosin 100 ppb single dye dilution EEMs and contour diagrams. *X*-axis range = 280 - 700 is nm, *y*-axis range = 220 – 520 nm.

The 100 PPB EO EEM/contour diagram displays a very similar pattern, with one exception: the 100 PPB EO EEM/ contour diagram displays *three* fluorescence centers. The three fluorescence centers displayed in the 100 PPB EO EEM/contour diagram occur at λ_{Ex} = 446 – 594 nm, λ_{Em} = 510 – 630 (primary fluorescence center), λ_{Ex} = 338 – 352 nm, λ_{Em} = 534 – 546 (long Ex wavelengths secondary fluorescence center), and λ_{Ex} = 300 – 312 nm, λ_{Em} = 530 – 550 (short Ex wavelengths secondary fluorescence center). The primary fluorescence center is intersected by the long Ex wavelength boundary of the graph space through the highest intensity center. Therefore, the longest Ex wavelength boundary of the primary EO fluorescence center is an approximation. The longest Em boundary of the southernmost secondary fluorescence center is also an approximation because the fluorescence center is intersected and skewed by scattered light. The presence of three, rather than two, fluorescence centers in EO EEMs and contour

diagrams produced through three-dimensional synchronous scanning may serve as an additional measure to distinguish FL from EO in aqueous dye trace samples.

The same characteristics used to differentiate FL and EO through both two and three-dimensional synchronous scanning may also be used to differentiate between RWT and SRB (locations of λ_{Ex} and λ_{Em} minima and maxima). Qualitative inspection of the shapes of the RWT and SRB fluorescence centers is not applicable in the examination of the RWT and SRB EEMs/contour diagrams largely because the primary fluorescence centers of the dyes are intersected by the longest Ex wavelength boundary of the graph so that only half or slightly less than half of the primary fluorescence centers are displayed in the EEMs/contour diagrams produced through the course of this research. The locations of the primary fluorescence centers are approximated by extrapolating the visible fluorescence centers into the longer Ex wavelengths as previously explained. The approximate locations of the RWT and SRB primary fluorescence centers are λ_{Ex} = 458 – 582 nm, λ_{Em} = 545 – 680 nm and λ_{Ex} = 462 – 578 nm, λ_{Em} = 535 – 680 nm, respectively. Note that the SRB primary fluorescence center is more severely truncated by the longest Ex wavelength boundary, so it is quite likely that the SRB λ_{Ex} is actually shifted toward longer wavelengths than reflected by the λ_{Ex} given here.

It is also difficult to discriminate between RWT and SRB EEMs/contour diagrams by qualitative interpretations because the portions of the EEMs/contour diagrams that may be seen are remarkably similar (Figure 28). The shape of the primary fluorescence centers seems to be identical and both dyes exhibit three secondary fluorescence centers at similar λ_{Ex} and λ_{Em} (see Table 17). No fluorescence features were identified through the application of three-dimensional synchronous scanning that might enhance

identification of RWT and SRB in dye trace samples apart from those features that are routinely used through two-dimensional synchronous scanning to identify fluorescent dyes.

6.2 Mixed Dye Dilution EEMs and Contour Diagrams

Mixed dye dilution synchronous scans and EEMs/contour diagrams are briefly discussed and summarized in the Results section. This section includes a comprehensive discussion of the mixed dye dilution EEMs/contour diagrams, including 1) comparison of synchronous scans and EEMs/contour diagrams of the mixed dye dilutions, 2) determination of fluorescence center locations, 3) identification of fluorescent dyes via fluorescence center locations where applicable, and 4) identification of any benefits of

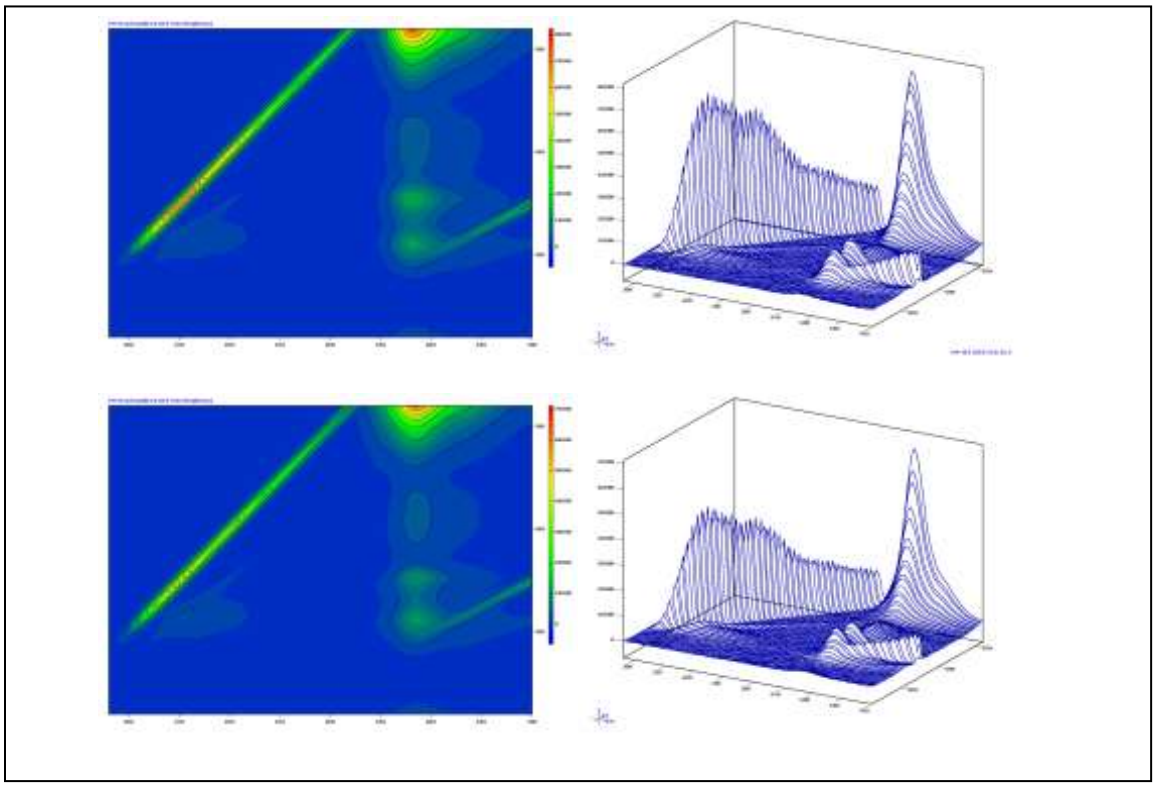

Figure 28: Comparison of rhodamine WT 100 ppb and sulphorhodamine B 100 ppb single dye dilution EEMs and contour diagrams. *X*-axis range = 280 - 700 is nm, *y*-axis range = 220 – 520 nm.

three-dimensional synchronous scanning as compared to two-dimensional synchronous scanning in the discrimination of fluorescent dyes in mixed dye dilutions.

6.2.1 FLEO 1:1 and FLEO 1:10

The two-dimensional synchronous scans of FLEO 1:1 and FLEO 1:10 display EO (Figure 29) as a shoulder on the FL fluorescence peak. The EEMs/contour diagrams of FLEO 1:1 and FLEO 1:10 each display one characteristic, low-intensity fluorescence center. No artifacts are present in the EEM/contour diagrams that might be comparable to the EO shoulder on the FL fluorescence peak displayed in the synchronous scan.

The primary fluorescence centers of FLEO 1:1 and FLEO 1:10 occur at λ_{Ex} = 464 – 510 nm, λ_{Em} = 498 – 548 nm and λ_{Ex} = 452 – 568 nm, λ_{Em} = 495 – 600 nm, respectively. The long wavelength Ex boundaries were determined by approximation since the long Ex boundary of the graph space intersects the primary fluorescence center above or through the highest intensity center. The shortest Em wavelength boundaries were also determined by approximation since the primary fluorescence centers are intersected and badly skewed by scattered light.

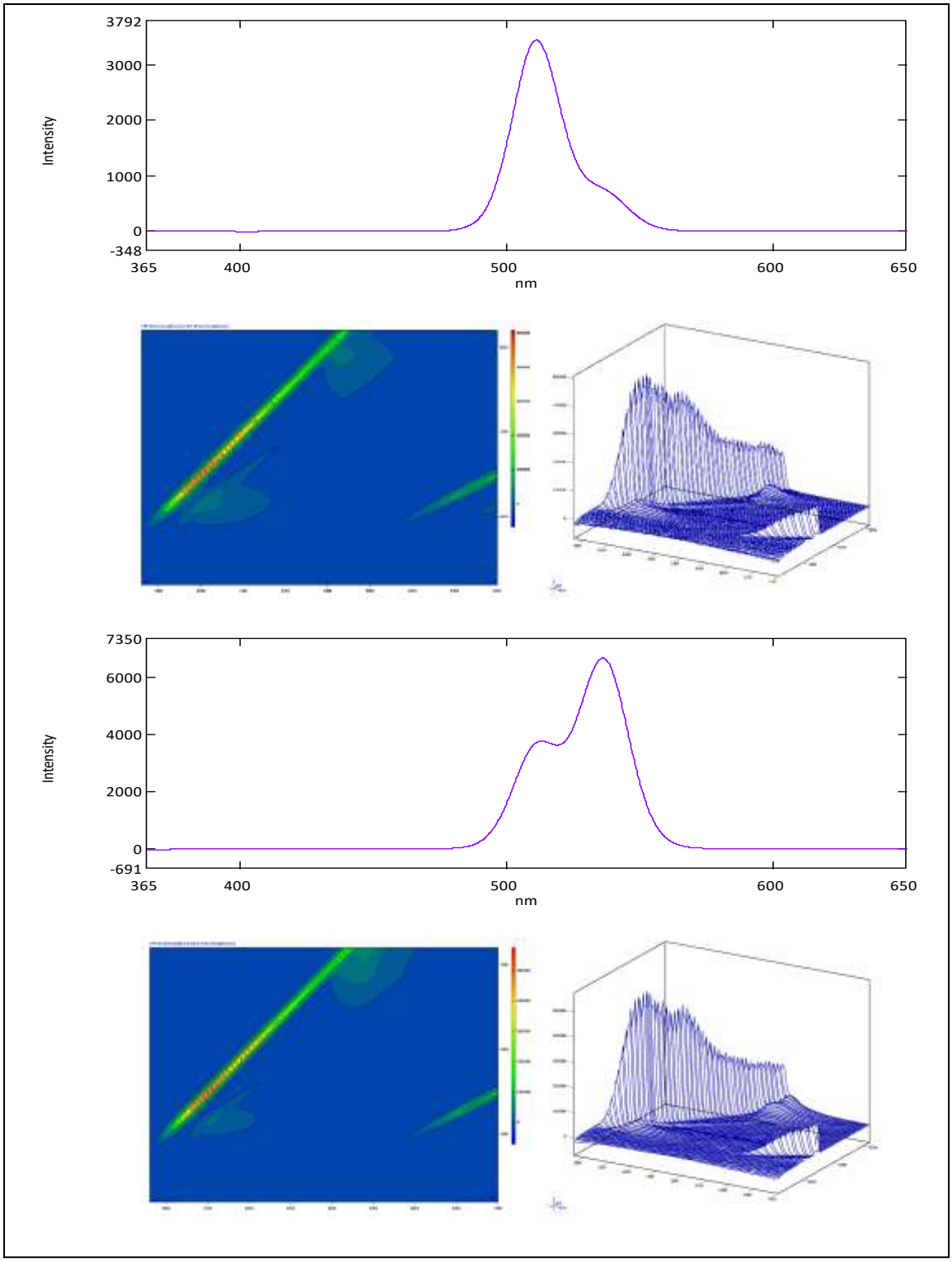

Figure 29: Comparison of FLEO 1:1 (top two rows) and FLEO 1:10 (bottom two rows) two-dimensional and three-dimensional synchronous scans. EEM and contour diagram *x*-axis range = 280 - 700 is nm, *y*-axis range = 220 – 520 nm.

The FLEO 1:1 primary fluorescence center does not correspond closely to the FL

or EO primary or secondary fluorescence centers. The FLEO 1:1 primary fluorescence center most closely corresponds to the single dilution FL and EO primary fluorescence centers, but even so the FLEO 1:1 primary fluorescence center λ_{Em} and λ_{Ex} minima and maxima are sometimes more than 50 nm from the location of FL and EO single dilution primary fluorescence centers.

The FLEO 1:10 primary fluorescence center does not correspond closely to the single dilution FL or EO primary or secondary fluorescence centers, though it corresponds the most closely to the single dilution FL and EO primary fluorescence centers. However, the FLEO 1:10 primary fluorescence center λ_{Em} and λ_{Ex} minima and maxima are sometimes more than 40 nm from the location of FL and EO single dilution primary fluorescence centers.

The characteristic fluorescence centers displayed in these EEMs/contour diagrams do not exhibit the usual shape observed in FL and EO single dye dilution fluorescence centers, but no specific qualitative fluorescence center characteristics seem sufficiently unique to distinguish FL from EO in these mixed dye dilution EEMs/contour diagrams.

6.2.2 FLEO 1:100

The FLEO 1:100 synchronous scan displays 1 ppb FL entirely absorbed by the 100 ppb EO fluorescence peak. Likewise, the EEM/contour diagram of FLEO 1:100 displays a single high intensity fluorescence center that is intersected and skewed by scattered light. The fluorescence center does not display the pattern typically displayed by FL and EO single dilution EEMs/contour diagrams. The EEM/contour diagram also displays two secondary fluorescence centers that are not continuous with the primary

fluorescence center and that are not intersected by scattered light. The two secondary fluorescence centers are continuous with one another.

The FLEO-1-100 primary fluorescence center occurs (Figure 30) at λ_{Ex} = 388 – 652 nm, λ_{Em} = 496 – 665 nm. The long wavelength Ex boundary of the primary fluorescence center λ_{Ex} was determined by approximation because the long wavelength Ex boundary of the graph space intersects the fluorescence center. The secondary fluorescence centers occur at λ_{Ex} = 288 – 322 nm, λ_{Em} = 516 – 585 nm (secondary fluorescence center *a*) and λ_{Ex} = 322 – 368 nm, λ_{Em} = 517 – 584 nm (secondary fluorescence center *b*).

The FLEO1:100 primary fluorescence center does not correspond closely to the FL or EO primary or secondary fluorescence centers. It corresponds the most closely to the FL and EO primary fluorescence centers, but even this correspondence is very limited (the FLEO 1:100 fluorescence center varies by up to 70 nm from the locations of single dilution FL and EO primary fluorescence centers). The primary fluorescence center also spans a broader λ_{Ex} and λ_{Em} than single dilution FL and EO primary fluorescence centers.

Secondary fluorescence center *a* does not correspond closely to any of the single dilution FL or EO primary or secondary fluorescence centers. Of these, secondary fluorescence center *a* corresponds the most closely to the single dilution FL secondary and single dilution EO tertiary fluorescence centers, but its location differs by up to 49 nm from the locations of these centers. Secondary fluorescence center *b* corresponds the most closely to the single dilution EO secondary fluorescence center, though a discrepancy up to 18 nm exists between the locations of these fluorescence centers. The

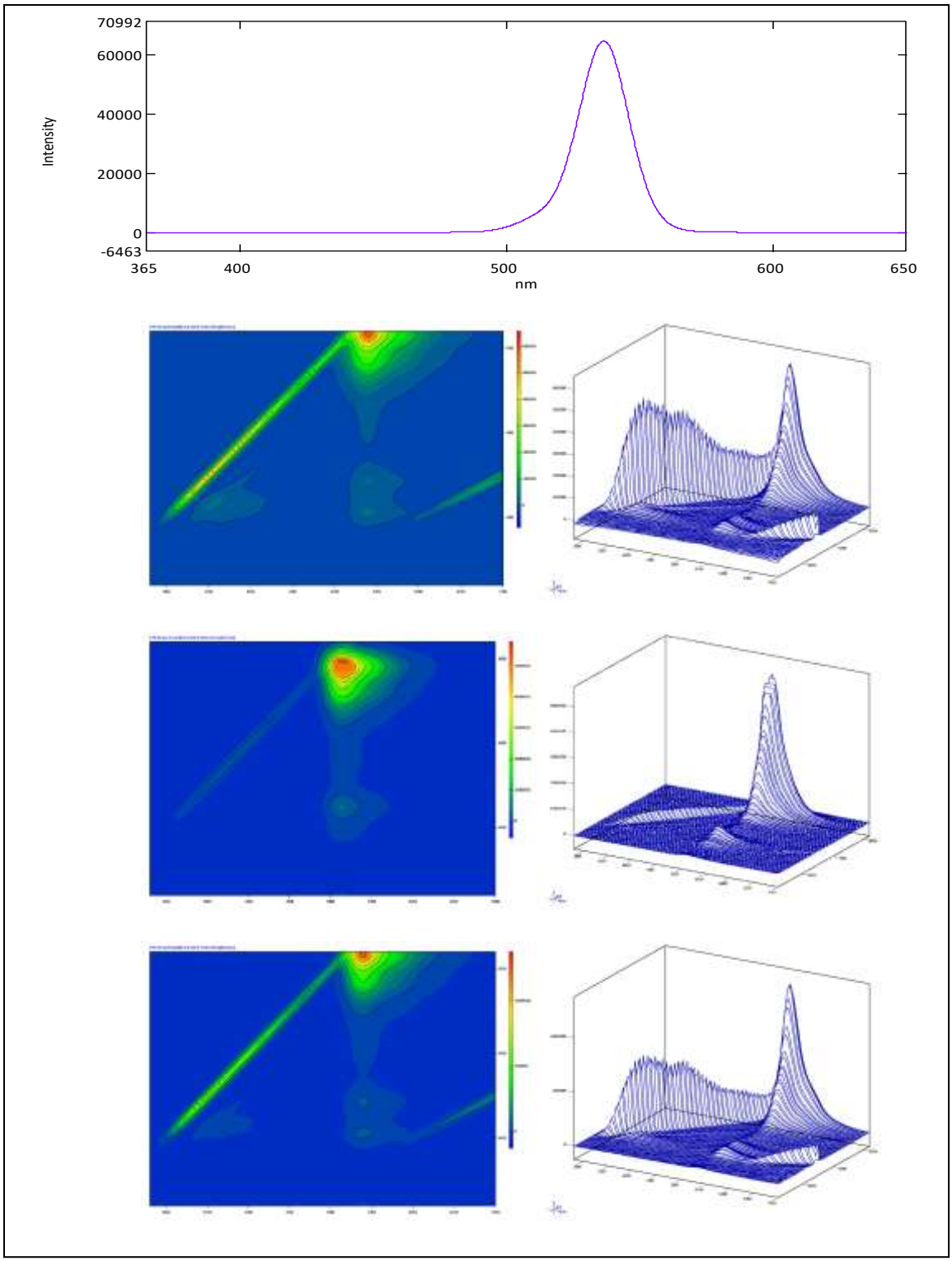

Figure 30: Comparison of FLEO 1:100 two and three-dimensional synchronous scans (top two rows), fluorescein 100 ppb single dye dilution EEMs and contour diagrams, and eosin 100 ppb single dye dilution EEMs and contour diagrams. EEM and contour diagram *x*-axis range = 280 - 700 is nm, *y*-axis range = 220 – 520 nm.

comparatively minimal 18 nm difference between the locations of single dilution EO secondary fluorescence center and secondary fluorescence center *b* likely indicates that the mixed dilution is compositionally dominated by EO. An overwhelming presence of FL would likely cause the secondary fluorescence center to be shifted more closely toward the position of single dilution FL secondary fluorescence centers. Instead, secondary fluorescence center *b* is more closely associated with the single dilution EO secondary fluorescence center.

No specific qualitative fluorescence center characteristics seem sufficiently unique to distinguish FL from EO in this mixed dye dilution EEMs/contour diagrams. However, three-dimensional synchronous scanning may offer one benefit to discriminating FL and EO present in a mixed dilution that two-dimensional synchronous scanning does not. Based on the relative locations of primary and secondary fluorescence centers, it is possible to determine whether FL or EO compositionally dominate the mixed dilution. By evaluating the correspondence of the location of the secondary fluorescence centers with the location of single dilution fluorescent dye secondary fluorescence centers, it is possible to determine if the mixed dilution is more heavily influenced by the presence of one fluorescent dye than another.

6.2.3 FLEO 10:1

The FLEO 10:1 synchronous scan displays 1 ppb EO entirely absorbed by the FL fluorescence peak due to FL's higher quantum yield. Likewise, the EEM/contour diagram displays one primary fluorescence center that is almost entirely within the graph space

and intersected by scattered light. The primary fluorescence center does not exhibit the fluorescence center shape usually observed in single dilution FL and EO EEMs/contour diagrams. The EEM/contour diagram also displays a secondary fluorescence center that is continuous with the primary fluorescence center by way of a low-intensity fluorescence pattern and is not intersected by scattered light.

The FLEO 10:1 primary fluorescence center is located at λ_{Ex} = 406 – 578 nm, λ_{Em} = 480 – 649 nm. The upper Ex boundary of the λ_{Ex} was determined by approximation because the longest Ex boundary of the graph space intersects the highest intensity fluorescence center. It was necessary to determine the shortest λ_{Em} boundary of the primary fluorescence center by approximation as well due to the interference of scattered light which causes skew of the fluorescence center. The FLEO 10:1 secondary fluorescence center is located at λ_{Ex} = 284 – 360 nm, λ_{Em} = 489 – 579 nm.

The FLEO 10:1 primary fluorescence center (Figure 31) does not correspond closely to the FL or EO primary or secondary fluorescence centers. Of these, the primary fluorescence center corresponds the most closely to the single dilution FL and EO primary fluorescence centers, though it differs in location by up to 56 nm from the FL primary fluorescence center and by up to 40 nm from the EO primary fluorescence center. The FLEO 10:1 secondary fluorescence center does not closely correspond to the single dilution FL or EO primary or secondary fluorescence centers. The secondary fluorescence centers differs in location by up to 43 nm from the single dilution FL secondary fluorescence center and by up to 48 nm from the single dilution EO tertiary fluorescence center. No specific qualitative fluorescence center characteristics seem

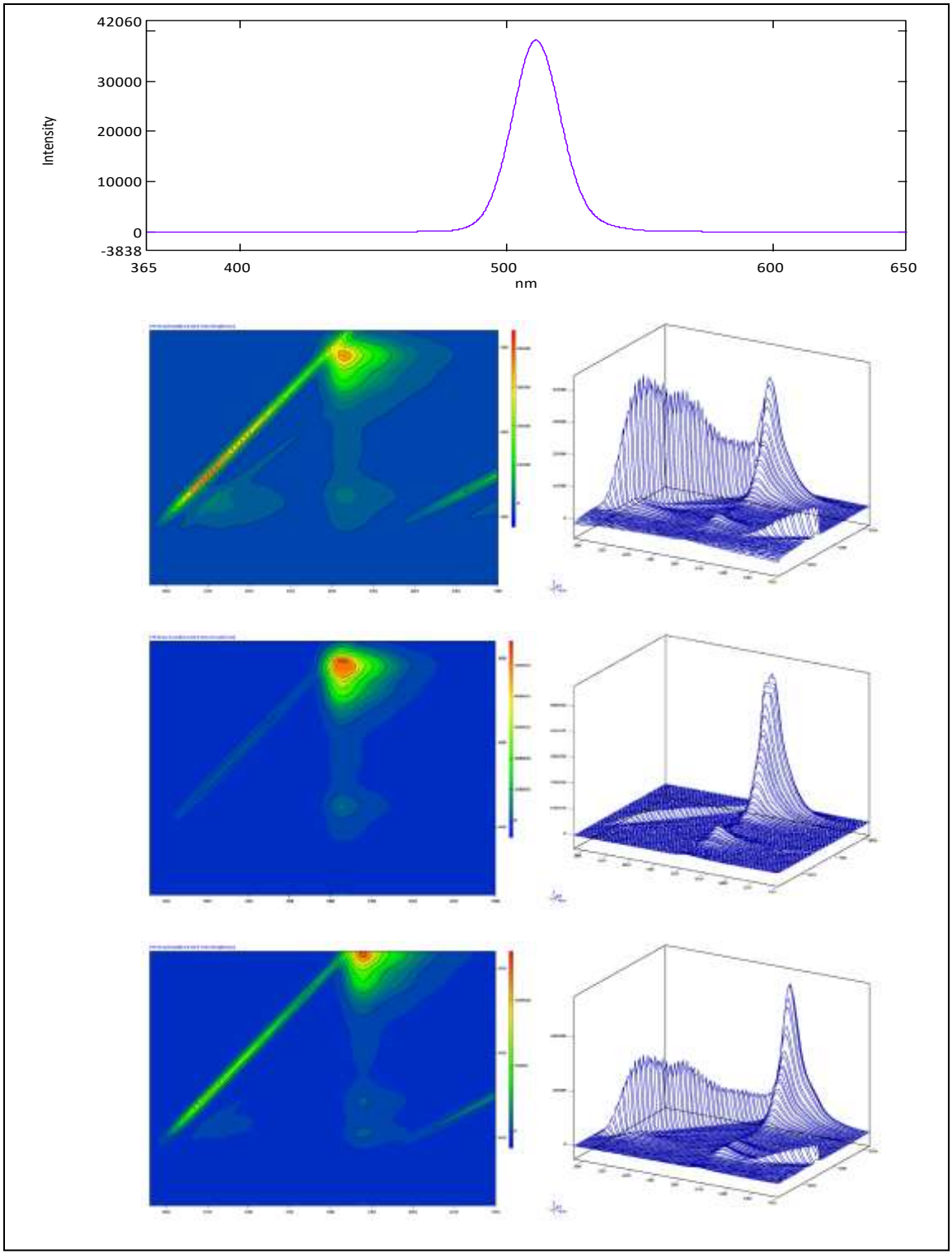

Figure 31: Comparison of FLEO 10:1 two and three-dimensional synchronous scans (top two rows), fluorescein 100 ppb single dye dilution EEMs and contour diagrams (third row from top), and eosin 100 ppb single dye dilution EEMs and contour diagrams (bottom row). EEM and contour diagram *x*-axis range = 280 - 700 is nm, *y*-axis range = 220 – 520 nm.

sufficiently unique to distinguish FL from EO in this mixed dye dilution EEMs/contour

diagrams.

6.2.4 FLEO 10:10

The FLEO 10:10 synchronous scan (Figure 32) displays EO as a small shoulder on the larger FL fluorescence peak and peak area is shared between the two dyes. No artifacts are present in the FLEO 10:10 EEM/contour diagram that might be comparable to the EO shoulder on the FL fluorescence peak displayed in the synchronous scan. Instead, the FLEO 10:10 EEM/contour diagram is remarkably similar to the FLEO 10:1 EEM/contour diagram and displays a primary fluorescence center that is almost entirely within the graph space and is intersected by scattered light. The primary fluorescence center does not exhibit the fluorescence center shape usually observed in single dilution FL and EO EEMs/contour diagram. The EEM/contour diagram also displays a secondary fluorescence center that is not continuous with the primary fluorescence center, nor is it intersected by scattered light.

The FLEO 10:10 primary fluorescence center is located at λ_{Ex} = 406 – 578 nm, λ_{Em} = 480 – 640 nm. The longest Ex wavelength boundary of the λ_{Ex} was determined by approximation because the longest Ex wavelength boundary of the graph space intersects the fluorescence center. The shortest Em wavelength λ_{Em} boundary of the primary fluorescence center was determined by approximation as well, as necessitated by scattered light interference and the resultant skew of the fluorescence center. The FLEO 10:10 secondary fluorescence center occurs at λ_{Ex} = 288 – 360 nm, λ_{Em} = 493 – 571 nm.

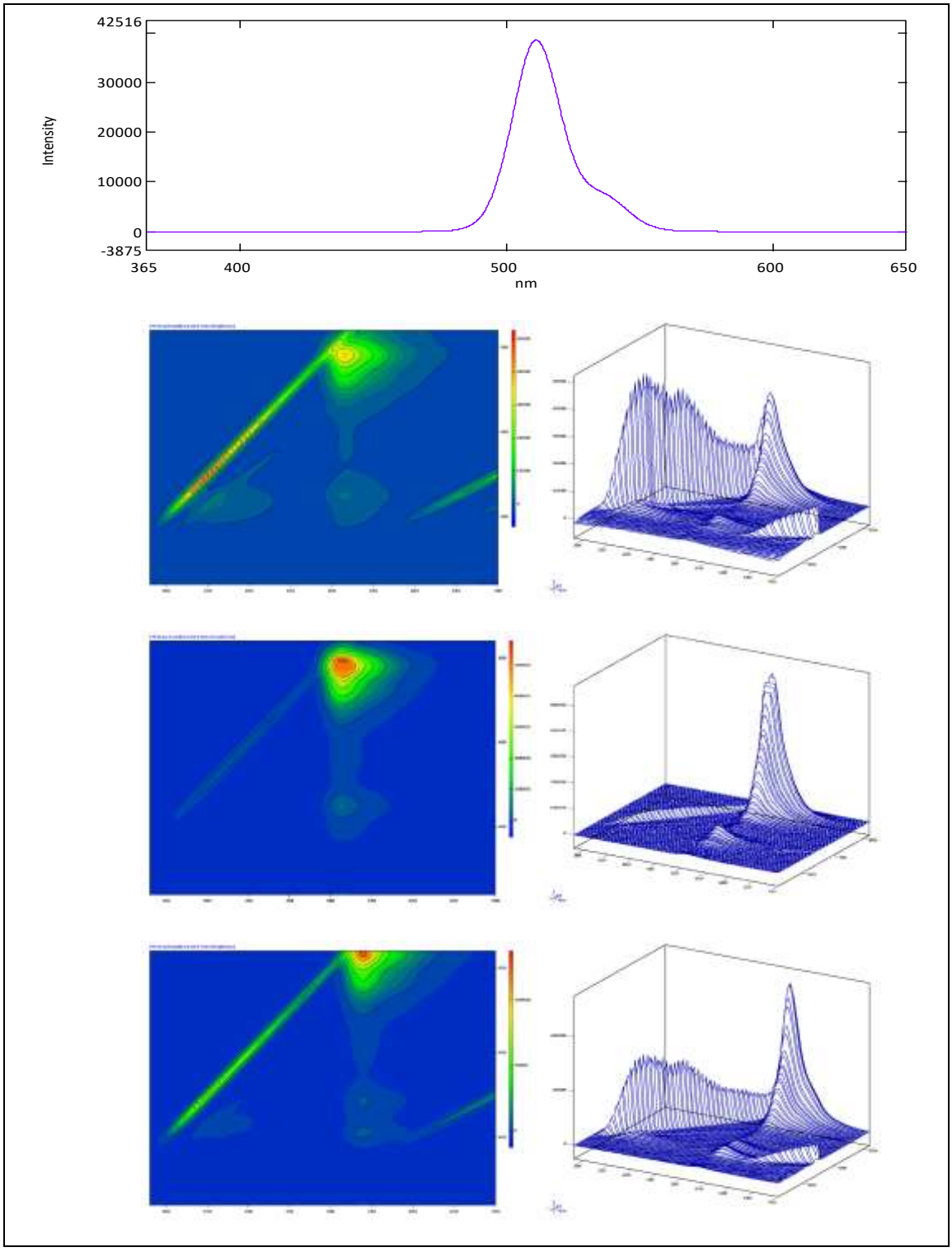

Figure 32: Comparison of FLEO 10:10 two and three-dimensional synchronous scans (top two rows), fluorescein 100 ppb single dye dilution EEMs and contour diagrams (third row from top), and eosin 100 ppb single dye dilution EEMs and contour diagrams (bottom row). EEM and contour diagram *x*-axis range = 280 - 700 is nm, *y*-axis range = 220 – 520 nm.

The FLEO 10:10 primary fluorescence center corresponds to the FLEO 10:1 primary fluorescence center to within 10 nm. The FLEO 10:10 primary fluorescence center does not correspond closely to the single dilution FL or EO primary or secondary fluorescence centers. Of these, the primary fluorescence center corresponds the most closely to the single dilution FL and EO primary fluorescence centers, though it differs in location by up to 56 nm from the FL primary fluorescence center and by up to 40 nm from the EO primary fluorescence center. The FLEO 10:10 secondary fluorescence center corresponds to the location of the FLEO 10:1 secondary fluorescence center to within 9 nm. The secondary fluorescence center does not closely correspond to the single dilution FL or EO primary or secondary fluorescence centers. The secondary fluorescence center varies by up to 35 nm from the single dilution FL secondary fluorescence center and by up to 48 nm from the single dilution EO tertiary fluorescence center.

Although the FLEO 10:1 and FLEO 10:10 primary fluorescence centers occur at very similar λ_{Ex} and λ_{Em} (to within 10 nm), as do the secondary fluorescence centers (to within 9 nm), no specific qualitative fluorescence center characteristics seem sufficiently unique to distinguish FL from EO in this mixed dye dilution EEMs/contour diagram.

6.2.5 FLEO 10:100

The FLEO 10:100 synchronous scan displays FL and EO as components of a bimodal peak where EO is the highest intensity peak. The FLEO 10:100 EEM/contour diagram does not seem to display the same bimodal fluorescence center trend but the shape of the FLEO 10:100 primary fluorescence pattern is especially unique, even as compared to the FL-EO mixed dye dilution EEM/contour diagrams, all of which have

exhibited primary fluorescence center patterns that differ from those exhibited by FL and EO single dilutions EEMs/contour diagrams. The primary fluorescence pattern appears to exhibit a “bean” shape, at least in the lower (visible) portion of the primary fluorescence center. The primary fluorescence center is intersected by the long wavelength Ex boundary of the graph space above the highest intensity center and is not intersected by scattered light. The FLEO 10:100 EEM/contour diagram also displays two secondary fluorescence centers that are nearly joined into a single secondary fluorescence center. The secondary fluorescence centers are not continuous with the primary fluorescence center.

The primary fluorescence center displayed in the FLEO 10:100 EEM/contour diagram (Figure 33) is located at λ_{Ex} = 388 – 652 nm, λ_{Em} = 495 – 655 nm. The longest wavelength Ex boundary of the λ_{Ex} was determined by approximation because the longest Ex boundary of the graph space intersects the highest intensity fluorescence center. The shortest wavelength λ_{Em} boundary of the primary fluorescence center was necessarily determined by approximation as well due to the interference of scattered light which causes skew of the fluorescence center toward shorter Em wavelengths. The secondary fluorescence centers are located at λ_{Ex} = 288 – 318 nm, λ_{Em} = 510 – 579 nm (secondary fluorescence center *c*) and λ_{Ex} = 318 – 368 nm, λ_{Em} = 499 – 575 nm (secondary fluorescence center *d*).

The FLEO 10:100 primary fluorescence center does not correspond closely to the FL or EO primary or secondary fluorescence centers. Of these, the primary fluorescence center corresponds the most closely to the single dilution FL and EO primary fluorescence centers, though it differs in location by up to 130 nm from the FL primary

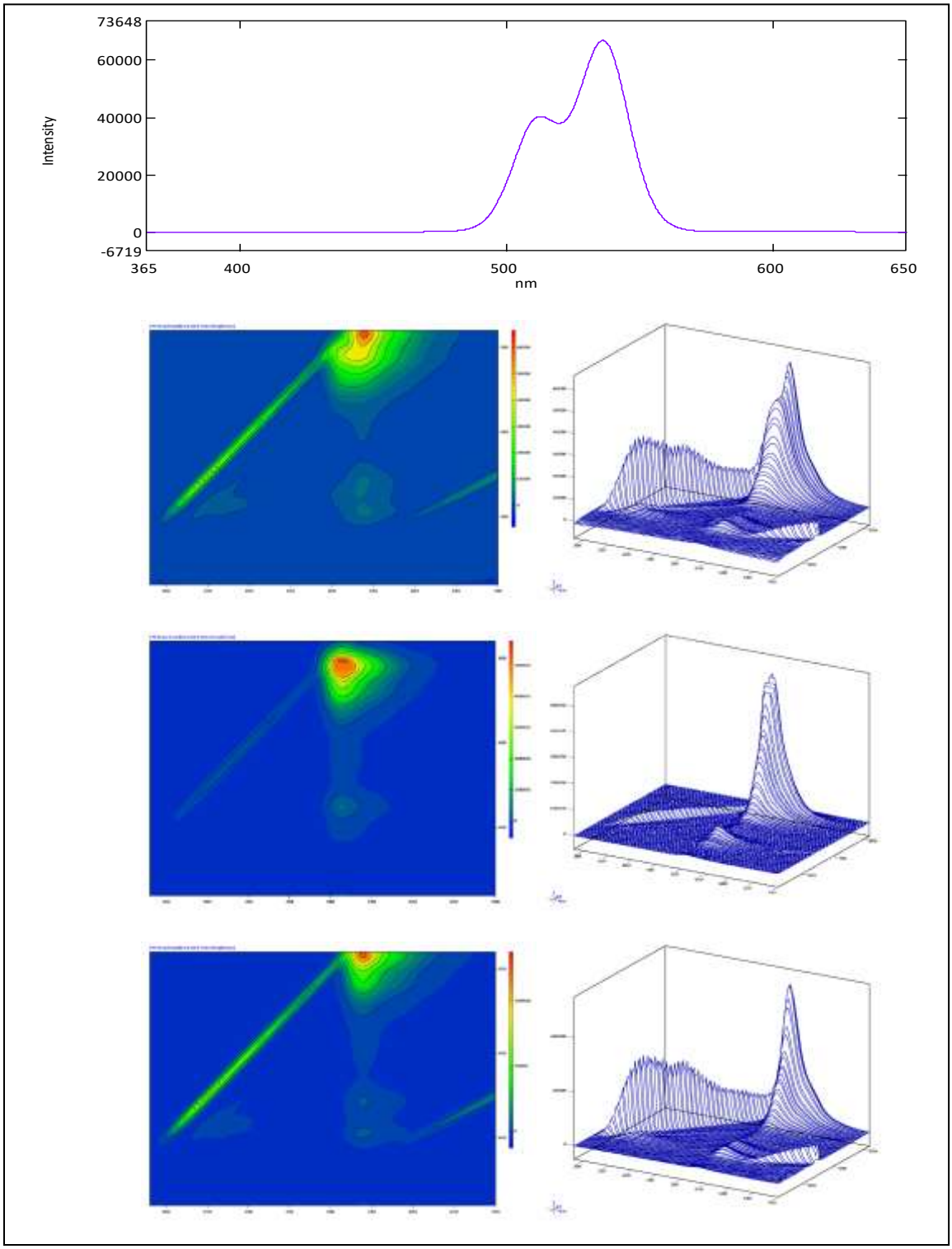

Figure 33: Comparison of FLEO 10:100 two and three-dimensional synchronous scans (top two rows), fluorescein 100 ppb single dye dilution EEMs and contour diagrams (third row from top), and eosin 100 ppb single dye dilution EEMs and contour diagrams (bottom row). EEM and contour diagram *x*-axis range = 280 - 700 is nm, *y*-axis range = 220 – 520 nm.

fluorescence center and by up to 58 nm from the EO primary fluorescence center. Secondary fluorescence center *c* does not correspond closely to the single dilution FL or EO primary or secondary fluorescence centers. Secondary fluorescence center *c* varies by up to 43 nm from the single dilution FL secondary fluorescence center and by up to 29 nm from the single dilution EO tertiary fluorescence center. Secondary fluorescence center *d* does not closely correspond to the single dilution FL or EO primary or secondary fluorescence centers and varies by up to 39 nm from the single dilution FL secondary fluorescence center and by up to 56 nm from the single dilution EO tertiary fluorescence center.

No specific qualitative fluorescence center characteristics seem sufficiently unique to distinguish FL from EO in this mixed dye dilution EEM/contour diagram. However, if future work utilized longer λ_{Ex} to investigate the interesting "bean" shape of the primary fluorescence center, it may be that the uniquely-shaped primary fluorescence center could provide insight that would allow discrimination of the FL and EO fluorescent dyes in the FLEO 10:100 mixed dye dilution.

6.2.6 RWTSRB 1:1, RWTSRB 1:10, RWTSRB 1:100, RWTSRB 10:1, RWTSRB 10:10, and RWTSRB 10:100

The RWTSRB 1:1, RWTSRB 1:10, RWTSRB1:100, RWTSRB 10:1, RWTSRB 10:10, and RWTSRB 10:100 synchronous scans display RWT and SRB as a single, indistinguishable peak.

6.2.7 RWTSRB 1:1 and RWTSRB 1:10

The RWTSRB 1:1 EEM/contour diagram is dominated by scattered light and does not capture the fluorescent dyes RWT or SRB. The RWTSRB 1:10 EEM/contour diagram captures only the shortest λ_{Ex} boundary of a fluorescence center and does not meaningfully capture the RWT or SRB fluorescent dyes.

6.2.8 RWTSRB 1:100

The RWTSRB 1:100 synchronous scan (Figure 34) display RWT and SRB as a single, indistinguishable peak. The RWTSRB 1:100 EEM/contour diagram captures the shorter wavelength portion of the λ_{Ex} of what is likely the primary fluorescence center and two secondary fluorescence centers. A third secondary fluorescence center is also displayed but does not exhibit fluorescence intensity greater than that which unites continuous primary and fluorescence centers. Therefore, it is not regarded as a true fluorescence center. The EEM/contour diagram displays added fluorescence artifacts that are not visible in the corresponding synchronous scan.

The primary fluorescence center of RWTSRB 1:100 is truncated by the longer Ex wavelength boundary of the graph space likely below the highest intensity fluorescence center. It is therefore difficult to state with any accuracy the approximate location or shape of the primary fluorescence center. The secondary fluorescence centers are located at λ_{Ex} = 288 – 332 nm, λ_{Em} = 565 – 610 nm (secondary fluorescence center *e*) and λ_{Ex} = 332 – 366 nm, λ_{Em} = 566 – 616 nm (secondary fluorescence center *f*). The long Em wavelength boundary of second fluorescence center *e* was determined by approximation

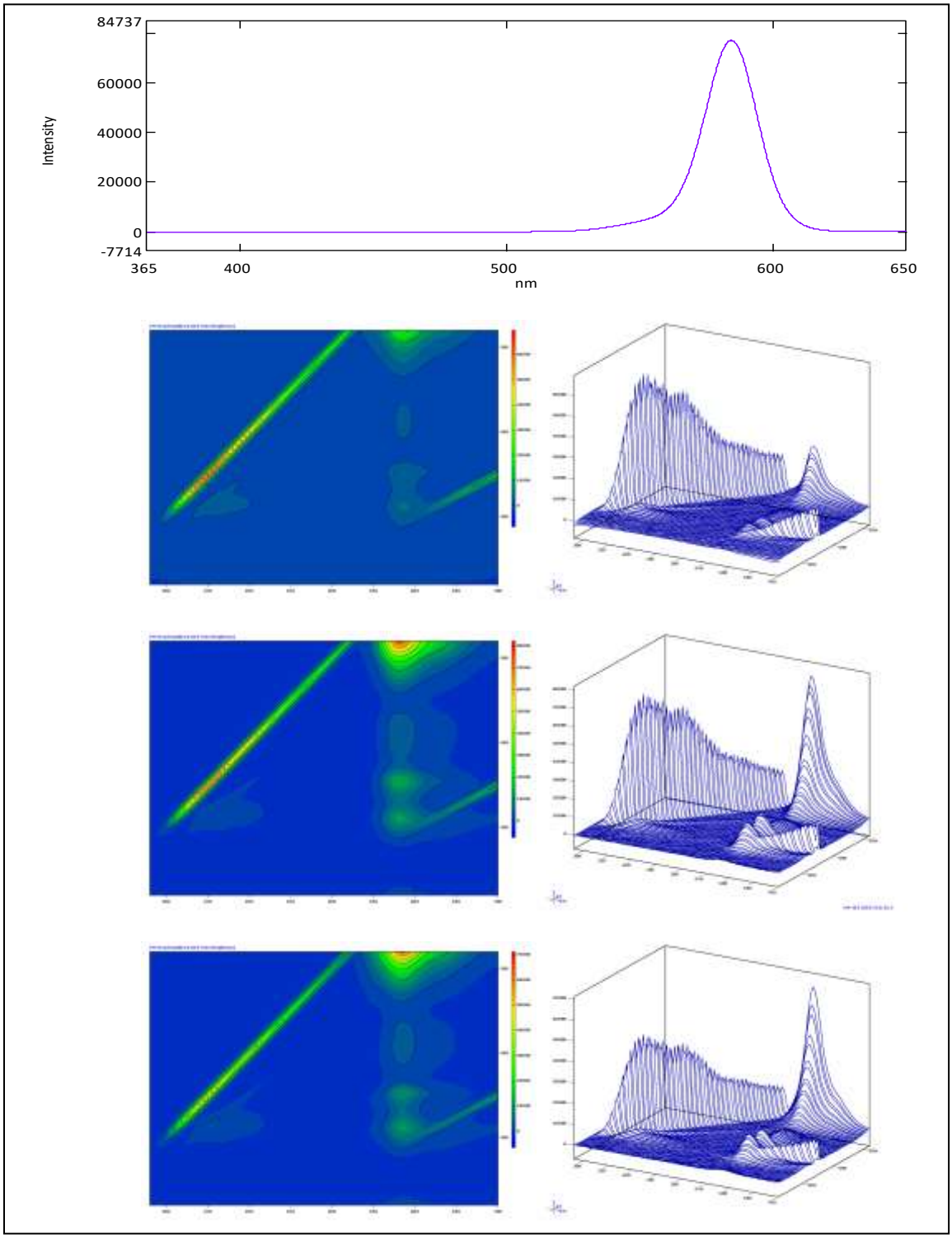

Figure 34: Comparison of RWTSRB 1:100 two and three-dimensional synchronous scans (top two rows), rhodamine WT 100 ppb single dye dilution EEM and contour diagram (third row from top), and sulphorhodamine B 100 ppb single dye dilution EEM and contour diagram (bottom row). EEM and contour diagram *x*-axis range = 280 - 700 is nm, *y*-axis range = 220 – 520 nm.

because the fluorescence center is intersected by scattered light along the longer Em wavelengths.

Although very little may be said about the primary fluorescence center due to the very limited view displayed in the EEM/contour diagram, secondary fluorescence center *e* corresponds nearly exactly (to within 2 nm) of the position of the quaternary SRB fluorescence center. Secondary fluorescence center *f* corresponds to the tertiary SRB fluorescence center to within 5 nm. Secondary fluorescence center *e* and *f* are likely attributable to the 100 ppb SRB component of the RWTSRB 1:100 mixed dilution. No attributes of the RWTSRB 1:100 EEM/contour diagram seem to aid in discrimination of the 1 ppb RWT from the 100 ppb SRB, though the location of secondary fluorescence centers *e* and *f* allow the identification of SRB in the mixed dilution even though the primary fluorescence center is only partially in view in the EEM/contour diagram.

6.2.9 RWTSRB 10:1 and RWTSRB 10:10

The RWTSRB 10:1 and RWTSRB 10:10 EEMs/contour diagrams capture the shorter wavelength portion of the λ_{Ex} of what is likely the primary fluorescence center, as well as what may be considered three secondary fluorescence centers. However, these secondary fluorescence centers do not exhibit fluorescence intensity greater than that which unites continuous primary and fluorescence centers in FL and EO EEMs/contour diagrams. Therefore, the three secondary fluorescence center patterns will not be considered true fluorescence centers. Due to the limited view of the primary fluorescence

center and the low intensity of the three secondary fluorescence centers, little information may be gleaned from the RWTSRB 10:1 and RWTSRB 10:10 EEMs/contour diagrams.

6.2.10 RWTSRB 10:100

The RWTSRB 10:100 EEM/contour diagram captures the shorter wavelength portion of the λ_{Ex} of what is likely the primary fluorescence center, as well as two secondary fluorescence centers that are continuous with the primary fluorescence center by a low intensity fluorescence pattern. The primary fluorescence center is truncated by the upper Ex wavelength boundary of the graph space likely below the highest intensity fluorescence center. It is therefore difficult to state with any accuracy the approximate location or shape of the primary fluorescence center. Even so, it is clear that the primary fluorescence center is intersected and skewed by scattered light. The secondary fluorescence centers are located at λ_{Ex} = 292 – 332 nm, λ_{Em} = 565 – 610 nm (secondary fluorescence center *g*) and λ_{Ex} = 332 – 366 nm, λ_{Em} = 566 – 608 nm (secondary fluorescence center *h*). The long Em wavelength boundary of second fluorescence center *g* was determined by approximation because the fluorescence center is intersected by scattered light along the longer Em wavelengths.

Although very little may be said about the RWTSRB 10:100 EEM/contour diagram (Figure 35) primary fluorescence center due to the very limited view displayed in the EEM/contour diagram, secondary fluorescence center *g* corresponds to the quaternary SRB fluorescence center to within 5 nm and secondary fluorescence center *h* corresponds to the tertiary SRB fluorescence center to within 3 nm, apart from the long Em wavelength boundary. The 12 nm discrepancy between the long Em wavelength

boundary of the tertiary SRB fluorescence center and secondary fluorescence center *h* is likely due to interference and skew of secondary fluorescence center *h* caused by

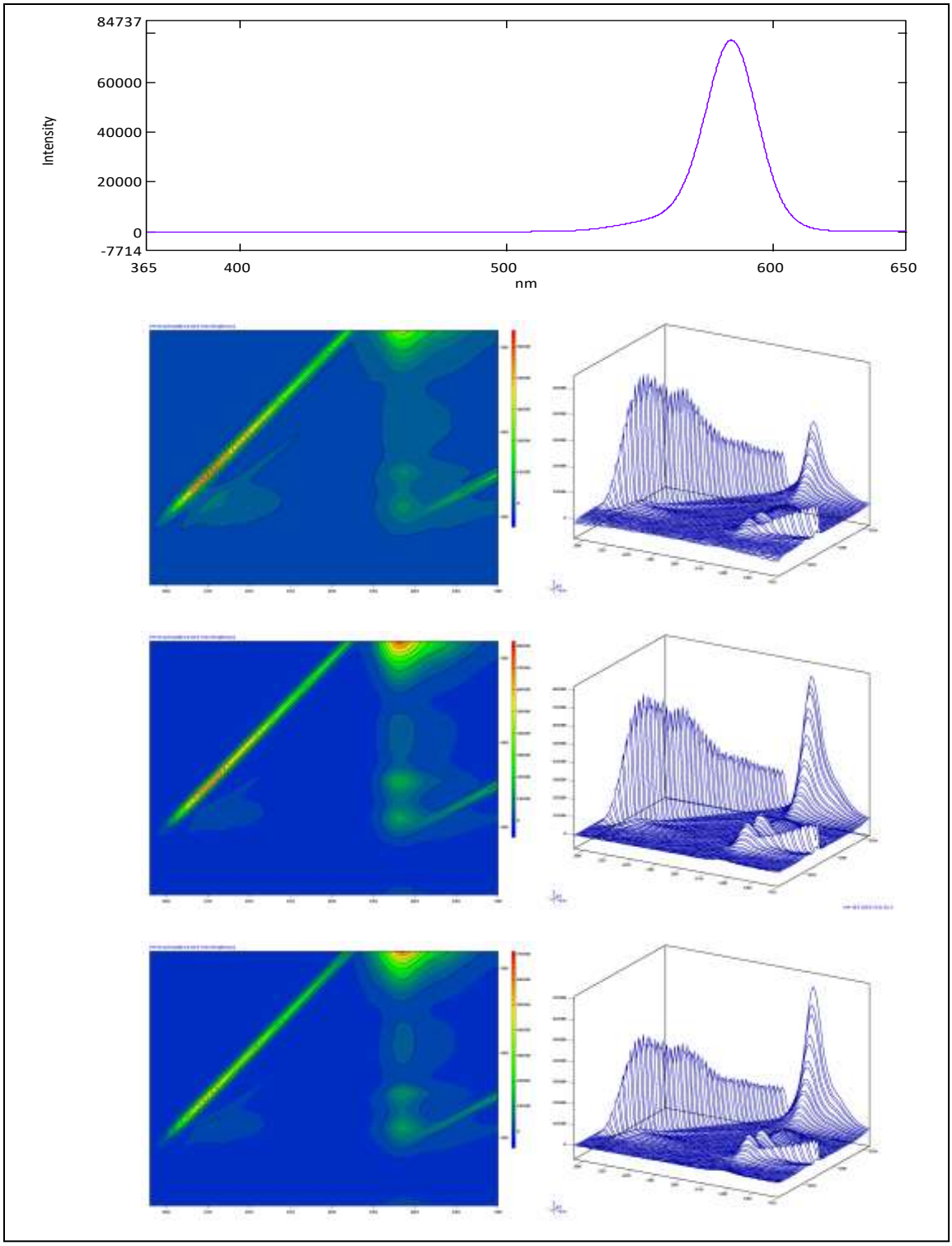

Figure 35: Comparison of RWTSRB 10:100 two and three-dimensional synchronous scans (top two rows), rhodamine WT 100 ppb single dye dilution EEM and contour diagram (third row from top), and sulphorhodamine B 100 ppb single dye dilution EEM and contour diagram (bottom row). EEM and contour diagram *x*-axis range = 280 - 700 is nm, *y*-axis range = 220 – 520 nm.

scattered light. Secondary fluorescence center *h* may reasonably be imagined to match the tertiary SRB fluorescence center more closely if scattered light patterns are abated. No attributes of the RWTSRB 1:100 EEM/contour diagram seem to aid in discrimination of the 1 ppb RWT from the 100 ppb SRB, though the location of secondary fluorescence centers *g* and *h* allow the identification of SRB in the mixed dilution even though the primary fluorescence center is only partially in view in the EEM/contour diagram.

6.2.11 RWTSRB 100:1

The RWTSRB 100:1 synchronous scan displays RWT and SRB as two intensely fluorescent discriminate peaks with only slight potential sharing of peak area. The intensities of the two dyes are remarkably close even though RWT is one hundred times the concentration of SRB. This is especially interesting because, as displayed in the single dilution synchronous scans, RWT and SRB fluoresce at comparable intensities at the same concentration. The RWTSRB 100:1 EEM/contour diagram displays a full primary fluorescence center that is intersected and skewed by scattered light and that extends a high-intensity fluorescence "lobe" or "arm" into longer Em and Ex wavelengths in the "northeastern" direction up and off the graph space. The upper Ex boundary of the graph space truncates the arm-like feature near its joint with the primary fluorescence center, but future studies may seek to employ longer λ_{Ex} wavelengths which may demonstrate that the arm-like feature in fact corresponds to the unique SRB fluorescence peak identified in the RWTSRB 100:1 synchronous scan.

The RWTSRB 100:1 EEM/contour diagram also displays what may be regarded as three low intensity secondary fluorescence centers that are not intersected by scattered

light (Figure 36). However, these secondary fluorescence centers are not more intense than the low intensity fluorescence pattern that renders primary and secondary fluorescence centers in FL:EO mixed dilution EEM/contour diagram continuous. Therefore, these secondary fluorescence centers, which do not exhibit the pattern usually exhibited by RWT:SRB mixed dilution secondary fluorescence centers, will not be regarded as true secondary fluorescence centers.

The primary fluorescence center is located at λ_{Ex} = 422 – 562 nm, λ_{Em} = 484 – 576 nm. The long Ex wavelength boundary of the primary fluorescence center was determined by approximation because the fluorescence center is truncated by the longer Ex boundary of the graph space above the highest intensity center. The short wavelength Em boundary of the primary fluorescence center was determined by approximation as well because the center is intersected by scattered light along the shorter Em wavelengths. The long Em boundary of the primary fluorescence center was also determined by approximation because the fluorescence center is continuous with an "arm"-like fluorescence artifact that extends into longer Ex and Em wavelengths. The chosen long Em wavelength boundary of the primary fluorescence center marks the location of the lowest fluorescence intensity (or the fluorescence "trough") between the primary fluorescence center and the arm-like feature.

The primary fluorescence center is located in the same general position as RWT and SRB primary fluorescence centers. Perhaps due to the interference of scattered light or the presence of the arm-like feature, the measurements do not correspond especially well with either the RWT or SRB primary fluorescence center.

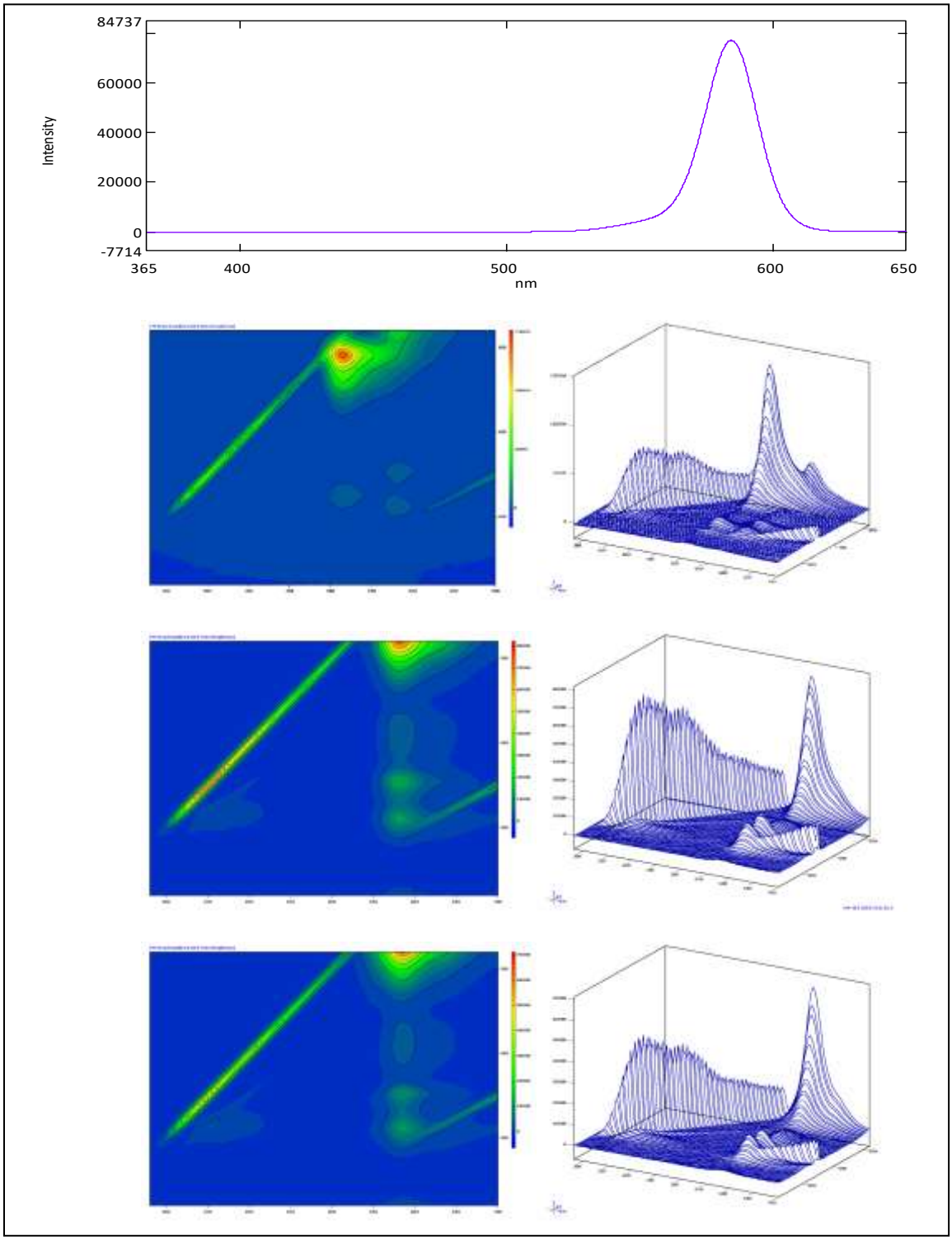

Figure 36: Comparison of RWTSRB 100:1 two and three-dimensional synchronous scans (top two rows), rhodamine WT 100 ppb single dye dilution EEM and contour diagram (third row from top), and sulphorhodamine B 100 ppb single dye dilution EEM and contour diagram (bottom row). EEM and contour diagram *x*-axis range = 280 - 700 is nm, *y*-axis range = 220 – 520 nm.

6.2.12 RWTSRB 100:10

The RWTSRB 100:10 synchronous scan displays only one homogenous fluorescence peak featuring no shoulders. The RWTSRB 100:10 EEM/contour diagram follows much the same pattern as that displayed in the RWTSRB 1:100, RWTSRB 10:1, RWTSRB 10:10, and RWTSRB 10:100 EEMs/contour diagrams. The RWTSRB 100:10 primary fluorescence center is bisected by the uppermost graph boundary through the highest intensity center and, although the view of the fluorescence center is limited, it is clear it is intersected by scattered light. The primary fluorescence center is continuous with three secondary centers located at shorter Ex wavelengths, which are also continuous with one another. The secondary fluorescence center located at the shortest Ex wavelengths is intersected by scattered light.

The RWTSRB 100:10 primary fluorescence center is located at λ_{Ex} = 462 – 578 nm, λ_{Em} = 545 – 680 nm. The long Ex wavelength boundary of the primary fluorescence center was determined by approximation because the fluorescence center is truncated by the longer Ex boundary of the graph space through the highest intensity center. The short Em boundary of the primary fluorescence center was determined by approximation as well because the center is intersected by scattered light along the shorter Em wavelengths. The three secondary fluorescence centers are located at λ_{Ex} = 288 – 332 nm, λ_{Em} = 560 – 606 nm (secondary fluorescence center *i*), λ_{Ex} = 332 – 380 nm, λ_{Em} = 559 – 631 nm (secondary fluorescence center *j*), and λ_{Ex} = 380 – 434 nm, λ_{Em} = 570 – 600 nm (secondary fluorescence center *k*). The long Em wavelength boundary of secondary fluorescence center *i* was determined by approximation because the fluorescence center is intersected by scattered light.

The RWTSRB 100:10 primary fluorescence center corresponds closely to the RWT primary fluorescence center (to within 5 nm). Secondary fluorescence center *i* corresponds closely to the RWT quaternary fluorescence center (to within 5 nm), secondary fluorescence center *j* corresponds closely to the RWT tertiary fluorescence center (to within 5 nm), and secondary fluorescence center *k* corresponds closely to the RWT primary secondary fluorescence center (to within 3 nm).

It is evident that the primary and secondary fluorescence centers displayed in RWTSRB 100:10 are artifacts resultant from the 100 ppb RWT component of the mixed dye dilution. No attributes of the RWTSRB 100:10 EEM/contour diagram seem to aid in discrimination of the 100 ppb RWT from the 10 ppb SRB, though future studies that employ longer λ_{Ex} wavelengths may identify the arm-like feature identified in the RWTSRB 100:1 EEM/contour diagram. This feature may prove useful in the discrimination of RWT from SRB in mixed dye dilutions.

6.2.13 RWTSRB 100:100

The RWTSRB 100:100 synchronous scan displays only one homogenous fluorescence peak featuring no shoulders. The RWTSRB 100:100 EEM/contour diagram follows much the same pattern as that displayed in the RWTSRB 1:100, RWTSRB 10:1, RWTSRB 10:10, and RWTSRB 10:100 EEMs/contour diagrams. The RWTSRB 100:100 primary fluorescence center captures the shorter wavelength portion of the λ_{Ex} of what is likely the primary fluorescence center. The primary fluorescence center is intersected by the uppermost graph boundary and, although the view of the fluorescence center is limited, it is clear the center is intersected by scattered light. What may be considered

three secondary fluorescence centers are also displayed in the EEM/contour diagram, though one of these is of an intensity equal to the fluorescence pattern that unifies primary and secondary fluorescence centers in FL:EO mixed dye dilution EEMs/contour diagrams. For this reason, only the two secondary fluorescence centers located at lower Ex wavelength ranges will be regarded as true secondary fluorescence centers. These two secondary fluorescence centers are continuous with one another by a low intensity fluorescence pattern and the secondary fluorescence center located at the shortest Ex wavelength ranges is intersected and skewed by scattered light.

Due to the limited view of the primary fluorescence center, little information may be gained from the RWTSRB 100:100 EEM/contour diagram (Figure 37) in relation to the location and shape of the primary fluorescence center. The two secondary fluorescence centers are located at λ_{Ex} = 294 – 332 nm, λ_{Em} = 564 – 610 nm (secondary fluorescence center *l*) and λ_{Ex} = 332 – 368 nm, λ_{Em} = 564 – 606 nm (secondary fluorescence center *m*). The long Em wavelength boundary of secondary fluorescence center *m* was determined by approximation because the fluorescence center is intersected by scattered light.

Secondary fluorescence center *l* corresponds closely to both the RWT quaternary fluorescence center (to within 6 nm) and the SRB quaternary fluorescence center (to within 7 nm). Secondary fluorescence center *m* corresponds more closely to the SRB tertiary fluorescence center (to within 15 nm) than the RWT tertiary fluorescence center (to within 30 nm). Although RWT and SRB are mixed into this dilution at equal concentrations (100 ppb), it is likely the fluorescent attributes of SRB dominate this

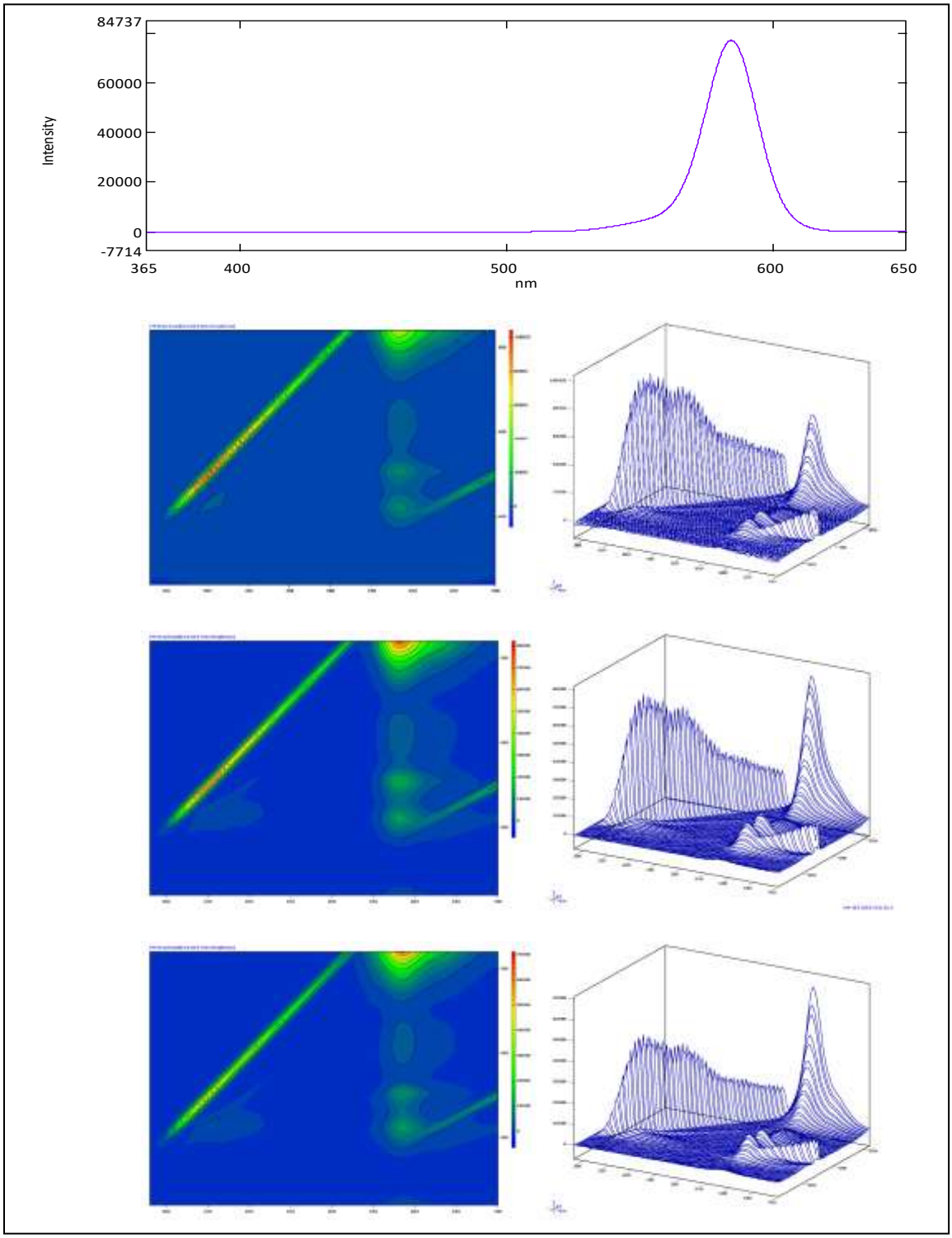

Figure 37: Comparison of RWTSRB 100:100 two and three-dimensional synchronous scans (top two rows), rhodamine WT 100 ppb single dye dilution EEM and contour diagram (third row from top), and sulphorhodamine B 100 ppb single dye dilution EEM and contour diagram (bottom row). EEM and contour diagram *x*-axis range = 280 - 700 is nm, *y*-axis range = 220 – 520 nm.

EEM/contour diagram due to SRB's higher quantum yield as compared to RWT. No attributes of the RWTSRB 100:10 EEM/contour diagram seem to aid in discrimination of the 100 ppb RWT from the 100 ppb SRB, though it may be possible to determine which of the dyes is present in higher concentrations with proper consideration of respective quantum yields and relative locations of primary and secondary fluorescence centers of RWT and SRB.

6.3 Lost River Cave Samples

6.3.1 Synchronous Scan Background Fluorescence

Several background fluorescence peaks were identified through the application of two-dimensional synchronous scanning and, more specifically, the application of the peak pick operation to the Lost River Cave fluorescent dye trace samples. The threshold was set to 0.01 nm and the number of points was set to five.

Peak α (Table 11) is present between λ_{Em} = ~385 – ~430 nm. In sample 009-0, the peak α Em maximum occurred at Em = 406.2 nm and 295 intensity units; in sample 022-0, the peak α Em maximum occurred at Em = 388.2 nm and 296 intensity units; in sample 023-0, the peak α Em maximum occurred at Em = 388.8 nm and 304 intensity units; and in sample 024-0, the peak α Em maximum occurred at Em = 388.6 nm and 306 intensity units. The Em maximum location varied by up to 18 nm, or 5%, and differed in intensity by up to 11 fluorescence intensity units, or 4%. Peak α exhibited a mean Em maximum of 393 nm.

Table 11: Statistical summary of Lost River Cave background fluorescence peak α.

Peak α	Range (nm)	Sample	Em Maxima (nm)	Fluorescence Intensity
	~385 - ~430	009-0	406.2	295
		022-0	388.2	296
		023-0	388.8	304
		024-0	388.6	306
	Count		4	4
	Mean		392.95	300.25
	Median		388.7	300
	Standard Deviation		8.836854644	5.560275773

Peak β (Table 12) fluoresces between λ_{Em} = ~390 – ~400 nm within the general range of peak α. Peak β exhibits an Em maximum at Em = 373 nm and 390 intensity units in sample 012-0, an Em maximum at Em = 374.0 nm and 305 intensity units in sample 017-0, an Em maximum at Em = 374.2 nm and 304 intensity units in sample 019-0, an Em maximum at Em = 374.8 nm and 305 intensity units in sample 020-0, an Em maximum at Em = 376.2 nm and 296 intensity units in sample 022-0, an Em maximum at Em = 375.2 nm and 398 intensity units in sample 023-0, and an Em maximum at Em = 377.2 nm and 313 intensity units in sample 024-0. The Em maximum of peak β varies by up to 4.2 nm, or 1 %, and the fluorescence intensity of peak β varies by up to 102 fluorescence intensity units, or 26%. Peak β exhibited a mean Em maximum at 375 nm.

Peak γ (Table 13) was measured between λ_{Em} = ~430 – ~460 nm. Peak γ exhibits an Em maximum at Em = 432.4 nm and 115 intensity units in sample 012-0 and Em = 416.0 nm and 198 intensity units in sample 024-0. The Em maximum of peak γ varied by

Table 12: Statistical summary of Lost River Cave background fluorescence peak β.

Peak β	Range (nm)	Sample	Em Maxima (nm)	Fluorescence Intensity
	~390 - ~400	012-0	373	390
		017-0	374	305
		019-0	374.2	304
		020-0	374.8	305
		022-0	376.2	296
		023-0	375.2	398
		024-0	377.2	313
	Count		7	7
	Mean		374.9428571	330.1428571
	Median		374.8	305
	Standard Deviation		1.41286605	43.95993847

Table 13: Statistical summary of Lost River Cave background fluorescence peak γ.

Peak γ	Range (nm)	Sample	Em Maxima (nm)	Fluorescence Intensity
	~430 - ~460	012-0	432.4	115
		024-0	416	198
	Count		2	2
	Mean		424.2	156.5
	Standard Deviation		11.59655121	58.68986284

16.4 nm, or 4%, and the fluorescence intensity varied by 83 fluorescence intensity units, or 42%. Peak γ exhibited a mean Em maximum at 424 nm.

Background fluorescence peaks α, β, and γ were not measured in any sample through the application of three-dimensional synchronous scanning. Comparisons of the locations of peaks α, β, and γ to the known locations of substances that often contribute to background fluorescence were attempted for the purpose of characterizing background fluorescence in the Lost River during the dye trace period. However, many published measurements refer only to Em and Ex maxima, and do not specify associated λ_{Ex} or λ_{Em}. This is especially problematic because the λ_{Em} were measured at a specific Ex

wavelength (Ex = 347 nm). Thus, although Ex = 347 may fall within the λ_{Ex} of the substance, only the Ex maximum (and not the λ_{Ex}) is published. Additionally, many measurements that were reported as λ_{Ex} and λ_{Em} do not include Ex = 347 within their chosen range.

Table 17 summarizes the fluorescence center measurements published in a variety of studies. Only three of these published measurements give an Ex maximum of 347 nm ± 1 nm (the peak maximum measured through this research may vary by up to 1 nm due to the chosen data interval of 2 nm). Hudson et al. (2008) reports an Ex/Em maxima at 347/461 nm for a humic-like peak based on surface water and effluent samples. Peak γ corresponds to this measurement the most closely, but the peak γ mean Em maximum (424 nm) differs from this measurement by 37 nm, or an 8% difference. Käss (1992) reports an Ex/Em maximum pair for the fluorescent dyes Tinopal CBS-X and Leucophor PBS of 346/435 nm and 348/430 nm, respectively. Again, peak γ corresponds to these measurements the most closely of the background fluorescence peaks. The peak γ Em maximum of 424 nm differs by 11 nm from the Tinopal CBS-X Em maxima (or a 3% difference) and by 6 nm from the Leucophor PBS Em maximum (or a 1% difference). Based on the available information, peak γ is therefore most likely attributable to the fluorescent dyes Tinopal CBS-X and, especially, Leucophor PBS. It is fundamentally feasible that peak γ should be attributed to Tinopal CBS-X and Leucophor PBS. These fluorescent dyes fall into the category of optical brighteners, which are often found in anthropogenically-impacted waterways as a result of many industrial processes and facilities, including tissue and paper mills (Baker 2002; Smart and Karunaratne 2002). It should be noted that the Em maximum of peak γ was determined through the

measurement of the peak in only two samples. Further studies should seek to develop a more robust measurement of the peak γ Em maximum.

Two of the published measurements given in Table 17 reference an λ_{Ex} that includes 347 nm. Muller et al. (2008) cite measurements originally published by Coble (1996) of two humic-like peaks that occur at λ_{Ex} = 320 – 360, λ_{Em} = 420 – 460 and λ_{Ex} = 304 – 347, λ_{Em} = 405 – 461. Peak γ corresponds to these measurements the most closely as well. The peak γ mean Em maximum of 424 nm is within the λ_{Em} of these two humic-like peaks (420 – 460 nm and 405 – 461 nm). It is reasonable that peak γ may be attributed to humic acids and optical brighteners. These substances emit light in the same range of the electromagnetic spectrum. In fact, a common impediment to the detection of optical brighteners used as fluorescent dye tracers is the presence of a broad "organics" peak at short Em wavelength ranges, into which optical brighteners are often absorbed unless a sufficiently large concentration of the tracer is injected (Smart and Karunaratne 2002; Coble 2007; Hudson et al. 2008; Muller et al. 2008).

Peaks α and β are not located within the same regions as substances whose Ex maxima are published as 347 nm or whose published λ_{Ex} includes Ex = 347 nm. To facilitate comparison of peaks α and β with fluorescent substances whose Ex and Em maxima alone are published, the following steps were performed: 1) The λ_{Ex} were estimated for those fluorescent substances in Table 17 for which the respective sources only specified the Ex maxima, 2) Those substances whose estimated λ_{Ex} contained Ex = 347 nm were selected, 3) The λ_{Em} were estimated for those fluorescent substances whose estimated λ_{Ex} contained Ex = 347 nm, and 4) The λ_{Em} of these fluorescent substances were compared to the λ_{Em} of the background fluorescence peaks in an effort to associate

background fluorescence peaks α and β with the fluorescence substances given in Table 17.

To facilitate the estimation of the λ_{Ex} of the substances in Table 17, the 1, 10, and 100 ppb FL fluorescent dye dilution EEMs/contour diagrams were evaluated to determine the distance of the Ex wavelength range min and max from the Ex maximum at varying concentrations. It was only possible to accurately estimate the λ_{Ex} of FL because only the FL fluorescence center was nearly completely captured by the EEM/contour diagram. The approximate locations of the FL fluorescence centers were verified by comparing the Ex maxima of the centers with the FL Ex maximum published in Käss (1992). The measured FL Ex maxima measured through this research were within 1% of the Ex maximum published by Käss (1992) (Tables 14, 15, and 16).

The 1 ppb FL Ex wavelength range min was approximately 8% different than the Ex max and the FL Ex wavelength range max was approximately 4% different than the Ex max. The 10 and 100 ppb FL Ex wavelength range mins were approximately 14% different than the Ex max and the FL Ex wavelength range maximums were approximately 6% different than the Ex max. By these measurements, it is clear that the majority of the area of the FL fluorescence center is located below the highest intensity center at shorter Ex wavelength ranges and the FL fluorescence center is asymmetrical along the Ex (*y*) axis. The more conservative percent differences (shorter wavelength

Concentration	Primary Center	Max Ex (nm)	Ex Start (nm)	Max - Start (nm)	% Diff	Ex End (nm)	End - Max (nm)	% Diff	Kass Ex Max (nm)	Variation (nm)	% Diff
100	FL	492	422	70	14.22764228	520	28	5.691056911	491	1	0.203665988
100	FL	492	422	70	14.22764228	520	28	5.691056911	438	54	12.32876712
10	FL	492	422	70	14.22764228	520	28	5.691056911	491	1	0.203665988
10	FL	492	422	70	14.22764228	520	28	5.691056911	438	54	12.32876712
1	FL	492	452	40	8.130081301	510	18	3.658536585	491	1	0.203665988
1	FL	492	452	40	8.130081301	510	18	3.658536585	438	54	12.32876712

Table 14: Fluorescein single dye dilution three-dimensional synchronous scan excitation range measurements.

Concentration	Primary Center	Max Em (nm)	Em Start (nm)	Max - Start (nm)	% Diff	Em End (nm)	End - Max (nm)	% Diff	Kass Em Max (nm)	Variation (nm)	% Diff
100	FL	517.5	480	37.5	7.246376812	610	92.5	17.87439614	512	5.5	1.07421875
10	FL	515	485	30	5.825242718	610	95	18.44660194	512	3	0.5859375
1	FL	514	495	19	3.696498054	566	52	10.11673152	512	2	0.390625
100	EO	540	510	30	5.555555556	630	90	16.66666667	538	2	0.371747212
10	EO	540	516	24	4.444444444	606	66	12.22222222	538	2	0.371747212
100	RWT	582.5	545	37.5	6.43776824	680	97.5	16.73819742	576	6.5	1.128472222
100	SRB	584	535	49	8.390410959	680	96	16.43835616	583	1	0.171526587
Mean					5.942328112			15.50045315			
Median					5.825242718			16.66666667			
Difference					0.117085394			1.166213513			

Table 15: Fluorescein, eosin, rhodamine WT, and sulphorhodamine B single dye dilution three-dimensional synchronous scan emission wavelength range measurements.

Source	Substance/Compound	Comments	Excitation Maximum (nm)	Emission Maximum (nm)	Δλ (nm)	Ex Start (nm)	Ex End (nm)	Em Start (nm)	Em End (nm)	Concidence of LRC BG Peak α λ_{Em}	Coincidence of LRC BG Peak β λEm
Baker 2001, p. 950	fulvic-like		339	422		311.88	352.56	396.68	489.52	33.32	3.32
Baker 2001, p. 950	fulvic-like		337	421		310.04	350.48	395.74	488.36	34.26	4.26
Baker 2001, p. 950	fulvic-like		339	420		311.88	352.56	394.8	487.2	35.2	5.2
Baker 2001, p. 950	fulvic-like		336	420		309.12	349.44	394.8	487.2	35.2	5.2
Sierra et al. 2005	humic acid--less intense center		360	520		331.2	374.4	488.8	603.2		
Käss 1992	Amino G-acid		359	450	91	330.28	373.36	423	522	7	
Käss 1992	Photine CU		345	435	90	317.4	358.8	408.9	504.6	21.1	
Käss 1992	Optical brightener		349	430	81	321.08	362.96	404.2	498.8	25.8	

Table 16: Published and estimated three-dimensional synchronous scanning measurements derived from three studies published by Baker (2001), Sierra et al. (2005), and Käss (1992) used to associate Lost River Cave background fluorescence peaks α and β with fluorescence substances known to permeate natural waterways.

range) exhibited by the 1 ppb FL EEM/contour diagram were used to estimate the λ_{Ex} of the fluorescent substances given in Table 17 due to the generally low concentration of background fluorescence. The λ_{Ex} were estimated by expanding the λ_{Ex} by 8% into the shorter Ex wavelength ranges and by 4% into the longer Ex wavelength ranges. Based on these estimated λ_{Ex}, the following fluorescent substances were considered for possible fit with background fluorescence peaks α and β: four cases of fulvic-like fluorescence measured by Baker (2001); one case of humic acid measured by Sierra et al. (2005); and the fluorescent dyes Amino G-Acid, Photine CU, and Optical Brightener published by Käss (1992).

Next, the λ_{Em} was estimated for each of the eight substances identified in the previous step. To facilitate the estimation of the λ_{Em}, the 1, 10, and 100 ppb FL; 10 and 100 ppb EO; 100 ppb RWT; and 100 ppb SRB fluorescent dye dilution EEMs/contour diagrams were evaluated to determine the distance of the Em wavelength range min and max from the Em maximum at varying concentrations (see Table 15). The average percent difference between the Em wavelength range min and Em maximum and Em wavelength range max and Em maximum, respectively, were then calculated from these measurements. The Em wavelength range min and Em wavelength range max percent difference were then respectively subtracted from and added to the Em maxima of the eight fluorescent substances to estimate the λ_{Em}. The approximate location of the FL, EO, RWT, and SRB fluorescence centers were verified by comparing the Em maxima of the centers with the FL, EO, RWT, and SRB Em maxima published by Käss (1992). The measured FL, EO, RWT, and SRB Em maxima measured through this research were within 2%, 1%, 2%, and 1%, respectively, of the Em maxima published by Käss (1992).

The seven EEM/contour diagrams of the four fluorescent dyes listed above were chosen to aid in the estimation of the λ_{Em} because they are the only EEM/contour diagrams that display complete fluorescence centers in the Em (*x*) direction. The λ_{Em} routinely used in the CHL to define two dimensional fluorescent dye peaks and calculate corresponding concentrations were not used to estimate the λ_{Em} of the eight fluorescence substances because, through the course of this research, it does not appear that Ex = 347, the excitation wavelength routinely used to excite samples in the CHL, is the ideal Ex wavelength for the detection of low-concentration FL, EO, RWT, and SRB. Ex = 347 is not the Ex max for any of the fluorescent dyes employed through this study and the λ_{Em} that corresponds to Ex = 347 is not necessarily fully diagnostic of the λ_{Em} of FL, EO, RWT, and SRB, nor of fluorescent substances that produce background fluorescence.

For all dilutions, there was, on average, approximately a 6% difference between the Em wavelength range min and the Em maximum. The average percent difference fell within about 2% percent of the median percent difference. For all dilutions, there was, on average, approximately a 16% difference between the Em wavelength range max and the Em maximum. The average percent difference fell within 7% percent of the median percent difference. It is evident that the areas of the primary fluorescence centers are concentrated in the longer Em wavelength regions and are not symmetrical about the Em (*x*) axis. As mentioned previously, the percent differences between the Em wavelength range min and the Em maximum and the Em wavelength range max and the Em maximum were then respectively subtracted from and added to the Em maximum of the eight fluorescent substances to estimate the λ_{Em}.

The mean Em maximum of peak α (Em = 393 nm) did not fall within the estimated λ_{Em} of any of the eight fluorescent substances. However, the estimated Em wavelength range of peak α (λ_{Em} = ~385 – ~430 nm) partially coincided with the estimated λ_{Em} of four fulvic-like peaks measured by Baker (2001) and the estimated λ_{Em} of Amino G-acid, Photine CU, and Optical Brightener published in Käss (1992). Peak α and the fulvic-like peaks measured by Baker (2001) shared the greatest extent of their λ_{Em} (between 33 and 36 nm), as compared to the extent peak α shared with Amino G-acid, Photine CU, and Optical Brightener (7, 21, and 26 nm, respectively). Although the estimated mean peak α maximum was not contained within any of the λ_{Em} of the eight fluorescent substances, it is most plausible that peak α is attributable to fulvic-like fluorescence, a product of the decomposition of natural organic matter, because peak α shared the greatest extent of its λ_{Em} with the fulvic-like peaks measured by Baker (2001).

The mean Em maximum of peak β (Em = 375 nm) also did not fall within the estimated λ_{Em} of any of the eight fluorescent substances. However, the estimated Em wavelength range of peak *β* (λ_{Em} = ~390 – ~400 nm) partially coincided with the estimated λ_{Em} of four fulvic-like peaks measured by Baker (2001) (between 3 and 6 shared nm). Although the estimated mean peak *β* maximum was not contained within any of the λ_{Em} of the eight fluorescent substances, it is most plausible that peak *β* is attributable to fulvic-like fluorescence as well because peak *β* shared the greatest extent of its λ_{Em} with the fulvic-like peaks measured by Baker (2001).

It is most certainly reasonable that both peaks α and *β* are attributable to fulvic acid-like fluorescence since the LRC samples were collected in a natural environment from a river system most certainly impacted by effluent containing chemical elements

derived from the process of decomposition of natural organic matter. Additionally, although peaks α and β did not correspond exactly to the fulvic acid-like fluorescence peaks measured by Baker (2001), the slight variations in their locations may reasonably be caused by pH differences, metal ion quenching, or differences in source vegetation and soil types, which have been shown to contribute variability of ± 20 nm (Baker and Genty 1999).

The second research objective of this study is to evaluate the ability of three-dimensional synchronous scanning to discriminate the fluorescent dye spectra of the common fluorescent dyes FL, EO, RWT, and SRB from background fluorescence in an anthropogenically-effected sampling environment. Through the application of two-dimensional synchronous scanning to the LRC samples, it was possible to identify and measure background fluorescence peaks α, β, and γ. It was also possible to create associations between the background fluorescence peaks and known sources of background fluorescence and tentatively characterize the background fluorescence of the LRC samples at the time of the LRC fluorescent dye trace. However, the background fluorescence peaks did not occur in the same region of the electromagnetic spectrum as the fluorescent dyes employed in this study and so discrimination of these background fluorescence peaks likely attributable to fulvic-acid like fluorescence, humic acid, and optical brighteners from FL, EO, RWT, and SRB is not appropriate. Furthermore, the background fluorescence peaks were not detected in the EEM/contour diagrams of the LRC samples.

Three-dimensional synchronous scanning did not enhance the discrimination of background fluorescence from the fluorescent dyes FL, EO, RWT, and SRB as compared

to two-dimensional synchronous scanning for two primary reasons: 1) The background fluorescence peaks did not fluoresce in the same region of the electromagnetic spectrum as the tracer dyes and so discrimination of background fluorescence of the humic acid, fulvic acid, and optical brightener varieties from these tracer dyes is unnecessary at concentrations likely to be found in the environment and 2) the background fluorescence peaks were not detected in the EEM/contour diagrams of the LRC samples.

6.3.1.1 Sample 022-0

FL is first detected in the synchronous scan of sample 022-0 at Em = 492.8 – 528.8 nm at a concentration of .004 ppb. It should be noted that .004 ppb is a smaller concentration than the smallest concentration FL PQL standard dilution (0.1 ppb) and so is outside the instrument calibration range. Background fluorescence peaks β and γ were also detected. The associated EEM/contour diagram displays one irregularly (angularly)-shaped primary fluorescence center at λ_{Ex} = 276 – 486 nm, λ_{Em} = 311 – 580 nm. The angularity of the fluorescence center is potentially caused by intersecting scattered light at about λ_{Ex} = 282 – 520 nm, λ_{Em} = 284 – 535 nm and the center seems to have one high intensity center. There are also two forms of scattered light present in the bottom right portion of the graph space at λ_{Ex} = 284 – 360 nm, λ_{Em} = 574 – 700 nm, though neither artifact is obviously intersecting the primary fluorescence center. No artifact resultant from the presence of background fluorescence or FL is evident in the 022-0 EEM/contour diagram.

The 022-0 EEM/contour diagram is nearly identical to the 021-0 EEM/contour diagram. This is especially interesting because the use of two-dimensional synchronous

scanning confirmed the presence of .004 ppb FL in the 022-0 sample and confirmed the lack of FL in the 021-0 sample. This comparison indicates that the 022-0 EEM/contour diagram, like the 021-0 EEM/contour diagram, is dominated by fluorescence patterns contributed by scattered light. Additionally, this comparison indicates that the three-dimensional synchronous scanning technique employed through this study failed to detect low concentrations of the fluorescent dye FL and low-intensity background fluorescence, especially as compared to current two-dimensional synchronous scanning techniques regularly employed in the CHL.

6.3.1.2 Sample 023-0

Through the use of two-dimensional synchronous scanning, FL was detected and measured in the 023-0 sample at greater than 600 fluorescence intensity units and a concentration of 0.092 ppb. Peak β and peak γ were also detected. The associated EEM/contour diagram displays the angular primary fluorescence center at λ_{Ex} = 282 – 446 nm, λ_{Em} = 311 – 570 nm. The fluorescence pattern attributable to scattered light occurs at about λ_{Ex} = 284 – 520 nm, λ_{Em} = 284 – 535 nm and intersects the primary fluorescence center. Two forms of scattered light are present in the bottom right portion of the graph space at λ_{Ex} = 292 – 362 nm, λ_{Em} = 580 – 700 nm. Unique to the 023-0 EEM/contour diagram, a secondary fluorescence center is displayed at λ_{Ex} = 462 – 508 nm, λ_{Em} = 500 – 637 nm. The short Em wavelength and both Ex boundaries were determined by approximation because the fluorescence artifact attributable to scattered light intersects the secondary fluorescence center at short Em wavelengths, the long Ex wavelength boundary of the graph space intersects the center above the highest intensity

point, and the primary fluorescence center is continuous with the secondary fluorescence center which renders discrimination of the two difficult.

The primary fluorescence center and fluorescence artifacts resultant from scattered light correspond to the primary fluorescence center and scattered light features displayed in 022-0 to within 11 nm (Figure 38), apart from the long wavelength Ex boundary of the primary fluorescence center, which corresponds to within 41 nm. The discrepancy between the primary fluorescence center measurements is likely due to interference by the secondary fluorescence center in the 023-0 EEM/contour diagram.

No artifact resultant from the presence of background fluorescence is evident in the 023-0 EEM/contour diagram. However, the secondary fluorescence center occurs in a region usually occupied by fluorescent dye primary fluorescence centers. The secondary fluorescence center does not correspond particularly well to any of the fluorescent dyes employed in this study, but measurement of the secondary fluorescence center may be less than accurate due to the aforementioned interference by scattered light and the primary fluorescence center. It is likely that the secondary fluorescence center may be attributed to FL.

In the case of sample 023-0, three-dimensional synchronous scanning failed to detect background fluorescence identified in the same sample using two-dimensional synchronous scanning. Three-dimensional synchronous scanning succeeded in the detection of FL in sample 023-0, but accurate measurement of the fluorescence center was thwarted by scattered light and the primary fluorescence center. Additionally, measurement of dye concentration is not possible using the three-dimensional analysis technique and software employed in this study.

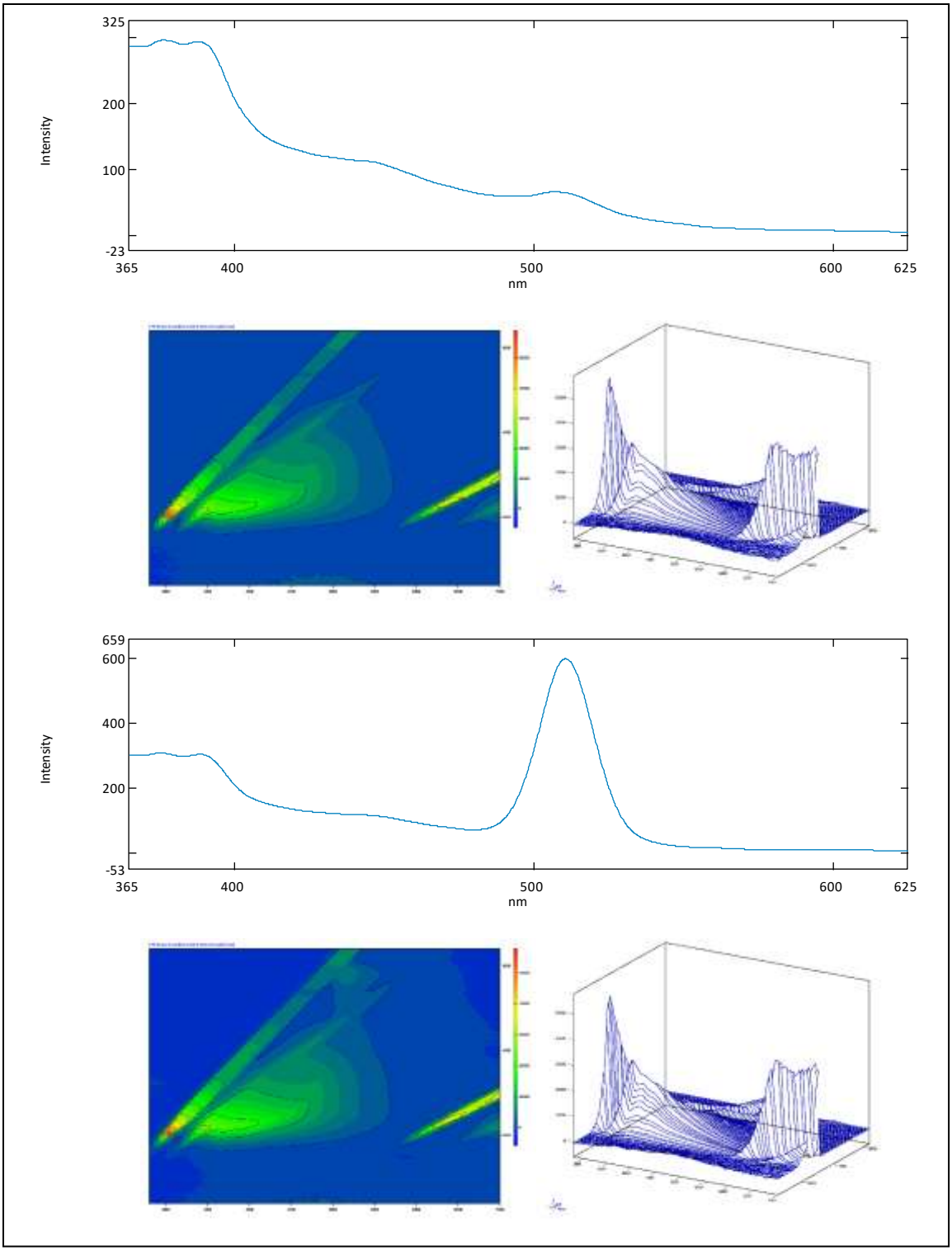

Figure 38: Comparison of Lost River Cave Sample 022-0 (top two rows) and Sample 023-0 (bottom two rows) two and three-dimensional synchronous scans. EEM and contour diagram *x*-axis range = 280 - 700 is nm, *y*-axis range = 220 – 520 nm.

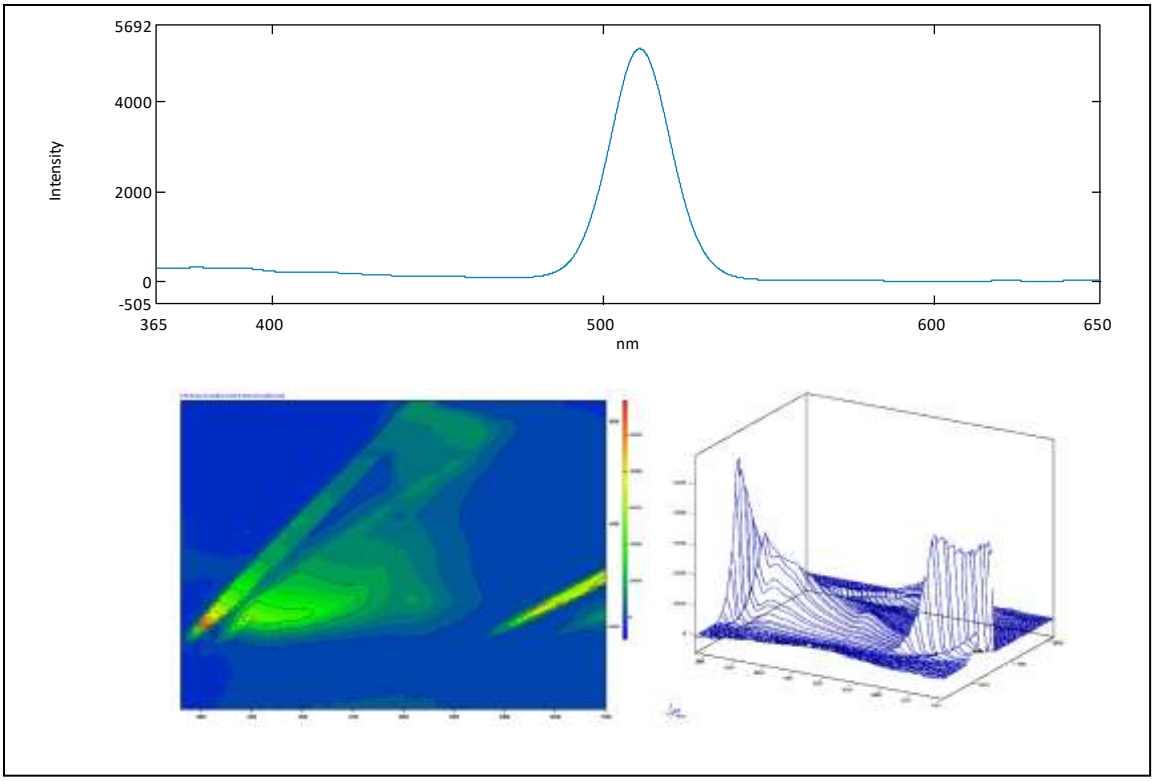

Figure 39: Comparison of Lost River Cave Sample 024-0 two and three-dimensional synchronous scans. EEM and contour diagram *x*-axis range = 280 - 700 is nm, *y*-axis range = 220 – 520 nm.

6.3.1.3 Sample 024-0

Through the use of two-dimensional synchronous scanning, FL, peak β, and peak γ were detected in the 024-0 sample (Figure 39), though the background fluorescence peaks are difficult to identify due to the course scale of the synchronous scan. Synchronous scans were produced of the 024-0 sample using both a high and low sensitivity setting because the FL is too highly concentrated to be accurately measured using the high sensitivity instrument setting. The low sensitivity synchronous scan minimized the appearance of instrumental noise and background fluorescence peaks and revealed that sample 024-0 contains 0.849 ppb FL that fluoresces at an intensity of about 5,000 fluorescence intensity units.

The 024-0 EEM/contour diagram displays the usual angular primary fluorescence center at λ_{Ex} = 276 – 525 nm, λ_{Em} = 314 – 590 nm, which is continuous with the secondary fluorescence center that occurs at λ_{Ex} = 418 – 525 nm, λ_{Em} = 465 – 615 nm. The primary fluorescence center short Em wavelength and long Ex wavelength boundaries were determined by approximation because the scattered light artifact at short Em wavelengths intersects the primary fluorescence center and the long Ex wavelength boundary of the center is obscured by the long Ex wavelength boundary of the graph space and the secondary fluorescence center. The secondary fluorescence center's short Em wavelength and both Ex boundaries were determined by approximation because the scattered light artifact interferes with measurement of the center at short Em wavelengths, the long Ex wavelength boundary of the graph space intersects the center above the highest intensity point, and the primary fluorescence center interferes with low Ex wavelength boundary measurements.

The primary fluorescence center exhibits the usual angular behavior exhibited in other LRC samples but is slightly more irregular, likely because the high sensitivity instrument setting is not the ideal setting for the measurement of the relatively highly-concentrated FL (the 024-0 EEM/contour diagram was produced using a high sensitivity instrument setting). Unique to sample 024-0, a tertiary fluorescence center is identified at short Ex wavelengths and λ_{Em} = 355 – 589 nm. Accurate measurement of the λ_{Ex} is not feasible because the low Ex wavelength boundary of the graph space severs the fluorescence center above the highest intensity point. Both the primary and secondary fluorescence centers are intersected and skewed by the linear fluorescence pattern that occurs at λ_{Ex} = 284 – 520 nm, λ_{Em} = 284 – 530 nm. The long Ex wavelength boundary of

the scattered light feature was defined by the long Ex boundary of the graph space. Other scattered light patterns occur at λ_{Ex} = 288 – 362 nm, λ_{Em} = 575 – 700 nm, but these scattered light patterns do not intersect the primary, secondary, or tertiary fluorescence centers. The long Em wavelength boundary of the scattered light pattern is defined by the long Em wavelength boundary of the graph space.

The primary fluorescence center corresponds to the primary fluorescence centers displayed in samples 022-0 and 023-0 to within 39 nm and 79 nm, respectively. The discrepancies between the 024-0 and other primary fluorescence centers is likely due to the irregularity of the 024-0 primary fluorescence center (the center exhibits a much wider λ_{Ex} in the 024-0 EEM/contour diagram). The secondary fluorescence center corresponds to the secondary fluorescence center displayed in sample 023-0 to within 44 nm. The discrepancy between the 023-0 and 024-0 secondary fluorescence centers is likely due to the entirely continuous nature of the primary and secondary fluorescence centers in the 024-0 sample and the subsequent difficulty in choosing an appropriate Ex wavelength to divide the two centers. The scattered light feature at short Em wavelengths corresponds to the same feature in samples 022-0 and 023-0 to within 6 nm, as do the scattered light features at long Em wavelengths.

As previously discussed, the secondary fluorescence center displayed in sample 024-0 occurs in a region usually occupied by fluorescent dye primary fluorescence centers and is most likely attributable to FL. The tertiary fluorescence center unique to 024-0 exhibits a long Ex wavelength boundary at about Ex = 260 nm, which is nearly 200 nm shorter than the short Ex wavelength boundaries of any of the fluorescent dyes used throughout this study. The long Ex wavelength upper boundary and λ_{Em} roughly

correspond to the location of humic and fulvic acids, but since the tertiary fluorescence center was not detected in either the 022-0 or 023-0 sample and synchronous scans of the 024-0 sample did not reveal that background fluorescence was present to a greater degree than in 022-0 or 023-0, it is more likely that the tertiary fluorescence center is an artifact resultant from the highly concentrated FL and high sensitivity instrument setting.

In the case of sample 024-0, three-dimensional synchronous scanning most likely failed to detect background fluorescence identified (albeit at extremely low levels) in the same sample using two-dimensional synchronous scanning. Three-dimensional synchronous scanning succeeded in the detection of FL in sample 024-0, but accurate measurement of the fluorescence center was thwarted by scattered light interference, primary fluorescence center interference, and choice of instrument setting. Additionally, measurement of dye concentration routinely conducted through two-dimensional synchronous scanning is not possible using the three-dimensional analysis technique and software employed in this study.

6.4 Summary of Project Limitations

Several project limitations bounded the effectiveness of this study. Two relatively minor limitations relate to the LRC sampling regime and resultant samples. The LRC samples analyzed through the course of this research only captured the beginning of the fluorescent dye breakthrough curve. Perhaps more information could have been gleaned from the LRC samples if the sampling regime was timed to more efficiently capture the entrance and exit of fluorescein in the system. Secondly, LRC sample 024-0 was inadvertently analyzed only in high sensitivity mode using three-dimensional

synchronous scanning. Perhaps more information could have been gleaned from LRC sample 024-0 if the sample had been analyzed in the low sensitivity mode which would have captured the full area and intensity of the FL fluorescence center.

A few more influential project limitations also bounded the effectiveness of this study: 1) lack of sample temperature control, 2) inability to quantify peak area and dye concentration using the 3D Spectrum mode, and 3) perhaps the most influential project limitation throughout the study, the influence of scattered light. First, although sample analysis is conducted quickly (within a matter of seconds) using two-dimensional synchronous scanning, analysis using three-dimensional synchronous scanning through this research was performed in about 12 – 15 minutes per sample. The samples were warmed to 30 °C in a water bath prior to analysis as per standard CHL procedures, but due to the extended analysis period required through high resolution three-dimensional synchronous scanning, the sample cooled to room temperature throughout the duration of the 12 – 15-minute analysis period. The temperature of the laboratory analysis was not always held constant over the sampling period and varied between 21 and 29 °C. No thermostatted cell holder was available through the course of this research and the variable room temperature, in addition to the cooling of the sample over the 10 – 15-minute analysis period, may have influenced the analytical results. It has been reported that some biological samples may fluoresce at a 10% difference in response to a temperature change of 1 °C (PerkinElmer 2000; Shimadzu 2015).

Next, fluorescent dye peak area and fluorescent dye concentration calculations are common through the application of two-dimensional synchronous scanning in the CHL and the routine use of the LabSolutions RF software. Calculation of peak area is an

intuitive feature of the Spectrum mode of the LabSolutions RF software package. However, the 3D Spectrum mode of the LabSolutions RF software employed to produce EEMs and contour diagrams through the course of this research does not incorporate any such feature. There is no intuitive method provided in the 3D Spectrum mode of the LabSolutions RF software package to quantify fluorescence center area or fluorescent dye concentration without modifications to the software or the use of external programs.

Finally, scattered light often interfered in the acquisition of clear and accurate EEMs and contour diagrams (Figure 40). In EEM/contour diagrams of low-concentration fluorescent dyes, the fluorescent dyes were usually not detected or measured and the EEM/contour diagrams were dominated by fluorescence patterns produced by scattered light. Since the fluorescent dyes were not detected at low concentrations using three-dimensional synchronous scanning, the presence of scattered light in these EEM/contour diagrams was not obviously obstructive. However, it should be noted that the fluorescence patterns caused by scattered light might be more prominent than any fluorescence resulting from the low concentration fluorescent dye, as reported by Soltzberg et al. (2012). Scattered light frequently and substantially affected the interpretation and measurement of high concentration dye fluorescence centers in EEMs and contour diagrams produced through the course of this research. Perhaps single dye dilution 10 ppb FL, 100 ppb FL, and .01 ppb RWT provide the most descriptive examples.

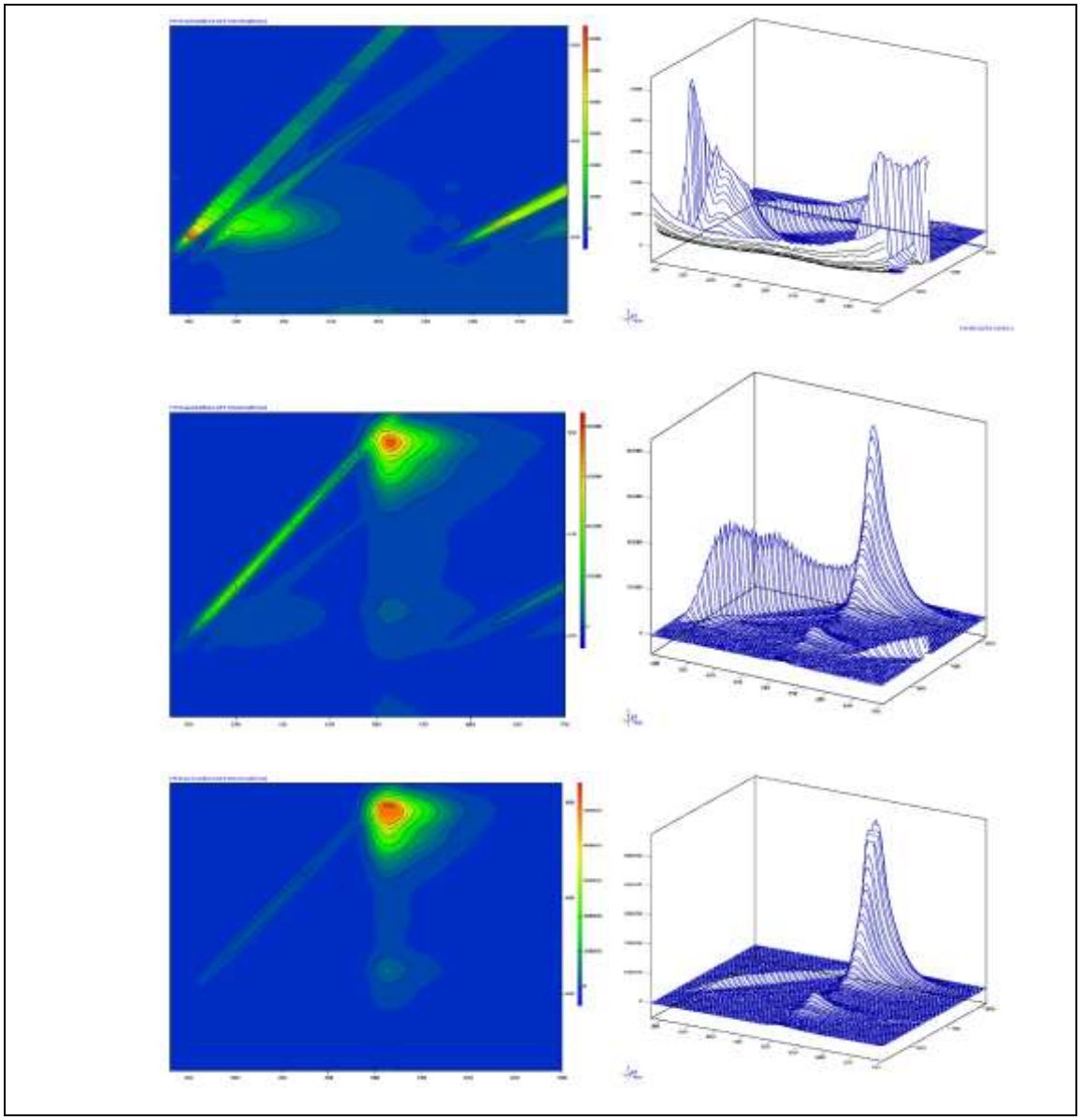

Figure 40: Examples of obstructive scattered light interference as displayed in single dye dilution RWT .01 ppb, FL 10 ppb, FL 100 ppb, and contour diagrams and EEMs, top to bottom. *X*-axis range = 280 - 700 is nm, *y*-axis range = 220 – 520 nm.

Consider the single dye dilution .01 ppb RWT EEM/contour diagram. This EEM/contour diagram exhibits four linear, diagonal fluorescence patterns that result from scattered light. From left to right, the diagonal fluorescence features are most likely attributable to zero order scattering, first order Raman scattering, and second order Raman scattering. Fluorescence patterns due to z*ero order scattering* arise when the emission detector measures the excitation radiation emitted by the xenon arc lamp. This

type of scattered light interference can generally be eliminated through the use of a sufficiently wide $\Delta\lambda$ (Gilbert Vial, Molecular Spectroscopy Product Specialist Shimadzu Scientific Instruments, May 2, 2019). The $\Delta\lambda$ employed to produce EEMs and contour diagrams through this study was 60 nm. The generally recommended minimum $\Delta\lambda$ is 10 nm (Gilbert Vial, Molecular Spectroscopy Product Specialist Shimadzu Scientific Instruments, May 2, 2019).

First order Raman scattering, the second diagonal fluorescent feature from the left, results from a shift in the energy of a scattered photon by a constant amount from the excitation photon energy (Soltzberg et al. 2012). This fluorescence too can generally be eliminated through choice of an appropriately wide $\Delta\lambda$ since, as discussed in Appendix A, increasing the separation of the λ_{Ex} from the λ_{Em} will ensure that the Raman scattering occurs within the wavelengths of the offset between λ_{Ex} and λ_{Em} rather than in the λ_{Em} itself (PerkinElmer 2000; Shimadzu 2015; Gilbert Vial, Molecular Spectroscopy Product Specialist Shimadzu Scientific Instruments, May 2, 2019).

Finally, *second order Raman scattering* results from a shift in the energy of a scattered photon by a constant amount from the excitation photon energy as well. However, in the case of second order scattering, the energy of a scattered photon appears at twice the excitation wavelength range. If the λ_{Em} of the EEM/contour diagram was wide enough, the Raman scattering could also be viewed at the third order, fourth order, fifth order, and so on (Gilbert Vial, Molecular Spectroscopy Product Specialist Shimadzu Scientific Instruments, May 2, 2019).

These fluorescence patterns caused by scattered light interfered in the measurement and interpretation of fluorescence centers of high concentration fluorescent

dye dilutions. Consider the single dye dilution 10 ppb FL EEM/contour diagram. The primary fluorescence center is intersected by zero order light scattering, thus hindering measurement of the short Em wavelength boundary and long Ex wavelength boundary of the center. The primary and secondary fluorescence centers are both affected by low intensity first and second order Raman scattering, but these fluorescence pattern do not substantially impede the measurement of the centers. Now consider the single dye dilution 100 ppb FL EEM/contour diagram. The greater concentration of FL renders the scattered light patterns less obtrusive, though the primary fluorescence center is still intersected by the zero order light scattering, which impedes the accurate measurement of the short Em wavelength and long Ex wavelength boundaries of the fluorescence center. Scattered light patterns have been observed to be less obtrusive in EEM/contour diagrams of high concentration dyes (Soltzberg et al. 2012).

Fluorescence patterns resultant from scattered light have been detected in EEMs and contour diagrams published in other studies as well, including Soltzberg et al. (2012), Baker (2001), and Qianqian et al. (2014). When choice of a sufficiently wide $\Delta\lambda$ does not alleviate the intrusion of scattered light into the EEMs and contour diagrams, wavelength-cutting filters are often installed in the spectrofluorophotometer that prevent light of a certain wavelength from entering the emission detector (Hudson et al. 2008; Gilbert Vial, Molecular Spectroscopy Product Specialist Shimadzu Scientific Instruments, May 2, 2019). Wavelength-cutting filters were not available for use through the duration of this research and choice of an appropriate large $\Delta\lambda$ did not alleviate the effects of scattered light.

7. Conclusions

7.1 Research Objectives and Conclusions

Through the course of this study, the proposed research objectives were both supported in some cases and not supported in others. The conclusions reached through the course of this research may be summarized according to the three primary research objectives: rigorously evaluate the potential of three-dimensional synchronous scanning and EEMs to 1) discriminate the fluorescent dye spectra of four common fluorescent dyes from one another, 2) discriminate fluorescent dye spectra of four common fluorescent dyes from background fluorescence in anthropogenically-effected sampling environments, and 3) enhance existing or establish new fluorescent dye detection and quantification methods in the field of dye tracing.

Research Objective 1 was satisfied through both two and three-dimensional analysis of single dye dilutions and mixed dye dilutions and comparisons of the resultant two-dimensional synchronous scans and EEMs/contour diagrams. Analysis of single dye dilutions yielded two primary conclusions: 1) The presence of three, rather than two, fluorescence centers in EO EEMs and contour diagrams may serve as an additional measure provided by three-dimensional synchronous scanning to distinguish FL from EO in aqueous dye trace samples, and 2) No fluorescence features were identified through EEMs/contour diagrams beyond those regularly identified through two-dimensional synchronous scans that might enhance identification of RWT and SRB in dye trace samples.

Analysis of mixed dye dilutions yielded four primary conclusions: 1) No specific qualitative fluorescence center characteristics displayed in the EEMs/contour diagrams

seem sufficiently unique to distinguish FL from EO or RWT from SRB beyond what is possible through two-dimensional synchronous scanning; 2) Through the use of three-dimensional synchronous scanning, it is possible to determine whether FL or EO compositionally dominate the sample by comparing the locations of the mixed dye secondary fluorescence centers to the locations of the FL and EO single dye dilution secondary fluorescence centers; 3) Through the use of three-dimensional synchronous scanning, it is possible to identify whether RWT or SRB are present in a sample mixture, although their primary fluorescence centers may not be visible in the chosen graph space, by comparing the locations of the mixed dye dilution secondary fluorescence centers to the locations of the RWT and SRB single dye dilution secondary fluorescence centers; and 4) through proper consideration of relative quantum yields and secondary fluorescence centers, it may be possible to determine whether RWT or SRB compositionally dominate a mixture, even if the primary fluorescence peaks are not visible in the graph space.

Research Objective 2 was satisfied through two-dimensional and three-dimensional synchronous scanning of twenty-four Lost River Cave water samples following an injection of fluorescein dye. Two-dimensional analysis of the LRC samples resulted in four primary conclusions: 1) Three background fluorescence peaks were present in the LRC samples (peaks α, β, and γ); 2) peak α is likely attributable to fulvic acids, or fulvic-like fluorescence; 3) peak β is most likely attributable to fulvic acids, or fulvic-like fluorescence; and 4) peak γ is most likely attributable to the optical brightener Leucophor PBS and humic acids, or humic-like fluorescence. Three-dimensional analysis of LRC samples resulted in one primary conclusion: three-dimensional synchronous

scanning did not enhance the discrimination of background fluorescence from the fluorescent dyes FL, EO, RWT, and SRB as compared to two-dimensional synchronous scanning.

Research Objective 3 was addressed as a matter of course through pursuit of satisfaction of Research Objectives 1 and 2. Prior to this study, the only fluorescent dye emission-excitation measurements identified in the literature were excitation and emission maxima provided by Käss (1992). Through the three-dimensional analysis of single dye dilutions of FL, EO, RWT, and SRB, full λ_{Ex} and λ_{Em} were established for each of the four dyes. These measurements may provide the foundation for optimizing two-dimensional synchronous scanning of samples containing fluorescent dyes and detection of fluorescent dyes employed in fluorescent dye traces. Through the course of this research and the determination of the λ_{Ex} and λ_{Em} of the four fluorescent dyes, it also became evident that the excitation wavelength regularly used in the CHL to excite samples through the course of two-dimensional synchronous scanning is likely not the ideal Ex wavelength for the detection of low concentration FL, EO, RWT, and SRB. Measurements made through this research may provide the foundation for optimizing two-dimensional synchronous scanning of fluorescent dye-containing samples in the CHL.

7.2 Future Work

Several adjustments if applied to further analysis of water samples containing FL, EO, RWT, or SRB may substantially enhance the analysis and the breadth of the results. Future three-dimensional synchronous scanning of fluorescent dyes should employ a

wider λ_{Ex}, or should be shifted to encompass longer excitation wavelengths to ensure measurement of the entire fluorescent dye primary fluorescence center. If within instrument limitations, the λ_{Ex} should range from 300 to 700 nm. Many primary fluorescence centers through the course of this study, especially those rendered by RWT and SRB, were truncated substantially or entirely omitted through the application of the chosen λ_{Ex} because the chosen λ_{Ex} spanned insufficiently long Ex wavelengths. Only FL primary fluorescence centers at high concentrations were fully visible through the course of this research. Furthermore, many EEMs/contour diagrams exhibited primary fluorescence centers of clearly unique shapes (for example, a bean-shaped feature in the FLEO 10:100 EEM/contour diagram and an arm-like feature in the RWTSRB 100:1 and RWTSRB 100:10 EEMs/contour diagrams) that may be clearly visible and provide additional information if longer Ex wavelengths are employed.

Alternatively, further studies may seek to employ more than one three-dimensional parameter set. The parameter set employed through this study may be slightly adjusted to fully capture the EO primary fluorescence center and low concentration FL primary fluorescence centers. An additional parameter set could be developed that employed longer Ex wavelengths and ensured measurement of the full RWT and SRB primary fluorescence centers.

Finally, future studies, especially any future studies performed in the CHL using three-dimensional synchronous scanning, may seek to use wavelength-cutting filters to eliminate fluorescence interference contributed by scattered light. Through the course of this study, usage of an appropriate $\Delta\lambda$ did not mitigate the effects of interference by

scattered light, which included obstruction of fluorescence center identification and measurement.

Following development of one or more optimum parameter sets for three-dimensional synchronous scanning of fluorescent dye dilutions and installation of wavelength-cutting filters (or otherwise mitigation of scattered light), future research may seek to establish methods by which "peak area," or in the case of EEMs/contour diagrams, primary fluorescence center area, may be quantified within or outside the analytical software. Developing the capacity to calculate the three-dimensional fluorescence center area would potentially allow the development of an area-concentration relationship like that used through two-dimensional synchronous scanning in the CHL to measure fluorescent dye concentrations. The development of this technique would render three-dimensional synchronous scanning equally as informative as, if not more informative than, two-dimensional synchronous scanning in the field of dye tracing.

Several components of the research performed through this study may benefit from repetition and verification. If a more suitable parameter set is developed for three-dimensional synchronous scanning of fluorescent dyes, the estimated λ_{Ex} and λ_{Em} of FL, EO, RWT, and SRB should be verified using a sample size greater than thirty and a statistical framework should be developed around the fluorescence center measurements to verify their significance. Through this process, the long Ex wavelength boundaries of the primary fluorescence centers of the four dyes should be verified since the upper Ex wavelength boundaries were nearly all defined by estimation. Estimation of the long Ex boundaries of the primary fluorescence centers was based on the assumption that fluorescence centers are symmetrical about the Ex (*y*) axis. However, as established in

the Discussion section, this assumption is false on the basis of the asymmetry of the FL 100 ppb primary fluorescence center. Through the course of this research, other boundaries of the fluorescence centers were also established by estimation as necessitated by interference of scattered light and limitations of the chosen parameter set. This assumption is generally flawed as well and all estimated boundaries of the fluorescence centers should be verified through future studies.

In addition to repetition and verification of several components of the research, several conclusions derived from the research should be verified as well. It is suggested through this work that the presence of three, rather than two, secondary fluorescence centers in EO EEMs and contour diagrams may serve as an additional measure to distinguish FL from EO in aqueous dye trace samples. This conclusion is founded upon observations drawn from one EO 100 ppb EEM/contour diagram and two FL EEM/contour diagrams (10 ppb and 100 ppb). Future work should endeavor to test this conclusion using a greater sample size and should evaluate the validity of this conclusion when applied to more dilute samples.

Further research should be conducted to characterize the Lost River. The LRC sample background fluorescence peak γ Em maxima was determined through the measurement of the peak in only two samples. Further studies should seek to develop a more robust measurement of peak γ in Lost River water samples. Further studies should also seek to develop a more robust characterization of the Lost River background fluorescence, and background fluorescence of karst waters impacted by anthropogenic contamination, in general. The background fluorescence measured in the Lost River during the study period is likely not representative of total background fluorescence in

the Lost River and very likely omits seasonal variation in background fluorescence (specifically, variations in concentrations of humic and fulvic acids). Further studies should fully investigate the background fluorescence of the Lost River.

8. References

Alexander, S. (2005). Spectral deconvolution and quantification of natural organic material and fluorescent tracer dyes. *Sinkholes and the Engineering and Environmental Impacts of Karst*, (144), 441-448.

American Public Health Association (1999). *Standard methods for the examination of water and wastewater, 15th ed*. APHA, AWWA, and WEF, Washington D.C.

Baedke, S., Krothe, N. (2000). Quantitative tracer test of the Beech Creek aquifer at the Ammunition Burning Grounds, Naval Surface Warfare Center, Crane, Indiana. In Sasowsky, I., Wicks, C. (eds.), *Groundwater Flow and Contamination Transport in Carbonate Aquifers* (15-30). Rotterdam: A. A. Balkema.

Baker (2001). Fluorescence excitation-emission matrix characterization of some sewage-impacted rivers. *Environmental Science and Technology 35*(5), 948-953.

Baker, A. (2002). Fluorescence excitation—emission matrix characterization of river waters impacted by a tissue mill effluent. *Environmental Science and Technology 36*(7), 1377-1382.

Baker, A., Curry, M. (2004). Fluorescence of leachates from three contrasting landfills. *Water Research 38*(10), 2605-2613.

Baker, A. and Genty, D. (1999). Fluorescence wavelength and intensity variations of cave waters. Journal of Hydrology *217*(1-2), 19-34.

Baker, A., Lamont-Black, J. (2001). Fluorescence of dissolved organic matter as a natural tracer of ground water. *Groundwater 39*(5), 745-750.

Behrens, H., Beims, U., Dieter, H., Dietze, G., Eikmann, T., Grummt, T., Leibundgut, C. (2001). Toxicological and ecotoxicological assessment of water tracers. *Hydrogeology Journal 9*(3), 321-325.

Benischke, R., Goldscheider, N., Smart, C. (2007). Tracer techniques. In Goldscheider, N., Drew, D. (Eds.), *Methods in Karst Hydrogeology* (147-170). London: Taylor and Francis Group.

Bennet, M. (2011). Multi-parameter quantitative mapping of microfluidic devices. Unpublished doctoral dissertation. The University of Edinburgh, United Kingdom.

Blair, R., Ray, J., and O'dell, P. (2012). Integrated surface water and groundwater assessment of large springs in the Green River Basin (BMU4, round 2). Kentucky Division of Water. Retrieved from: http://water. ky.

gov/groundwater/Documents/NPS0503-IntegratedSWGWAssessmentGreenRiver.pdf.

(a) Bledsoe, L. (2019). *Analysis on Shimadzu RF-6000*. Internal Crawford Hydrology Laboratory document: unpublished.

(b) Bledsoe, L. (2019). *Standard operating procedures*. Internal Crawford Hydrology Laboratory document: unpublished.

Bloembergen, N. (1967). The stimulated raman effect. *American Journal of Physics 35*(11), 989-1023.

Cherry, J., Freeze, R. (1979). *Groundwater*. New Jersey, USA: Prentice Hall.

Coble, P. (1996). Characterization of marine and terrestrial DOM in seawater using excitation-emission matrix spectroscopy. *Marine chemistry 51*(4), 325-346.

Crain, A. (2002). Pesticides and nutrients in karst springs in the Green River Basin, Kentucky, May-September 2001. United States Geological Survey Factsheet 133-01. Retrieved from https://pubs.er.usgs.gov/publication/fs13301.

Crawford Hydrology Laboratory (2019). *Karst groundwater investigation research procedures*. Bowling Green, KY: Lee Anne Bledsoe. Retrieved from http://dyetracing.com/.

Crawford Hydrology Laboratory (n.d.). What is karst? Retrieved from http://yunus.hacettepe.edu.tr/~harun/karst.htm.

Crawford, N. (1984). Toxic and explosive fumes rising from carbonate aquifers: a hazard for residents of sinkhole plains. *Sinkholes: Their Geology, Engineering, and Environmental Impact*. Balkema, Rotterdam: 297-304.

Crawford, N. (2000). Microgravity investigations of sinkhole collapses under highways. In *Proceedings of the 1st SAGEEP Conference 1* (1-13).

Crawford, N., Hoffman, W. (1989). The karst landscape in warren county. In *Warren County Comprehensive Plan Technical Volume*. Bowling Green, KY: Western Kentucky University.

Currens, J. (1995). Generalized Block Diagram of the Western Pennyroyal Karst. Lexington, KY: KGS, Map and Chart 16, Series XII, 2001.

Currens, J. (2002). *Kentucky is Karst Country!: What You Should Know about Sinkholes and Springs* (Information Circular 4, Series XII). University of Kentucky: Kentucky Geological Society.

De Waele, J., Plan, L., Audra, P. (2009). Recent developments in surface and subsurface karst geomorphology: An introduction. *Geomorphology 106*, 1-8.

Fiore, J., del Carmen Scapini, M., Olivieri, A. (2013). Excitation–emission matrices applied to the study of urban effluent discharges in the Chubut River (Patagonia, Argentina). *Environmental monitoring and assessment 185*(8), 6909-6919.

Goldberg, M., Weiner, E. (1993). Fluorescence spectroscopy in environmental and hydrological sciences. In *Fluorescence Spectroscopy* (213-241). Berlin: Springer.

Goldscheider, N., Andreo, B. (2007). The geological and geomorphological framework. In Goldscheider, N., Drew, D. (Eds.), *Methods in Karst Hydrogeology* (9-23). London: Taylor and Francis Group.

Goldscheider, N., Drew, D., Worthington, S. (2007). Introduction. In Goldscheider, N., Drew, D. (Eds.), *Methods in Karst Hydrogeology* (1-8). London: Taylor and Francis Group.

Goldscheider, N. (2012). A holistic approach to groundwater protection and ecosystem services in karst terrains. *AQUA mundi 2*, 117-124.

Goldscheider, N., Meiman, J., Pronk, M., Smart, C. (2008). Tracer tests in karst hydrogeology and speleology. *International Journal of Speleology 37*(1), 27-40.

Göppert, N., Goldscheider, N. (2007). Solute and colloid transport in karst conduits under low- and high-flow conditions. *Groundwater 46*(1), 61-68.

Granger, D., Fabel, D., Palmer, A. (2001). Pliocene-Pleistocene incision of the Green River, Kentucky, determined from radioactive decay of cosmogenic ^{26}Al and ^{10}Be in Mammoth Cave sediments. *Geological Society of America Bulletin 113*(7), 825-836.

Groves, C. (1987). Lithologic controls on karst groundwater flow, Lost River groundwater basin, Warren County, Kentucky. [Master's thesis, Western Kentucky University]. WKU TopScholar.

Hudson, N., Baker, A., Ward, D., Reynolds, D., Brunsdon, C., Carliell-Marquet, C., and Browning, S. (2008). Can fluorescence spectrometry be used as a surrogate for the Biochemical Oxygen Demand (BOD) test in water quality assessment? An example from South West England. *Science of the total environment*, *391*(1), 149-158.

Ibsen Photonics A/S (2020). Signal-to-noise ratio and dynamic range definitions. Farum, Denmark. Retrieved from https://ibsen.com/wp-content/uploads/Tech-Note-The-Signal-to-Noise-Ratio-SNR-and-Dynamic-Range-DR.pdf.

Ingram, K., Dow, K., Carter, L., Anderson, J., and Sommer, E. (Eds.). (2013). *Climate of the Southeast United States: variability, change, impacts, and vulnerability*. Washington, DC: Island Press.

Käss, W. (1992). *Tracing technique in geohydrology*. Rotterdam, Netherlands: A.A. Balkema.

Keppy, N. and Allen, M. (2008). Understanding spectral bandwidth and resolution in the regulated laboratory. *Thermo Fisher Scientific Technical Note, 51721*.

Kraus, T. (2016). *Excitation-emission matrix*. Found in USGS Organic Matter Research Lab, https://ca.water.usgs.gov/OMRL/OpticalProperties.html.

Lost River Cave.org (n.d.). *Lost River Cave Weddings and Rentals Wedding Photo Gallery*. https://www.lostrivercave.org/weddings-rentals/#wedding-photo-gallery.

Meus, P., Käss, W., Schnegg, P. (2006). Background and detection of fluorescent tracers in karst groundwater. *Karst, climate change and groundwater 18*, 65-75.

Miller, R. (2019). *Mystery gasoline vapors force closing of tours and boat rides inside Lost River Cave*. Western Kentucky University Public Radio. Retrieved from https://www.wkyufm.org/post/mystery-gasoline-vapors-force-closing-tours-and-boat-rides-inside-lost-river-cave#stream/0.

Murck, B., Skinner, B., and Porter, S. (1997). *Dangerous Earth: An Introduction to Geologic Hazards.* John Wiley & Sons.

National Oceanic and Atmospheric Association (NOAA) (2020). Bowling Green Warren County Airport 1981-2010 Climate Normals. [Data set]. Retrieved from https://www.ncdc.noaa.gov/cdo-web/.

Ovesný, M. (2016). *Computational methods in single molecule localization microscopy* (Doctoral dissertation). Charles University, Prague.

Palmer, A. (1981). *A Geological Guide to Mammoth Cave National Park*. Teaneck, New Jersey: Zephyrus Press.

Palmer, A. (1991). Origin and morphology of limestone caves. *Geological Society of America Bulletin 103*, 1-21.

Palmer, A. (2007). *Cave geology 454*. Dayton: Cave books.

Panchompoo, J., Aldous, L., Baker, M., Wallace, M., and Compton, R. (2012). One-step synthesis of fluorescein modified nano-carbon for Pd (II) detection via fluorescence quenching. *Analyst 137*(9), 2054-2062.

Patra, D., Mishra, A. (2002). Total synchronous fluorescence scan spectra of petroleum products. *Analytical and Bioanalytical Chemistry 373*(4), 304-309.

PerkinElmer. (2000). An introduction to fluorescence spectroscopy. Buckinghameshire, UK. Retrieved from https://www.chem.uci.edu/~dmitryf/manuals/Fundamentals/Fluorescence%20Spectroscopy.pdf.

Pronk, M., Goldscheider, N., Zopfi, J. (2006). Dynamics and interaction of organic carbon, turbidity, and bacteria in a karst aquifer system. *Hydrogeology Journal 14*(4), 473-484.

Pronk, M., Goldscheider, N., Zopfi, J. (2007). Particle-size distribution as indicator for fecal bacteria contamination of drinking water from karst springs. Environmental Science & Technology, *41*(24), 8400-8405.

Qianqian, X., Fei, C., Yun, Z., Lei, C., and Jun, L. (2014). Analysis of spectra and intensity of 3D florescence of phenol dissolved in water. In *International Conference on Mechatronics, Control and Electronic Engineering* (MCE-14). Atlantis Press.

Ray, J., Currens, J. (1998). Mapped Groundwater Basins in the Beaver Dam 30 x 60 Minute Quadrangle. Kentucky Geological Survey Map and Chart Series 19.

Reynolds, D. (2014). The Principles of Fluorescence. In Coble, P., Lead, J., Baker, A., Reynolds, D., Spencer, R. (Eds.), *Aquatic Organic Matter Fluorescence* (3-34). New York, NY: Cambridge University Press.

Rubio, S., Gomez-Hens, A., and Valcarcel, M. (1986). Analytical applications of synchronous fluorescence spectroscopy. *Talanta*, *33*(8), 633-640.

Ryan, M., Meiman, J. (1996). An examination of short-term variations in water quality at a karst spring in Kentucky. *Groundwater 34*(1), 23-30.

Sasowsky, R. (2000). Carbonate aquifers: a review of thoughts and methods. In Sasowsky, I., Wicks, C. (Eds.), *Groundwater Flow and Contamination Transport in Carbonate Aquifers* (1-14). Rotterdam: A. A. Balkema.

Shahbazy, M., Vasighi, M., Kompany-Zareh, M., Ballabio, D. (2016). Oblique rotation of factors: a novel pattern recognition strategy to classify fluorescence excitation–emission matrices of human blood plasma for early diagnosis of colorectal cancer. *Molecular BioSystems*, *12*(6), 1963-1975.

Shimadzu (2012). LabSolutions: Data acquisition and processing theory guide. Kyoto, Japan. Shimadzu Corporation.

Shimadzu (2015). Shimadzu spectrofluorophotometer RF-6000 instruction manual. Kyoto, Japan: Shimadzu Corporation.

Sierra, M., Donard, O., Lamotte, M., Belin, C., Ewald, M. (1994). Fluorescence spectroscopy of coastal and marine waters. *Marine Chemistry 47*(2), 127-144.

Sierra, M., Giovanela, M., Parlanti, E., Soriano-Sierra, E. (2005). Fluorescence fingerprint of fulvic and humic acids from varied origins as viewed by single-scan and excitation/emission matrix techniques. *Chemosphere, 58*(6), 715-733.

Sliney, D. (2016). What is light? The visible spectrum and beyond. *The Scientific Journal of the Royal College of Ophthalmologists*, 30(2), 222-229.

Smart, C., Karunaratne, K. (2002). Characterisation of fluorescence background in dye tracing. *Environmental Geology 42*(5), 492-498.

Smart, P., Laidlaw, I. (1977). An evaluation of some fluorescent dyes for water tracing. *Water Resources Research 13*(1), 15-33.

Smart, C., Simpson, B. (2002). Detection of fluorescent compounds in the environment using granular activated charcoal detectors. *Environmental Geology 42*(5), 538-545.

Soltzberg, L., Lor, S., Okey-Igwe, N., and Newman, R. (2012). 3D fluorescence characterization of synthetic organic dyes. *American Journal of Analytical Chemistry*, 3(9), 622-631.

Sun, H., Sakka, Y., Shirahata, N., Gao, H., Yonezawa, T. (2012). Experimental and theoretical studies of photoluminescence from $Bi_8^{2+}$and Bi_5^{3+} stabilized by $[AlCl_4]^-$ in molecular crystals. *Journal of Materials Chemistry 22*(25), 12837-12841.

Tejada, S. (1985). EPA goes underground at Kentucky Superfund site. EPA Journal, *11*(6), 26-27.

Thomas, M. (2012). Root-mean square error compared to, and contrasted with, standard deviation. *Surveying and Land Information Science 72*(3), 107-108.

Thompson, M. and Ellison, S. (2005). A review of interference effects and their correction in chemical analysis with special reference to uncertainty. *Accreditation and Quality Assurance, 10*(3), 82-97.

Verhoeven, G. (2017). The reflection of two fields: electromagnetic radiation and its role in (aerial) imaging. *AARGNEWS 55*, 13-18.

Visit Bowling Green Kentucky (2016). *Bowling Green, Kentucky Things to Do: Caves and Nature around Bowling Green, Ky*. https://www.visitbgky.com/things-to-do/caves-nature/.

Wehry, E. (1997). Molecular fluorescence and phosphorescence spectrometry. In F. Settle (Ed.), *Handbook of instrumental techniques for analytical chemistry* (507-539). New Jersey: Prentice Hall.

Weiss, J. (1943). Fluorescence of Organic Molecules. *Nature 152*, 176-178.

Wu, F., Evans, R., and Dillon, P. (2003). Separation and characterization of NOM by high-performance liquid chromatography and on-line three-dimensional excitation emission matrix fluorescence detection. *Environmental Science and Technology, 37*(16), 3687-3

9. Appendix A: Fluorescence Theory

What is commonly called *fluorescence spectrometry* is an "umbrella term" that includes both fluorescence and phosphorescence spectrometry and may be more aptly termed "photoluminescent spectroscopy." The discussion begins with an explanation of fundamental aspects of spectrofluorophotometric analysis. Analysis by spectrofluorophotometer involves exposing a sample to radiation of a given distribution of wavelengths called an *excitation spectrum.* Fluorescent substances in the sample absorb the energy and then emit an *emission spectrum* which is measured by the instrument (in this case, a Shimadzu RF 6000 Spectrofluorophotometer (Figure 41).

Figure 41: Shimadzu RF-6000 fluorescence spectrofluorophotometer.

Wehry (1997) defined photoluminescence as, "a type of optical spectroscopy in which a molecule is promoted to an electronically excited state by absorption of ultraviolet, visible, or near infrared radiation. The excited molecule then decays back to the ground state, or to a lower-lying excited electronic state, by emission of light" (Wehry 1997, p. 509). More specifically, when a molecule in the base state S_0 is exposed to light, the electrons of the molecule experience an increase in kinetic energy because a

significant fraction of the molecules of the fluorescent substance absorb a proton. The increase in kinetic energy causes the molecule to move to a higher-energy level: an excited singlet state S_1. The excited molecule then transitions to a lower energy level, a triplet state T_1, without radiating energy. Finally, the excited molecule radiates energy in the form of heat or light (photons), which causes it to completely return to a base state S_0. The light emitted as the molecule transitions from an excited state S_1 to a triplet state T_1 to the base state S_0 is called *phosphorescence*. The light the molecule emits from a triplet state T_1 to a base state S_0 is called *fluorescence* (Smart and Laidlaw 1977; Wehry 1997; Baker and Genty 1999; Reynolds 2014; Shimadzu 2015) (Figure 42).

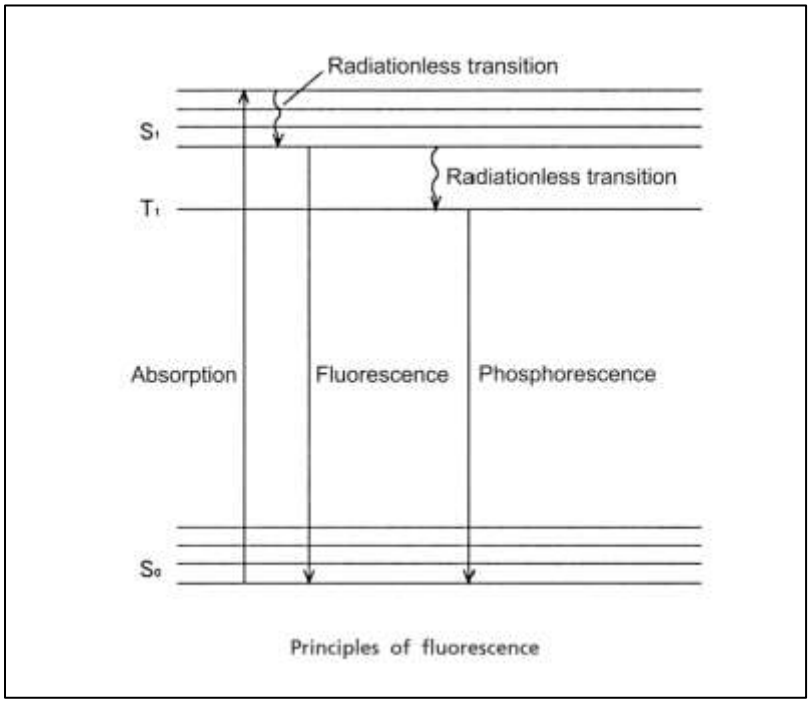

Figure 42: Jablonski energy diagram (Shimadzu 2015).

Several fundamental concepts of fluorescence are relevant in the course of basic fluorescence spectrometry: Stoke's Law and Stoke's Shift, wavelength offset, quanta, quantum efficiency, and the quantum yield of fluorescence (Q). First let it be said that

measurement of fluorescence parameters is generally made in terms of their *wavelengths* (distance between two consecutive crests in an electromagnetic wave) in units of nanometers (nm) (Sliney 2016). These measurements dictate the variety of energy as displayed in the figure below (Figure 43).

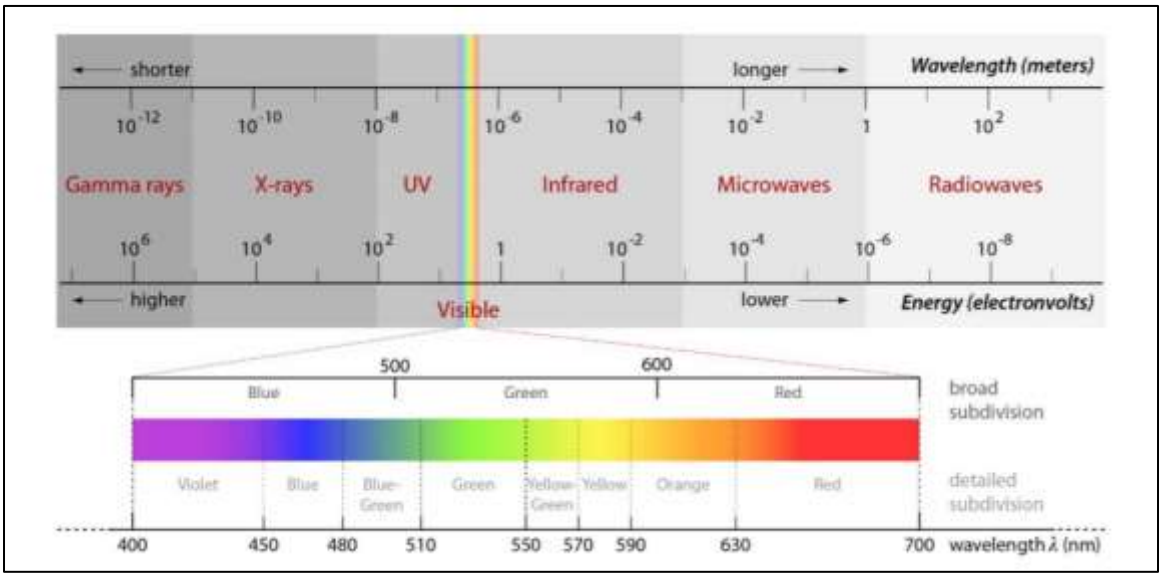

Figure 43: The full electromagnetic spectrum, including a more detailed perspective of the visible light range (Verhoeven 2017).

After a given molecule is excited by a certain wavelength of light to an excited state S_1, it radiates energy in the form of light as it returns to a base state S_0. Part of the energy that excited the molecule is lost as vibration or heat energy, which causes the molecule to radiate light at longer wavelengths than the wavelength of the light that excited it. This phenomenon is governed by *Stoke's Law* (Shimadzu 2015). Stoke's Law is relevant because it directs the instrument operator to scan longer wavelengths to measure the fluorescence of a sample than the wavelength of the light used to irradiate the sample (Shimadzu 2015). It is also relevant because it provides the basis for the phenomena whereby the maximum in the emission spectrum of a substance occurs at a longer wavelength than the maximum in the absorbance spectrum of the same substance.

The difference between these maxima is known as *Stoke's Shift* and usually ranges from 20 to 50 nm (Wehry 1997) (Figure 44).

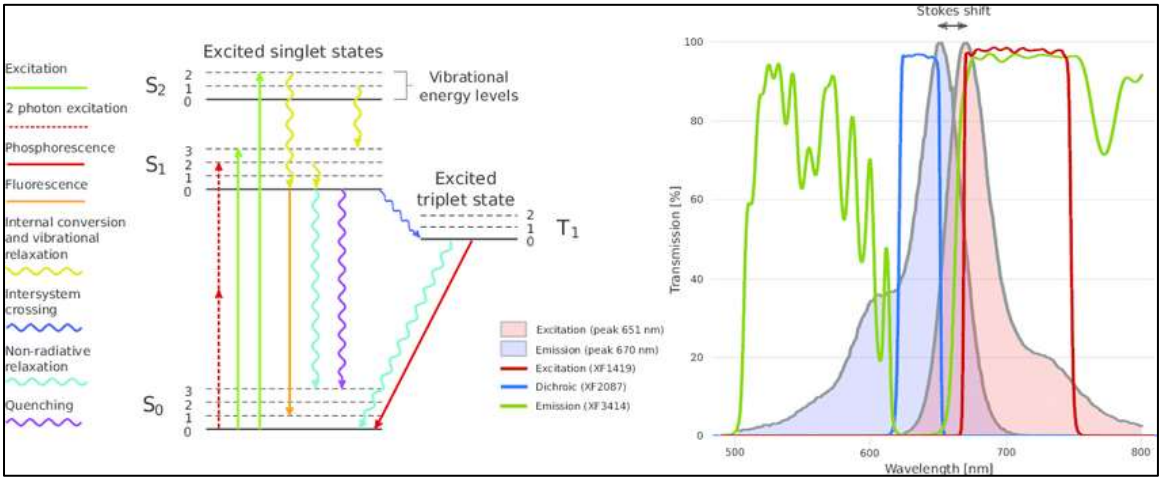

Figure 44: Jablonski diagram, Stokes shift, and wavelength offset (Ovesný 2016).

Stoke's shift is a fundamental principle of fluorescence spectroscopy and mandates the careful consideration and choice of *wavelength offset (Δλ)*. The Δλ is the difference in nanometers between the wavelength of light that the instrument operator sets to excite the substance and the wavelength of light absorbed or emitted by the substance that the instrument operator chooses to measure. It is rarely if ever within the instrument's capacity to measure the entire possible emission or absorption wavelength range in response to the entire possible range of excitation wavelengths—most instruments only measure the spectral range between 200 and 1000 nm. The Δλ is a critical consideration in fluorescent spectroscopy because improper consideration of the wavelength offset may result in inability to measure the full synchronous spectra of a substance, discussed below (Rubio et al. 1986; Wehry 1997).

Other pertinent concepts related to fluorescence spectroscopy include quantum efficiency and quantum yield of fluorescence. However, to facilitate explanation of these

fundamental concepts, it is necessary to discuss the nature and units of energy. It is necessary to assume that energy is composed of discrete units called quanta. The energy *E* of one quantum is proportional to its frequency of oscillation, as described by (PerkinElmer 2000):

$$E = hv = \frac{hc}{\lambda}\ erg \qquad (2)$$

where v = frequency, λ = related wavelength, and h = Planck's constant (6.624×10^{-27} ergs/second). However, the energy of only one quantum is usually too small for practical considerations and instead energy is usually discussed in terms of an *einstein*, or the amount of energy *E* associated with *N* quanta, or a mole of photons (where $N = 6.023 \times 10^{23}$, or Avogadro's number). The amount of energy per einstein is proportional to the frequency of the light, or radiation (PerkinElmer 2000). It is now possible to discuss fundamental concepts related to energy in terms of quanta and einsteins.

The *quantum efficiency* is the efficiency with which excited molecules return to a base state S_0 through decomposition, reaction, or emission. The quantum efficiency of a compound dictates that the excitation spectrum of a compound will be identical to the absorbance spectra of the same compound. Quantum efficiency of an excited molecule in the case of photoluminescent processes may be defined as:

$$\Phi E = \frac{einsteins\ emitted}{einsteins\ absorbed}\ or\ \frac{No.of\ quanta\ emitted}{No.of\ quanta\ absorbed} \qquad (3)$$

where ΦE is quantum efficiency of a substance, which never exceeds unity (PerkinElmer 2000, p. 6).

The *quantum yield of fluorescence (Q)* is the fraction of the electronically-excited molecules in a substance that will decay to a ground state S_0 by fluorescence. A high quantum yield indicates a high fluorescence intensity. A low quantum yield indicates a low fluorescence intensity, or no fluorescence. Mathematically, the quantum yield of fluorescence is defined by:

$$Q = \frac{n_c}{n_c + n_f + \sum n_0} \qquad (4)$$

where Q = quantum yield of fluorescence, n_c = frequency of light emission, n_f = frequency of radiationless transition, and n_0 = other frequencies (chemical reaction, etc.)

The quantum yield of fluorescence is the frequency of the waves of emitted light divided by the sum of the frequency of the emitted light, the frequency of the transition of the molecules from the T_1 to the S_0 state, and any other frequencies caused by processes other than the fluorescent decay of the excited molecules from the S_1 to the S_0 states. Nonradiative decay processes (processes other than fluorescence by which a molecule decays from an excited state to a ground state) include quenching (a process by which other chemical constituents within the substance prevent it from fluorescing when irradiated) or chemical reactions like photodecomposition and biodegradation (Smart and Laidlaw 1977; Wehry 1997; Shimadzu 2015). The quantum yield of fluorescence is relevant because it indicates to the instrument operator to what degree a substance may be expected to fluoresce, or if a substance may be expected to fluoresce at all. Quantum

yield values have been developed for certain compounds, including some fluorescent dyes (Wehry 1997).

Many of the components of fluorescence are controlled and measured through the practice of fluorescence spectroscopy. These components include the absorbance, excitation, emission, and synchronous spectra of a substance. The results of these analyses are traditionally displayed on two-dimensional graphs (for example, Figure 45) where fluorescence intensity is displayed in fluorescence intensity units on the *y*-axis and wavelength on the *x*-axis.

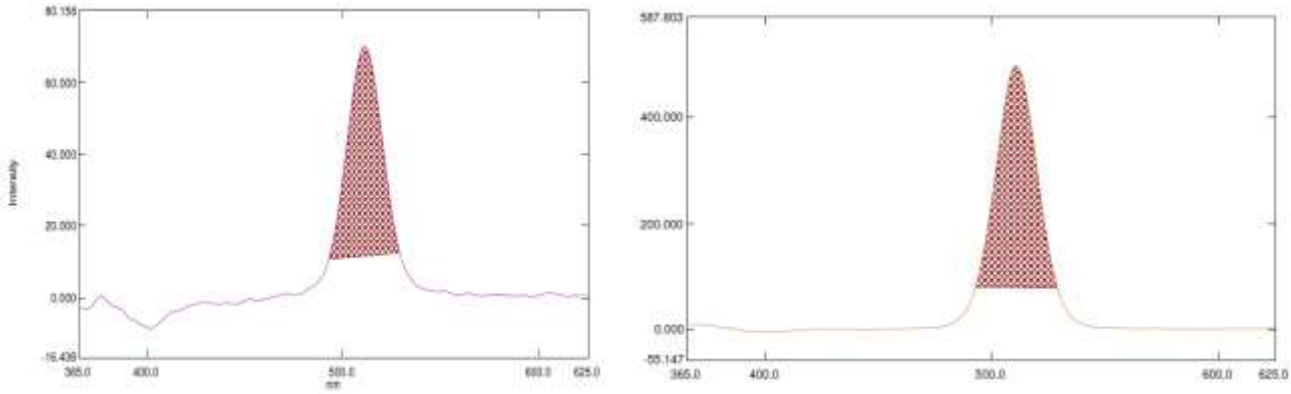

Figure 45: Two-dimensional synchronous scans of .01 PPB (left) and 0.1 PPB (right) fluorescein standard dilutions.

The *absorbance spectrum* (Figure 46) is the spectrum of wavelengths of excitation radiation (light used to irradiate the fluorescent compound) at which the fluorescent compound absorbs radiation (photons) and may become excited (a sufficient portion of the molecules move to an excited singlet state S_1). It is not, however, a record of the

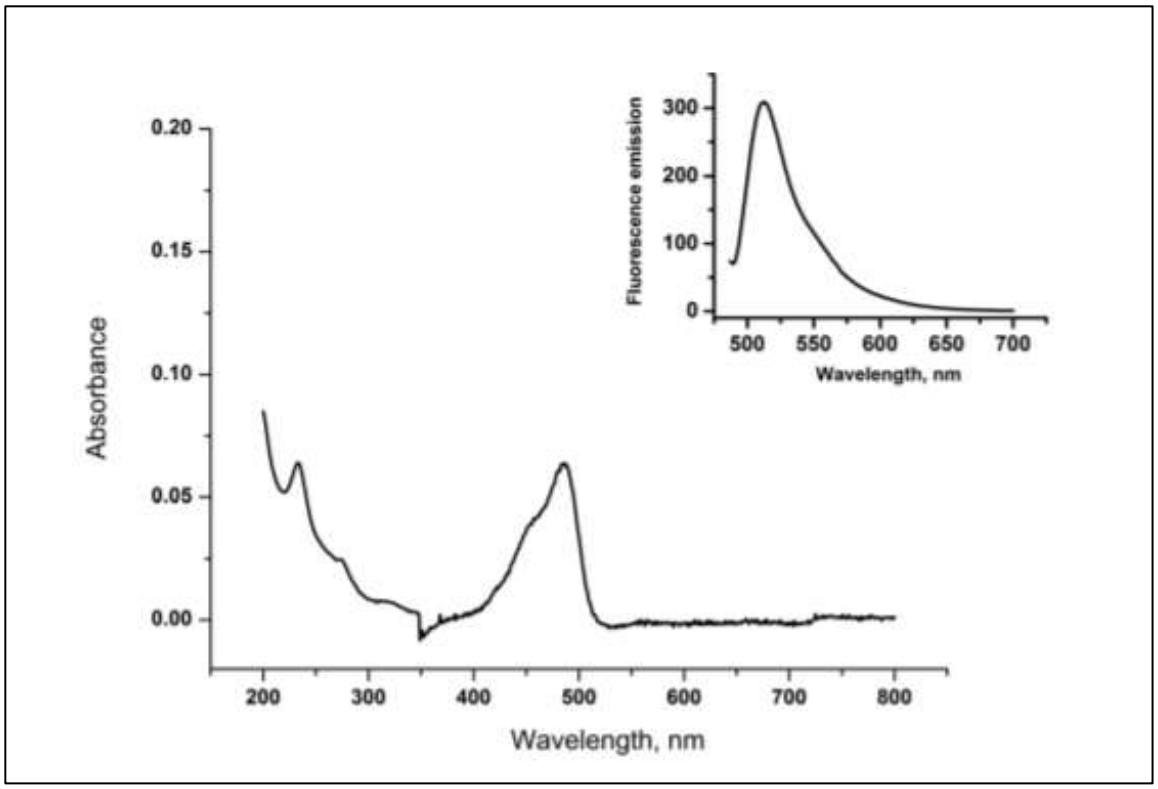

Figure 46: UV-Vis absorption spectrum of 10 μM fluorescein in water, with max absorbance observed at ~485 nm. Inset: fluorescence emission spectrum of 5 μM fluorescein in water (Ex = 485 nm) with emission max peak wavelength of 511.94 nm (Panchompoo et al. 2012).

excitation wavelengths at which the fluorescent compound will emit fluorescence.

Absorbance of a fluorescent compound is defined by a version of the Beer-Lambert Law (PerkinElmer 2000, p. 16):

$$\log_{10} \frac{Io}{I} = Ecl \qquad (5)$$

where I = intensity of the transmitted light, Io = intensity of incident light, E = molecular extinction coefficient, c = concentration in gm moles/L^{-1}, l = pathlength of sample, and $\log_{10} \frac{Io}{I}$ is = the absorbance of the compound.

By measuring the absorbance spectra of a substance, one may determine if a substance is fluorescent. If absorption does not occur at all, the substance will not fluoresce. Alternately, a substance will fluoresce most intensely when excited within the absorption peak wavelength range. More specifically, the maximum fluorescence intensity of a particular fluorescent compound will occur when the wavelength offset between the excitation and emission spectra correspond to the difference between the wavelengths of the absorption and emission maxima (Rubio et al. 1986; Wehry 1997; PerkinElmer 2000; Sierra et al. 2005; Shimadzu 2015). Wavelength offset will be discussed shortly.

The excitation spectrum (λ_{Ex}) is the spectrum of wavelengths of irradiating light at which the fluorescent compound will emit fluorescence (Figure 47). With few exceptions, the λ_{Ex} of a substance is identical to its absorption spectrum. The λ_{Ex} of a substance may be determined by measuring the fluorescence intensity of an irradiated substance at a set emission wavelength while varying the wavelength of the excitation light over a specified interval (Wehry 1997). The emission spectrum (λ_{Em}) of a fluorescent compound is the range of wavelengths of light that the molecules of an irradiated compound emit as they decay from a triplet state T_1 to a singlet state S_1. The λ_{Em} of a fluorescent compound may be measured by holding the excitation radiation at a constant wavelength while the light emitted by the fluorescent substance is measured along a specified range of wavelengths (Wehry 1997). The intensity of the λ_{Em} of a fluorescent substance is directly proportional to the excitation radiation and there is sometimes a slight overlap

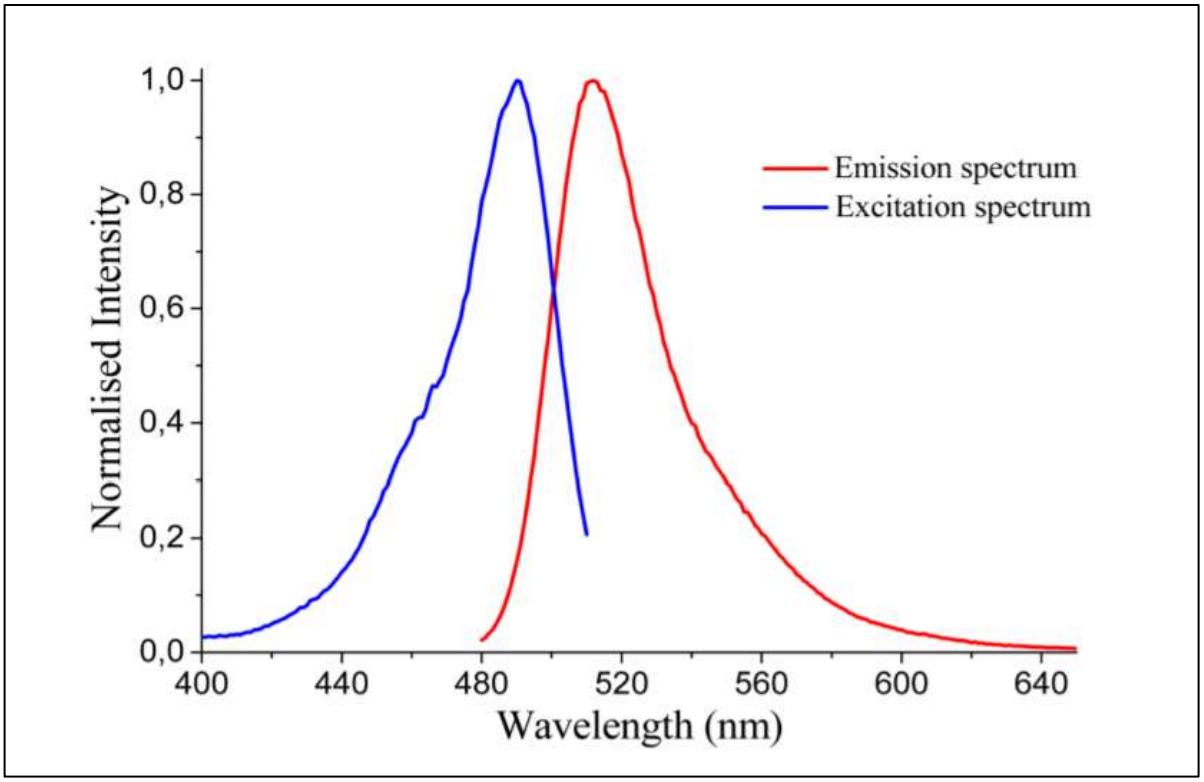

Figure 47: Excitation and emission spectra of fluorescein (Bennett 2011).

between the absorption and λ_{Em} of a fluorescent compound (Wehry 1997; PerkinElmer 2000).

The synchronous spectrum encompasses aspects of both λ_{Ex} and λ_{Em} in that both the λ_{Ex} and λ_{Em} are varied and monitored. The *synchronous spectra* of a fluorescent compound is the collection of λ_{Em} that are produced in response to radiation of a specified range of excitation wavelengths at specified intervals. The synchronous scan spectrum may be measured by measuring each λ_{Em} that is emitted in response to radiation of a certain excitation wavelength at specified intervals along a specified range of excitation wavelengths. The instrument operator chooses the excitation wavelength at which the results are displayed, and the wavelengths of the light emitted by the fluorescent substance are plotted on the *x*-axis against the fluorescence intensities of the light at each

emission wavelength on the *y*-axis on a graph. These graphs are known as *synchronous scans*. The intensity (*I*) reported in any synchronous scan is often reported in arbitrary fluorescence units (AFU) and is dependent upon the nature of the λ_{Ex} and λ_{Em}, as well as on the wavelength offset between the excitation λ_{Ex} and emission λ_{Em} wavelengths. Fluorescence intensity may be expressed as:

$$I_s = KcdE_x(\lambda_{ex})E_m(\lambda_{ex} + \Delta\lambda) \quad (6)$$

or, alternately,

$$I_s = KcdE_x(\lambda_{em} - \Delta\lambda)E_m(\lambda_{em}) \quad (7)$$

where E_x is the excitation function at a given excitation wavelength ($\lambda_{ex} = \lambda_{em} - \Delta\lambda$), E_m is the emission intensity at the corresponding emission wavelength ($\lambda_{em} = \lambda_{ex} + \Delta\lambda$), *c* is the analyte concentration, *d* is the thickness of the sample, and *K* is a characteristic luminescence constant comprising the "instrumental geometry factor" and related parameters (Rubio et al. 1986, p. 633).

Note that λ_{Em} and λ_{Ex} will not be identical for a given substance due to Stoke's shift. To account for Stoke's shift, the synchronous spectra of a fluorescent substance is not measured without consideration of an appropriate wavelength offset. The idea of a $\Delta\lambda$ between light of a distinct emission wavelength that is emitted in response to light of a distinct excitation wavelength may be expanded to apply to the full synchronous spectrum of a substance (full set of excitation wavelengths and emission wavelengths). As an example, the specified excitation wavelength range of a measured synchronous spectrum may begin at 250 nm, but the specified emission range of the same synchronous

spectrum may begin at 253. Synchronous scanning is heavily dependent on the chosen $\Delta\lambda$ since choosing an appropriate $\Delta\lambda$ ensures that the appropriate range of emission wavelengths is measured for each excitation wavelength. The fluorescence signal will be measurable only when the excitation and emission signals may both occur over the selected $\Delta\lambda$. The shape and bandwidth of a fluorescence spectrum are also functions of the chosen $\Delta\lambda$ (Rubio et al. 1986; Wehry 1997; Sierra et al. 2005).

The measurement of synchronous spectra, called *synchronous scanning*, is often the desired mode of fluorescence measurement because synchronous scanning provides more information than the measurement of absorbance, excitation, or emission spectra alone; is more useful in discriminating fluorescent compounds from one another; and is more useful in the discrimination of the fluorescence of the compound of interest from background fluorescence. Synchronous scanning has been used to characterize the fluorescence signatures of a wide variety of substances, including petroleum products, tissue mill effluent, humic and fulvic acids in a variety of natural aqueous samples, aqueous samples taken from waters impacted by sewage, landfill leachate, etc. (Goldberg and Weiner 1993; Sierra et al. 1994; Wehry 1997; Baedke and Krothe 2000; Baker 2001; Baker 2002; Patra and Mishra 2002; Smart and Simpson 2002; Baker and Curry 2004). The fluorescence signatures of common fluorescent dyes have also been established (Käss 1992). The following tables display fluorescence characteristics of many common fluorescent dyes and fluorescent compounds (Tables 17 and 18).

Table 14: Fluorescence properties of some common organic substances.

Source	Substance/ Compound	Comments	Excitation Maximum or Range (nm)	Emission Maximum or Range (nm)
Baker 2001, p. 949	tryptophan		275	350
Baker 2001, p. 949	fulvic-like		320-340	410-430
Baker 2001, p. 949	humic-like		370-390	460-480
Baker 2001, p. 950	fulvic-like		330	418
Baker 2001, p. 950	fulvic-like		339	422
Baker 2001, p. 950	fulvic-like		337	421
Baker 2001, p. 950	fulvic-like		329	416
Baker 2001, p. 950	fulvic-like		339	420
Baker 2001, p. 950	fulvic-like		336	420
Baker 2001, p. 950	fulvic-like		332	416
Baker 2001, p. 950	fulvic-like		329	414
Baker 2001, p. 950	protein (troptophan) luminescence		278	363
Baker 2001, p. 950	protein (troptophan) luminescence		278	340
Baker 2001, p. 950	protein (troptophan) luminescence		278	357

Source	Substance/ Compound	Comments	Excitation Maximum or Range (nm)	Emission Maximum or Range (nm)
Baker 2001, p. 950	protein (troptophan) luminescence		281	356
Baker 2001, p. 950	protein (troptophan) luminescence		279	353
Baker 2001, p. 950	protein (troptophan) luminescence		279	360
Baker 2001, p. 950	protein (troptophan) luminescence		278	360
Baker 2001, p. 950	protein (troptophan) luminescence		276	370
Sierra et al. 2005	fulvic acid--most intense center		260	460
Sierra et al. 2005	fulvic acid--less intense center		310	440
Sierra et al. 2005	humic acid--less intense center		265	325
Sierra et al. 2005	humic acid--less intense center		360	520
Muller et al. 2008, p. 8038	TYLIS	tyrosine-like substances	265-285	395-315
Muller et al. 2008, p. 8038	TRYLIS	tryptophan-like substances	260-295	335-370
Muller et al. 2008, p. 8038	HULIS	humic-like substances	300-340	390-475
Muller et al. 2008, p. 8040	tyrosine-like peak		275	305
Muller et al. 2008, p. 8040	trytophan-like peak		275	340
Muller et al. 2008, p. 8040	humic-like peak (exact intensity maximum dependent upon source--terrestrial,		320-360	420-460

Source	Substance/ Compound	Comments	Excitation Maximum or Range (nm)	Emission Maximum or Range (nm)
	anthropogenic, or agriculture)			
Hudson et al. 2008, p. 2	humic- like (from decomposition of plant material)--Peak C		304-347	405-461
Hudson et al. 2008, p. 2	humic- like (from decomposition of plant material)--Peak A		217-261	395-449
Hudson et al. 2008, p. 2	tryptophan-like peak--Peak T (most intense)		275-296	330-378
Hudson et al. 2008, p. 2	tryptophan-like peak--Peak T2 (less intense)		216-247	329-378
Hudson et al. 2008, P. 1-2	tryptophan-like peak	maximum of overall potential range	275	340
Hudson et al. 2008, p. 14	tryptophan-like peak	based on all samples (surface water and effluent)	296	378
Hudson et al. 2008, p. 14	tryptophan-like peak	based on all samples (surface water and effluent)	247	378
Hudson et al. 2008, p. 14	humic-like peak	based on all samples (surface water and effluent)	347	461
Hudson et al. 2008, p. 14	humic-like peak	based on all samples (surface water and effluent)	261	449

Table 15: Käss (1992) fluorescent dye properties.

Substance/ Compound	Comments	Excitation Maximum or Range (nm)	Emission Maximum or Range (nm)	Δλ (nm)
Uranine	I.e. Fluorescein	491	512	21
Uranine	I.e. Fluorescein	438	512	74
Eosin		516	538	22
Rhodamine B		554	576	22
Sulforhodamine B		564	583	19
Amidorhodamine B		530	551	21
Rhodamine WT		554	580	26
Rhodamine 6G		526	552	26
Erythrosine		525	547	22
Rose bengale		518	535	17
Dichlorfluorescein		502	518	16
Pyranine 108%	At pH 9.5	455	512	57
Pyranine 108%	at pH <2	405	445	40
Na-naphthionate		320	430	110
Amino G-acid		359	450	91
Lanaperl fast yellow		469	508	39
Lissamine		432	508	76
Tinopal CBS-X		346	435	79
Leucophor PBS	Liquid form	348	430	82
Photine CU		345	435	90
Optical brightener		349	430	81

10. Appendix B: Complete Collection of Two and Three-Dimensional Synchronous Scans

10.1 Single Dye Dilution Two-Dimensional Synchronous Scans

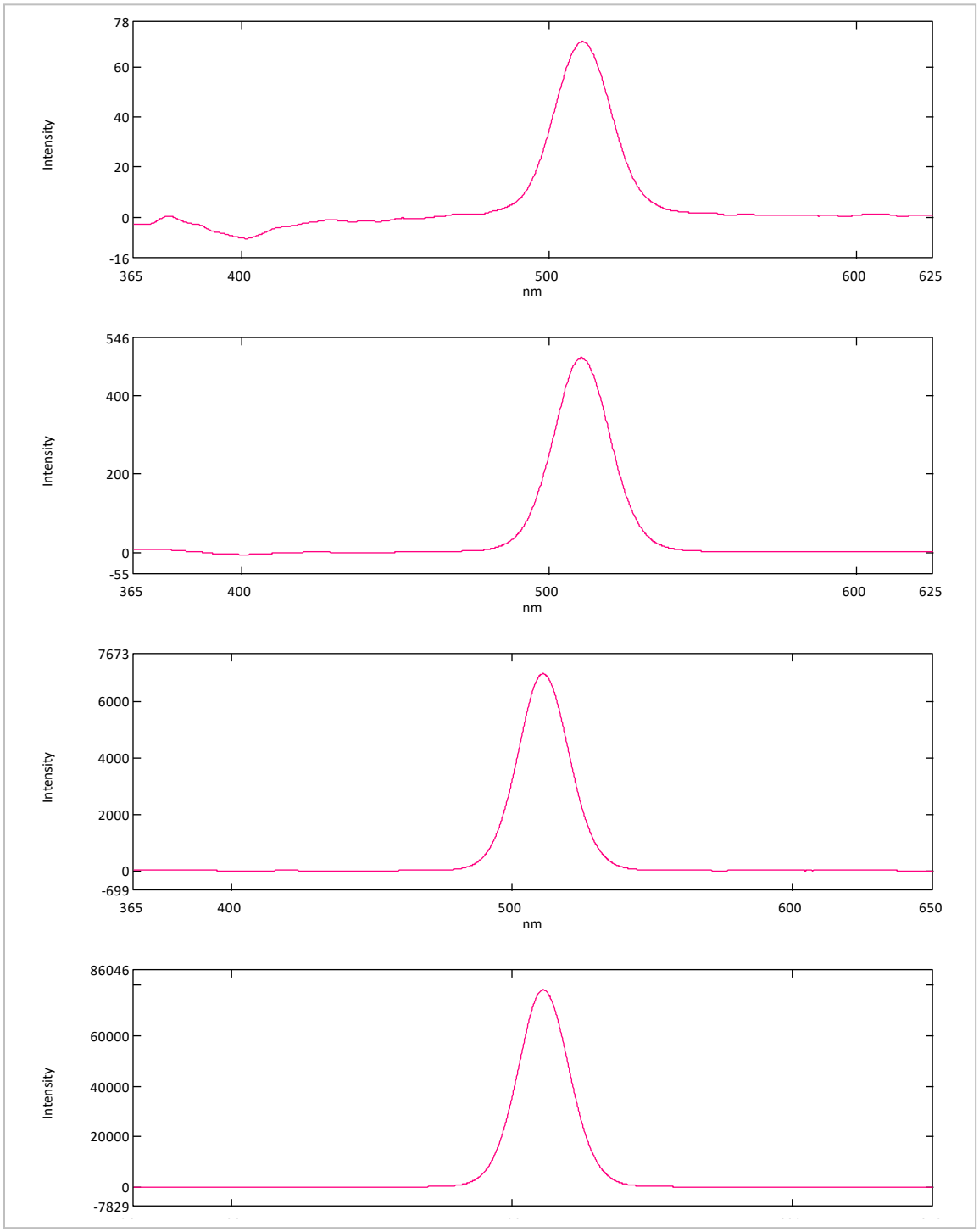

Figure 48: Top to bottom, two-dimensional synchronous scans of fluorescein .01, 0.1, 1, and 10 ppb single dye dilutions.

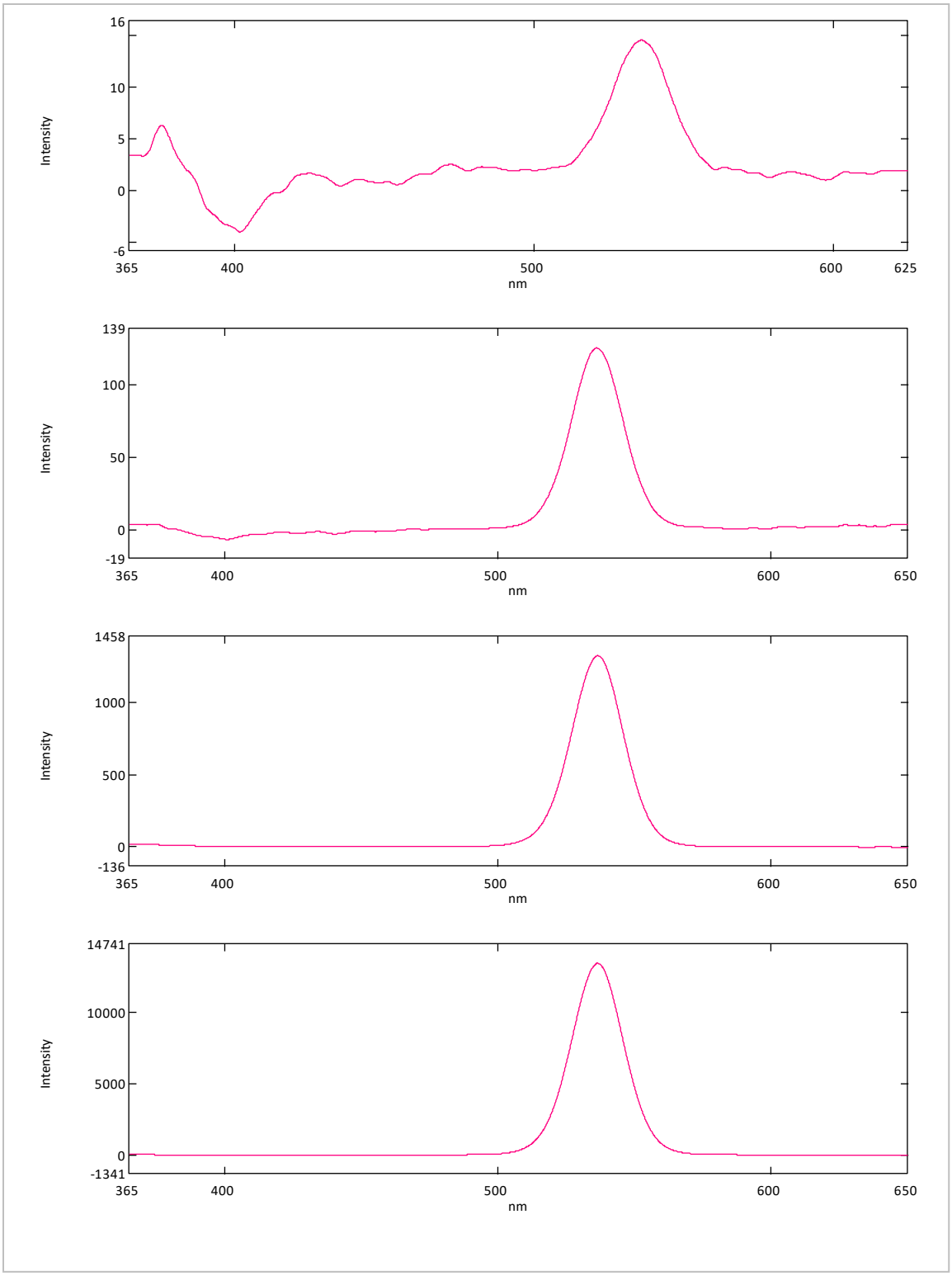

Figure 49: Top to bottom, two-dimensional synchronous scans of eosin .01, 0.1, 1, and 10 ppb single dye dilutions.

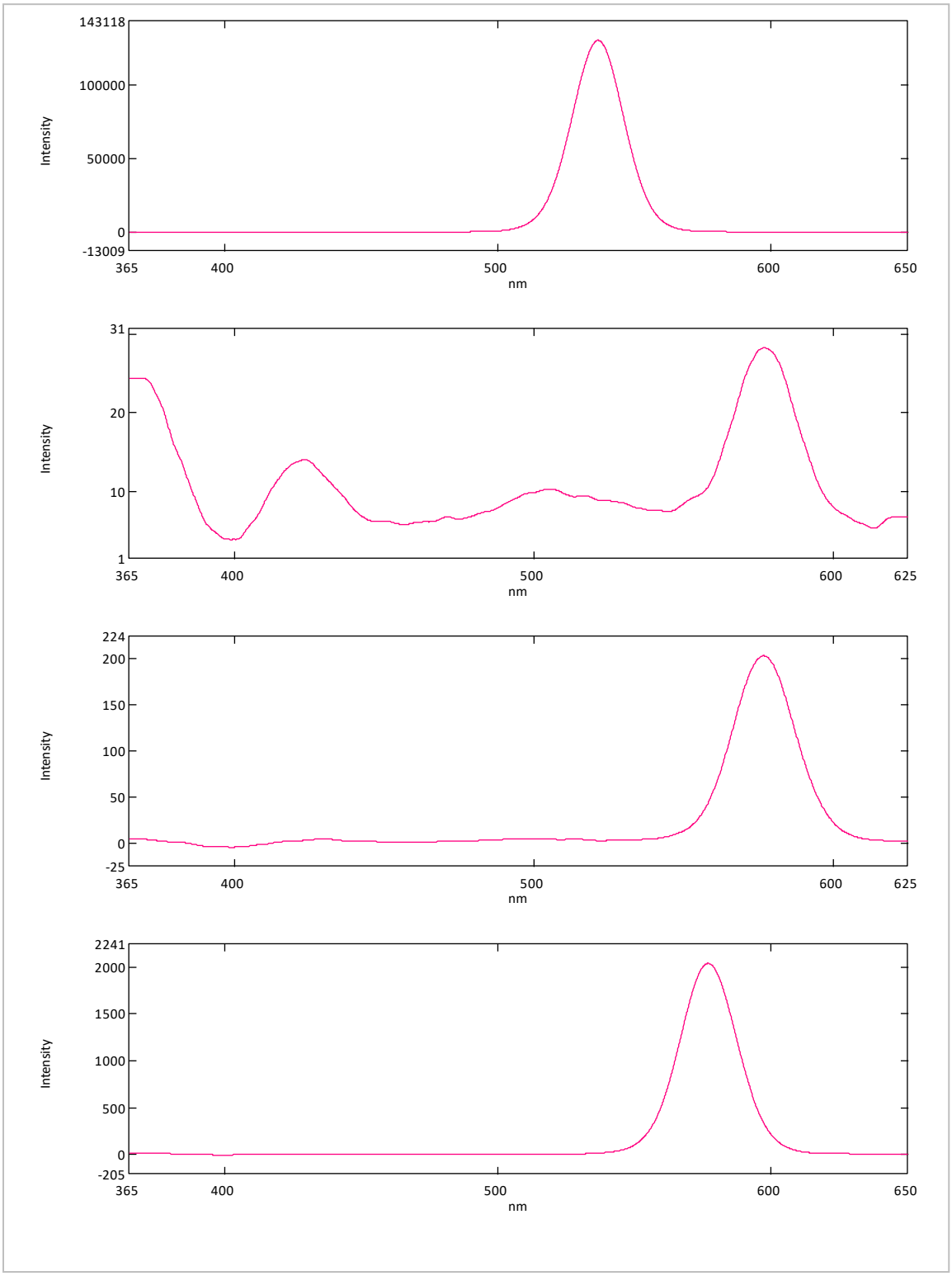

Figure 50: Top to bottom, two-dimensional synchronous scans of eosin 100 ppb and rhodamine WT .01, 0.1, and 1 ppb single dye dilutions.

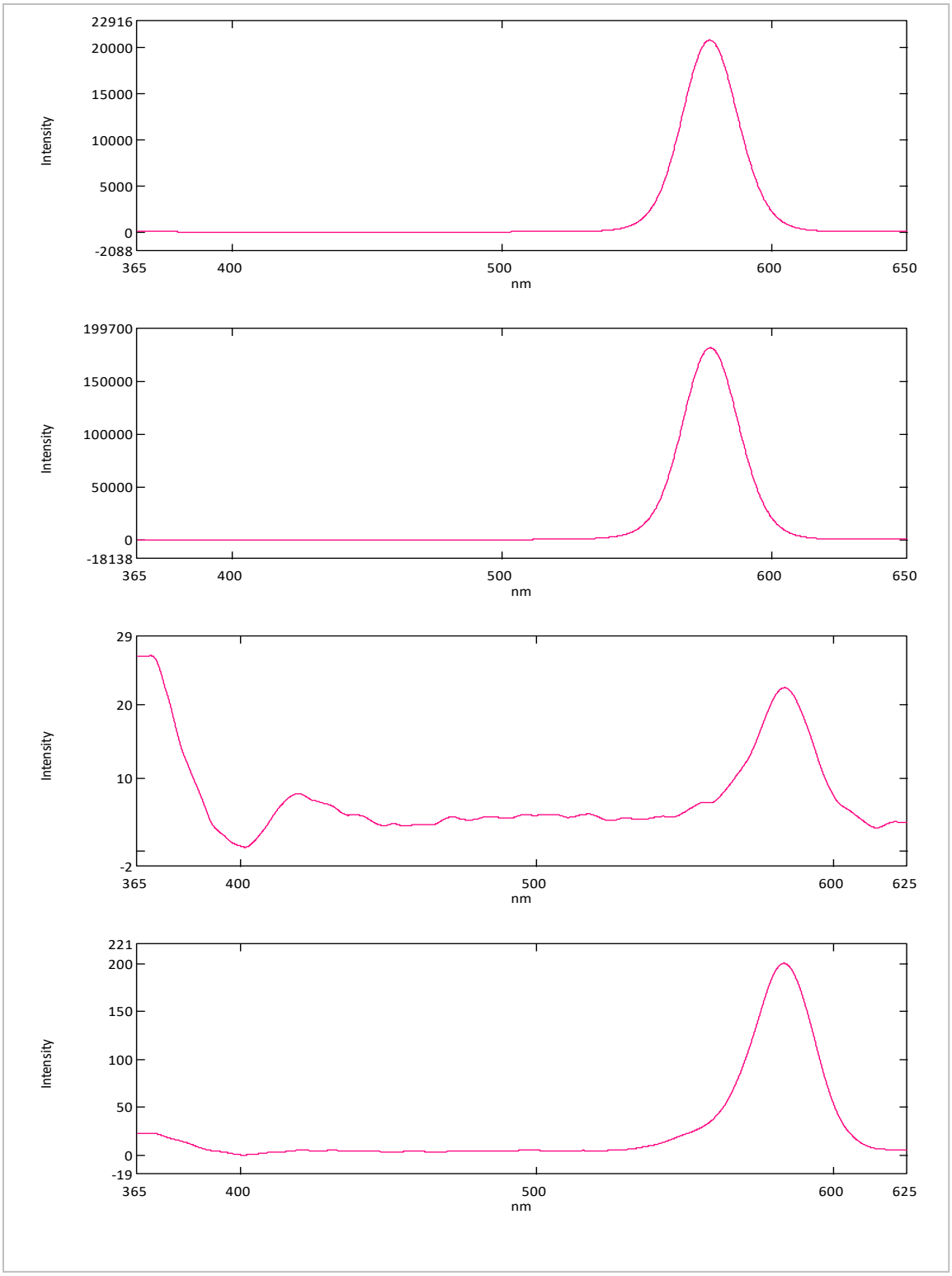

Figure 51: Top to bottom, two-dimensional synchronous scans of rhodamine WT 10 and 100 ppb and sulphorhodamine B .01 and 0.1 ppb single dye dilutions.

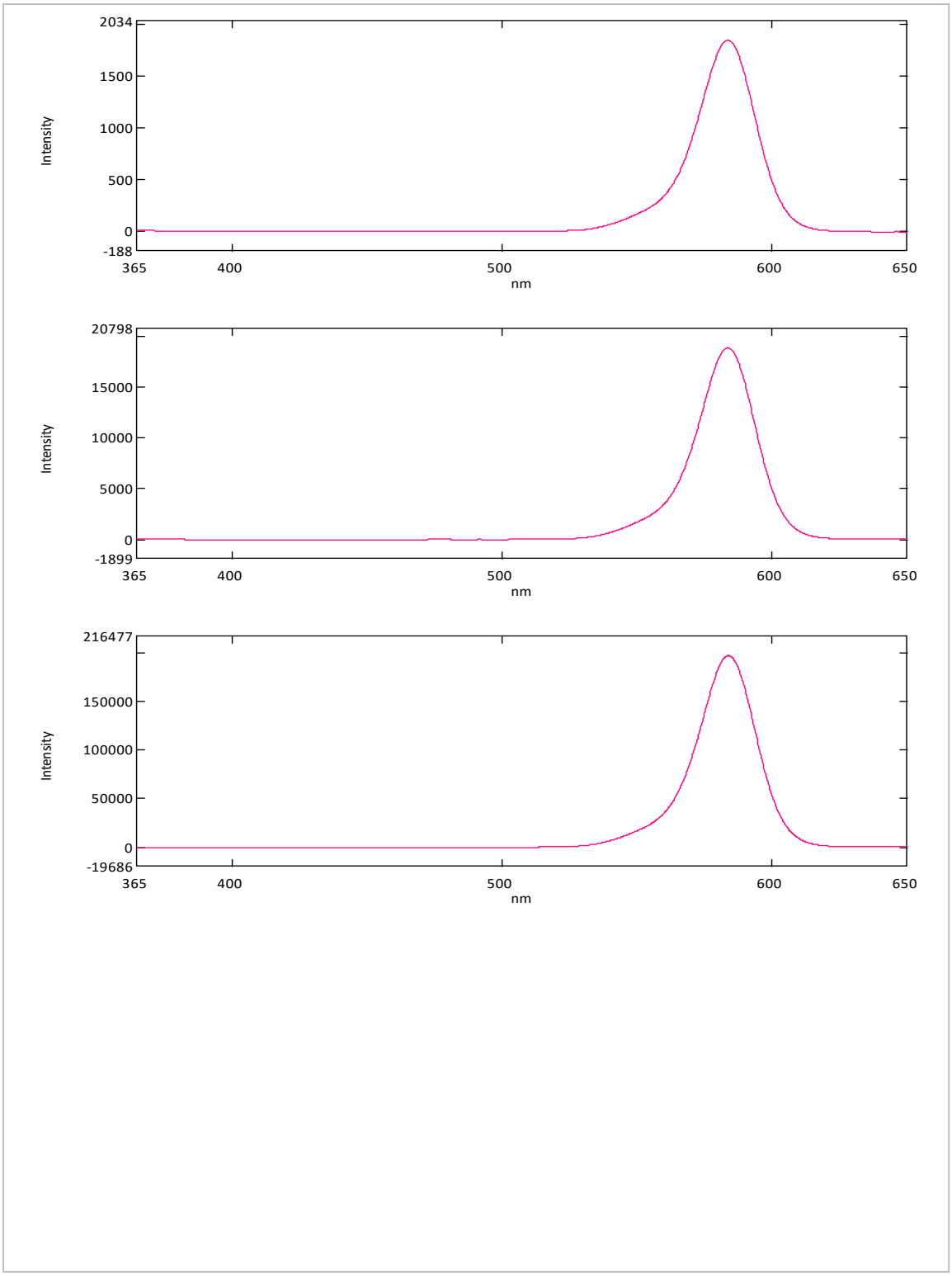

Figure 52: Top to bottom, two-dimensional synchronous scans of sulphorhodamine B 1, 10, and 100 ppb single dye dilutions.

10.2 Single Dye Dilution Three-Dimensional Synchronous Scans

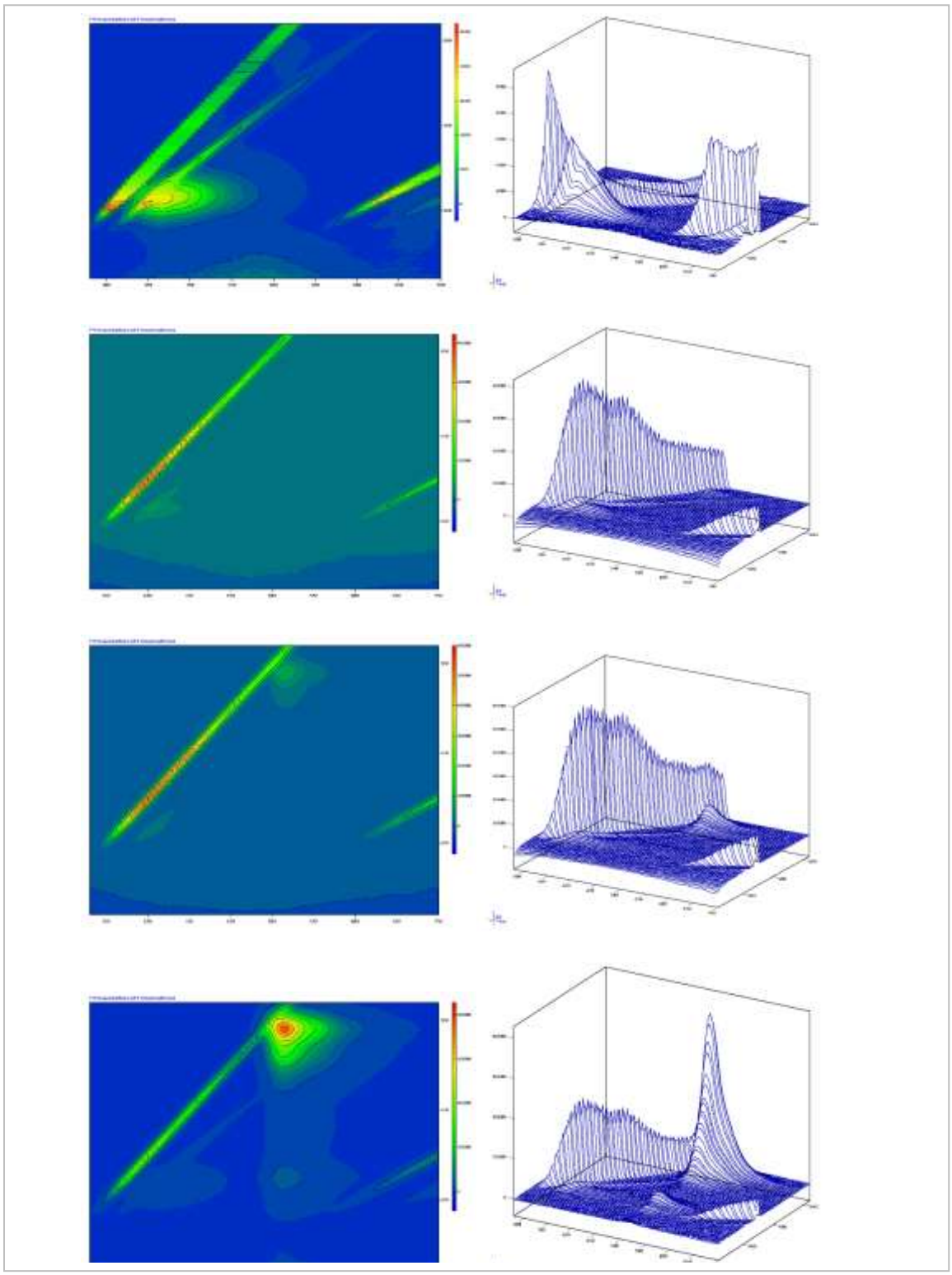

Figure 53: Top to bottom, three-dimensional synchronous scans of fluorescein, .01, 0.1, 1, and 10 ppb single dye dilutions. X-axis range = 280 - 700 is nm, Y-axis range = 220 – 520 nm.

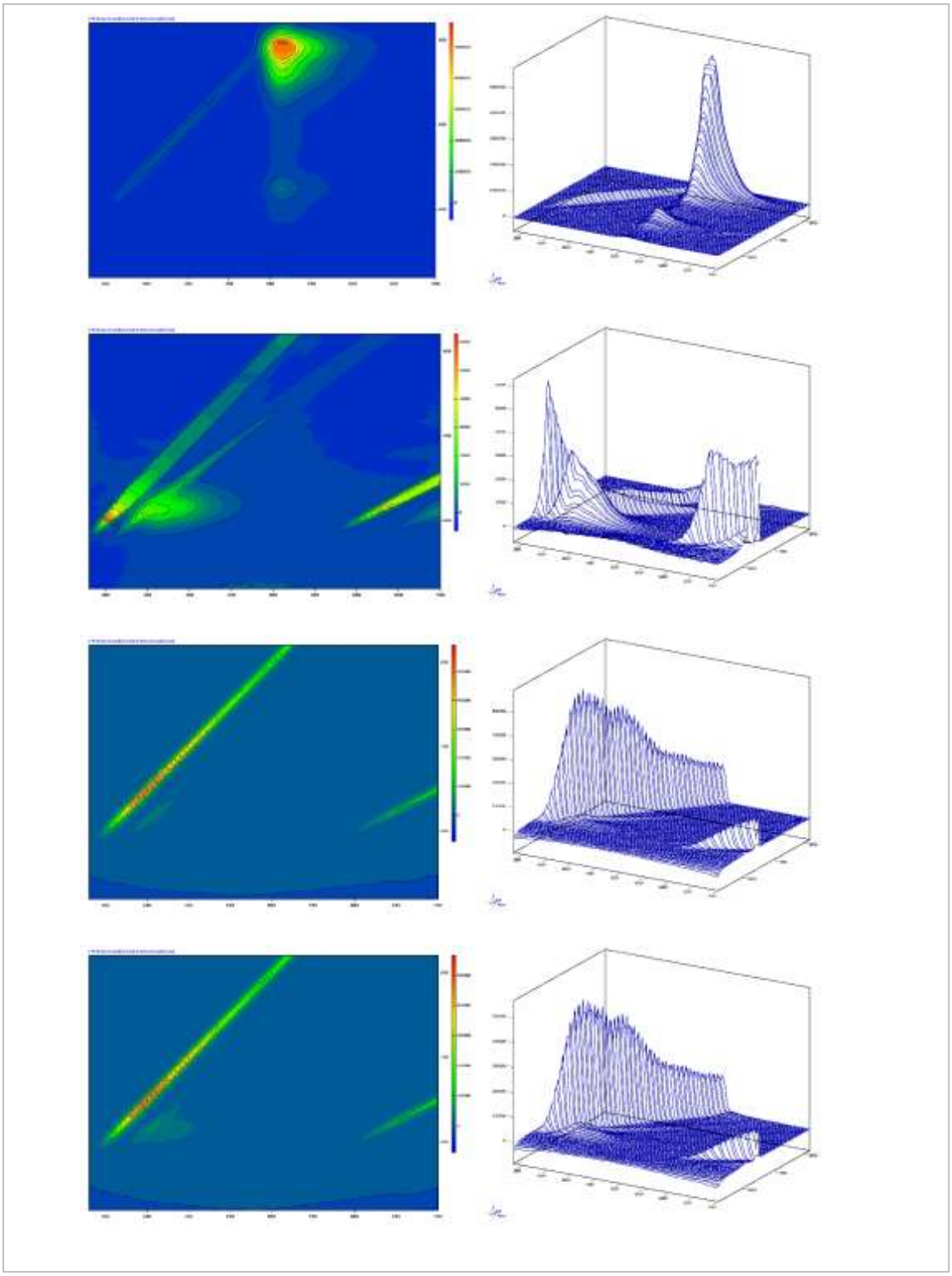

Figure 54: Top to bottom, three-dimensional synchronous scans of fluorescein 100 ppb and eosin .01, 0.1, and 1 ppb single dye dilutions. X-axis range = 280 - 700 is nm, Y-axis range = 220 – 520 nm.

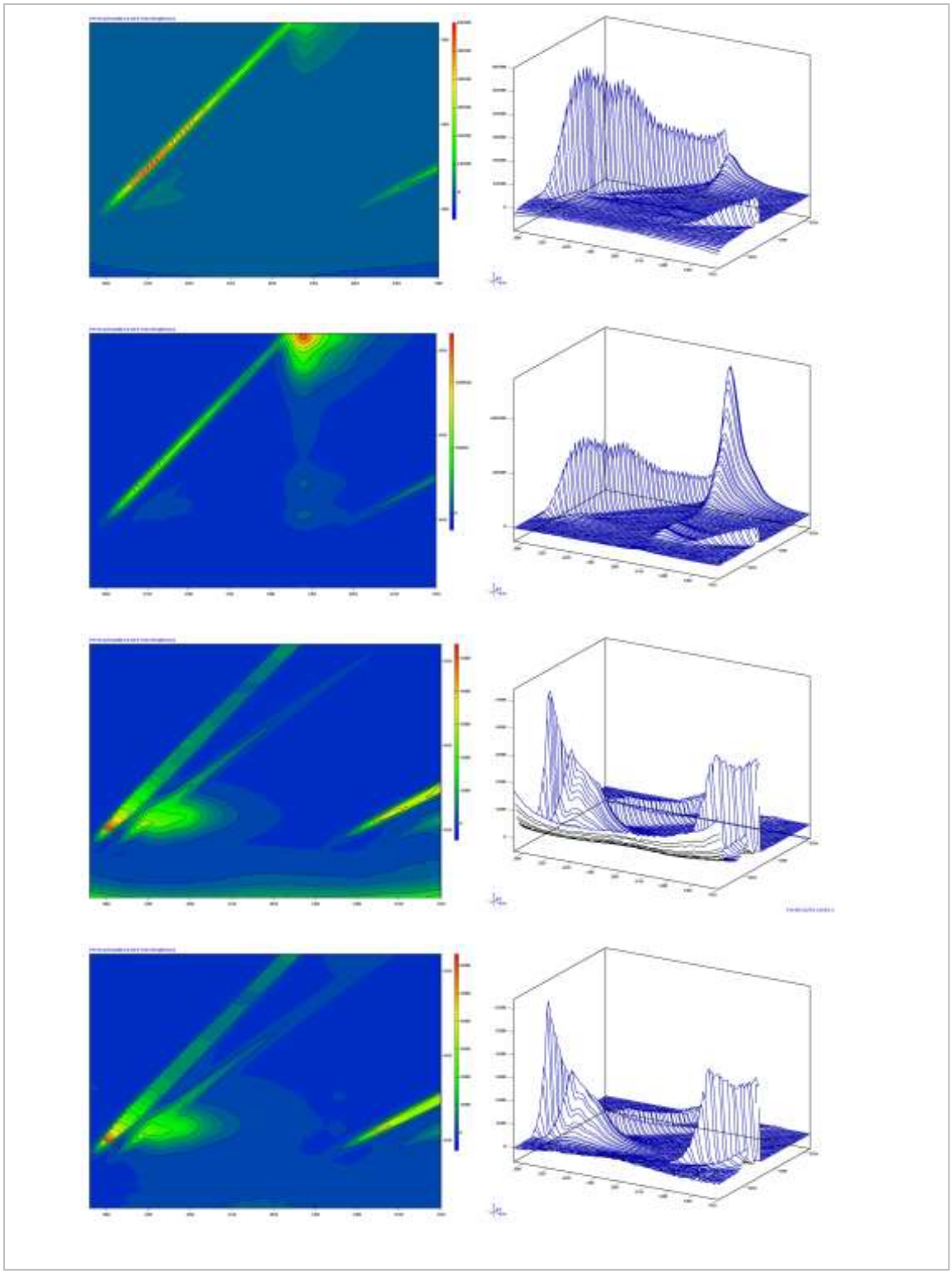

Figure 55: Top to bottom, three-dimensional synchronous scans of eosin 10 and 100 ppb and rhodamine WT .01 and 0.1 ppb single dye dilutions. X-axis range = 280 - 700 is nm, Y-axis range = 220 – 520 nm.

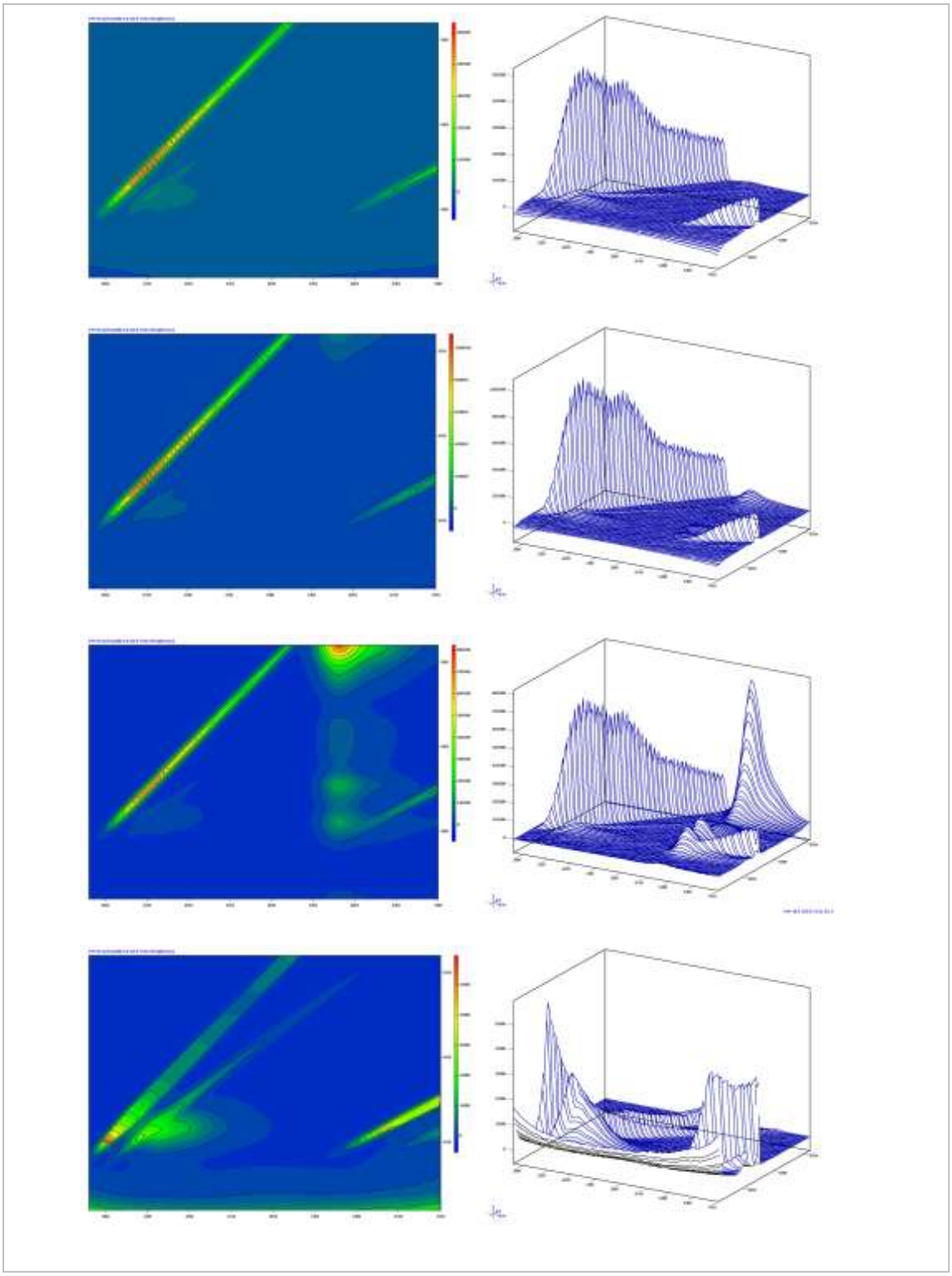

Figure 56: Top to bottom, three-dimensional synchronous scans of rhodamine WT 1, 10, and 100 ppb and sulphorhodamine B .01 ppb single dye dilutions. X-axis range = 280 - 700 is nm, Y-axis range = 220 – 520 nm.

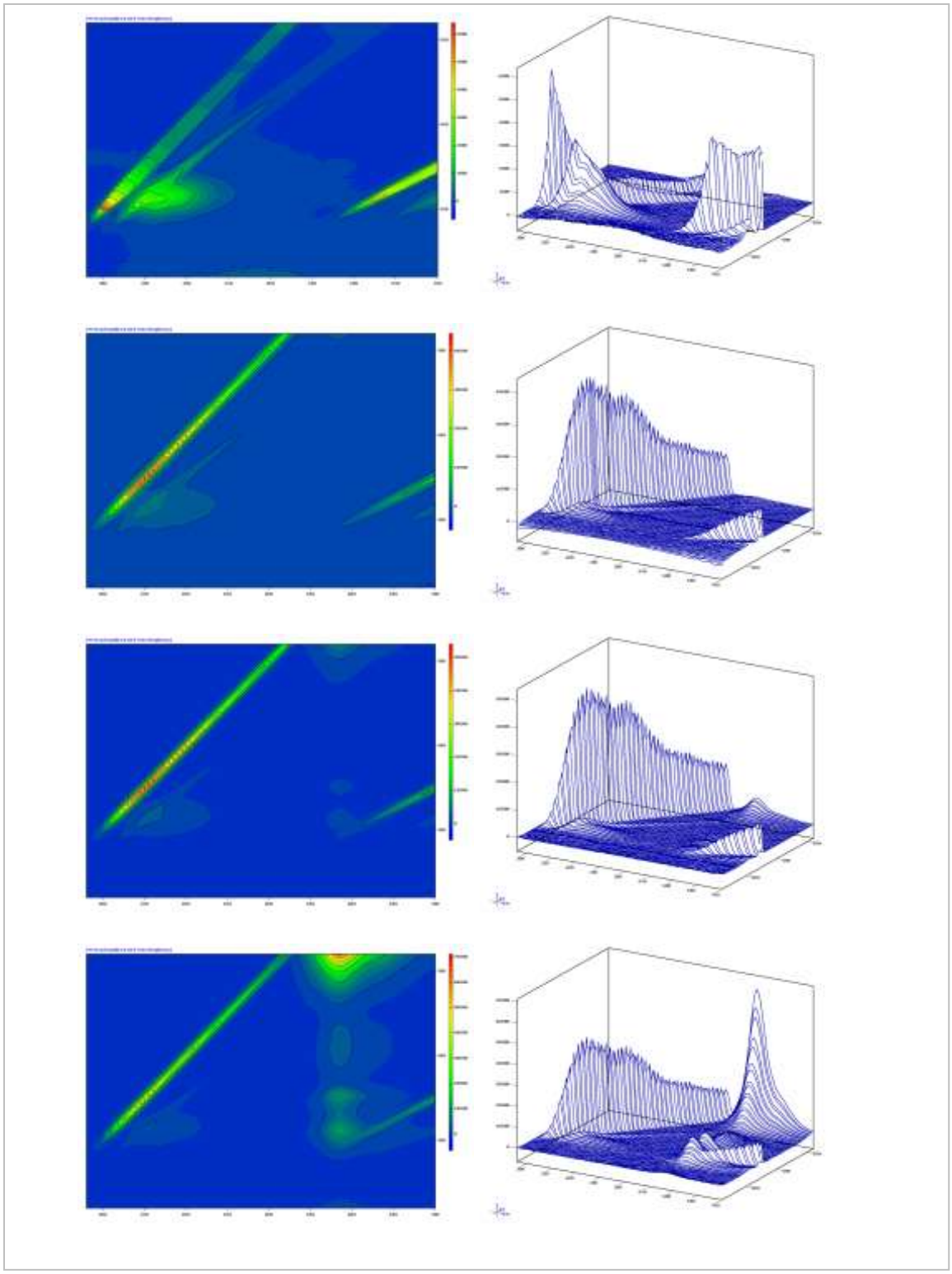

Figure 57: Top to bottom, three-dimensional synchronous scans of sulphorhodamine B 0.1, 1, 10, and 100 ppb single dye dilutions. X-axis range = 280 - 700 is nm, Y-axis range = 220 – 520 nm.

10.3 Mixed Dye Dilution Two-Dimensional Synchronous Scans

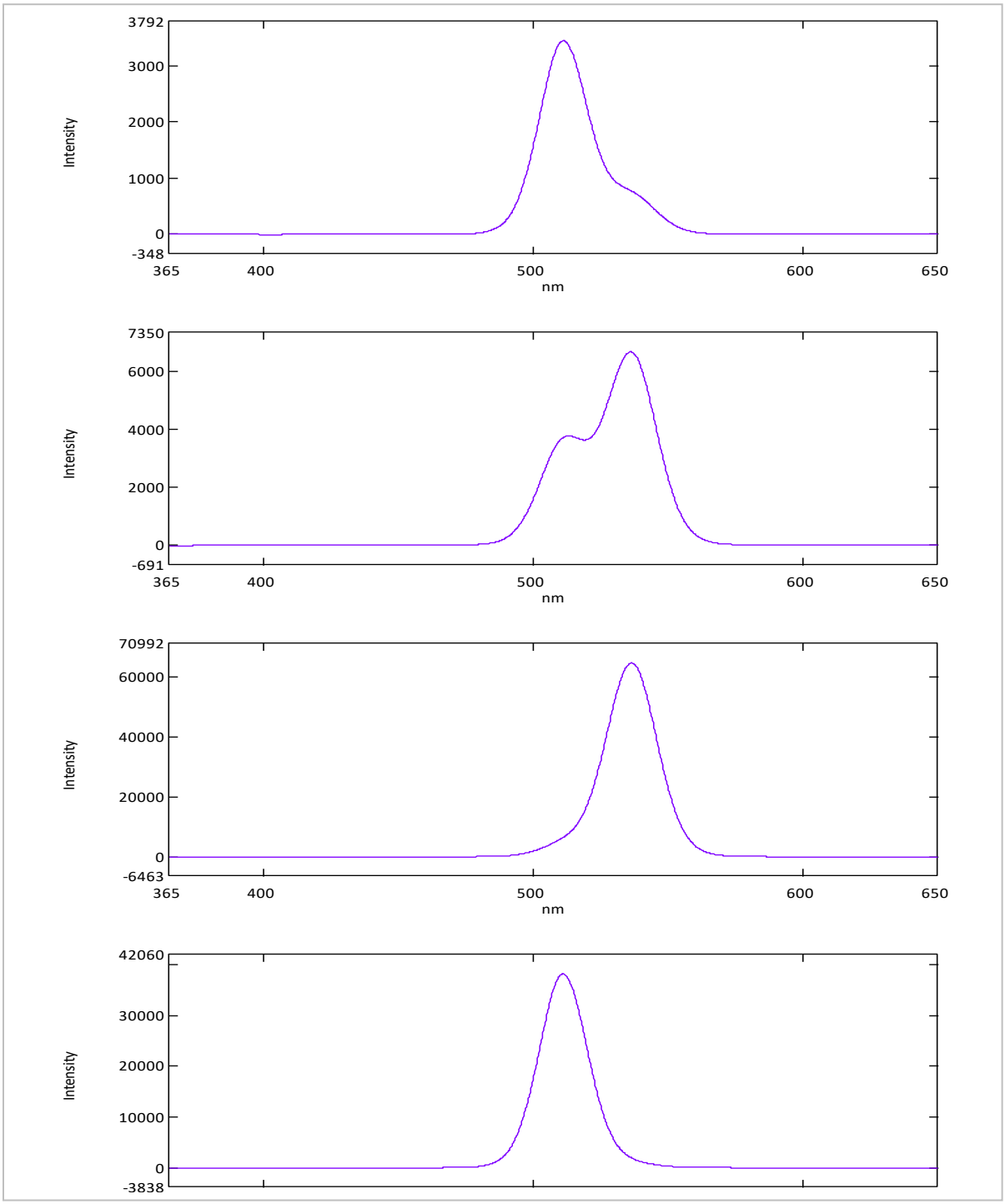

Figure 58: Top to bottom, two-dimensional synchronous scans of FLEO 1:1, FLEO 1:10, FLEO 1:100, and FLEO 10:1 mixed dye dilutions.

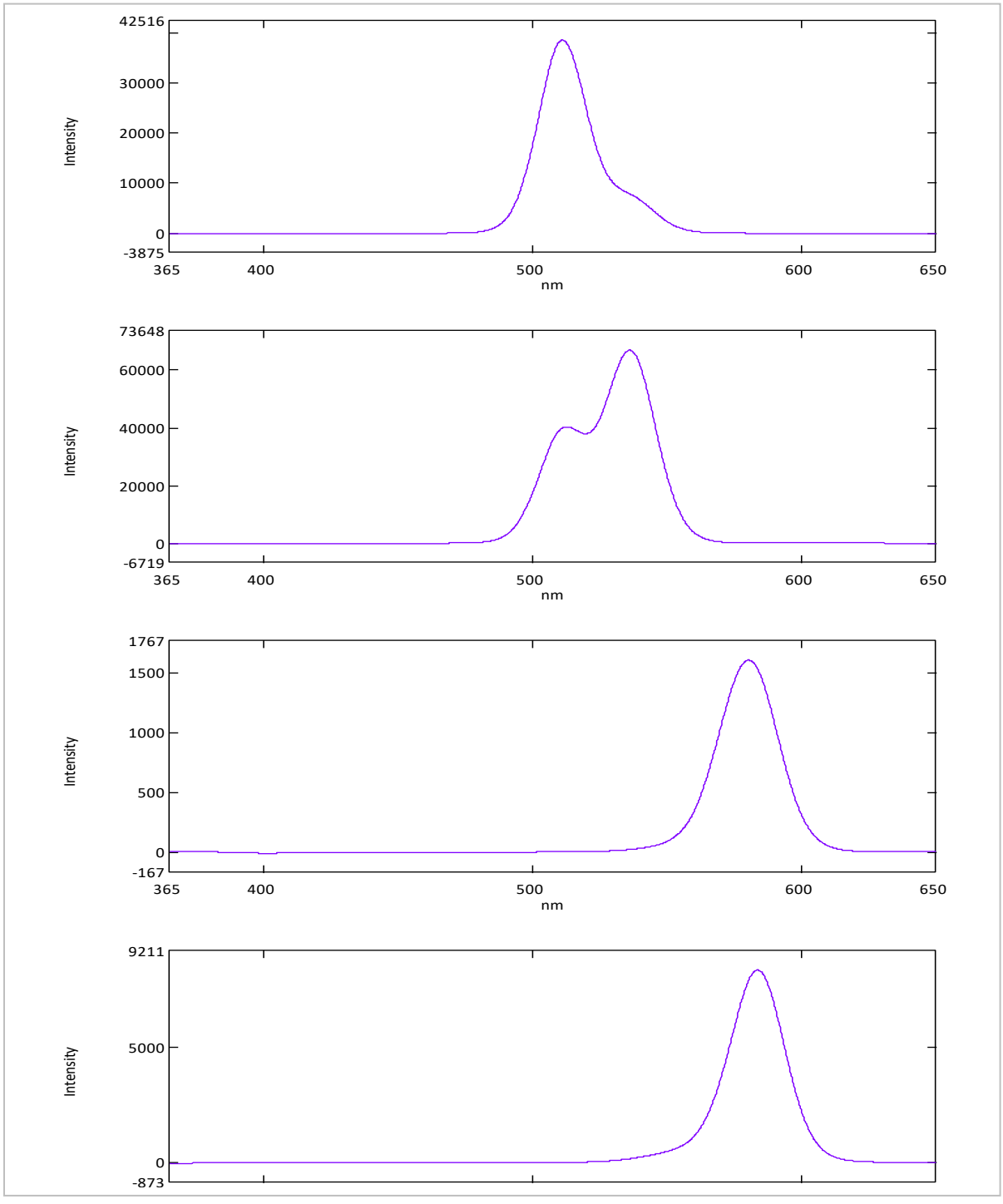

Figure 59: Top to bottom, two-dimensional synchronous scans of FLEO 10:10, FLEO 10:100, RWTSRB 1:1, and RWTSRB 1:10 mixed dye dilutions.

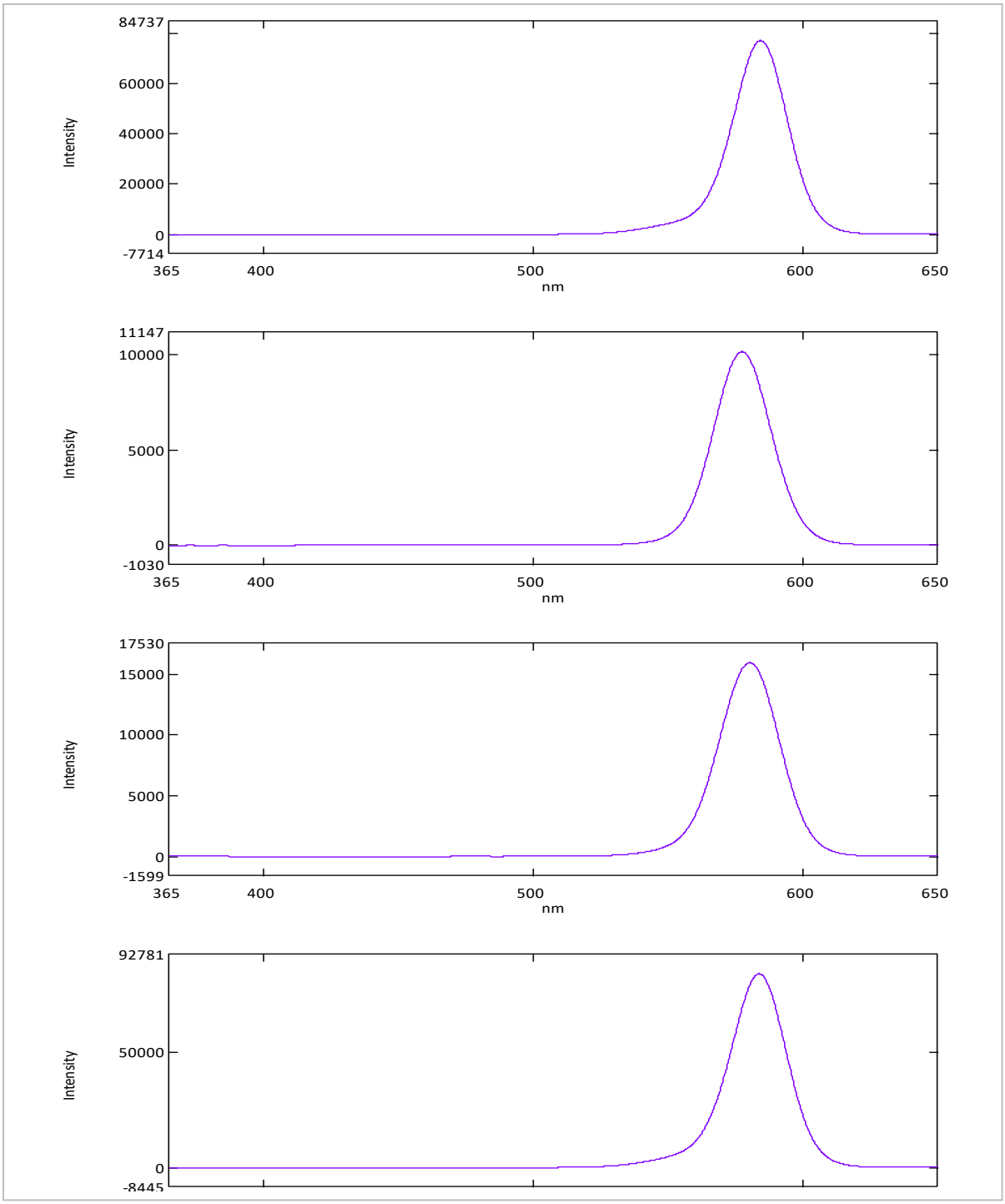

Figure 60: Top to bottom, two-dimensional synchronous scans of RWTSRB 1:100, RWTSRB 10:1, RWTSRB 10:10, and RWTSRB 10:100 mixed dye dilutions.

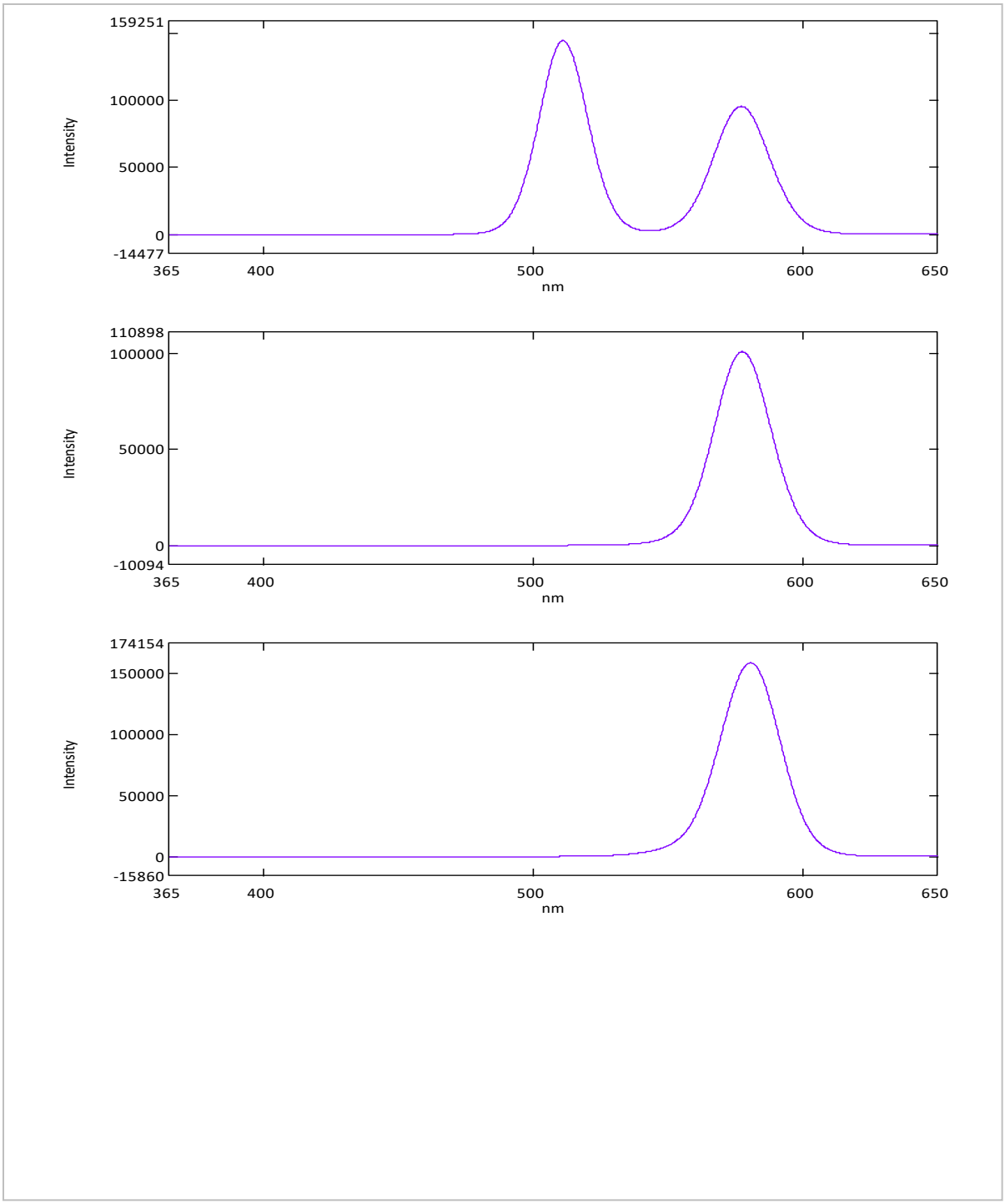

Figure 61: Top to bottom, two-dimensional synchronous scans of RWTSRB 100:1, RWTSRB 100:10, and RWTSRB 100:100 mixed dye dilutions.

10.4 Mixed Dye Dilution Three-Dimensional Synchronous Scans

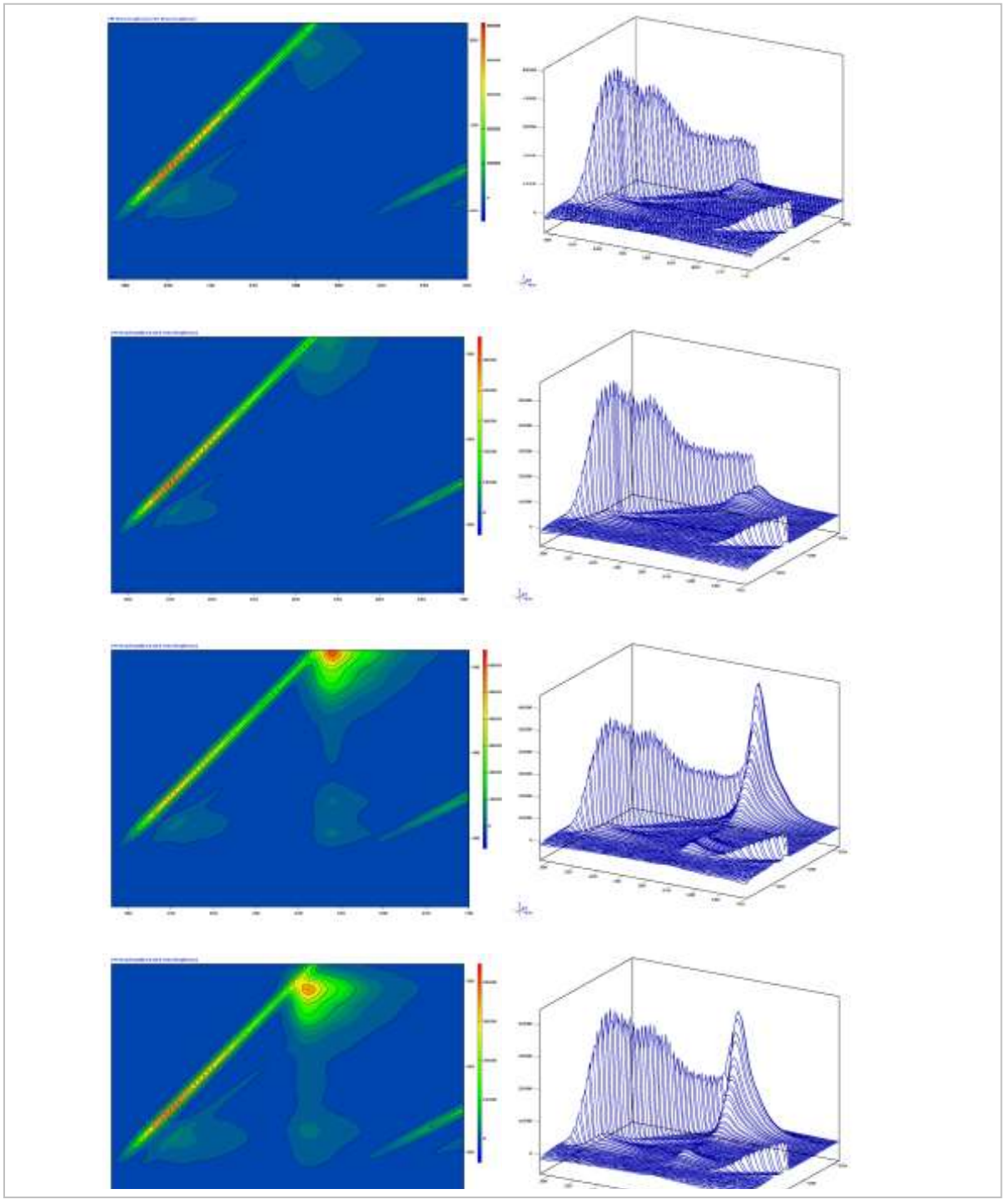

Figure 62: Top to bottom, three-dimensional synchronous scans of FLEO 1:1, FLEO 1:10, FLEO 1:100, and FLEO 10:1 mixed dye dilutions. X-axis range = 280 - 700 is nm, Y-axis range = 220 – 520 nm.

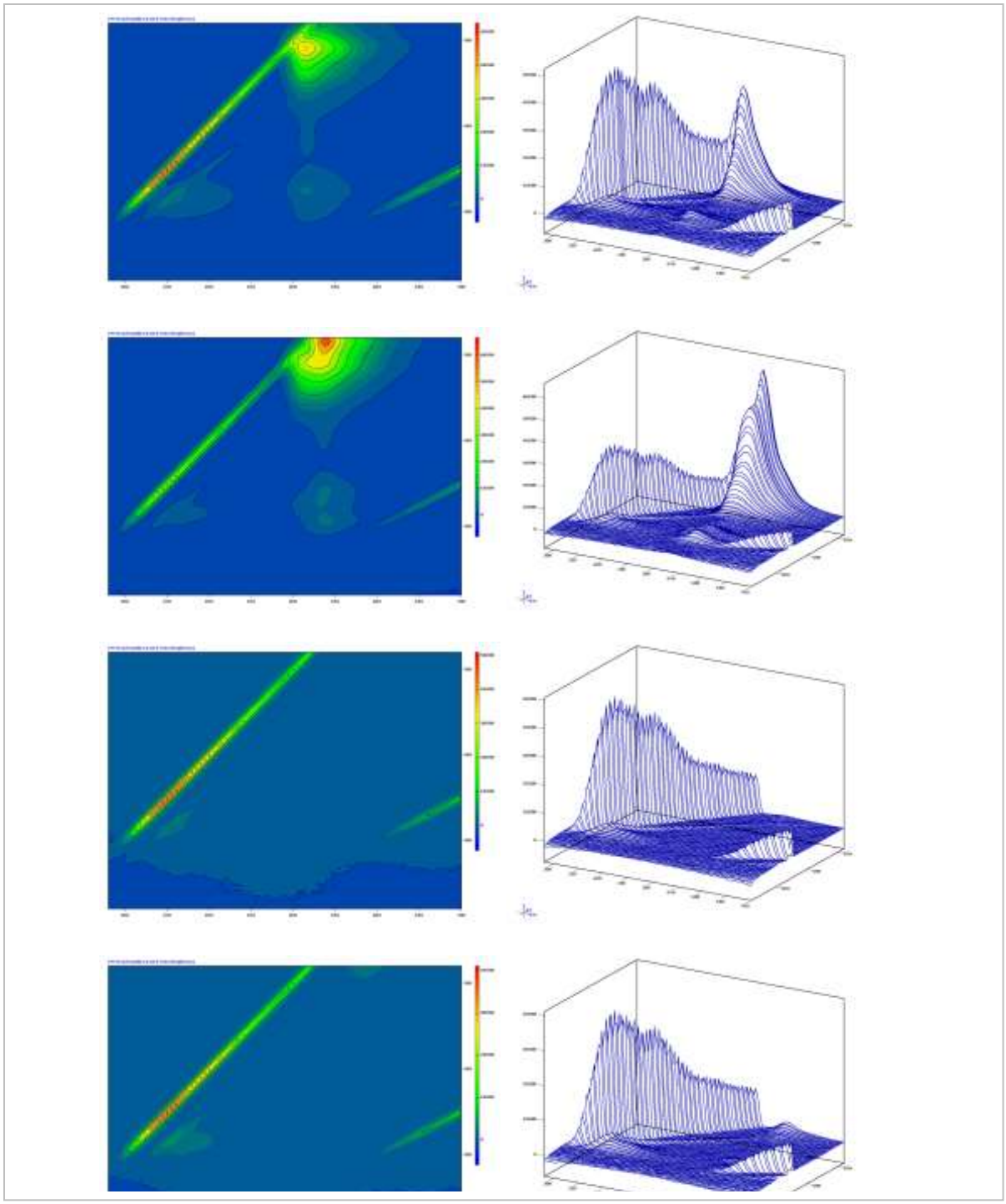

Figure 63: Top to bottom, three-dimensional synchronous scans of FLEO 10:10, FLEO 10:100, RWTSRB 1:1, and RWTSRB 1:10 mixed dye dilutions. X-axis range = 280 - 700 is nm, Y-axis range = 220 – 520 nm.

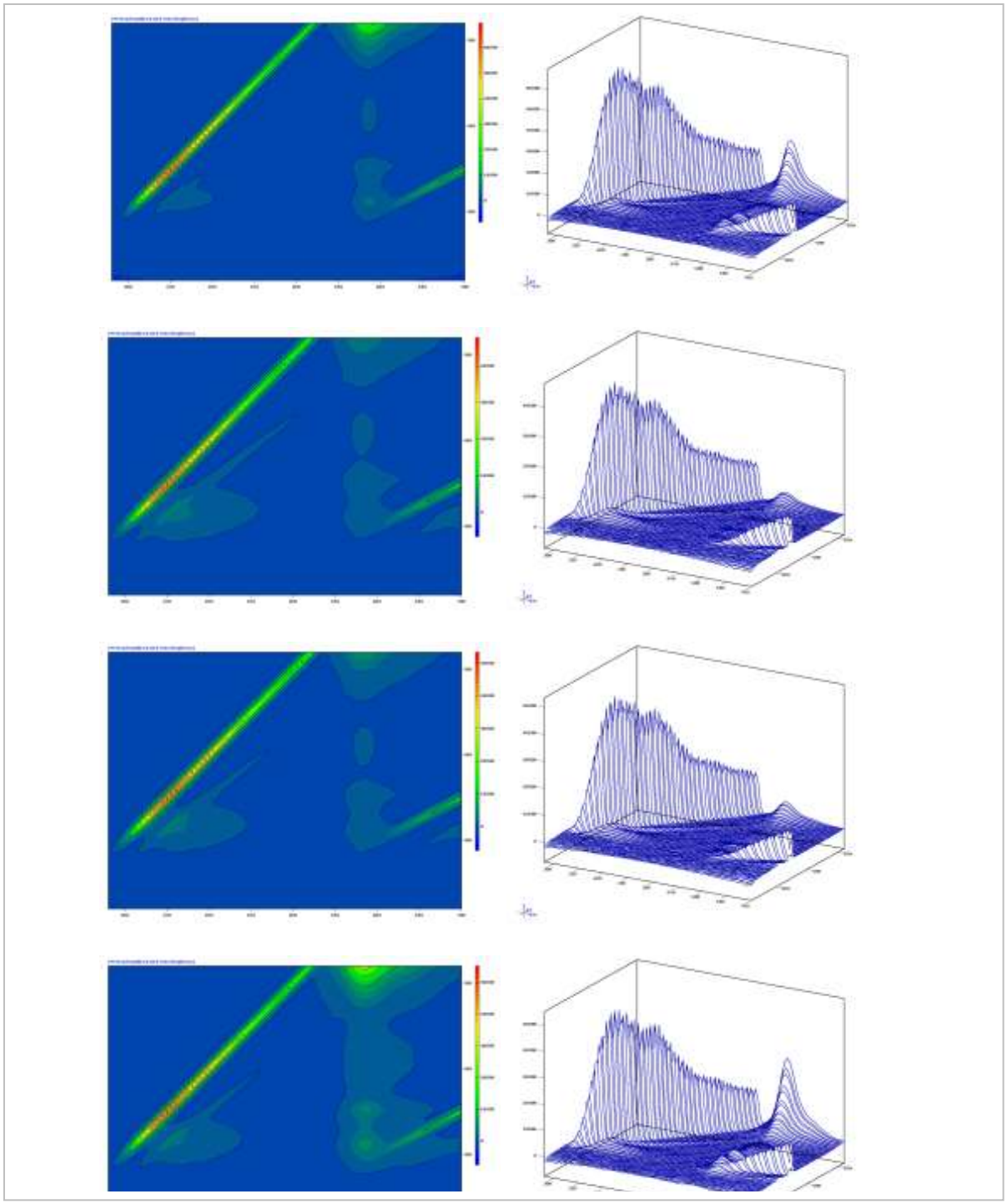

Figure 64: Top to bottom, three-dimensional synchronous scans of RWTSRB 1:100, RWTSRB 10:1, RWTSRB 10:10, and RWTSRB 10:100 mixed dye dilutions. X-axis range = 280 - 700 is nm, Y-axis range = 220 – 520 nm.

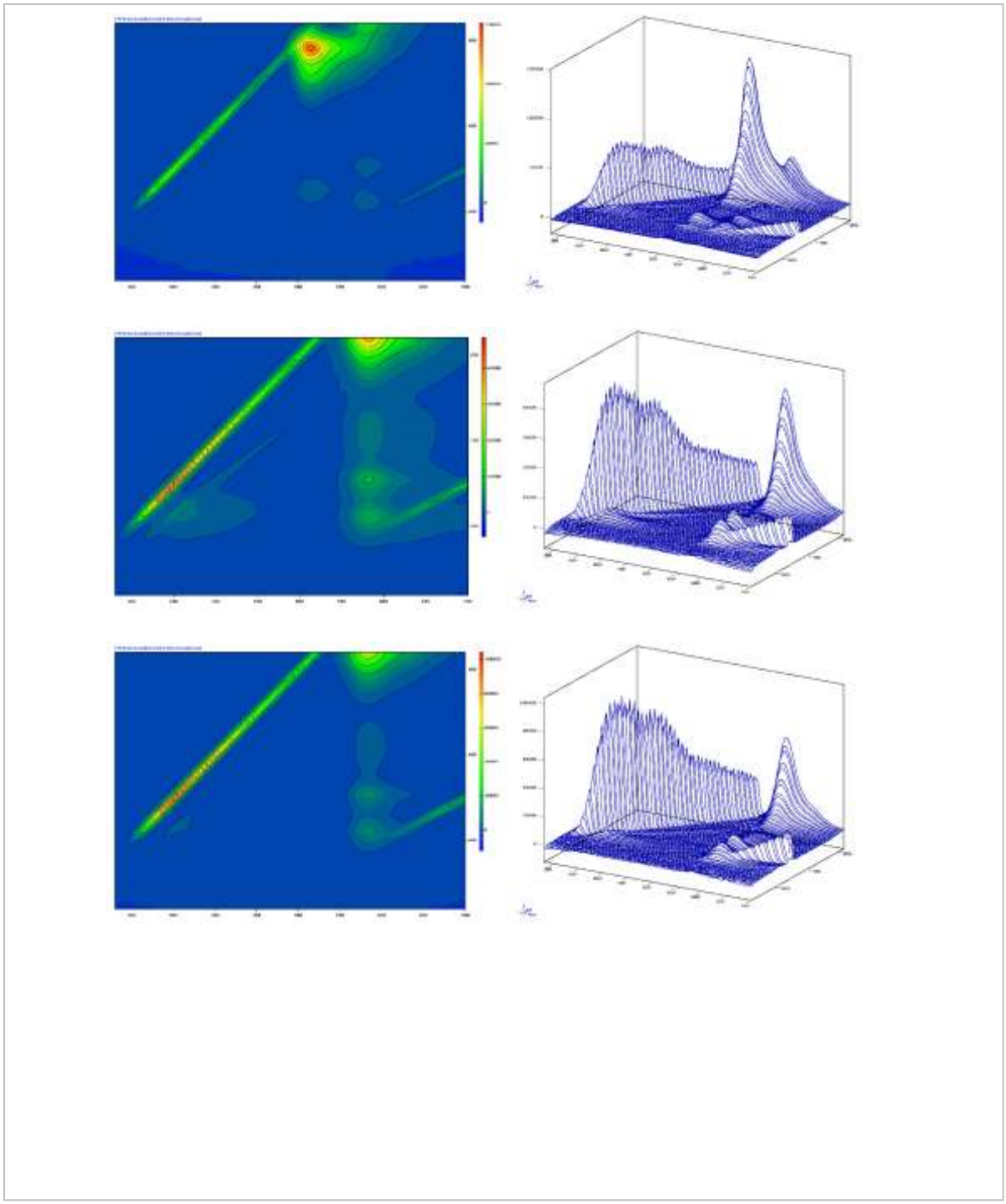

Figure 65: Top to bottom, three-dimensional synchronous scans of RWTSRB 100:1, RWTSRB 100:10, and RWTSRB 100:100 mixed dye dilutions. X-axis range = 280 - 700 is nm, Y-axis range = 220 – 520 nm.

10.5 Lost River Cave Two-Dimensional Synchronous Scans

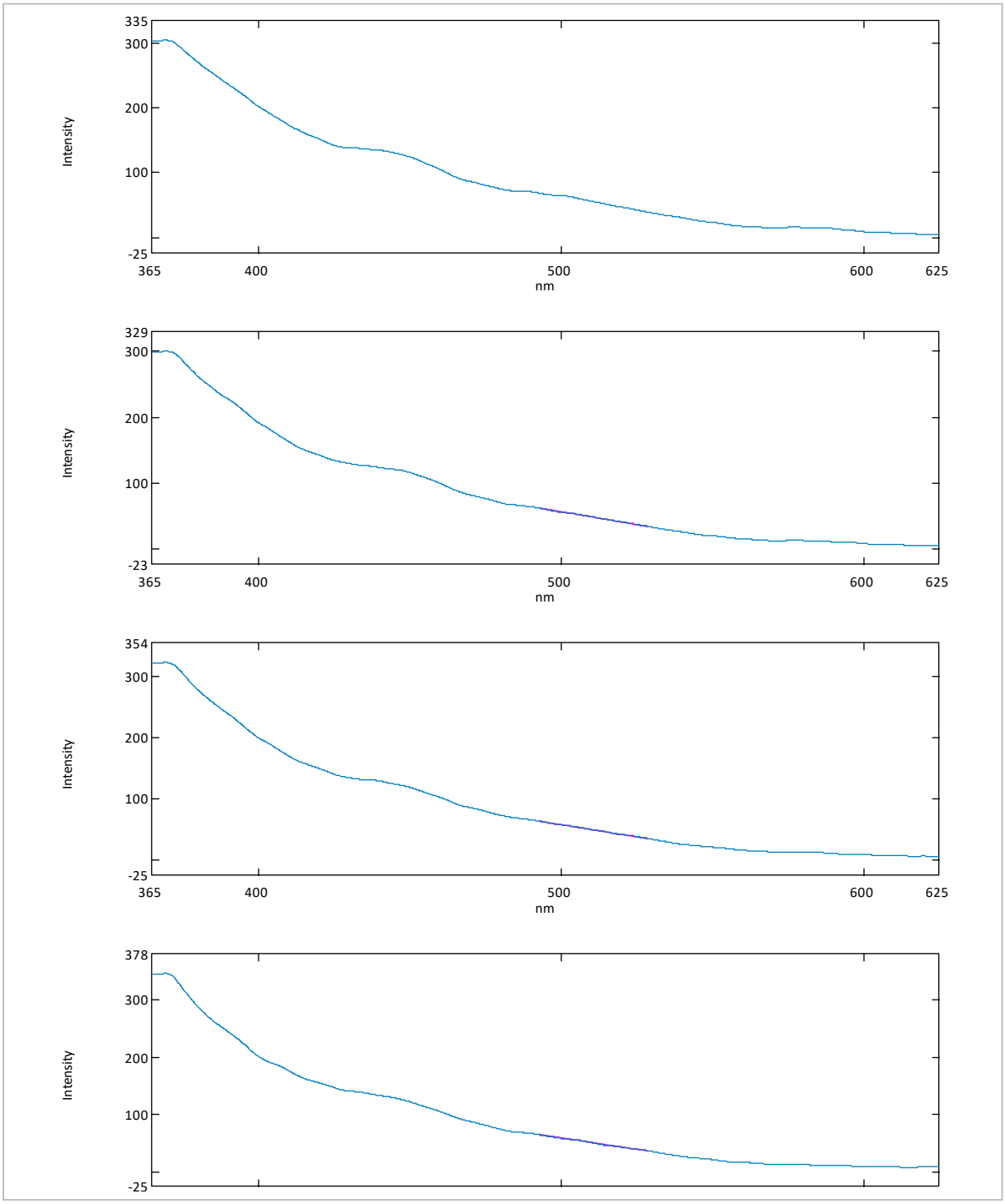

Figure 66: Top to bottom, two-dimensional synchronous scans of Lost River Cave 001, 002, 003, and 004 water samples.

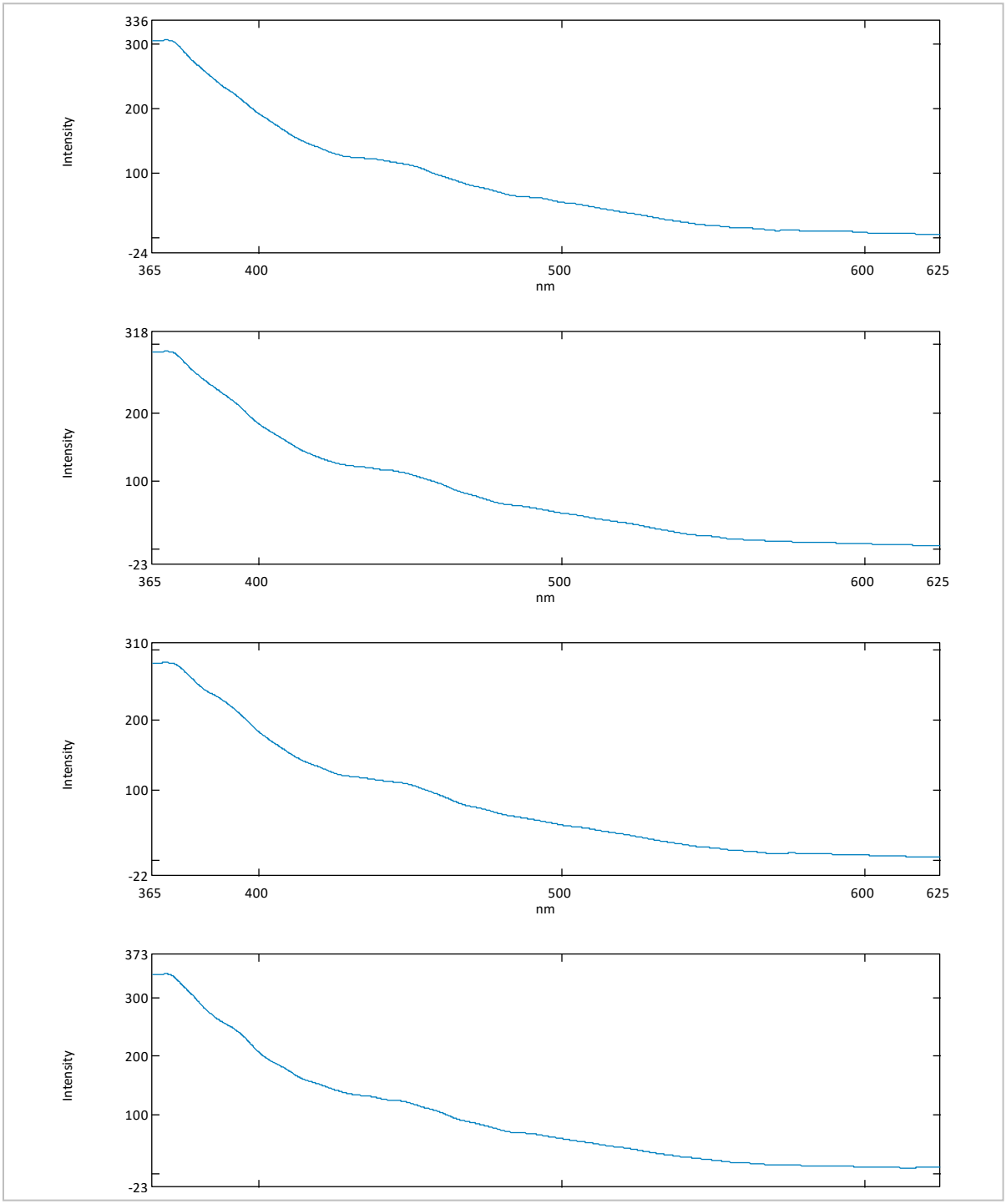

Figure 67: Top to bottom, two-dimensional synchronous scans of Lost River Cave 005, 006, 007, and 008 water samples.

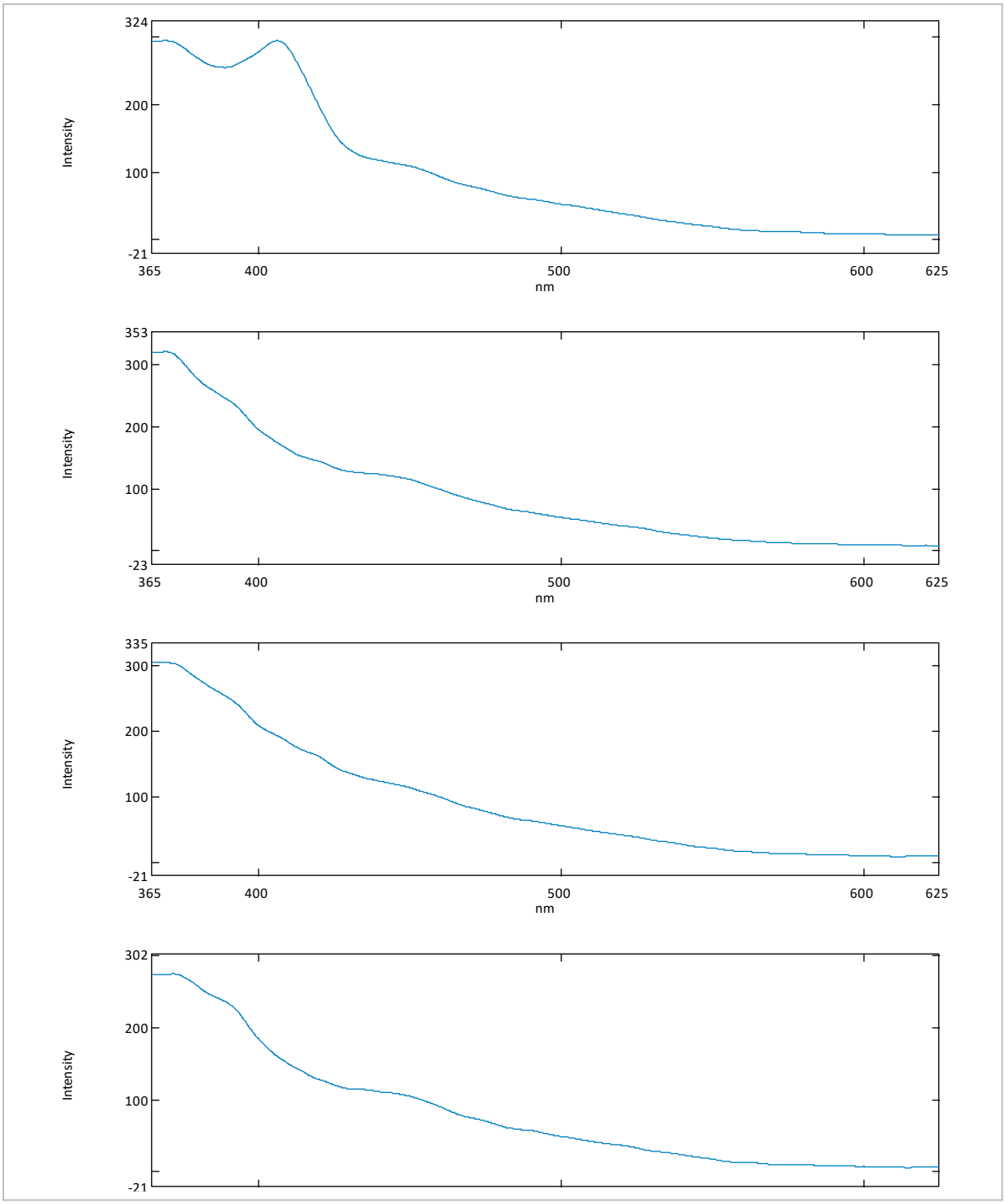

Figure 68: Top to bottom, two-dimensional synchronous scans of Lost River Cave 009, 010, 011, and 012 water samples.

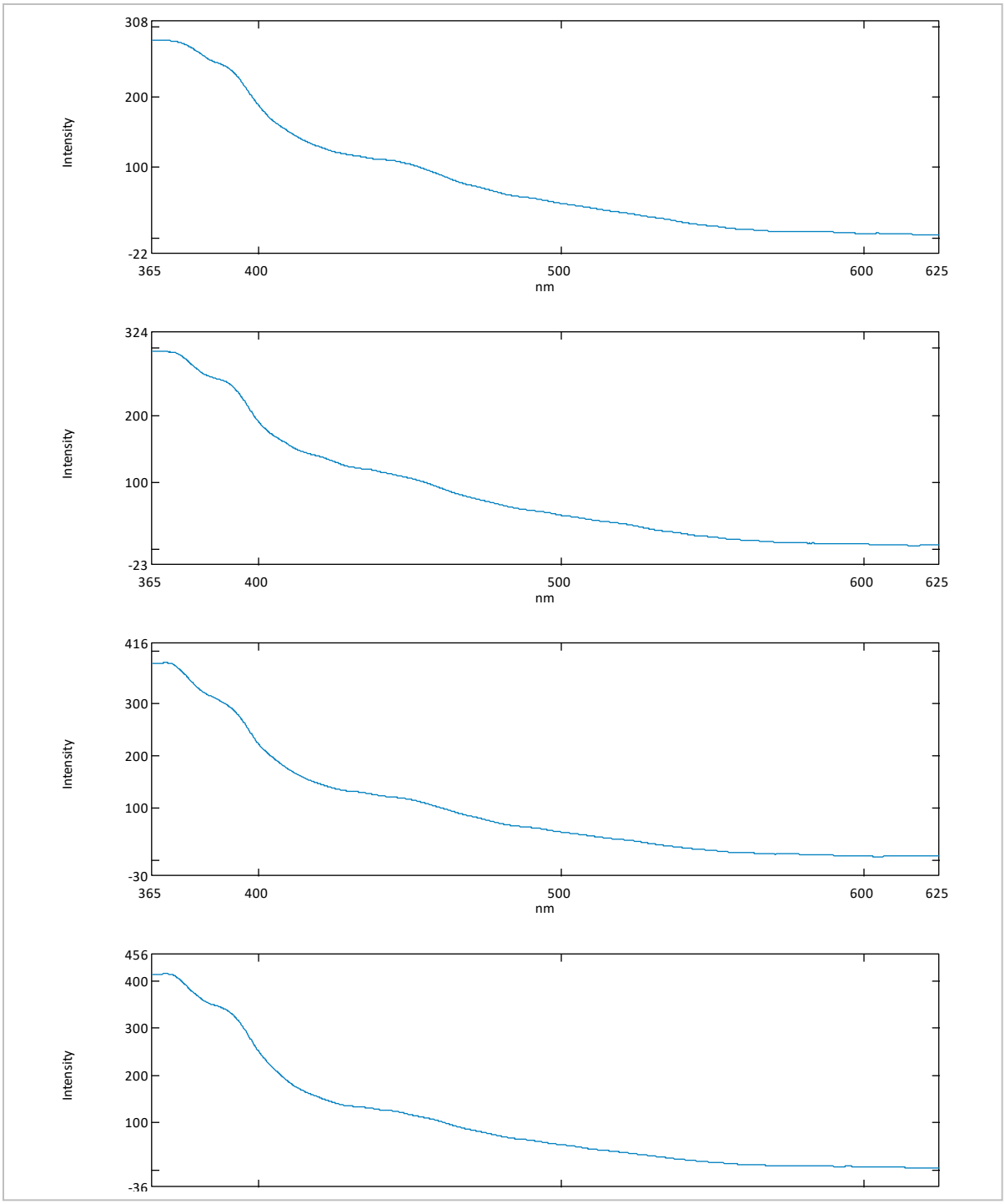

Figure 69: Top to bottom, two-dimensional synchronous scans of Lost River Cave 013, 014, 015, and 016 water samples.

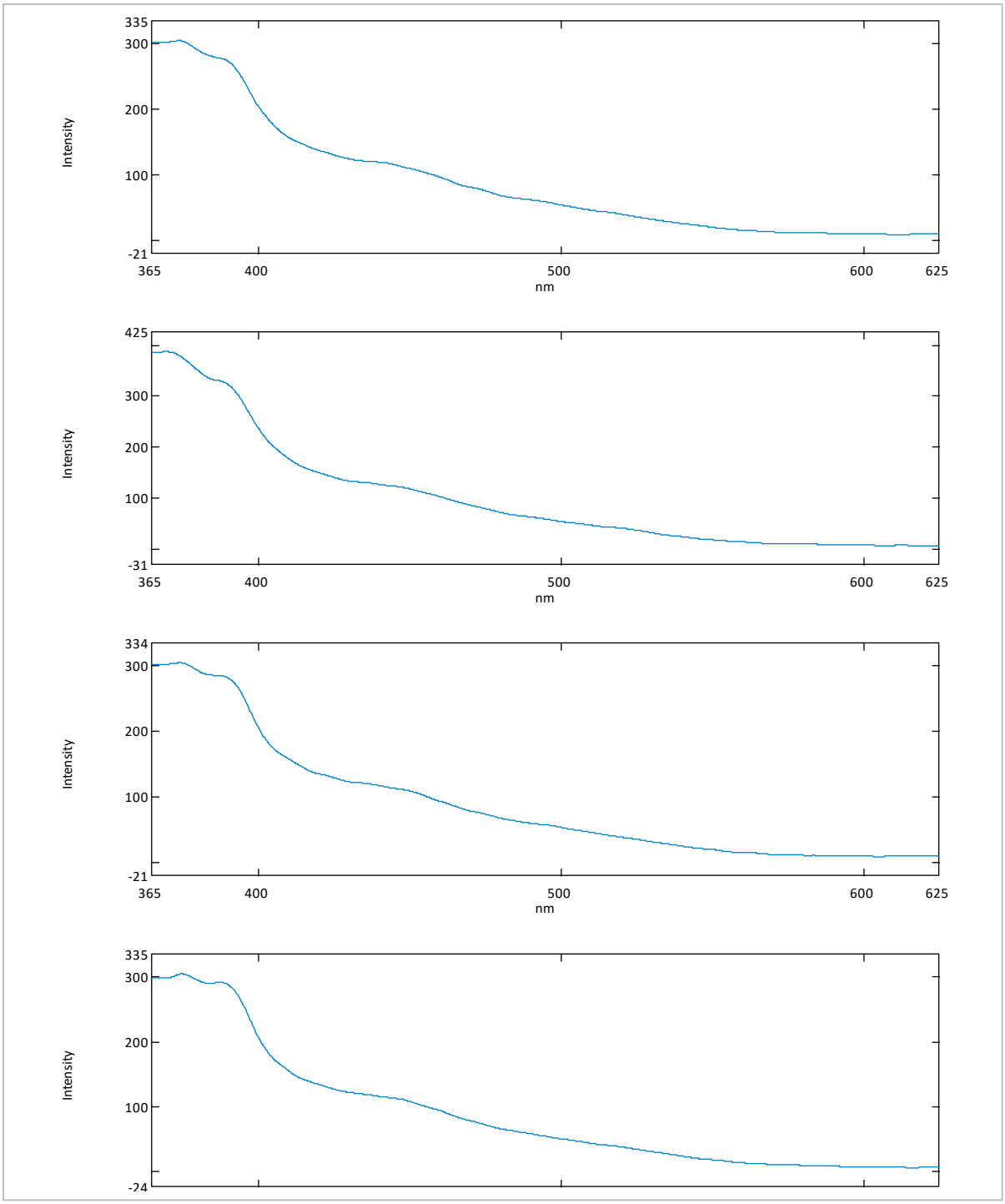

Figure 70: Top to bottom, two-dimensional synchronous scans of Lost River Cave 017, 018, 019, and 020 water samples.

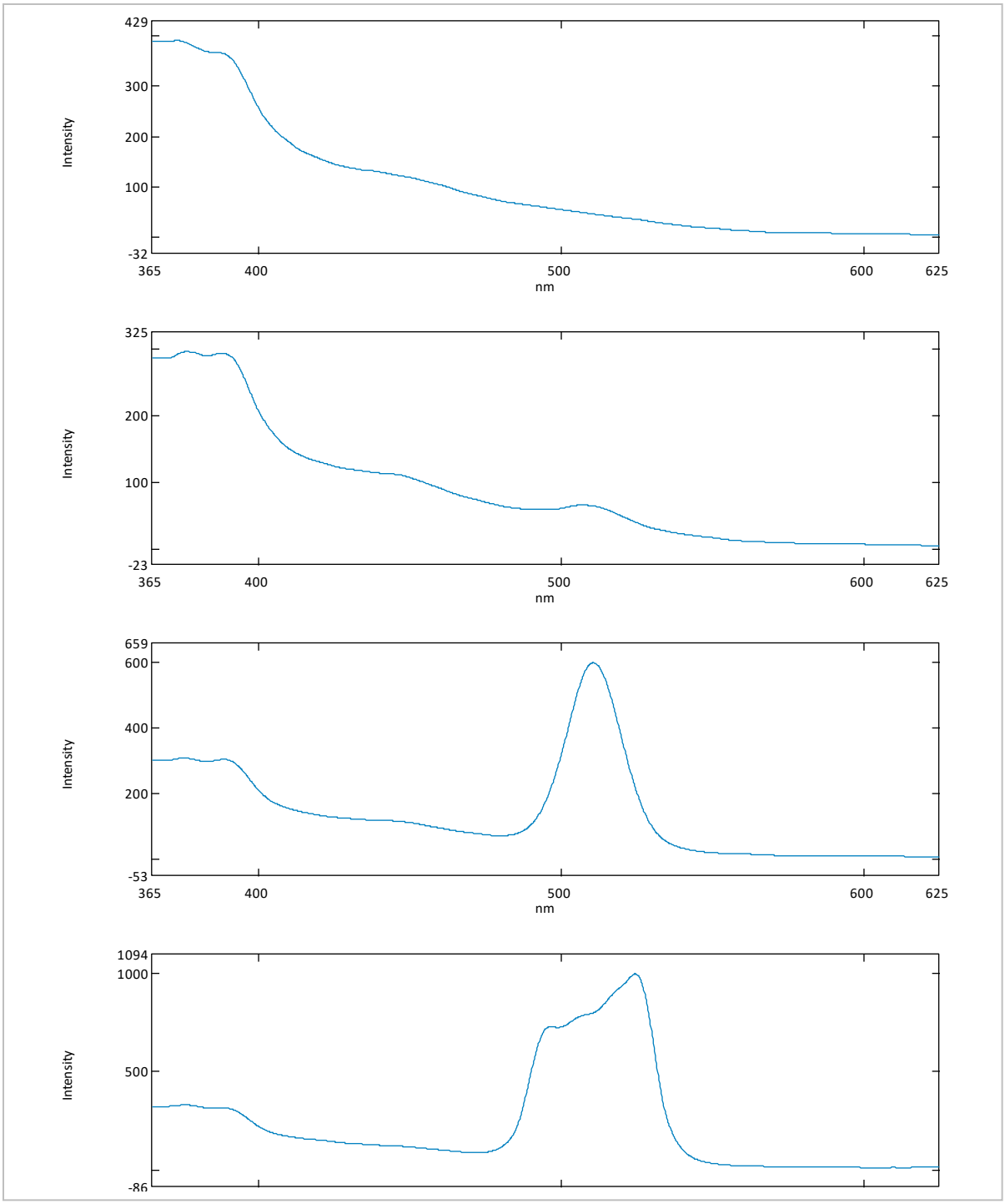

Figure 71: Top to bottom, two-dimensional synchronous scans of Lost River Cave 021, 022, 023, and 024 water samples.

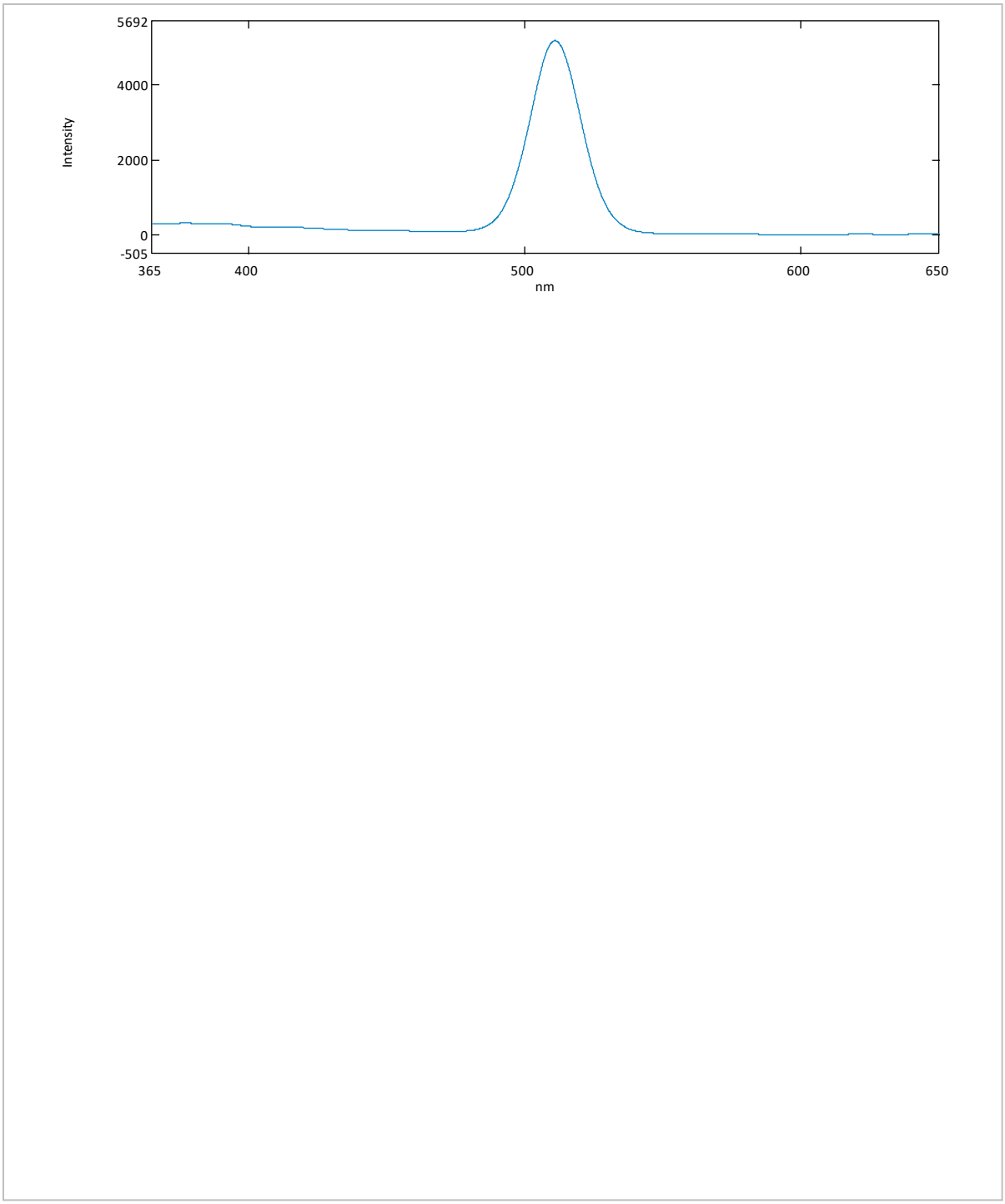

Figure 72: Low sensitivity two-dimensional synchronous scan of Lost River Cave 024 water sample.

10.6 Lost River Three-Dimensional Synchronous Scans

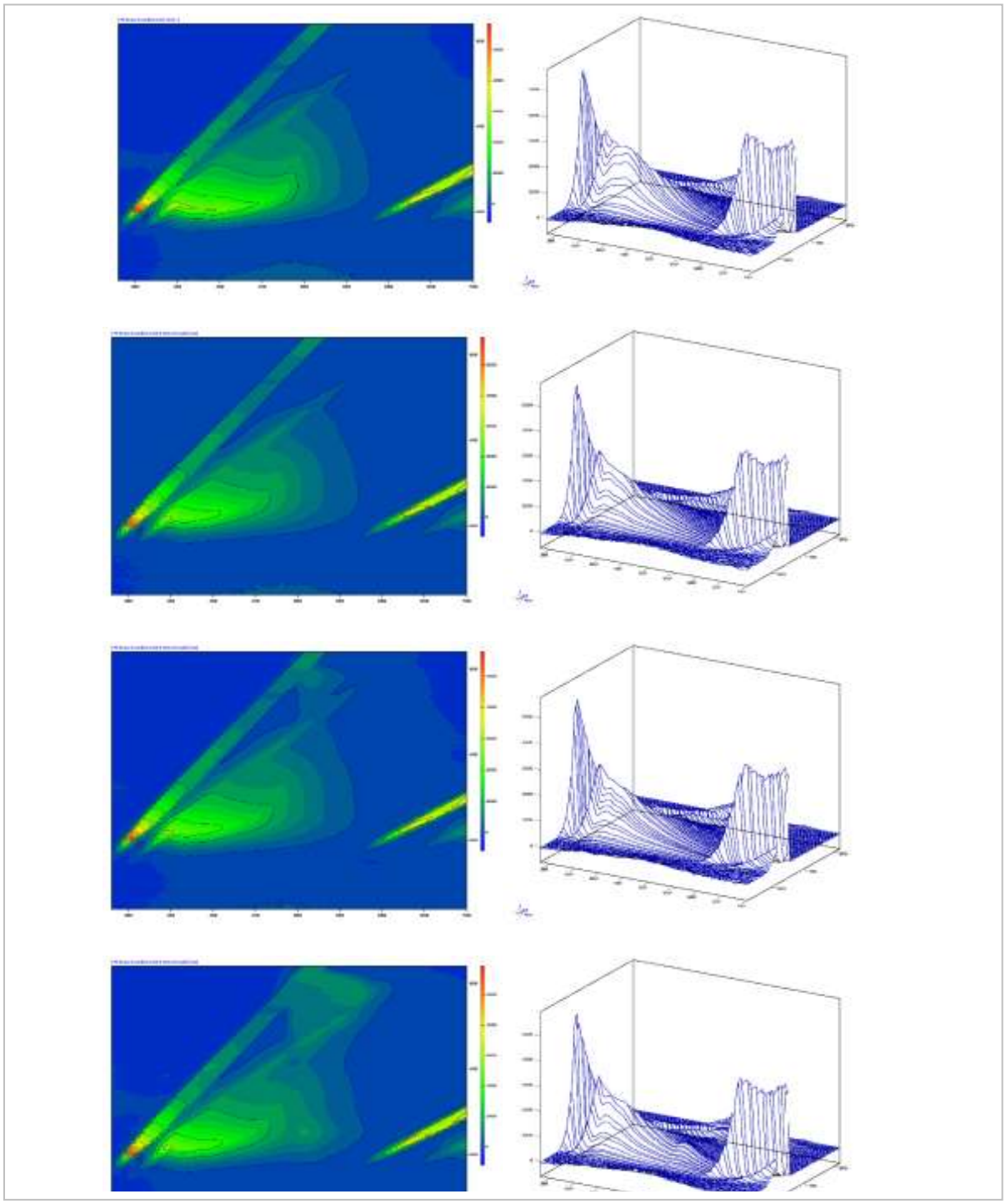

Figure 73: Top to bottom, three-dimensional synchronous scans of Lost River Cave 021, 022, 023, and 024 water samples. X-axis range = 280 - 700 is nm, Y-axis range = 220 – 520 nm.